# Oxidation Kinetics of Methylphosphonic Acid in Supercritical Water: Experimental Measurements and Model Development

by
Patricia A. Sullivan

B.S., Chemical Engineering
University of Notre Dame, 1999

M.S., Chemical Engineering Practice
Massachusetts Institute of Technology, 2002

Submitted to the Department of Chemical Engineering
in partial fulfillment of the requirements for the degree of

DOCTOR OF PHILOSOPHY IN CHEMICAL ENGINEERING

at the

MASSACHUSETTS INSTITUTE OF TECHNOLOGY

[February 2004]
November, 2003





Signature of Author: _____
Department of Chemical Engineering
November 10, 2003

Certified by: _____
Professor Jefferson W. Tester
Thesis Supervisor

Accepted by: _____
Professor Daniel Blankschtein
Professor of Chemical Engineering
Chairman, Committee for Graduate Students

# Oxidation Kinetics of Methylphosphonic Acid in Supercritical Water: Experimental Measurements and Model Development

by
Patricia A. Sullivan

Submitted to the Department of Chemical Engineering on November 10, 2003 in partial fulfillment of the requirements for the degree of Doctor of Philosophy in Chemical Engineering

## ABSTRACT

Above its critical point ($T_c$=374 °C, $P_c$=221 bar), the physical properties of pure water change drastically from liquid-like to dense gas-like behavior. Supercritical water is a nonpolar solvent with moderate densities (approximately 0.1 g/mL) and gas-like diffusivities and viscosities. Above 450 °C, radical pathways dominate due to the higher temperatures and decreased ionic reaction rates when the ion-dissociation constant of water is less than $10^{-19}$. Supercritical water is employed as an oxidation medium for the destruction of dilute organic aqueous waste streams because organic compounds and gases are both soluble in supercritical water. Oxidation proceeds quickly and completely without interphase mass transfer limitations, with characteristic reaction times of one minute needed for total conversion of C/H/N/O organic compounds to water, carbon dioxide, and molecular nitrogen.

With this as a motivation, the supercritical water oxidation kinetics of the model organophosphorus compound, methylphosphonic acid (MPA or $PO(OH)_2CH_3$), was the primary focus of this thesis. Organophosphorus oxidation in supercritical water is being considered as a destruction method for stockpiled organophosphorus chemical warfare agents. MPA is a refractory intermediate and its reaction kinetics are important for the complete oxidation of larger organophosphorus compounds. Previous experimental MPA oxidation studies focused on determining the conditions necessary to achieve high destruction efficiencies at excess oxygen and long residence times. The primary goal of our research was to improve the mechanistic understanding of MPA oxidation kinetics in supercritical water. Our approach was to experimentally measure MPA oxidation rates and product yields at well-defined operating conditions and to develop both microscopic and macroscopic models, ranging from regressed global models to an elementary reaction mechanism, to quantify MPA oxidation kinetics in supercritical water.

MPA hydrolysis and oxidation rates were experimentally measured in a laboratory-scale plug flow reactor. The effects of MPA concentration (0.5 to 1.0 mM), oxygen concentration (1.0 to 3.8 mM), temperature (478 to 572°C) and pressure (138 to 277 bar) on oxidation rates were determined for residence times ranging from 3.0 to 9.5 s. Conversion due to hydrolysis was less than 6% after $\tau$=7 s at all temperatures studied. For $\tau$=7 s at stoichiometric conditions and $P$=246 bar, low conversion ($X$<30% at $\tau$=10 s) was observed at $T$<503 °C, while almost complete conversion ($X$=99%) occurred at $T$=571 °C. The only phosphorus-containing product was phosphoric acid, while the carbon-containing intermediates, carbon monoxide and methane, were present in varying concentrations in addition to final carbon-containing product, carbon

dioxide. Methane was only a minor product, with a carbon yield less than 20% at all experimental conditions. MPA oxidation rates varied with oxygen concentration and pressure (or water density), but were relatively independent of initial MPA concentration.

A global MPA oxidation rate law was regressed from the data with its dependence on temperature, MPA concentration, oxygen concentration, and water concentration quantified. The regressed parameters were a pre-exponential factor of $10^{14.0\pm1.6}$ ($s^{-1}$ $M^{-1.47}$), an activation energy of 228±22 kJ/mol, a first-order MPA dependence, an oxygen order of 0.30±0.18, and a water order of 1.17±0.30 (all parameters to 95% confidence). A four-pathway model was also developed where MPA reacted to form the carbon-containing intermediates, CO and $CH_4$, with subsequent reactions of $CH_4$ to form CO and CO to form $CO_2$. From these results, the reaction rate and oxygen dependence for each pathway was estimated. This macroscopic model can be used to predict the fate of all carbon at different operating conditions during MPA oxidation.

The first step in the development of an MPA SCWO elementary reaction rate model was to accurately estimate organophosphorus thermochemistry and transition state theory reaction rates by employing *ab initio* calculations using the CBS-Q method in Gaussian 98. Current organophosphorus combustion mechanisms contain few MPA reaction pathways and all rate constants are estimated with high uncertainty (Korobeinichev *et al.*, 2000; Glaude *et al.*, 2000). Through the *ab initio* calculations, rate constants were estimated for newly identified reaction pathways, such as MPA hydrogen abstraction reactions and $P^{\bullet}O(OH)_2$ reactions. As part of this study, calculated transition state theory rate constants were compared to estimated organophosphorus rate constants from literature combustion mechanisms to determine their accuracy. Reactions involving P-O bonds were typically overestimated by several orders of magnitude in the combustion mechanisms because the P-O bond is much stronger than similar C-O or N-O bonds.

An MPA SCWO elementary reaction rate model was developed with 94 new organophosphorus reactions and 14 new organophosphorus intermediates. This model improved on previous organophosphorus combustion models by adding hydrogen abstraction reaction channels that were necessary to properly predict the experimentally measured MPA product yields. The MPA SCWO model correctly predicts the concentration profiles of MPA and its carbon-containing products at temperatures between 478 and 572 °C at stoichiometric conditions and 246 bar. The model also qualitatively predicts that MPA oxidation rates increase with increasing oxygen concentration, as found experimentally, but was unable to predict that MPA oxidation rates increase with increasing water concentration. This limitation could be due to an incomplete representation of water's role as both a solvent and a reactant in supercritical water. This model introduced new organophosphorus reaction pathways and intermediates that could also be important in other organophosphorus combustion mechanisms.

Thesis Supervisor: Jefferson W. Tester
Herman P. Meissner Professor of Chemical Engineering

# Acknowledgements

The best part of my time here at MIT has been the people that I've met. And to think that I almost didn't visit this school because I was convinced that I wouldn't like it here until my dad insisted that I give it a try. I was pleasantly surprised by all the nice and interesting people that I met then and I contine to be impressed by the amazing friends that I have met here and I look forward to the great things that they will all do one day.

I must first thank my advisor, Jeff Tester, who provided the right mixture of guidance and freedom so that I could define my project and pursue interesting avenues. Jeff treats all of his students like we're family and he creates a friendly group atmosphere that makes working much easier and more enjoyable. I must also thank my thesis committee for all of their helpful insight to my project. The members always brought up interesting ideas and questions during our meetings which really helped me along the way. I need to especially thank Bill Green for patiently answering all my modeling questions and concerns. I would not have been able to develop the model without his expertise and guidance. In addition, I also need to thank Sumathy Raman for all the help and time that she put into the ab initio study with me. She is a wonderfully kind and helpful teacher who is always willing to answer the silliest questions.

I also need to thank the past and present members of the Tester group with whom I spent countless hours in the basement, including Josh, Mike, Paul, Murray, Jason, Heather, Brian, Chad, Russ, and Anish (fellow basement dweller). We always had the right mix of discussing football teams one second and someone's research problems the next second. I must wish the best of luck to Jason and Russ, who are carrying on the SCWO torch in the laboratory. Along with all of my friends in the basement, I must also thank my friends at MIT, Kim, April, Kevin, Paul, Ian, and sometimes Ley, who came and rescued me from the reactor or Chemkin to make sure that I ate lunch most days. It will be hard to leave here and no longer have the "lunch knock" anymore.

Finally, I need to thank my family (Pat, Judy, Sean, and Meghan) who have always been there to support me through all of life's adventures. As I finish up grad school here, I only hope that Sean has as rewarding experience at Georgia Tech as I've had here (even though he did switch from chemical engineering to biomedical engineering). And finally, I need to thank my husband, Jim, who has been there for me through all the ups and downs of my grad school career and who kept me almost sane during our time here.

# Table of Contents

# List of Figures

# List of Tables

# 1 Introduction and Background

In this thesis, the oxidation kinetics of organophosphorus compounds in supercritical water (SCW) were examined. Motivation for research in this area is provided by the fact that supercritical water oxidation (SCWO) is being considered as a destruction method for stockpiled organophosphorus nerve agents, but their oxidation kinetics in SCW have not been thoroughly characterized. To provide a background for this investigation, the properties of supercritical water and the advantages of SCWO are discussed along with previous SCWO kinetic research. In addition, introductory information on organophosphorus chemical warfare agents is presented, including their chemical structure, common destruction methods, and previous SCWO research on these organophosphorus compounds

## 1.1 Supercritical Water Oxidation

Supercritical water behaves as a nonpolar, dense gas that can solvate both organics, like benzene or butane, and light gases, like $O_2$, $N_2$ or $CO_2$, removing interphase mass transfer limitations for oxidation. SCWO has been used to remediate dilute aqueous waste streams that are otherwise difficult to treat. To improve the understanding of SCWO technology and increase its use as a remediation method, basic research has focused on both fundamental studies and engineering issues. To better predict and model supercritical water processes, fundamental research has been conducted on SCW physical property measurements, equation of state development, phase nucleation and phase equilibria, and measurement and prediction of oxidation rates for model compounds. Engineering studies have been targeted at improving problematic issues for the SCWO process, such as efficient heat transfer, salt deposition and plugging in the reactor, and materials corrosion.

### *1.1.1 Supercritical Water*

A substance is considered "supercritical" when it is above both its critical pressure and temperature. As the temperature or pressure of a two-phase vapor-liquid system nears the critical point, the densities of the vapor and the liquid phase approach each other until they become a single phase at the critical point. As long as both the temperature and pressure are above the critical point, the substance remains a single phase. In the supercritical phase, the substance exhibits characteristics of both gases and liquids in what can be best described as a high density vapor phase or a low density liquid phase.

As a substance passes through the critical point, physical properties such as density, dielectric constant, dissociation constant, and viscosity exhibit dramatic changes due to the different environment. The changes in density and dielectric constant influence the solubility characteristics of these fluids, such that compounds that are insoluble at ambient conditions become miscible in the supercritical phase. Supercritical fluids are widely used in applications that take advantage of these changes in solubility. Since the solubility is dependent on the density, separations are much easier and less costly in supercritical fluids because they can be simply achieved by decreasing the pressure.

Two of the most popularly studied supercritical fluids are carbon dioxide and water. Carbon dioxide has a relatively moderate critical temperature ($T_c$) of 31.1 °C and critical pressure ($P_c$) of 73.8 bar. Extraction is one common application of supercritical $CO_2$ due to its enhanced solubility of many organics and its ease of separation by simply lowering the pressure (McHugh and Krukonis, 1994). Currently, industrial processes employ supercritical $CO_2$ to decaffeinate coffee beans and to extract oils or flavors from materials. Supercritical $CO_2$ has also been

studied as an alternative solvent in which to conduct reactions, such as organic syntheses, enzymatic reactions, and polymerizations (McHugh and Krukonis, 1994).

Water's critical point is at much more extreme conditions than $CO_2$'s critical point. Water has a critical temperature ($T_c$) of 374°C, a critical pressure ($P_c$) of 221 bar, and a critical density ($\rho_c$) of 0.32 g/cm$^3$. Supercritical water has been exploited for its ability to solvate both organics and gases and thus be an excellent medium for organic oxidation. Supercritical water is miscible with organic compounds and gases because the physical properties mimic nonpolar behavior, drastically different than those of ambient liquid water or steam. For example, the changes in water density and dielectric constant with temperature at $P$=250 bar are shown in Figure 1-1 (Haar *et al.*, 1984). At subcritical temperatures, the water density decreases slightly as the temperature increases from ambient temperatures. However, once the fluid passes through water's critical temperature ($T_c$=374 °C), the density decreases sharply to less than 0.2 g/cm$^3$. The supercritical water density is an order of magnitude lower than that of liquid water and is two orders of magnitude higher than typical gas densities (on the order of $10^{-03}$ g/cm$^3$). At SCW densities, gases, such as nitrogen or oxygen, are completely miscible with water.

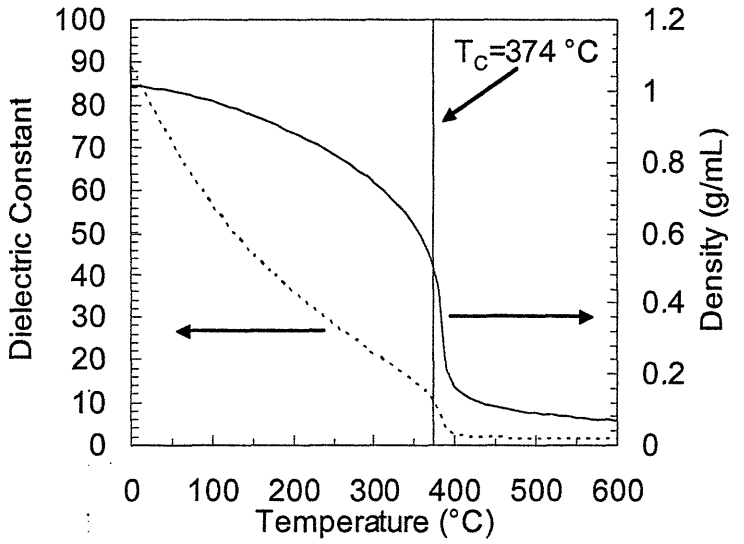


**Figure 1-1: The effect of temperature on water density and dielectric strength at 250 bar from Haar *et al.* (1984)**

The dielectric constant is the measure of a solvent's ability to shield charge or to stabilize a charge separation. At ambient liquid conditions, water is a polar fluid with a high dielectric constant, approximately equal to 80, due to hydrogen bonding and the high density of liquid water. As the temperature increases, the higher solvent energy leads to decreased hydrogen bonding and lower densities. As the intermolecular distance between water molecules increases, there is less solvent shielding and the dielectric constant decreases, as shown in Figure 1-1. At hydrothermal temperatures between 250 and 350°C, water behaves like a moderately polar organic solvent with a dielectric constant between 20 and 30, while at supercritical temperatures greater than 400 °C and pressures above 250 bar, water becomes nonpolar with a dielectric constant of 1 to 2. Due to the sharp decrease in dielectric constant, the solubility of nonpolar, organic compounds in supercritical water increases dramatically.

Solubility behavior in supercritical water is also characterized by the drastic change in the ion-dissociation constant. The ion-dissociation constant, $K_w$, is defined as the product of the

activities of the hydrogen ($H^+$) and hydroxyl ($OH^-$) ions and is a measure of water's ability to solvate ions. Typically at room temperature, the ion-dissociation constant is $10^{-14}$ with the activities of $H^+$ and $OH^-$ each equal to $10^{-07}$. The ion-dissociation constant is shown in Figure 1-2 at 250 bar from correlations by Marshall and Franck (1981) and Bandura and Lvov (2000). The supercritical $K_w$ values for Bandura and Lvov were measured at lower water densities in an effort to more accurately determine the ion-dissociation constant at supercritical conditions for densities less than 0.4 g/mL. As the temperature increases, at a constant pressure of 250 bar, the dissociation constant increases to a maximum value of $10^{-11}$ at $T$=250 °C in the liquid phase and decreases sharply past the critical point. The larger dissociation constant at subcritical temperatures can lead to increased hydrolysis reaction rates, especially for acid and base catalyzed reactions. As the temperature increases further past the critical point, the dissociation constant decreases dramatically to less than $10^{-19}$ where water remains in molecular form and does not readily dissociate. Since ions do not dissociate at these conditions, supercritical water does not support ionic reactions and salts become insoluble.

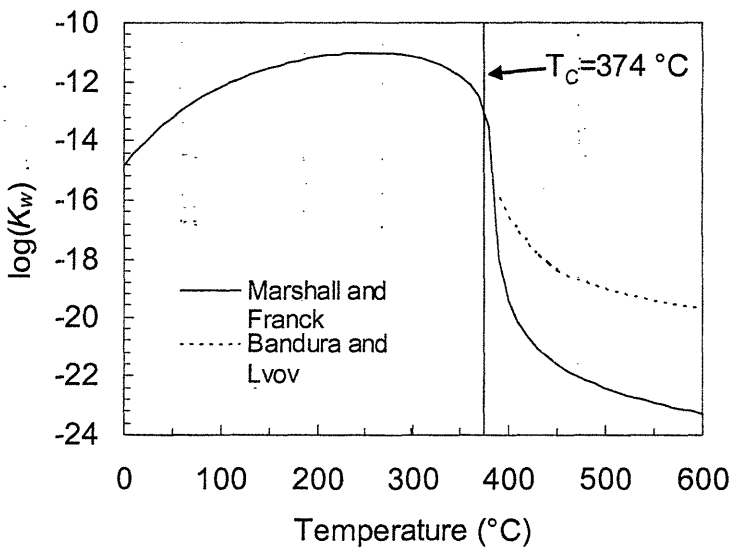


**Figure 1-2: The effect of temperature on the ion-dissociation constant of water, $K_w$, at 250 bar from Marshall and Franck (1981) and Bandura and Lvov (2000)**

With the lower dielectric constant, density, and ion dissociation constant, SCW is an ideal solvent for oxidation of organic compounds. Organic compounds and oxygen are both soluble in SCW, removing mass-transfer limitations. The higher temperatures, along with increased molecular diffusivity and a lower viscosity, lead to increased reaction rates. Reactions proceed primarily via radical pathways, as reactions through ionic pathways decrease significantly due to the much lower ion-dissociation constant. With these attributes of SCW, at typical operating conditions, oxidation proceeds quickly and completely with residence times less than one minute needed to achieve destruction efficiencies greater than 99.99% (Tester *et al.*, 1993a).

### *1.1.2 Supercritical Water Oxidation Applications*

Supercritical water oxidation (SCWO) is often employed as an alternative remediation method to incineration. The reaction kinetics in SCWO are similar to those in incineration since radical reactions dominate. However, due to the lower operating temperatures ($T$<700 °C), reactions can occur by different radical pathways, avoiding the formation of harmful compounds, such as dioxins, which occurs at elevated temperatures. For nitrogen-containing compounds, $NO_x$ compounds are typically formed at incineration temperatures ($T$>1000 °C). At lower SCWO operating temperatures, the reaction channels for $NO_x$ compounds are avoided and the final nitrogen-containing oxidation products are mostly molecular $N_2$ with a small amount of $N_2O$.

In supercritical water, the final oxidation products for C/H/N/O compounds are water, carbon dioxide, and molecular nitrogen. For compounds containing heteroatoms such as chlorine, sulfur, and phosphorus, oxidation also produces the corresponding mineral acids: HCl, $H_2SO_4$, and $H_3PO_4$. Introduction of these acids in SCW can cause corrosion, so these acids are often neutralized to their corresponding salts by addition of a strong base, such as NaOH. Once

formed, the insoluble salts precipitate out of solution and are removed to prevent plugging of the SCWO reactor.

Supercritical water oxidation is most often used for remediation of dilute organic aqueous waste streams that are not suitable for incineration or selective adsorption. Incineration is not a viable economic option for organic aqueous waste streams with concentrations less than 25 wt% due to the amount of energy required to sustain reaction (Tester *et al.*, 1993a). For these more dilute waste streams, SCWO can typically achieve destruction and removal efficiency levels greater than 99.99% with short residence times and a minor energy input due to the lower temperatures. SCWO has also been employed to destroy dangerous compounds, such as chemical warfare agents and propellants (Shaw and Dahmen, 2000). Incineration of these compounds can be problematic because of the possibility of accidental releases of unburned toxic compounds in the stack gas to the environment. SCWO occurs in a completely enclosed process that is not in contact with the outside environment and has been targeted as an incineration alternative for the destruction of these highly toxic compounds.

A brief review of SCWO applications is presented here. More detailed information on SCWO applications can be obtained from the SCWO technology reviews listed below. Earlier reviews of SCWO technology include those written by Freeman (1985), Modell (1989), and Thomason *et al.* (1990). More recently, Tester *et al.* (1993a) reviewed various aspects of SCWO, including its effectiveness for waste treatment, the status of commercial development, process engineering issues, and a summary of relevant research that has been conducted in the field. Gloyna and Li (1995) reviewed the engineering aspects of SCWO. Savage *et al.* (1995) first reviewed reactions in supercritical fluids, then subsequently reviewed organic reactions in SCW (Savage, 1999). Tester and Cline (1999) discussed oxidation kinetics and corrosion in

SCW and further research needs to better understand these processes. Shaw and Dahmen (2000) reviewed the current state of SCWO technology for the destruction of toxic organic materials. Recently, Kritzer and Dinjus (2001) discussed the current major issues in SCWO and provided a review of the current reactor design research.

The ability of SCWO to effectively treat a variety of dilute aqueous organic waste streams, ranging from sewage sludges to pharmaceutical waste streams, has been demonstrated by many studies. Supercritical water oxidation was first employed to destroy polychlorinated biphenyls (PCBs) and DDT without the formation of dioxins by MODAR (Thomason and Modell, 1984). Since then, SCWO has also been shown to effectively treat sewage sludge, including human metabolic waste (Hong *et al.*, 1987, 1988), municipal sludge (Shanableh and Gloyna, 1991), a mixture of municipal sludge and distillery wastewater (Goto *et al.*, 1998), pulp and paper sludge (Modell *et al.*, 1992) and a mixture of primary clarifier sludge with bleach plant effluent (Cooper *et al.*, 1997). Additionally, the first full-scale SCWO sludge processing plant was recently built in Harlingen, TX to process municipal waste (Griffith and Raymond, 2002). Other waste streams that have been treated include pharmaceutical and biopharmaceutical waste (Johnston *et al.*, 1988), dinitrotoluene (DNT) process wastewater (Li *et al.*, 1993), and polymer process effluents (Schmieder and Abeln, 1999).

Supercritical water oxidation has also been targeted by the Departments of Defense and Energy as a destruction method for weapons, chemical warfare agents, explosives, and propellants (Shaw and Dahmen, 2000). SCWO is an attractive treatment method for these dangerous compounds, because the SCWO reactor is fully enclosed so that accidental release to the environment does not occur. SCWO has been demonstrated to effectively treat wastes, such as chemical warfare agents (Spritzer *et al.*, 1995; Snow *et al.*, 1996), propellants (Buelow, 1990),

smokes and dyes (Rice *et al.*, 1994), and explosives (Harradine *et al.*, 1993). SCWO was chosen to be part of the process to destroy the chemical warfare agent, VX, in 1998 (NRC, 1998). Additional discussion on the SCWO process as a destruction method for chemical warfare agents is included in Section 1.2.

### *1.1.3 SCWO Process Description*

Any SCWO process, at laboratory scale or plant scale, contains certain key steps such as pressurization, preheating, salt removal, and heat recovery. An example of a typical SCWO flowchart is shown in Figure 1-3.

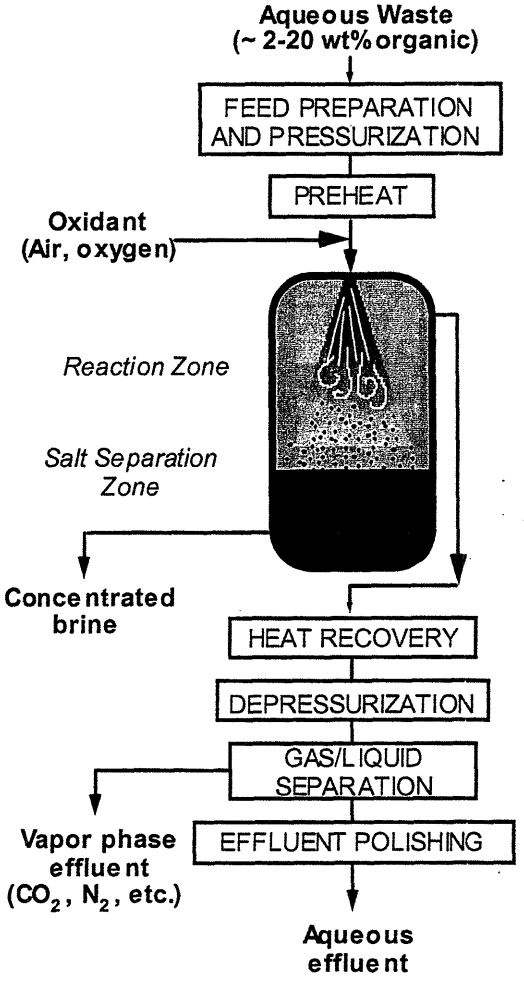


**Figure 1-3: Schematic of a typical SCWO process**

The first step in any SCWO process is pretreatment of the feed stream and pressurization to operating pressures, typically greater than 250 bar. Two feed streams, an organic and an oxidant stream, are fed to the reactor separately. The oxidant feed stream can be compressed air, liquid oxygen, or aqueous hydrogen peroxide that decomposes to form molecular oxygen and water during preheating. The choice of oxidant is usually determined by the scale of the operation and the economic costs. For the organic waste stream, some method of pretreatment may be necessary depending on the concentration and condition of the organic feed stream. For solids-containing waste streams, such as sludges, the solids must be macerated before being pumped to the high operating pressures in an effort to increase the lifetime of high-pressure pumps. The organic concentration in the feed stream determines the amount of heat generated from oxidation that is available to preheat the incoming feed stream once the reactor effluent exits the reactor. To achieve an optimal heating value, the organic waste stream may be diluted or auxiliary fuel may be added before it is fed to the reactor. If the feed stream contains heteroatoms, such as P, S, or Cl, a caustic may be added to the feed stream to neutralize any acid that may be formed and prevent corrosion.

After the feed is pressurized to the system operating pressure, it is preheated to 300 to 400 °C before entering the reactor by heat transfer from the reactor effluent by countercurrent heat exchange. The oxidant feed stream is usually also preheated before it mixes with the organic stream. When the oxidant and organic feed streams are mixed, heat generated from the exothermic oxidation reaction can increase reactor temperatures to between 550 and 650°C. At these conditions, complete destruction of most organics occurs very rapidly.

To prevent salt deposition and plugging, the SCWO reactor is typically equipped with a salt separation method. When salts are formed from the oxidation of heteroatom containing

waste compounds, they fall out of solution since they are insoluble in the SCWO reactor. Many different reactor designs have been studied to prevent the precipitated salts from accumulating on the reactor walls and eventually plugging the reactor as reviewed in two recent articles (Hodes *et al.*, 2003; Marrone *et al.*, 2003). Most of these reactor designs involve a cooler water stream where precipitated salts can dissolve. For example, in the process in Figure 1-3, a temperature gradient across the tank reactor is employed so that the salts precipitate into the cooler water to form a concentrated brine.

Once the reactor effluent exits the reactor, it is quenched by contact with the inlet feed stream. The cooled effluent is then depressurized to a two-phase gas and liquid waste stream, which is separated using a gas-liquid separator. The vapor phase contains unreacted oxygen, carbon dioxide, and nitrogen (if air was used or if N-heteroatoms are present), which can all be released to the atmosphere. The aqueous effluent often contains small amounts of dissolved metals that can be removed to sufficiently low levels for discharge or use as potable water using effluent polishing methods, such as ion exchange (Tester *et al.*, 1993a).

In spite of the advantages of SCWO treatment, there are some problems/drawbacks with this process that have prevented SCWO from widespread application. Three problems are highlighted in the recent review article by Kritzer and Dinjus (2001): corrosion of the reactor system, salt deposition and plugging, and lack of experimental data for reliable cost evaluation for scale-up. Another problem that has precluded SCWO from reaching a larger industrial scale is the capital investment required. Critical reactor materials are high nickel alloys, which are much more expensive than stainless steel. The high-pressure pumps required for this process can be very expensive, especially if a solids-containing stream, like sludges, is introduced.

Corrosion occurs when high concentrations of halogen, sulfur and phosphorus-containing organics are heated to SCW temperatures. Corrosion has been a serious problem for chemical warfare agent destruction by SCWO (Shaw and Dahmen, 2000). Many of the large chemical warfare agents undergo hydrolysis in the preheater, producing acids, such as $H_2SO_4$, which dissociate at subcritical temperatures and corrode the preheater tubing. A number of corrosion-resistant materials have been tested in SCWO reactors, including nickel alloys, Inconel and Hastelloy, and titanium. Each material is resistant to certain acids; however, the problem is that no one alloy has been found that can prevent corrosion by all acids (Kritzer and Dinjus, 2001).

Another major issue for SCWO development is the management of salt deposition and plugging in the reactor that was recently reviewed by Marrone *et al.* (2003) and Hodes *et al.* (2003). An alternative method to prevent corrosion in the preheater is to add a caustic to the organic feed stream so that acids, once formed, will react with the caustic and form salts in the preheater, thus preventing corrosion. However, at SCW temperatures, these salts become insoluble and precipitate out of solution in the SCWO reactor. The salts that are formed in supercritical water are sticky in nature and difficult to remove from reactor surfaces. A number of reactor designs have been introduced to prevent salt precipitation and plugging on the walls of the SCWO reactor. These designs include the transpiring wall reactor, the reversible flow tubular reactor, and adsorption/reaction on a fluidized solid phase (Marrone *et al.*, 2003). The transpiring wall reactor contains an inner porous tube through which cooler supercritical or subcritical water flows to form a protective film on the inner wall. Other research has focused on removing the precipitated salts from reactor walls by mechanical methods such as brushing or scraping or by chemical methods such as reactor flushing or using additives. For further

information on salt precipitation and removal, refer to the complete review of the current status of salt precipitation in SCWO technology (Marrone *et al.*, 2003).

### *1.1.4 Previous Basic Kinetic Research in SCWO*

SCWO provides a rich landscape of research needs with a variety of problems to examine, from improving fundamental understanding of chemical and physical phenomena in SCW to engineering design research. Materials and corrosion research has focused on evaluating corrosion-resistant materials and improving fundamental understanding of corrosion mechanisms in SCWO (Kriksunov and MacDonald, 1995; Tester and Cline, 1999; Kritzer *et al.*, 1999; Kritzer *et al.*, 2000; Mitton *et al.*, 2000; Mitton *et al.*, 2001). Salt behavior in SCW has been studied extensively from fundamental studies of phase behavior and nucleation and growth kinetics to alternative reactor design studies (Armellini and Tester, 1991, 1993; Armellini *et al.*, 1994; McGuinness, 1995; Mueggenburg *et al.*, 1995; LaRoche *et al.*, 1997; Tester *et al.*, 1998; Hurst *et al.*, 2002).

Another major SCWO research area is measurement and prediction of SCWO reaction kinetics. SCWO kinetic data and predictive models are necessary for scale-up and reactor design for SCWO processes. In order for SCWO to become practical for the destruction of wastes, better understanding of the kinetics and reaction mechanisms for compounds that would undergo treatment is needed. To this end, research in our group and others has focused on determining SCWO kinetics of model compounds. Some studies have only measured destruction efficiencies, while other studies also determined global kinetic rate expressions and elementary rate mechanisms.

For the past 20 years, our research group at MIT has characterized the hydrolysis, oxidation, and pyrolysis of a variety of model compounds in sub and supercritical water. Model

compounds were chosen either because they were stable intermediates in the oxidation of larger compounds or because they would be present in the feed streams of actual SCWO processes. For each of these compounds, a well-defined set of data was typically obtained by varying temperature, pressure or density, residence time, and organic or oxidant concentrations. In our research group, multi-scale modeling tools are typically employed to gain a better understanding of the reaction mechanism. Macroscopic level models include global rate laws and macroscopic rate constants for major pathways regressed from experimental data. Predictive models have also been developed to determine the elementary reactions by which oxidation occurs. Elementary reaction rate models are adapted from lower pressure and higher temperature combustion conditions to SCW conditions and are then compared to SCWO experimental data. *Ab initio* calculations have also been employed to calculate transition state theory rate constants for individual elementary reactions.

Initial research in our group focused on smaller compounds that would be intermediates in the oxidation scheme of larger molecules. The studied compounds included carbon monoxide (Helling and Tester, 1987; Holgate *et al.*, 1992; Holgate and Tester, 1994a, 1994b), hydrogen (Holgate and Tester, 1993; Holgate and Tester, 1994a, 1994b), methane (Webley and Tester, 1991), methanol (Webley and Tester, 1989; Tester *et al.*, 1993b; Phenix, 1998), and ammonia (Webley *et al.*, 1991; Helling and Tester, 1988). In more recent studies, larger model compounds have also been studied that would be present in real waste streams. Some of these larger compounds underwent significant hydrolysis as well as oxidation, including acetic acid (Meyer *et al.*, 1995), glucose (Holgate *et al.*, 1995), methylene chloride (Marrone *et al.*, 1995; Marrone et al, 1998a; Marrone *et al.*, 1998b; Salvatierra *et al.*, 1999), thiodiglycol (Lachance *et al.*, 1999), and methyl-tert butyl ether (Taylor *et al.*, 2001; 2002). Other large, refractory

compounds that do not have significant hydrolysis rates include benzene (DiNaro *et al.*, 2000a; 2000b) and ethanol (Helling and Tester, 1988; Schanzenbacher *et al.*, 2002). Predictive, elementary reaction rate models were developed for hydrogen, carbon monoxide, methane, and benzene with varying degrees of success (Webley and Tester, 1991; Holgate *et al.*, 1994b; DiNaro *et al.*, 2000b).

First-order rate constants for oxidation (Figure 1-4) and hydrolysis (Figure 1-5) of the model compounds studied in our laboratory are shown below. From Figure 1-4, most of the compounds undergo significant oxidation on similar time scales between 500 and 600 °C. The alcohols, ethanol and t-butanol, are more labile while methane and ammonia are the most refractory compounds that have been studied in our laboratory. For the hydrolysis rates, shown in Figure 1-5, methylene chloride and MTBE both exhibited a maximum in hydrolysis rate at subcritical temperatures. This non-Arrhenius behavior is due to changes in water's physical properties as it passes through the critical temperature of 374 °C.

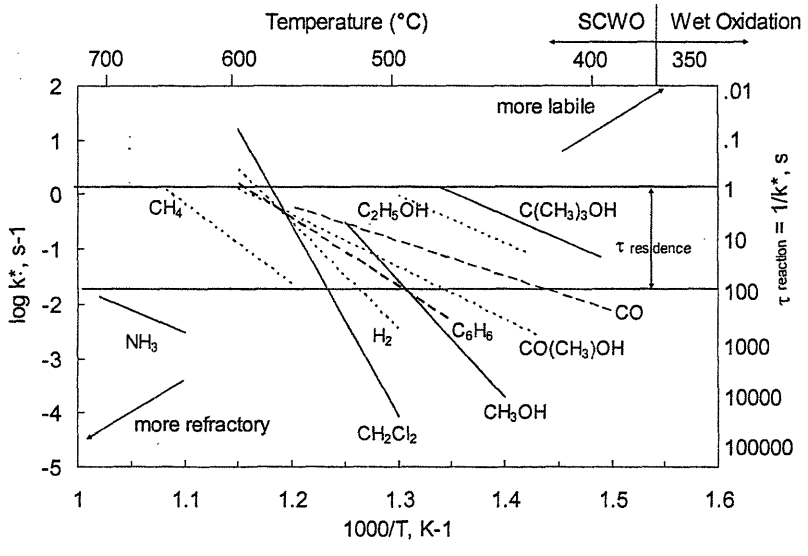


**Figure 1-4: Arrhenius plot of first-order oxidation rates for model compounds studied in our laboratory**

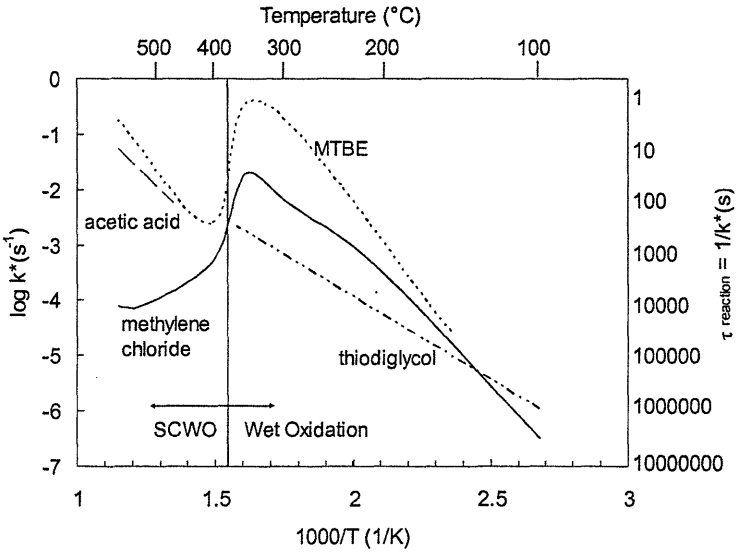


**Figure 1-5: Arrhenius plot of first-order hydrolysis rates for model compounds studied in our laboratory**

Many other research groups have also conducted SCWO kinetic studies. A brief description of work from some of the major contributors is described here. At the University of Michigan, Professor Savage and coworkers have studied the oxidation kinetics of a variety of model compounds. The oxidation kinetics of phenol and substituted phenols were measured both with and without catalysts (Thornton and Savage, 1992a, 1992b; Gopalan and Savage, 1995; Martino and Savage, 1997, 1999a, 1999b; Yu and Savage, 1999, 2000a, 2000b). They have also studied methane and methanol oxidation kinetics and developed elementary reaction rate models for these compounds and their mixtures (Brock and Savage, 1995; Brock *et al.*, 1996, 1998; Savage *et al.*, 1998; Savage *et al.*, 2000). Recent work in this group has focused on determining the effect of water concentration on SCWO reaction rates (Akiya and Savage, 2000a, 2000b; Henrickson and Savage, 2003).

At the University of Texas, Professor Gloyna and coworkers have studied the oxidation kinetics of a variety of waste compounds. Most of these studies focused on high destruction kinetics with excess oxygen to determine the conditions necessary for complete destruction for

reactor design applications. Model compounds that have been examined include phenol (Li *et al.*, 1997), n-octanol (Li *et al.*, 1997), pyridine (Crain *et al.*, 1993), dinitrotoluene (Li *et al.*, 1993), acetamide (Lee and Gloyna, 1992), and acetic acid (Li *et al.*, 1997). This research group has also examined the oxidation kinetics of sludges in depth (Crain *et al.*, 2000; Blaney *et al.*, 1995; Shanableh and Gloyna, 1991). Researchers in this group have also studied the SCWO kinetics of organophosphorus compounds (Turner, 1993; Bianchetta *et al.*, 1999). These studies are summarized in Section 1.2.2 where the previous work on SCWO of organophosphorus compounds is discussed.

At Sandia National Laboratories, a research group led by Steve Rice has conducted many studies utilizing in situ Raman spectroscopy to measure oxidation rates of model compounds and the concentration profiles of their products and reaction intermediates. They have provided insight into reaction kinetics for model compounds such as methane (Steeper *et al.*, 1996), methanol (Rice *et al.*, 1996), isopropyl alcohol (Hunter *et al.*, 1996), and ethanol (Rice and Croiset, 2001). They have also studied the decomposition rate of hydrogen peroxide in supercritical water, which is an important reaction for radical generation in SCWO (Croiset *et al.*, 1997; Croiset and Rice, 1998).

At Los Alamos National Laboratory, Steve Buelow and coworkers have studied the oxidation kinetics of propellants and chlorinated hydrocarbons (Harradine *et al.*, 1993; Foy *et al.*, 1996). This group has also examined using alternative oxidants, such as nitrates, in SCW for compounds, such as ammonia, EDTA, and acetic acid (DellOrco *et al.*, 1995; Proesmans *et al.*, 1997; DellOrco *et al.*, 1997).

While at the University of Delaware, Professor Klein's group studied the oxidation and hydrolysis kinetics of a variety of compounds. Oxidation studies focused on measuring

oxidation rates of alcohols and acetic acids and developing lumped reaction models for these compounds (Boock and Klein, 1993; Iyer *et al.*, 1998). Hydrolysis studies were conducted on a variety of compounds, including nitriles (Izzo *et al.*, 1999; Iyer and Klein, 1997), 1-nitrobutane (Iyer *et al.*, 1996), nitroanilines (Wang *et al.*, 1995), and substituted anisoles (Klein *et al.*, 1992).

The majority of the previous kinetic studies have focused primarily on the oxidation of hydrocarbons or nitrogen-containing compounds in SCW. Few studies have been conducted on SCWO of phosphorus-containing compounds, as is discussed further in Section 1.2.2. The SCWO kinetics of organophosphorus compounds are important for applications, such as the destruction of organophosphorus chemical warfare agents, and further SCWO research on these compounds would be beneficial to the SCWO field.

## 1.2 ORGANOPHOSPHORUS CHEMISTRY

Our study of the oxidation kinetics of organophosphorus compounds was motivated by the U.S. Army's interest in using SCWO as a remediation method for the destruction of organophosphorus nerve agents. In this section, the chemistry of organophosphorus nerve agents is discussed as well as the common destruction methods for these compounds to set the stage for our selection of methylphosphonic acid (MPA) as the model compound for this study.

### *1.2.1 Organophosphorus Chemical Warfare Agents*

As mandated by the 1997 Chemical Weapons Convention (CWC), the stockpiles of chemical warfare agents in the U.S., numbering 30,600 tons originally, must be destroyed by 2007 (NRC, 1999). Chemical warfare agents are classified into two groups, organophosphorus nerve agents and blister agents. The organophosphorus nerve agents such as VX, Sarin (GB), and Soman (GD), shown in Figure 1-6, are acetylcholinesterase inhibitors that can cause death

within ten minutes of exposure. The blister agents, such as Lewisite and mustard, blister exposed tissue and can cause respiratory damage.

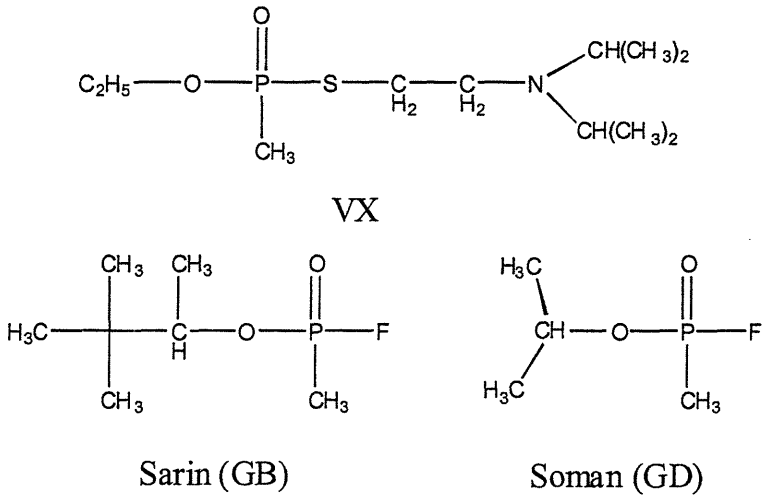


**Figure 1-6: Organophosphorus nerve agents**

Since the 1970's, the primary destruction method for these agents and the assorted contaminated munitions, containers, and packing material has been incineration. Incineration results in complete destruction of these agents; however, there have been increased levels of public disapproval for incineration due to health and safety concerns about possible contaminated emissions from incineration, as well as accidental releases that could occur in handling these warfare agents for treatment (NRC, 1999). Thus, the U.S. Department of Defense, its research laboratories, and industry have focused attention on alternative technologies to detoxify these chemical warfare agents. Universities such as MIT, U. of Texas, and U. of Delaware have provided supporting research for this effort (Shaw and Dahmen, 2000).

One alternative warfare agent destruction method is neutralization followed by post-processing to achieve complete remediation (NRC, 1998). This two-step process is the chosen destruction method for remediation of the bulk agents, mustard gas and VX. Neutralization, using sodium hydroxide, has a destruction efficiency greater than 99.9999% for the warfare

agent, but the effluent contains compounds that must be treated for acceptable disposal (NRC, 1998). For mustard gas, the neutralized effluent is treated by microbial degradation to achieve complete destruction. The destruction method that the U.S. Army has chosen for the VX hydrolysis products is SCWO because it was deemed the most likely to completely mineralize the compounds in the effluent, removing the need for further processing (NRC, 1998). The VX neutralized effluent contains ethylmethylphosphonic acid (EMPA), methylphosphonic acid (MPA), and VX-thiol, as shown in Figure 1-7. According to the CWC, the organophosphorus compounds, EMPA and MPA, qualify as Schedule 2 precursors because they have a P-C bond and could conceivably be used to reproduce the nerve agent. These organophosphorus compounds retain the P-C bond from VX because the P-C bond is inert to acidic and basic hydrolysis (Cordeiro *et al.*, 1986; Schowanek and Verstraete, 1991). To completely destroy these compounds, a post-processing method that occurs through radical mediated pathways should be used, such as SCWO.

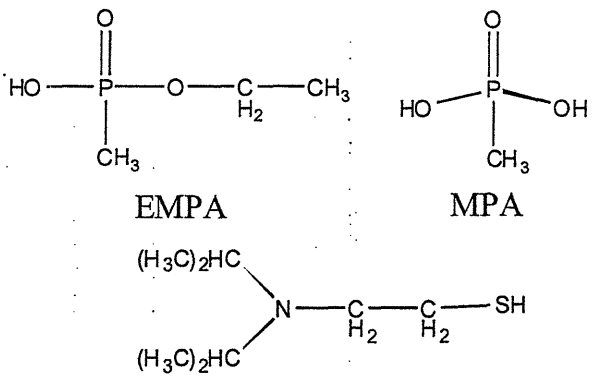


**Figure 1-7: VX neutralization products**

### *1.2.2 Basic Research on Organophosphorus Destruction Kinetics*

Many laboratories have studied destruction kinetics of the organophosphorus nerve agents to assess the effectiveness of different destruction methods. Due to nerve agents' toxicity,

most researchers perform experiments with organophosphorus simulants that retain the important chemistry of the agents without the toxicity. The two most commonly used organophosphorus simulants are dimethyl methylphosphonate (DMMP or $PO(OCH_3)_2CH_3$ ) and diisopropyl methylphosphonate (DIMP or $PO(OC(CH_3)_3)_2CH_3$). These compounds do not contain the fluorine or sulfur groups which contribute to the toxicity of the nerve agents in Figure 1-6, however they do retain the 4-coordinated phosphorus structure of the nerve agent.

The destruction research in three major areas is presented along with how they pertain to SCWO of the VX hydrolysate. Many researchers have studied incineration of chemical warfare agents since this is the primary agent destruction method. These studies are relevant to examine because agent destruction occurs by radical pathways in incineration and these pathways should be similar to those in SCWO. Neutralization studies are discussed because the neutralization products become reactants in the SCWO process. Finally, the few earlier SCWO studies of organophosphorus compounds are reviewed and evaluated.

*Organophosphorus Incineration Research*

Motivated by incineration applications, Professor Fisher's group at Cornell University has studied the gas-phase pyrolysis of the organophosphorus simulants, diethyl methylphosphonate (DEMP) and DIMP in a quartz flow tube reactor (Zegers and Fisher, 1996; Zegers and Fisher, 1998). These studies focused on identification of decomposition products and analysis of the unimolecular decomposition kinetics. DEMP pyrolysis, studied at 529 to 634 °C (802 to 907 K), residence times of 15 to 125 ms, and a pressure of 47 torr (0.063 bar), produced ethylene, ethanol, EMPA, and MPA. The DIMP pyrolysis products were propylene, isopropanol, isopropyl methylphosphonate (IMP), and MPA at 527 to 627 °C (800 to 900 K) and

residence times of 15 to 90 ms. DEMP and DIMP reacted by unimolecular decomposition to form alcohols or alkenes and unimolecular decomposition rates were calculated for both species.

Combustion of the organophosphorus stimulant, DMMP, in oxygen-containing flames has been studied by many researchers (Werner and Cool, 1999; Korobeinichev *et al.*, 1999, 2000, 2001; Glaude *et al.*, 2000; MacDonald *et al.*, 2001; Nogueira and Fisher, 2003). Werner and Cool (1999) measured concentration profiles for DMMP and its intermediates in a $H_2/O_2$ flame using laser-ionization mass spectrometry. From identified intermediates, such as $PO_2OCH_3$, $PO_2CH_3$, and $PO(OH)(CH_3)(OCH_3)$, Werner and Cool inferred possible radical pathways and developed a DMMP kinetic model. This work provided insight into possible reaction pathways for organophosphorus compounds, but the model was unable to predict the concentration profiles for many of the measured intermediates.

At the Institute of Chemical Kinetics and Combustion in Novosibirsk, Russia, Korobeinichev *et al.* reported on the combustion of DMMP and trimethyl phosphate (TMP) in a $H_2/O_2$ flame in a series of articles (Korobeinichev *et al.*, 1999, 2000, 2001). Korobeinichev *et al.* (2000) measured concentration profiles of DMMP and its intermediates and products using molecular-beam mass spectrometry. They identified certain compounds that were not found in Werner and Cool's (1999) study, mainly MPA and phosphoric acid. Korobeinichev *et al.* (2000) adapted Werner and Cool's kinetic model to include reaction rates for MPA and phosphoric acid and modified other reaction rates after model comparison with experimental data to improve predictions. The resulting kinetic model was in good agreement with the experimental concentration profiles for DMMP and the final combustion products.

A modeling study was recently conducted by Glaude *et al.* (2002) to assess the ability of different organophosphorus simulants (DMMP, DIMP, and TMP) to mimic the combustion

kinetics of the nerve agent, sarin. Glaude *et al.* (2002) found that DIMP was the only organophosphorus simulant that predicted similar combustion results to those predicted for sarin combustion. The governing reaction for sarin combustion was a six-center molecular elimination, where a H on the isopropyl group was abstracted by the P=O bond and propene was formed. The other simulants, DMMP and TMP, do not contain the isopropyl group and could not predict reaction through this pathway. Results from this study indicate that organophosphorus reaction pathways need to be better understood for the appropriate choice of simulant compounds. The organophosphorus combustion experiments and models provide insights into possible reaction pathways and intermediates that could be present during SCWO.

*Organophosphorus Neutralization Research*

The purpose of neutralization is to detoxify the warfare agent and to produce an effluent that can be easily treated for complete destruction (Yang, 1999). Neutralization with caustic aqueous solutions was the detoxification method for sarin before incineration became the standard chemical agent destruction method in 1982 (U.S. Congress, 1992). For neutralization processes, kinetic and solubility measurements of the actual nerve agents have been conducted by the U.S. Army research laboratories (Yang *et al.*, 1992; Yang, 1995; Yang, 1999). Using simulants for neutralization studies is not as effective because neutralization rates are strongly affected by solubilities, which differ between the simulants and the actual nerve agents in different solvents. Most of the neutralization research has focused on measuring solubilities and reaction rates and identifying neutralization products in different neutralization solutions, such as aqueous alkali, basic hydrogen peroxide, aqueous bleach, and oxone (Yang, 1995).

Sarin and soman detoxification requires removal of the fluorine group from the nerve agent. The neutralization rates for these compounds are typically fast as these compounds are

soluble in most neutralization solutions and react quickly. VX detoxification rates are typically slower because VX has limited solubility in many of the neutralization solutions and the P-S bond is more difficult to cleave than the P-F bond in sarin and soman. The two primary methods of VX detoxification are nucleophilic substitution with cleavage of the P-S bond and hydrolysis initiated by oxidation at sulfur (Yang, 1999). Neutralization with a sodium hydroxide solution proceeds by nucleophilic substitution at the P-O and P-S bonds on VX. One product, $PO(OH)(OC_2H_5)(CH_3)$, is nontoxic; however, the other product, $PO(OH)(SCH_2CH_2Ni\text{-}Pr_2)(CH_3)$, is a highly toxic thioic acid byproduct (Yang, 1999). To ensure that the thioic acid is converted to a nontoxic byproduct, neutralization is conducted at elevated temperatures in concentrated NaOH solutions. The U.S. Army's chosen method for VX detoxification is nucleophilic substitution in NaOH at elevated temperatures to produce the hydrolysis products that are shown in Figure 1-7. These hydrolysis products are the compounds that would be fed to the SCWO reactor for post-processing.

*Organophosphorus Supercritical Water Oxidation Research*

Two previous experimental studies of organophosphorus oxidation kinetics in SCW have been conducted at the University of Texas (Turner, 1993 and Bianchetta *et al.*, 1999). These studies have examined compounds with similar chemistry to the caustic hydrolysis products, EMPA and MPA, shown in Figure 1-7. Turner (1993) reported that DMMP hydrolyzed quickly and completely to MPA and methanol at temperatures of 300 to 520 °C, a pressure of 276 bar, and residence times of 7 to 57 s in the preheater section of a tubular reactor system. In essence, Turner's experiments measured the co-oxidation kinetics of a mixed MPA and methanol feed stream. Due to the low temperature range studied, MPA conversions were generally less than

50%. A global rate law for MPA and methanol co-oxidation regressed from Turner's data yielded first-order behavior with respect to both MPA and oxygen concentrations.

More recently, Bianchetta *et al.*'s (1999) MPA SCWO study focused on measuring rates at high conversion, with over half of the experiments at conversions greater than 90% to represent more practical treatment applications. The experiments in this study were conducted at temperatures between 400 and 594 °C, residence times between 3 and 83 s, a pressure of 276 bar, and oxygen concentrations at 110 to 200% of stoichiometric amounts. At 550 °C, 276 bar, and 200% stoichiometric oxygen, conversions of greater than 99% were measured at residence times less than 20 s. Reaction pathways were inferred from the analysis of carbon-containing intermediates and products, and a global rate law was regressed from the experimental data. First-order rate constants were also estimated for the major reaction pathways.

The two organophosphorus SCWO studies at the University of Texas have helped to improve our knowledge of SCWO kinetics of organophosphorus compounds. These studies determined that the oxidation kinetics of MPA are pertinent for destruction of most organophosphorus compounds in SCW since MPA is a refractory intermediate in the oxidation and hydrolysis of larger organophosphorus compounds. Bianchetta *et al.* (1999) explored the conditions necessary for complete destruction of MPA with excess oxygen. However, these studies have failed to provide a fundamental, mechanistic understanding of organophosphorus oxidation kinetics in supercritical water, which is important for process development and operation. Our approach to better quantify organophosphorus oxidation kinetics in supercritical water is presented next in Chapter 2.

## 1.3 REFERENCES

Akiya, N. and P. Savage, "Effect of water density on hydrogen peroxide dissociation in supercritical water. 1. Reaction equilibrium." *J. Phys. Chem. A* **104**(19), 4433-4440 (2000a).

Akiya, N. and P. Savage, "Effect of water density on hydrogen peroxide dissociation in supercritical water. 2. Reaction kinetics." *J. Phys. Chem. A* **104**(19), 4441-4448 (2000b).

Armellini, F. J. and J. W. Tester, "Experimental methods for studying salt nucleation and growth from supercritical water." *J. Supercrit. Fluids* **4**(4), 254 (1991).

Armellini, F. J. and J. W. Tester, "Solubility of sodium-chloride and sulfate in subcritical and supercritical water vapor from 450-500 degrees C and 100-250 bar." *Fluid Phase Equilib.* **84**, 123-142 (1993).

Armellini, F. J., J. W. Tester and G. T. Hong, "Precipitation of sodium-chloride and sodium-sulfate in water from sub- to supercritical conditions - 150 to 550-degrees-C, 100 to 300 bar." *J. Supercrit. Fluids* **7**(3), 147-158 (1994).

Bandura, A. V. and S. N. Lvov, "The ionization constants of water over a wide range of temperatures and densities." in *Steam, water, and hydrothermal systems: Physics and chemistry meeting the needs of industry*, P. R. Tremaine, P. G. Hill, D. E. Irish and P. V. Palakrishnan, Eds., NRC Press, Ottawa, (2000).

Bianchetta, S., L. Li and E. F. Gloyna, "Supercritical water oxidation of methylphosphonic acid." *Ind. Eng. Chem. Res.* **38**, 2902-2910 (1999).

Blaney, C., L. Li, E. F. Gloyna and S. U. Hossain, "Supercritical water oxidation of pulp and paper mill sludge as an alternative to incineration." in *Innovations in Supercritical Fluids*, K. W. Hutchenson and N. R. Foster, Eds., ACS Symposium Series, **608**, American Chemical Society, Washington, D.C., 444-455 (1995).

Boock, L. and M. T. Klein, "Lumping strategy for modeling the oxidation of C1-C3 alcohols and acetic-acid in high-temperature water." *Ind. Eng. Chem. Res.* **32**(11), 2464-2473 (1993).

Brock, E. E. and P. E. Savage, "Detailed chemical kinetics model for supercritical water oxidation of $C_1$ compounds and $H_2$." *AIChE J.* **41**(8), 1874-1888 (1995).

Brock, E., Y. Oshima, P. Savage and J. Barker, "Kinetics and mechanism of methanol oxidation in supercritical water." *J. Phys. Chem.* **100**, 15834-15842 (1996).

Brock, E., P. Savage and J. Barker, "A reduced mechanism for methanol oxidation in supercritical water." *Chem. Eng. Sci.* **53**(5), 857-867 (1998).

Buelow, S. J., "Destruction of propellant components in supercritical water." LA-UR-90-1338, Los Alamos National Laboratory, (1990).

Cooper, S. P., H. G. Folster, S. A. Gairns and E. G. Hauptmann, "Treatment of lagoon sludge, primary clarifier sludge, and bleach plant effluent by supercritical water oxidation." *Pulp Pap. Can.* **98**(10), 37-41 (1997).

Cordeiro, J. L., D. L. Pompliano and J. W. Frost, "Degradation and detoxification of organophosphonates: Cleavage of the carbon to phosphorus bond." *J. Am. Chem. Soc.* **108**, 332-334 (1986).

Crain, N., S. Tebbal, L. Li and E. F. Gloyna, "Kinetics and reaction pathways of pyridine oxidation in supercritical water." *Ind. Eng. Chem. Res.* **32**(10), 2259-2268 (1993).

Crain, N., A. Shanableh and E. F. Gloyna, "Supercritical water oxidation of sludges contaminated with toxic organic chemicals." *Water Sci Technol* **42**(7-8), 363-368 (2000).

Croiset, E., S. F. Rice and R. G. Hanush, "Hydrogen peroxide decomposition in supercritical water." *AIChe J.* **43**(9), 2343-2352 (1997).

Croiset, E. and S. F. Rice, "Direct observation of $H_2O_2$ during alcohol oxidation by $O_2$ in supercritical water." *Ind. Eng. Chem. Res.* **37**(5), 1755-1760 (1998).

Dell'Orco, P., B. Foy, E. Wilmanns, L. Le, J. Ely, K. Patterson and S. Buelow, "Hydrothermal oxidation of organic compounds by nitrate and nitrite." in *Innovations in Supercritical Fluids*, K. W. Hutchenson and N. R. Foster, Eds., ACS Symposium Series, **608**, American Chemical Society, Washington, D.C., 179-96 (1995).

Dell'Orco, P. C., E. F. Gloyna and S. J. Buelow, "Reactions of nitrate salts with ammonia in supercritical water." *Ind. Eng. Chem. Res.* **36**(7), 2547-2557 (1997).

DiNaro, J., J. Tester, J. Howard and K. Swallow, "Experimental measurements of benzene oxidation in supercritical water." *AICHE J.* **46**(11), 2274-2284 (2000a).

DiNaro, J., J. Howard, W. Green, J. W. Tester and J. Bozzelli, "Elementary reaction mechanism for benzene oxidation in supercritical water." *J Phys Chem A* **104**(45), 10576-10586 (2000b).

Foy, B. R., K. Waldthausen, M. A. Sedillo and S. J. Buelow, "Hydrothermal processing of chlorinated hydrocarbons in a titanium reactor." *Environ Sci Technol.* **30**(9), 2790-2799 (1996).

Freeman, H., "Supercritical water oxidation." in *Innovative Thermal Hazardous Organic Waste Treatment Processes: Pollution Technology Review No. 125*, Eds., Noyes Publications, Park Ridge, NJ, 25-29 (1985)

Glaude, P. A., H. J. Curran, W. J. Pitz and C. K. Westbrook, "Kinetic study of the combustion of organophosphorus compounds." *Proceedings of the Combustion Institute* **28**, 1749-1756 (2000).

Glaude, P. A., C. Melius, W. J. Pitz and C. K. Westbrook, "Detailed chemical kinetic reaction mechanisms for incineration of organophosphorus and fluoro-organophosphorus compounds." *Proceedings of the Combustion Institute* **29**, 2469-2476 (2002).

Gloyna, E. F. and L. Li, "Supercritical water oxidation research and development update." *Environ. Progress* **14**(3), 182 (1995).

Gopalan, S. and P. E. Savage, "Phenol oxidation in supercritical water: From global kinetics to a detailed mechanistic model." in *Innovations in Supercritical Fluids*, K. W. Hutchenson and N. R. Foster, Eds., ACS Symposium Series, **608**, American Chemical Society, Washington, D.C., 217-231 (1995).

Goto, M., T. Nada, A. Ogata, A. Kodama and T. Hirose, "Supercritical water oxidation for the destruction of municipal excess sludge and alcohol distillery wastewater of molasses." *J. Supercrit. Fluids* **13**(1-3), 277-282 (1998).

Griffith, J. W. and D. H. Raymond, "The first commercial supercritical water oxidation sludge processing plant." *Waste Manage.* **22**(4), 453-459 (2002).

Haar, L., J. S. Gallagher and G. S. Kell, *NBS/NRC Steam Tables*. Hemisphere Publishing Corp., New York (1984).

Harradine, D. M., S. J. Buelow, P. Dell'Orco, R. B. Dyer, B. Foy, J. M. Robinson and J. A. Sanchez, "Oxidation chemistry of energetic materials in supercritical water." *Hazard. Waste Hazard. Mater.* **10**(2), 233-246 (1993).

Helling, R. K. and J. W. Tester, "Oxidation kinetics of carbon monoxide in supercritical water." *Energy Fuels* **1**(5), 417-423 (1987).

Helling, R. K. and J. W. Tester, "Oxidation of simple compounds and mixtures in supercritical water - carbon monoxide, ammonia, and ethanol." *Environ Sci Technol.* **22**(11), 1319-1324 (1988).

Henrikson, J. T. and P. Savage, "Water-density effects on phenol oxidation in supercritical water." *AIChE J.* **49**(3), 718-726 (2003).

Hodes, M., P.A. Marrone, G.T. Hong, K.A. Smith and J. W. Tester, "Salt precipitation and scale control during supercritical water oxidation – part A: Fundamentals and research." *J. Supercrit. Fluids* in press (2003).

Holgate, H. R., P. A. Webley, J. W. Tester and R. K. Helling, "Carbon monoxide oxidation in supercritical water: the effects of heat transfer and the water-gas shift reaction on observed kinetics." *Energy Fuels* **6**(5), 586-597 (1992).

Holgate, H. R. and J. W. Tester, "Fundamental kinetics and mechanisms of hydrogen oxidation in supercritical water." *Combust. Sci. Technol.* **88**(5-6), 369-397 (1993).

Holgate, H. R. and J. W. Tester, "Oxidation of hydrogen and carbon monoxide in sub- and supercritical water: reaction kinetics, pathways, and water-density effects. 1. Experimental results." *J. Phys. Chem.* **98**(3), 800-809 (1994a).

Holgate, H. R. and J. W. Tester, "Oxidation of hydrogen and carbon monoxide in sub- and supercritical water: reaction kinetics, pathways, and water-density effects. 2. Elementary reaction rate modeling." *J. Phys. Chem.* **98**(3), 810-822 (1994b).

Holgate, H. R., J. C. Meyer and J. W. Tester, "Glucose hydrolysis and oxidation in supercritical water." *AICHE J.* **41**(3), 637-648 (1995).

Hong, G. T., P. K. Fowler, W. R. Killilea and K. C. Swallow, "Supercritical water oxidation: Treatment of human waste and system configuration tradeoff study." *Proceedings of 17th Intersociety Conference on Environmental Systems*, Seattle, WA, July 13-15 (1987)

Hong, G. T., W. R. Killilea and T. B. Thomason, "Supercritical water oxidation: Space applications." *ASCE Space '88 Proceedings*, Albuquerque, NM, August 29-31 (1988)

Hunter, T. B., S. F. Rice and R. G. Hanush, "Raman spectroscopic measurement of oxidation in supercritical water .2. Conversion of isopropyl alcohol to acetone." *Ind. Eng. Chem. Res.* **35**(11), 3984-3990 (1996).

Hurst, W. S., M. S. Hodes, W. J. Bowers, V. E. Bean, J. E. Maslar, P. Griffith and K. A. Smith, "Optical flow cell and apparatus for solubility, salt deposition and Raman spectroscopic studies in aqueous solutions near the water critical point." *J. Supercrit. Fluids* **22**(2), 157-166 (2002).

Iyer, S., G. R. Nicol and M. T. Klein, "Hydrothermal reactions of 1-nitrobutane in high-temperature water." *J. Supercrit. Fluids* **9**(1), 26-32 (1996).

Iyer, S. D. and M. T. Klein, "Effect of pressure on the rate of butyronitrile hydrolysis in high-temperature water." *J. Supercrit. Fluids* **10**(3), 191-200 (1997).

Iyer, S., P. Joshi and M. Klein, "Automated model building and modeling of alcohol oxidation in high temperature water." *Environ. Progress* **17**(4), 221-233 (1998).

Izzo, B., M. T. Klein, C. LaMarca and N. C. Scrivner, "Hydrothermal reaction of saturated and unsaturated nitriles: Reactivity and reaction pathway analysis." *Ind. Eng. Chem. Res.* **38**(4), 1183-1191 (1999).

Johnston, J. B., R. E. Hannah, V. L. Cunningham, B. P. Daggy, F. M. Sturm and R. M. Kelly, "Destruction of pharmaceutical and biopharmaceutical wastes by the MODAR supercritical water oxidation process." *Biotechnology* **6**(12), 1423-1427 (1988).

Klein, M. T., Y. G. Mentha and L. A. Torry, "Decoupling substituent and solvent effects during hydrolysis of substituted anisoles in supercritical water." *Ind. Eng. Chem. Res.* **31**(1), 182-187 (1992).

Korobeinichev, O. P., S. B. Ilyin, V. M. Shvartsberg and A. A. Chernov, "The destruction chemistry of organophosphorus compounds in flames - I: Quantitative determination of final phosphorus-containing species in hydrogen-oxygen flames." *Combust. Flame* **118**(4), 718-726 (1999).

Korobeinichev, O. P., S. B. Ilyin, T. A. Boshova, V. M. Shvartsberg and A. A. Chernov, "The chemistry of the destruction of organophosphorus compounds in flames -III: The destruction of DMMP and TMP in a flame of hydrogen and oxygen." *Combust. Flame* **121**(4), 593-609 (2000).

Korobeinichev, O. P., T. A. Bolshova, V. M. Shvartsberg and A. A. Chernov, "Inhibition and promotion of combustion by organophosphorus compounds added to flames of CH4 or H-2 in O-2 and Ar." *Combust. Flame* **125**(1-2), 744-751 (2001).

Kriksunov, L. B. and D. D. Macdonald, "Corrosion in supercritical water oxidation systems: a phenomenological analysis." *J. Electrochem. Soc.* **142**(12), 4069-73 (1995).

Kritzer, P., N. Boukis and E. Dinjus, "Factors controlling corrosion in high-temperature aqueous solutions: a contribution to the dissociation and solubility data influencing corrosion processes." *J. Supercrit. Fluids* **15**(3), 205-227 (1999).

Kritzer, P., N. Boukis and E. Dinjus, "Transpassive dissolution of alloy 625, chromium, nickel, and molybdenum in high-temperature solutions containing hydrochloric acid and oxygen." *Corrosion* **56**(3), 265-272 (2000).

Kritzer, P. and E. Dinjus, "An assessment of supercritical water oxidation (SCWO) - Existing problems, possible solutions and new reactor concepts." *Chem. Eng. J.* **83**(3), 207-214 (2001).

La Roche, H. L., M. Weber and C. Trepp, "Design rules for the wallcooled hydrothermal burner (WHB)." *Chem. Eng. Technol.* **20**(3), 208-211 (1997).

Lachance, R., J. Paschkewitz and J. W. Tester, "Thiodiglycol hydrolysis and oxidation in sub- and supercritical water." *J. Supercrit. Fluids* **16**, 133-147 (1999).

Lee, D. S. and E. F. Gloyna, "Hydrolysis and oxidation of acetamide in supercritical water." *Environ Sci Technol.* **26**(8), 1587-1593 (1992).

Li, L., E. F. Gloyna and J. E. Sawicki, "Treatability of DNT process waste-water by supercritical water oxidation." *Water Environ. Res.* **65**(3), 250-257 (1993).

Li, L., P. Chen and E. F. Gloyna, "Pilot-plant validation of kinetic models for supercritical water oxidation." *Chem. Ox.* **4**, 219 (1997).

Macdonald, M. A., F. C. Gouldin and E. M. Fisher, "Temperature dependence of phosphorus-based flame inhibition." *Combust. Flame* **124**(4), 668-683 (2001).

Marrone, P. A., R. Lachance, J. DiNaro, B. D. Phenix, J. C. Meyer, J. W. Tester and W. A. Peters, "Methylene chloride oxidation and hydrolysis in supercritical water." in *Innovations in Supercritical Fluids*, K. W. Hutchenson and N. R. Foster, Eds., ACS Symposium Series, **608**, American Chemical Society, Washington, D.C., 197-216 (1995).

Marrone, P. A., T. A. Arias, W. A. Peters and J. W. Tester, "Solvation effects on kinetics of methylene chloride reactions in sub and supercritical water: Theory, experiment, and ab initio calculations." *J. Phys. Chem. A.* **102**(35), 7013-7028 (1998a).

Marrone, P. A., P. M. Gschwend, K. C. Swallow, W. A. Peters and J. W. Tester, "Product distribution and reaction pathways for methylene chloride hydrolysis and oxidation under hydrothermal conditions." *J. Supercrit. Fluids* **12**(3), 239-254 (1998b).

Marrone, P.A., M. Hodes, K.A. Smith and J.W. Tester, "Salt precipitation and scale control in supercritical water oxidation – part B: Commercial/ full-scale applications." *J. Supercrit. Fluids* in press (2003).

Marshall, W. L. and E. U. Franck, "Ion product of water substance, 0-1000 °C, 1-10,000 bars. New international formulation and its background." *J. Phys. Chem. Ref. Data* **10**(2), 295 (1981).

Martino, C. J. and P.E. Savage, "Supercritical water oxidation kinetics, products, and pathways for $CH_3$- and CHO- substituted phenols." *Ind. Eng. Chem. Res.* **36**(5), 1391-1400 (1997).

Martino, C. J. and P. Savage, "Supercritical water oxidation kinetics and pathways for ethylphenols, hydroxyacetophenones, and other monosubstituted phenols." *Ind. Eng. Chem. Res.* **38**(5), 1775-1783 (1999a).

Martino, C. J. and P. Savage, "Oxidation and thermolysis of methoxy-, nitro-, and hydroxy-substituted phenols in supercritical water." *Ind. Eng. Chem. Res.* **38**(5), 1784-1791 (1999b).

McGuinness, T. C., "Supercritical water oxidation reactor apparatus and method." US Patent. #5348051 (1995).

McHugh, M. A. and V. J. Krukonis, *Supercritical Fluid Extraction: Principles and Practice.* Butterworth Publishers, Stoneham, MA (1994).

Meyer, J. C., P. A. Marrone and J. W. Tester, "Acetic acid oxidation and hydrolysis in supercritical water." *AIChE J.* **41**(9), 2108-2121 (1995).

Mitton, D. B., J. H. Yoon, J. A. Cline, H. S. Kim, N. Eliaz and R. M. Latanision, "Corrosion behavior of nickel-based alloys in supercritical water oxidation systems." *Ind. Eng. Chem. Res.* **39**(12), 4689-4696 (2000).

Mitton, D. B., N. Eliaz, J. A. Cline and R. M. Latanision, "An overview of the current understanding of corrosion in SCWO systems for the destruction of hazardous waste products." *Mater. Technol.* **16**(1), 44-53 (2001).

Modell, M., "Supercritical water oxidation." in *Standard Handbook of Hazardous Waste Treatment and Disposal*, H. M. Freeman, Ed., McGraw Hill, New York, 8.153-8.168 (1989)

Modell, M., J. Larson and S. F. Sobczynski, "Supercritical water oxidation of pulp mill sludges." *Tappi J.* **75**(6), 195-202 (1992).

Mueggenberg, H. H., D. C. Rousar and M. F. Young, "SCWO reactor with wall conduits for boundary flow control." US Patent. #5387398 (1995).

Nogueira, M. F. and E. M. Fisher, "Effects of dimethyl methylphosphonate on premixed methane flames." *Combust. Flame* **132**(3), 352-363 (2003).

NRC, "Using Supercritical Water Oxidation to Treat Hydrolysate from VX Neutralization." Commission on Engineering and Technical Systems, Washington, D.C., (1998).

NRC, "Review and Evaluation of Alternative Technologies for Demiliarization of Assembled Chemical Weapons." Commission on Engineering and Technical Systems, Washington, D.C., (1999).

Phenix, B., "Hydrothermal oxidation of simple organic compounds." PhD Thesis, Department of Chemical Engineering, Massachusetts Institute of Technology, Cambridge, MA, (1998).

Proesmans, P. I., L. Luan and S. J. Buelow, "Hydrothermal oxidation of organic wastes using ammonium nitrate." *Ind. Eng. Chem. Res.* **36**(5), 1559-1566 (1997).

Rice, S. F., C. A. LaJeunesse, R. G. Hanush, J. D. Aiken and S. C. Johnston, "Supercritical water oxidation of colored smoke, dye, and pyrotechnic compositions." SAND94-8209, Sandia National Laboratory, (1994).

Rice, S. F., T. B. Hunter and Å. C. Rydén, "Raman spectroscopic measurement of oxidation in supercritical water. 1. Conversion of methanol to formaldehyde." *Ind. Eng. Chem. Res.* **35**(7), 2161-2171 (1996).

Rice, S. and E. Croiset, "Oxidation of simple alcohols in supercritical water III. Formation of intermediates from ethanol." *Ind. Eng. Chem. Res.* **40**(1), 86-93 (2001).

Salvatierra, D., J. D. Taylor, P. A. Marrone and J. W. Tester, "Kinetic study of hydrolysis of methylene chloride from 100 to 500 degrees C." *Ind. Eng. Chem. Res.* **38**(11), 4169-4174 (1999).

Savage, P. E., S. Gopalan, T. I. Mizan, C. J. Martino and E. E. Brock, "Reactions at supercritical conditions: Applications and fundamentals." *AIChE J.* **41**(7), 1723-1778 (1995).

Savage, P., J. Yu, N. Stylski and E. Brock, "Kinetics and mechanism of methane oxidation in supercritical water." *J. Supercrit. Fluids* **12**, 141-153 (1998).

Savage, P. E., "Organic chemical reactions in supercritical water." *Chem. Rev.* **99**(2), 603 (1999).

Savage, P., J. Rovira, N. Stylski and C. Martino, "Oxidation kinetics for methane/methanol mixtures in supercritical water." *J. Supercrit. Fluids* **17**, 155-170 (2000).

Schanzenbacher, J., J. D. Taylor and J. W. Tester, "Ethanol oxidation and hydrolysis rates in supercritical water." *J. Supercrit. Fluid* **22**(2), 139-147 (2002).

Schmeider, H. and J. Abeln, "Supercritical water oxidation: State of the art." *Chem Eng Technol.* **22**(11), 903 (1999).

Schowanek, D. and W. Verstraete, "Hydrolysis and free radical mediated degradation of phosphonates." *J. Environ. Qual.* **20**, 769-776 (1991).

Shanableh, A. and E. F. Gloyna, "Supercritical water oxidation - wastewaters and sludges." *Water Sci Technol* **23**(1-3), 389-398 (1991).

Shaw, R. W. and N. Dahmen, "Destruction of toxic organic materials using supercritical water oxidation: Current state of the technology." in *Supercritical Fluids*, E. Kiran, Ed., Kluwer Academic Publishers, Netherlands, (2000)

Snow, R. H., W. Sabato, K. Taylor, G. C. Sresty, K. Downey, D. Hazlebeck and D. Jensen, "Demilitarization of chemical agents by hydrolysis and supercritical water oxidation." *Proceedings of ERDEC Scientific Conference on Chemical and Biological Defense Research*, 359 (1996).

Spritzer, M. H., D. A. Hazlebeck and K. W. Downey, "Supercritical water oxidation of chemical agents and solid propellants." *J. Energ. Mater.* **13**(3&4), 185-212 (1995).

Steeper, R. R., S. F. Rice, I. M. Kennedy and J. D. Aiken, "Kinetics measurements of methane oxidation in supercritical water." *J. Phys. Chem.* **100**(1), 184-9 (1996).

Taylor, J. D., J. I. Steinfeld and J. W. Tester, "Experimental measurement of the rate of methyl tert-butyl ether hydrolysis in sub- and supercritical water." *Ind. Eng. Chem. Res.* **40**(1), 67-74 (2001).

Taylor, J. D., F. A. Pacheco, J. I. Steinfeld and J. W. Tester, "Multiscale reaction pathway analysis of methyl tert-butyl ether hydrolysis under hydrothermal conditions." *Ind. Eng. Chem. Res.* **41**(1), 1-8 (2002).

Tester, J. W., H. R. Holgate, F. J. Armellini, P. A. Webley, W. R. Killilea, G. T. Hong and H. E. Barner, "Supercritical water oxidation technology." in *Emerging Technologies in Hazardous Waste Management*, W. D. Tedder and F. G. Pohland, Eds., ACS Symposium Series, **518**, American Chemical Society, Washington, D.C., 35-76 (1993a).

Tester, J. W., P. A. Webley and H. R. Holgate, "Revised global kinetic measurements of methanol oxidation in supercritical water." *Ind. Eng. Chem. Res.* **32**(1), 236-239 (1993b).

Tester, J. W., P. A. Marrone, M. M. DiPippo, K. Sako, M. T. Reagan, T. A. Arias and W. A. Peters, "Chemical reactions and phase equilibria of model halocarbons and salts in sub- and supercritical water (200-300 bar, 100-600 degrees C)." *J. Supercrit. Fluids* **13**(1-3), 225-240 (1998).

Tester, J. W. and J. A. Cline, "Hydrolysis and oxidation in sub- and supercritical water: Connecting process engineering science to molecular interactions," *Corrosion,* **55**, 1088 (1999).

Thomason, T. B. and M. Modell, "Supercritical water destruction of aqueous wastes." *Hazardous Waste* **1**(1), 453-467 (1984).

Thomason, T. B., G. T. Hong, K. C. Swallow and W. R. Killilea, "The MODAR Supercritical Water Oxidation Process." in *Innovative Hazardous Waste Treatment Technology Series, Volume 1:Thermal Processes*, H. M. Freeman, Eds., Technomic Publishing Co., Lancaster, PA, 31-42 (1990)

Thornton, T. D. and P. Savage, "Phenol oxidation pathways in supercritical water." *Ind. Eng. Chem. Res.* **31**(11), 2451-2456 (1992a).

Thornton, T. D. and P. Savage, "Kinetics of phenol oxidation in supercritical water." *AIChE J* **38**(3), 321-327 (1992b).

Turner, M. D., "Supercritical water oxidation of dimethyl methylphosphonate and thiodiglycol." PhD Thesis, University of Texas at Austin, (1993).

U.S.Congress, Office of Technology Assessment, *Disposal of Chemical Weapons: Alternative Technologies - Background Paper*, OTA-BP-O-95, Washington, DC: U.S. Government Printing Office, (1992).

Wang, X. G., L. U. Gron, M. T. Klein and T. B. Brill, "The influence of high-temperature water on the reaction pathways of nitroanilines." *J. Supercrit. Fluid* **8**(3), 236-249 (1995).

Webley, P. A. and J. W. Tester, "Fundamental kinetics of methanol oxidation in supercritical water." in *Supercritical Fluid Science and Technology*, K. P. Johnston and J. M. L. Penninger, Eds., ACS Symposium Series, **406**, American Chemical Society, Washington, D.C., 259-275 (1989).

Webley, P. A. and J. W. Tester, "Fundamental kinetics of methane oxidation in supercritical water." *Energy and Fuels* **5**, 411-419 (1991).

Webley, P. A., J. W. Tester and H. R. Holgate, "Oxidation kinetics of ammonia and ammonia-methanol mixtures in supercrtical water in the temperature range 530-700°C at 246 bar." *Ind. Eng. Chem. Res.* **30**(8), 1745-1754 (1991).

Werner, J. H. and T. A. Cool, "Kinetic model for the decomposition of DMMP in a hydrogen/oxygen flame." *Combust. Flame* **117**, 78-98 (1999).

Yang, Y. C., J. A. Baker and J. R. Ward, "Decontamination of chemical warfare agents." *Chem. Rev.* **92**(8), 1729-1743 (1992).

Yang, Y.-C., "Chemical reactions for neutralising chemical warfare agents." *Chem. Ind.* **9**, 334-337 (1995).

Yang, Y.-C., "Chemical detoxification of nerve agent VX." *Acc. Chem. Res.* **32**(2), 109-115 (1999).

Yu, J. and P. Savage, "Catalytic oxidation of phenol over $MnO_2$ in supercritical water." *Ind. Eng. Chem. Res.* **38**(10), 3793-3801 (1999).

Yu, J. and P. Savage, "Phenol oxidation over $CuO/Al_2O_3$ in supercritical water." *Appl Catal B-Environ* **28**(3-4), 275-288 (2000a).

Yu, J. and P. Savage, "Kinetics of catalytic supercritical water oxidation of phenol over $TiO_2$." *Environ. Sci. Technol.* **34**(15), 3191-3198 (2000b).

Zegers, E. J. and E. M. Fisher, "Gas-phase pyrolysis of diethyl methylphosphonate." *Comb. Sci. Tech.* **116-117**, 69-89 (1996).

Zegers, E. J. P. and E. M. Fisher, "Gas-phase pyrolysis of diisopropyl methylphosphonate." *Combust. Flame* **115**, 230-240 (1998).

# 2 Objectives and Approach

The purpose of this research is to provide a quantitative mechanistic understanding of organophosphorus oxidation kinetics for model systems in supercritical water. The model organophosphorus compound chosen for this study was methylphosphonic acid (MPA) because it is a key, refractory intermediate in the oxidation of organophosphorus agents. In sub- and supercritical water, larger organophosphorus compounds hydrolyze to form MPA, which is quite refractory with little hydrolysis in supercritical water. The oxidation kinetics of MPA are important for all organophosphorus compounds as MPA oxidation is a rate limiting step in complete destruction of organophosphorus compounds.

Although the oxidation kinetics of MPA in SCW have been previously examined by Bianchetta *et al.* (1999), their work exclusively focused on measuring MPA destruction efficiencies at long residence times in the presence of excess oxygen concentrations. For optimal reactor design and operation, the MPA oxidation mechanism needs to be better understood and the effects of operating variables, such as residence time, oxygen concentration, and water density and concentration, on MPA oxidation rates needs to be determined. Also, development of a predictive model for MPA oxidation kinetics could provide a useful tool for reactor design, not necessarily constrained to the experimental operating range from which it was determined. An MPA elementary reaction mechanism would also provide improved mechanistic understanding of important reaction channels during MPA oxidation.

The approach used to achieve these objectives consisted of four main elements:

1) *Experimentally measure MPA hydrolysis and oxidation rates and product yields to quantify reaction kinetics.* These experiments were conducted on the plug flow reactor that has been used for most of the previous SCWO experiments performed in this

laboratory. The effects of different operating parameters, such as temperature, residence time, fuel equivalence ratio, reactor pressure or water density, and initial MPA concentration, on MPA oxidation rates and product yields were determined by systematic variation of each of these operating variables. We focused on conditions of moderate conversion because these data have less uncertainty and the effects of operating parameters on MPA oxidation rates can be better quantified. Proper identification and measurement of stable carbon-containing and phosphorus-containing intermediates and products was important to deduce the MPA oxidation mechanism in SCW. Experimental methods and results are presented in Chapter 3.

2) *Develop macroscopic models from data regression.* Macroscopic models were regressed from the experimental data to correlate MPA oxidation rates and product yields in supercritical water because they are pertinent for SCWO process design and optimization. An MPA global rate law was developed from nonlinear regression of the MPA oxidation data to estimate the pre-exponential factor, activation energy, and MPA, oxygen, and water dependence on MPA oxidation rates. A macroscopic four-pathway model was also formulated to calculate MPA oxidation rates and carbon yields of methane, carbon monoxide and carbon dioxide at different operating conditions. From nonlinear regression, the pre-exponential factor, activation energy, and oxygen dependence for each global pathway in this macroscopic model was estimated. Development of the multiple pathway global model helps to assess the conditions required for complete conversion all carbon to the final carbon-containing product, $CO_2$. Global and macroscopic modeling results are presented in Section 3.4 of Chapter 3.

3) *Conduct ab initio calculations on organophosphorus combustion chemistry.* Early work on combustion of organophosphorus compounds has provided few MPA reaction pathways and intermediates available for inclusion in an MPA elementary reaction rate model. To develop an MPA elementary reaction rate model, both reliable thermochemistry and reaction rates are needed. Without experimental data, *ab initio* quantum chemical calculations can be used to predict thermochemistry and reaction rates. Thus, the thermochemistry of MPA and its reaction intermediates and transition state theory rate constants for postulated MPA reaction pathways were estimated from *ab initio* calculations. Another part of this *ab initio* study was to assess the accuracy of estimated organophosphorus rate constants in combustion mechanisms to determine how well general rate estimation methods work for organophosphorus reactions. The *ab initio* calculation methods and results are discussed in Chapter 4.

4) *Develop an MPA SCWO elementary reaction rate model.* Since global rate laws can only be reliably used in the operating range from which they were regressed, a more fundamental approach is needed that employs an elementary reaction rate network model to predict MPA oxidation rates over a wide range of conditions. Development of this model would also provide insight into important MPA reaction channels. Typically, specific elementary reactions are taken from combustion models for the same model compound and modified to apply at SCW conditions of higher pressures and lower temperatures. However, since there are only a few MPA elementary reactions in the literature, the MPA SCWO model development focused on hypothesizing possible reaction pathways and estimating reaction rates for these pathways. Predicted MPA oxidation rates and product yields from the model were then compared to the MPA

SCWO experimental data to assess the model accuracy. Additionally, important MPA reaction pathways were identified from rate of production analysis. The development of the MPA elementary reaction model and its predicted results are discussed in Chapter 5.

# 3 Experimental Procedures and Results for MPA Oxidation in Supercritical Water

The primary goal of this experimental study was to characterize the hydrolysis and oxidation kinetics of MPA in SCW. A total of 71 experiments were conducted to systematically explore the effects of temperature, time, oxygen concentration, MPA concentration, and pressure (or water density) on MPA conversion and on its product distribution. Once the data were obtained, a global rate expression was regressed with its dependence on MPA, oxygen, and water concentrations determined. Also, macroscopic reaction rates for major pathways were estimated from the data to determine the relative reaction rates in the MPA oxidation scheme.

## 3.1 Description of the Bench Scale SCWO System

All experiments for this study were conducted on the bench-scale plug flow reactor that was previously modified by Phenix (1998) and DiNaro (1999). No significant modifications of this apparatus were made for the current work. The reactor system, as used for this work, is shown in Figure 3-1. The reactor system consisted of four major sections; the feed preparation and pressurization stage, the preheating system, the reactor stage, and the letdown system and sample collection.

### *3.1.1 Feed Preparation and Pressurization Stage*

This section of the reactor system consisted of the feed tanks, feed solutions, and two HPLC pumps that were required for delivery of the feed solutions to the reactor (Figure 3-1). Organic and oxygen saturators were also available to prepare dissolved solutions of gaseous compounds, such as methane or oxygen, for delivery to the reactor system. However, as the

saturators were not employed for these experiments, they have not been included in the system description. For a description of the oxygen and organic saturators in the reactor system, refer to Holgate (1993).

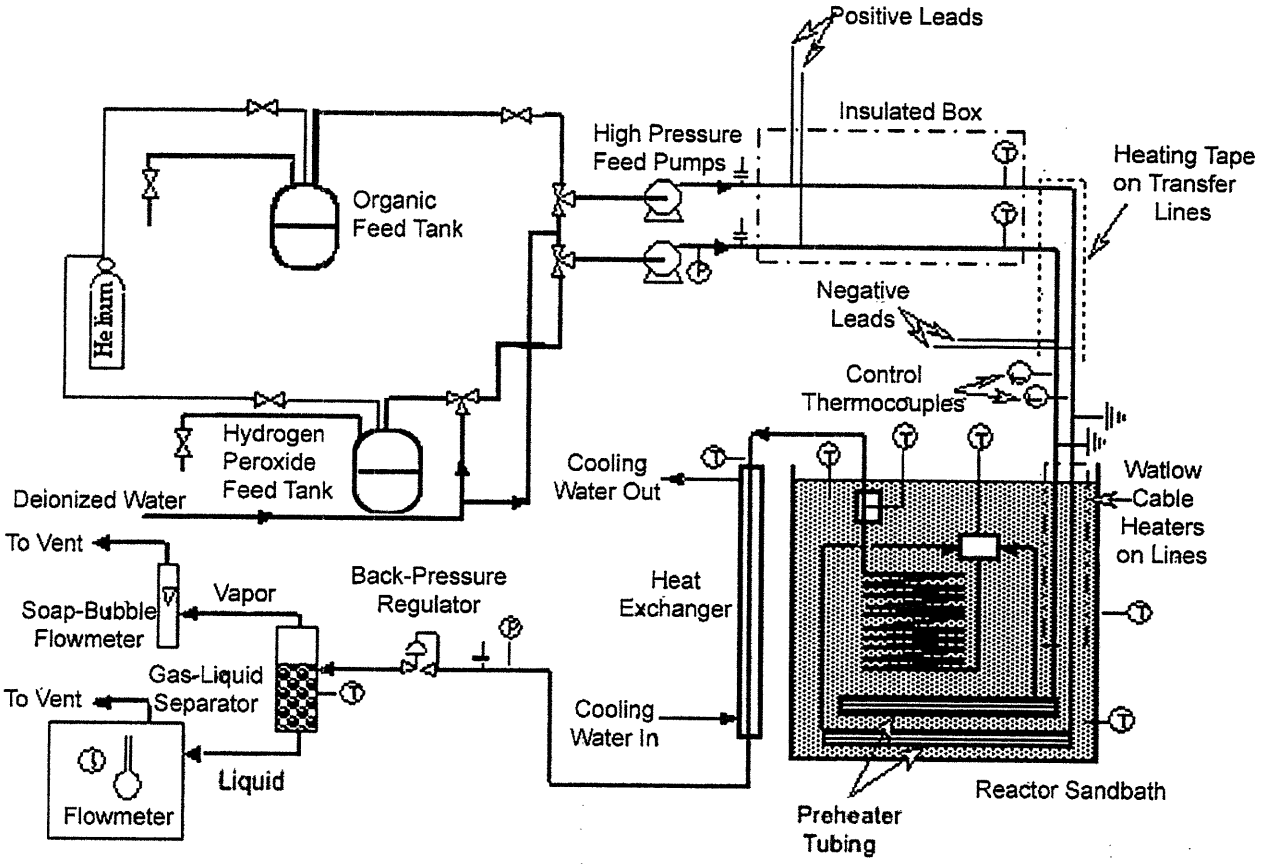


**Figure 3-1: Plug flow reactor system**

The purpose of this section of the reactor system was to prepare aqueous solutions of the organic compound (MPA) and the oxidant (hydrogen peroxide) and to separately pressurize these feeds to the operating reactor pressure by the HPLC pumps. All reactor feed solutions were made from deionized water obtained by delivery of house distilled water to a Barnstead Nanopure-A water purification system. The Barnstead system had four cartridges in the following order: a MACROpure cartridge (p/n D0836) to remove organics and colloids, an

Ultrapure cartridge (p/n K0809) that had a mixed bed resin for cation/anion removal, an ORGANICfree cartridge (p/n D0820) for removal of TOC, and a 0.2 μm filter cartridge (p/n D0749).

The water feed tank was a large reservoir for holding deionized water. This feed tank was degassed with helium to remove all residual oxygen from the water and pressurized with a helium head pressure of 1.7 bar. During heatup and cooldown, pure water was pumped through both of the HPLC pumps to the reactor from this tank. The water feed tank was connected by 340SS tubing to three-way valves that were located before the pumps on both the organic and oxidant feed lines. These valves allowed for the pump feeds to be switched from the organic or oxidant solutions to the water feed tank. During hydrolysis experiments (reaction of the organic in the absence of oxygen), the water feed tank delivered water through the oxidant feed pump throughout the experiment.

All experiments performed in this thesis used the organic feed tank for holding prepared aqueous solutions of MPA. The organic feed tank was a 5 liter plastic-coated glass feed vessel with a conical bottom (Kontes, p/n 953901-5002). To prepare MPA feed solutions, MPA (Aldrich Chem. Co, 98%, p/n 28,986-8) was used as received and the desired mass was measured using an analytical balance (Mettler Toledo, AG240). The MPA was dissolved in deionized water in a volumetric flask and the contents were then transferred to the feed vessel where the solution was magnetically stirred. The feed solution was degassed with helium to ensure that no oxygen was present in the organic feed solution. The tank was then capped and pressurized with 1.7 bar of helium to provide adequate head pressure to deliver the solution to the HPLC organic feed pump via 1/8-in. (3.2-mm) O.D. teflon tubing. Organic feed samples were withdrawn from the feed tank by a sampling line, made of 1/8-in. (3.2-mm) O.D. teflon

tubing, and an on/off valve. A second sampling valve was located on the tubing between the feed tank and the HPLC pump to ensure that the concentrations in the feed tank and the inlet tubing were the same.

Hydrogen peroxide ($H_2O_2$) was used as the oxidant feed for all of the experiments reported in this study. Using $H_2O_2$ allowed for higher reactor oxygen concentrations than were available with pure oxygen saturators. As first reported by Rice at Sandia National Laboratories, $H_2O_2$ can be used as an oxygen source in an SCWO reactor since it decomposes in the preheating section via the following global reaction producing oxygen and water:

$$2\ H_2O_2 \leftrightarrow O_2 + 2\ H_2O \qquad \text{(R1)}$$

Phenix (1998) performed a set of experiments to ensure that complete destruction of $H_2O_2$ to $O_2$ and $H_2O$ occured in the preheater before the oxidant feed stream reached the reactor. Methanol conversions with a saturated oxygen feed and a $H_2O_2$ feed were compared to assess if the $H_2O_2$ had any affect on oxidation kinetics. The experiments showed that the oxidation kinetics were unaffected by the use of $H_2O_2$. Any residual $H_2O_2$ in the feed stream at the reactor inlet could have a dramatic effect on oxidation results because at higher temperatures, $H_2O_2$ decomposes quickly to two OH radicals which could increase the organic oxidation rates.

To prepare the hydrogen peroxide feed solution, a 30 wt% aqueous solution of A.C.S. grade $H_2O_2$ (Aldrich Chemical Co., p/n 21,676-3; VWR, p/n MK524004) was used as received and diluted with deionized water to the desired concentration. The hydrogen peroxide solution was transferred to the hydrogen peroxide feed tank, a 4 liter HDPE reservoir (Dionex, p/n 39164), where the solution was degassed with helium and the headspace was pressurized with 1.7 bar of helium. A teflon tube sampling line with an on/off valve extended from the hydrogen peroxide feed tank to allow for sampling of the feed solution. Once sampled, the concentration

of $H_2O_2$ was verified using the ceric ion titration method described in Section 3.2.1. The reservoir was connected to the HPLC oxidant feed pump using 1/8-in. (3.2-mm) O.D. teflon tubing. Since $H_2O_2$ decomposition is catalyzed by metals, the reservoir, tubing and valves for the hydrogen peroxide feed system before the pump were all made of plastic (HDPE, ETFE, or PTFE) to minimize the breakdown of $H_2O_2$ to form $O_2$ before the pump. The presence of $O_2$ bubbles in the feed could affect the pump's operation.

The organic and oxidant feed streams were pressurized to the reactor pressure, typically 246 bar, and delivered to the system via two independent, digital HPLC pumps (Rainin, SD-200). Each pump had a 25 mL/min pump head which could increment flow at 0.001 mL/min and was rated for operation at 4,600 psig (318 bar) at maximum flow. Each pump also had a pulse-dampening pressure module; so, the total pressure fluctuations measured downstream were only ±2 bar at the normal operation pressure of 246 bar (±0.8%).

The organic, hydrogen peroxide, and water feed tanks needed to be pressurized with sufficient head pressure to ensure the feeds were delivered to the suction-side of the pump faster than the pump drew the solution on the intake stroke of the pump's piston. Without the head pressure, air bubbles could form in the piston chamber and the pump would not deliver the desired flowrate. A Tefzule ferrule (Upchurch, p/n P-300) and an 1/8-in. Delrin nut (Upchurch, p/n P-301) connected the 1/8-in. O.D. teflon tubing from the organic and hydrogen peroxide feed tanks to the pump inlet. Each pump had a pressure transducer which displayed the pressure at the pump's exit. For a secondary measurement of the feed pressure, there was a pressure gauge on the oxidant feed line just after the pump.

Although the HPLC pumps allow the flowrate to be set through the digital interface, it was observed that the actual flowrate was slightly higher than the setpoint when the pumps were

installed in the reactor system. As a result, each pump was calibrated for use in the reactor system. The pump calibration curves calculate the actual flowrate of each pump as a function of the pump setpoint, the total system pressure, and the suction-side pressure. These calibration curves were used to determine the flowrate delivered from the pumps in the design of experiments and for data analysis. The calibrations that were used were the same as those developed by Phenix (1998). The calibration curves were checked periodically and found not to deviate significantly from the measured results.

### *3.1.2 Preheating System*

The preheating system separately heated the pressurized organic and oxidant lines to operating temperature before the two feeds mixed at the reactor entrance. Preheating was extremely important in this reactor system to ensure that the feed streams were at the reactor temperature before they enter the reactor inlet. There were two subsections of the preheating system: the direct ohmic preheating section followed by preheating coils that were located in the heated, fluidized sandbath which housed the reactor. The direct ohmic heating system was added by Phenix (1998) because it provided more accurate temperature control and allowed preheating to higher temperatures than were achievable with the previous preheating apparatus, a preheater sandbath. All heated tubing in the preheater and reactor sections was made of the nickel alloys, Hastelloy 276 or Inconel 625, to prevent against material failure since SCWO is a corrosive environment for stainless steel components. Additionally, all high pressure fittings in the reactor section were constructed of Hastelloy 276.

The direct ohmic heating (DOH) section of the preheater separately heated the aqueous organic and oxidant feeds to reaction temperature using resistive heating. This system was an adaptation of the DOH system used at Los Alamos National Laboratory. Heating was

accomplished by applying a voltage across independent 9.5-m lengths of 1/16-in. (1.6-mm) O.D. x 0.01-in. (0.25-mm) wall HC-276 tubing. Given that the resistance of the preheater tubing was 11 Ohms, up to 1300 Watts of power could be generated with application of the full 120 VAC, which was sufficient power to heat the feed streams to reaction temperature. To apply the voltage to the tubing, the positive lead of a 120 VAC line was clamped to the upstream end of each 9.5-m coil, and the negative lead was clamped to the downstream end. A back-up ground was also attached to the tubing immediately after the negative lead to direct the electricity to the ground in the event that contact was lost between the negative lead and the coil.

At the beginning of each DOH preheater and immediately upstream of the contact point of the positive lead there was a short section of high-pressure 1/8-in. (3.2-mm) O.D. x 0.04-in. (1.0-mm) I.D. PEEK tubing followed by a check valve (Nupro, p/n SS-53S4). The PEEK tubing electrically isolated the upstream section of the reactor, and the check valve prevented hot water from flowing back through the PEEK tubing should upstream pressure be lost.

Each 9.5-m coiled tubing section was thermally and electrically insulated using two layers of high-temperature Nextel sleeving (Omega, p/n XC-116 and SXC-316). Electrical insulation was necessary to prevent contact between the organic and oxidant DOH coils and to avoid the short circuiting that would occur if the successive coils of the preheater tubing came into contact. These insulated coils were housed in a 20-cm x 36-cm x 66-cm insulated box made of Kaowool board and fiber bond cement (Lynn Ceramics). Loose, bulk alumina-silicated ceramic fiber (Lynn Ceramics) was packed around the coils and completely filled the box to provide additional insulation. The last approximately 0.5-m of the 9.5-m DOH preheating coils, situated just before the preheaters enter the reactor sandbath, were not located inside the insulated box due to the geometric constraints of the system. To prevent heat loss, these sections

of the preheating lines were traced with Samox heat tape (Thermolyne, p/n BWH102060, 1-in. wide x 6-ft. long, 904 W) and were wrapped with alumina-silicated ceramic fiber. Power to the heat tape was controlled by a Thermolyne Percentage Power Controller (Thermolyne, Type CN45500, 120 VAC, 15 A) with the power setting set to "HI".

Temperature regulation of the DOH system was accomplished by controlling the supplied voltage levels, which were specified by 1/32-in. Type K thermocouples located immediately after the negative leads and the back-up grounds on each preheater line. The thermocouple tips were centered in the flow streams, and their output wass routed to Omega PID temperature controllers (Omega, p/n CN9141A). Zero-voltage-switched, silicon controlled rectifier (SCR) power controllers (Omega, p/n CR71Z-230, 240VAC, 30 A) regulated the percentage of complete sine waves delivered to the preheaters based on the signal from the Omega PID controllers.

Between the DOH heating system and the reactor sandbath, there was a 30-cm section of preheater tubing on each of the feed streams that was actively heated by resistive cable heaters (Watlow, p/n 62H24A6X, 1/16-in. (1.6-mm) O.D. x 2-ft. (61-cm) long, 10 V, 240 W max) which were wrapped around the preheater tubing. The power to the cable heaters was controlled by variable transformers (Powerstat, p/n 3PN117C, 0-120 V, 12 A). The tubing and cable heaters were insulated with Zetex insulating wrap (1-in. wide) and alumina-silicate ceramic fiber to prevent heat loss.

Additional preheater tubing was contained in the fluidized reactor sandbath (Techne, FB-08). Once the organic and oxidant streams entered the sandbath, each stream passed through an additional 5.2 m coiled length of 1/16-in. (1.6-mm) O.D. x 0.01-in. (0.25-mm) wall HC-276

tubing. This additional tubing served to ensure that the feeds entered the reactor inlet at the desired temperature.

### *3.1.3 Reactor System*

Since most of the preheating load was accomplished by the DOH system, the main purpose of the Techne FB-08 fluidized sandbath was to provide an isothermal environment for the reactor. The sandbath operated at temperatures up to 700 °C, and the temperature was controlled by a Eurotherm PID controller which used a Type K thermocouple located in the sand as its sensing element. The sand temperature at the bottom and the top of the sandbath was also measured with 1/16-in. Type K thermocouples located in the sandbath. With proper fluidization, the measured temperatures of the three thermocouples were within 2-3 °C of each other.

Mixing of the organic and oxidant feed streams was accomplished in a specially modified 1/8-in. HC-276 cross from High Pressure Equipment (p/n 60-24HF2). The feed streams entered the cross in a side-entry configuration at an angle of 90° from each other. To increase the rate of mixing of the two feed streams, the internal diameters of the two arms of the cross through which the feed streams entered were reduced from their original 1/16-in. (1.6-mm) I.D. to 0.01-in. (0.25-mm) I.D. by press fitting short lengths of 1/16-in. (1.6-mm) O.D. x 0.01-in. (0.25-mm) I.D. 316SS tubing into those arms. The smaller diameter tubing increased the rate of mixing of the feed streams by increasing their inlet velocities as is discussed in further detail in Phenix (1998). The modification to the mixing tee was done to accelerate the mixing rates that had caused induction times on the order of one to two seconds for previous oxidation data on this apparatus. A 1/16-in. Type K thermocouple was seated in a side port of the cross and its tip extended into the fluid to ensure accurate measurement of the fluid temperature. An HC-276 1/8-in. to 1/4-in.

adapter (High Pressure Equipment, p/n 60-21HF4HM2) occupied the fourth port which connected the 1/4-in. (6.35-mm) O.D. reactor to the mixing cross.

The reactor itself was a 1/4-in. (6.35-mm) O.D. x 0.067-in. (1.7-mm) I.D. 4.71 m coiled length of Inconel 625 tubing with an internal volume of 10.71 $cm^3$. At the end of the reactor, there was another 1/4-in. to 1/8-in. adapter connected to an 1/8-in. HC-276 tee from High Pressure Equipment (p/n 60-23HF2). A second 1/16-in. Type K thermocouple was seated in this tee, and its tip was positioned in the flowstream to allow temperature monitoring at the end of the reactor. The temperature at the reactor entrance and exit were typically within 2 to 3 °C of each other at normal operating temperatures of 450 to 600 °C.

After the reactor outlet tee, a 26-cm length of 1/4-in. (6.35-mm) O.D. x 1/16-in. (1.6-mm) I.D. HC-276 insulated tubing connected the reactor outlet to the heat exchanger outside of the sandbath. This 26-cm section of tubing, referred to as the riser, had an internal volume of 0.51 $cm^3$. The temperature was measured at the end of this riser with a 1/32-in. Type K thermocouple, but it was not monitored in the riser section. Since only a portion of the riser was located in the sand, the riser was non-isothermal as evidenced by a measured temperature drop of 50 to 150°C from the reactor outlet to the end of the riser. It is unknown at what point in the riser reaction stopped and what the volumetric flowrate was in the riser due to the strong relationship between density and temperature at these conditions.

Accurate measurement of the total reactor volume is important for determination of the residence time in the reactor. The total reactor volume included the reactor (10.71 $cm^3$), the fittings (0.28 $cm^3$), and the riser volume (0.51 $cm^3$). As pointed out, reaction probably did not occur in the entire riser volume; however, the non-isothermal riser only accounted for 4% of the total reactor volume. When the volume uncertainty was propagated to the residence time

uncertainty, it resulted in a 2 or 3% uncertainty in the reactor residence time. To calculate the reactor residence time, the volume was assumed to be 11.23 $cm^3$, estimating that reaction took place in approximately half of the riser volume.

### *3.1.4 Letdown System and Sample Collection*

The purpose of this section was to cool and depressurize the reactor effluent to ambient conditions so that the outlet gas and liquid concentrations and flowrates could be measured. After exiting the reactor sandbath, the reactor effluent entered the inner tube of a shell-and-tube heat exchanger and was immediately quenched. The inner tube of the heat exchanger was a 3-m length of 1/4-in. (6.35-mm) O.D. x 0.065-in (1.65-mm) wall HC-276 tubing and the outer wall shell was a 2.4-m length of 1/2-in. (1.3-cm) O.D. x 0.035-in. (0.89-mm) wall copper tubing. The cooling water source was the building cold water supply which was pre-filtered through a 10 μm spiral-wound prefilter cartridge (VWR, p/n 26303-052).

Downstream of the heat exchanger, there was a pressure transducer (Dynisco, Model 832) which measured the system pressure. The pressure read at this transducer was typically the same as that read by the pressure gauge located on the oxidant stream feed line within the accuracy of the two instruments. After the pressure transducer, a spring-loaded, manual backpressure regulator (Tescom, p/n 26-3200) controlled system pressure. Upon passing through the backpressure regulator, the effluent was flashed to atmospheric pressure.

After the backpressure regulator, the effluent became two phases and the resulting vapor and liquid streams were separated in a gas-liquid separator constructed of 20-cm of 1/2-in. (1.3-cm) O.D. 316SS tubing packed with 4-mm borosilicate glass beads. The gas exited the top of the separator and passed through a sampling port and a soap-bubble flowmeter before it was vented to the hood. Gas samples were taken from the sampling port with a gas-tight syringe, and the gas

flowrate was measured using the soap-bubble flowmeter and a stopwatch. The liquid exited the bottom of the separator into a 1/8-in. (3.2-mm) O.D. 316SS liquid sampling line. Liquid samples were collected from this line, and the flowrate was measured using a Class A volumetric flask and a stopwatch.

### *3.1.5 Health and Safety*

There were many potential hazards associated with the operation of this high-pressure, high-temperature reactor system. There risks included: overpressurization of the reactor system, electric shock from the DOH system, inhalation of the alumina from the sandbath, burns from the hot fluid, heated metal or the alumina from the sandbath, and exposure to toxic chemicals. The following procedures were adopted to ensure operator safety.

The risk of overpressurization of the reactor system was minimized in several ways. First, the digital HPLC pumps automatically shut down if the pressure exceeded the maximum pump pressure of 4600 psig (318 bar). There was also a rupture disk (High Pressure Equipment) downstream of the heat exchanger set to burst at 4,500 psig (311 bar) +6%, -3%. Finally, the entire reactor system was housed inside 3/8-in. (0.95-cm) to 1/2-in. (1.3-cm) Lexan mounted on a Unistrut frame to protect the operators should a piece of metal under pressure let go.

The primary safety concerns about the DOH system were the conduction of electricity upstream or downstream of the DOH system which could impair electrical equipment and shock the operator if the conductive metal tubing was touched. The DOH system was electrically isolated from the upstream system by the PEEK tubing, and downstream of the negative lead there was a backup ground which conducted the current to ground if the negative lead lost contact with the tubing. All electrically conducting sections of the DOH system were well insulated to eliminate the possibility of individuals accidentally contacting any electrically

conducting metal tubing. There were three readily accessible locations to cut power to the DOH system at any time, including the main circuit breaker.

The chromatographic grade alumina (VWR, AX0611-1) that was used in the fluidized sandbath is harmful to the lungs when inhaled due to the particulate size. To prevent against inhalation, the fluidized sandbath was located inside a ventilated Lexan box. The sandbath itself had an air reclamation system which recaptured expelled sand, and ventilation of the Lexan box prevented any escaped sand from entering the laboratory. Whenever it was necessary to work on or around the fluidized sandbath, dust masks were worn to prevent sand inhalation.

The temperatures in the heated sections of the system were in excess of 500 °C which could cause severe burns if any heated material were contacted. To prevent against inadvertent burns, all heated sections of the system were located inside Lexan shielding. Additionally, all heated metal was either located in the sandbath or was enclosed in insulation, so the operator could not directly contact hot metal. If any heated section of the reactor did develop a leak, the hot fluid was contained inside both the insulation or sandbath and the Lexan shielding.

Exposure to the organic feed and the liquid and vapor effluent was minimized, and the proper personal protective equipment was worn when feeds and samples had to be handled. The organic feed tank was kept in a hood in a plastic coated, glass vessel. In the event that the feed tank developed a leak, the organic was entirely contained inside this hood. The vapor-phase reactor effluent was vented directly to this same hood, and the liquid sample collection port was enclosed in a ventilated box. This active ventilation system ensured that organic vapors would not be present in the laboratory.

### *3.1.6 Reactor Operation and Data Collection*

To conduct an experiment on this apparatus, the system was first pressurized and heated to the desired temperature and pressure. During this stage, deionized water from the feed tank was fed through the reactor system. Once a steady flowrate, typically 5 mL/min for each pump, had been established, the system was pressurized using the backpressure regulator. Then, the first stage of preheating began by setting the sandbath temperature to the desired temperature and turning on the power controllers for the cable heaters and heat tape. At this point, the cooling water for the heat exchanger was also turned on to cool the reactor effluent. The DOH preheating system was activated a short time later.

While the system was heating, the MPA and $H_2O_2$ feed solutions were prepared. MPA and $H_2O_2$ samples were taken for analysis from the feed vessels before the reactor feed was switched to the organic and oxidant feeds. At the end of the day, an additional set of MPA and $H_2O_2$ samples were analyzed to ensure that the inlet organic and oxidant concentrations did not change over the course of a set of experiments. Once the reactor system reached the desired temperature, the pump flowrates were set to the appropriate flowrate for the set residence time and the pump feeds were switched from the water feed tank to the organic and oxidant feed vessels using the three-way valves on each feed line. Once the organic and oxidant flows had begun, an hour was required to achieve steady state conditions. Typically, two and a half to three hours were needed before data collection could begin.

A typical experiment, where kinetic data were measured at a single pressure, temperature, residence time, and initial organic and oxygen concentration, lasted about one hour. During this hour, at least six liquid and gas flowrate measurements were made. In addition, three to six liquid and gas effluent samples were collected for analysis. Gas samples were taken by inserting

a gas-tight teflon tipped syringe into the septa-sealed sampling port located above the gas/liquid separator and withdrawing a 200 μL sample which was immediately injected onto one of the gas chromatographs. Liquid samples were collected from the liquid sampling line at the bottom of the gas/liquid separator into 2 mL amber autosampler vials capped with PTFE/silicone caps and were later injected onto the ion chromatograph. The pressure was read and recorded from the pressure transducer located just before the back pressure regulator with every flowrate measurement. The temperatures at several different locations were logged to a computer in ten second intervals. After obtaining at least three consistent measurements of the gas-phase concentrations and collecting six liquid samples, that HPLC pump setpoints were changed for the next set of conditions or the reactor was shut down. After the conditions were changed, an additional hour was required to achieve steady state at the new set of conditions. Typically, data at three sets of conditions were collected in one day.

The temperature measurements were recorded by logging thermocouple measurements every ten seconds using HOTMUX software from DCC Corporation. Temperatures were recorded at thermocouples at the end of the DOH preheater system of both the organic and oxidant feeds, in the mixing cross at the reactor inlet, in the tee at the reactor outlet, in the tee at the end of the riser before the heat exchanger, and at the top and bottom of the sandbath. For each set of conditions, the ambient temperature and pressure were also measured to calculate the Henry's law coefficients and to determine the aqueous solubility of the gas phase compounds in the vapor effluent.

## 3.2 Analytical Methods and Analysis

During the course of one experiment, between three and six liquid and vapor samples were collected for analysis. The gas samples were immediately analyzed by gas

chromatography, while the liquid samples were analyzed by ion chromatography. MPA feed samples were first diluted before being analyzed on the ion chromatograph. The $H_2O_2$ feed concentrations were determined by ceric ion titration.

The measured outlet and feed concentrations along with the reactor temperature and pressure, the ambient temperature and pressure, and the vapor and liquid flowrates were then used to calculate the kinetic parameters. The important values to calculate for each experiment were the residence time, the initial reactor concentrations of MPA and $O_2$, the fuel equivalence ratio, the MPA conversion, the apparent first-order rate constant, and the reactor concentrations of intermediate and final products. Additionally, the carbon yields and carbon fractions for all carbon-containing species were calculated and the phosphorus and carbon balances were determined to assess that all reactants and products were correctly accounted for. The confidence intervals for all measured and calculated values were determined and reported at the 99% confidence interval.

### *3.2.1 Product Analysis*

An ion chromatograph was employed to analyze both MPA feed solutions and the liquid-phase effluent concentrations of MPA and phosphoric acid. Since the MPA feed concentrations were typically higher than 2,000 ppm, the feed solution was diluted with deionized water before it was injected on the ion chromatograph. The maximum MPA and phosphoric acid concentration that could be analyzed on this system was approximately 1,200 ppm. Due to dilution by the oxidant stream and conversion in the reactor, the effluent did not typically require dilution before injection on the ion chromatograph.

The ion chromatograph consisted of a Dionex IonPac AS11 anion column (Dionex, p/n 044076) with a Dionex IonPac AG11 guard column (Dionex, p/n 044078), a Rainin HPXL

pump, a Dionex Anion Self-Regenerating Suppressor ASRS-I (Dionex, p/n 053946), a Dionex DS3 Detection Stabilizer (Dionex, p/n 044130), and a Dionex ED40 electrochemical detector (Dionex, p/n 046297) operated in conductivity mode with a 21 mM NaOH eluent at a flowrate of 1 mL/min. During the course of these experiments, the Rainin HPXL pump was replaced with a Dionex IP25 Isocratic pump (Dionex, p/n 054046). All parts of the IP25 pump, including the pump head, are made of PEEK to prevent leaching that could occur when the basic elent contacts the metal parts of the pump.

The eluent was 21 mM NaOH, which has a much higher conductivity than the relative conductivity of the analyzed compounds. Between the column and the detector, the fluid flowed through the Dionex Anion Self-Regenerating Suppressor. This suppressor worked as an electrochemical cell, with the NaOH eluent flowing concurrently between two water chambers with a cation exchange membrane between them. Hydronium ($H^+$) ions were produced at the anode in the water chamber and flowed across the cation membrane to react with the hydroxyl ($OH^-$) anions and form water. After the eluent passed through the suppressor, it mainly consisted of neutral water. The analyte then entered the detector, allowing for detection of the low conductivity species.

Multiple analyses of the MPA feed samples and the effluent samples were made. Four to six diluted MPA feed samples were usually measured in triplicate, while the six liquid effluent samples were measured in duplicate. These results were then used to calculate the average concentrations and standard deviations of the feed and liquid phase effluent concentrations. The ambient concentrations were used to determine the actual reactor concentrations for the data analysis.

To analyze the gas effluent, three separate gas chromatographs were employed. For the light gases, such as hydrogen, oxygen, nitrogen, carbon monoxide, carbon dioxide, and methane, an HP 5890 Series II GC was used with a thermal conductivity detector (TCD) and helium as the carrier gas. To ensure complete separation of the gases, two columns were connected in series with an air actuated switching valve (HP Valving Option 404). The first column was a 5-ft (1.5-m) x 1/8-in. (3.2-mm) 60/80 mesh Carboxen 100 column which separated the carbon containing gases, but did not retain $H_2$, $O_2$, or $N_2$. The second column was an 8-ft (2.4-m) x 1/8-in. (3.2-mm) 60/80 mesh Molsieve 5A column which then separated the $H_2$, $O_2$, and $N_2$ and passed them onto the detector. Carbon monoxide was less retained on the Carboxen column than $CH_4$ or $CO_2$ and also passed through the Molsieve column to the detector. However, to avoid irreversible absorption of $CO_2$ on the Molsieve column, the switching valve reversed the carrier gas flow prior to the $CO_2$ and $CH_4$ reaching the column. $CO_2$ and $CH_4$ then flowed back through the Carboxen column before reaching the detector. The elution order for this GC was $H_2$, $O_2$, $N_2$, CO, $CO_2$, and $CH_4$. The average gas phase concentrations and the corresponding standard deviations of $O_2$, $N_2$, CO, and $CO_2$ for three to six gas phase samples were determined on this instrument.

A second HP 5890 Series II GC with an FID detector used a helium carrier gas to analyze for light hydrocarbons, such as methane. The 200 μL gas sample was injected into a glass wool packed, split/splitless capillary inlet liner (HP, p/n 19251-60540). The column was a bonded Astec PLOT column (Astec Gas Pro, p/n 81103) that can separate hydrocarbons up to C-10. The average gas phase concentration and standard deviation for methane was determined on this GC from three to six gas phase samples.

A third HP 5890 Series II with a TCD detector employed nitrogen as the carrier gas to analyze for helium and hydrogen. Hydrogen could also be detected on the other TCD at higher concentrations, but the nitrogen carrier gas was required for the detection of the low concentrations that are found in the gas phase effluent. This GC also used the 60/80 mesh Carboxen 1000 and 60/80 mesh Molsieve 5A for separation. The average gas phase concentrations of He and $H_2$ were calculated along with their standard deviations with this GC for three to six gas phase samples.

The hydrogen peroxide concentration was measured by ceric ion titration to determine the inlet oxygen concentration to the reactor. For this titration, a $H_2O_2$ sample was titrated with the strong oxidant, tetravalent cerium ion, in the presence of ferroin indicator. Once the $H_2O_2$ was completely oxidized by the cerium ion, the cerium ion then oxidized the indicator, causing the ferroin indicator to change from bright orange to light blue. The amount of cerium ion that was required to change the color of the ferroin indicator was directly proportional to the concentration of $H_2O_2$. The titration was performed using a Hach digital titrator (Hach Co., p/n 16900-01) and Hach hydrogen peroxide reagents (Hach Co., p/n 22928-00). To perform the titration, 30 mL of deionized water and 2 mL of 19.2 N $H_2SO_4$ were magnetically stirred in a 50 mL Erlenmeyer flask on a magnetic stir plate. Then, 500 μL of the $H_2O_2$ feed sample were added to the flask using a Gilson 1000 μL Pipetman pipette along with one drop of ferroin indicator solution. The solution in the flask was then titrated with 0.5 N ceric ion solution with the digital titrator until the solution changed color from orange to blue. The number of digits was read from the digital titrator and was used to calculate the $H_2O_2$ feed concentration from a calibration equation. This measurement was conducted on a sample at the beginning and at the

end of day, in triplicate for each sample. The average $H_2O_2$ concentration and its standard deviation was then determined from these six measurements.

### *3.2.2 Data and Error Analysis*

For each experiment, the reactor temperature and pressure, the ambient temperature and pressure, and the vapor and liquid flowrates were measured and recorded. Additionally, from analytical measurements, the ambient concentrations of MPA and $H_2O_2$ in the feed samples, MPA and phosphoric acid in the liquid phase effluent samples, and $O_2$, $N_2$, CO, $CO_2$, $CH_4$, He, and $H_2$ in the gas-phase effluent samples were measured. From these measurements, the inlet and outlet reactor concentrations and the residence time could be calculated. Once these values were calculated, the kinetic data including conversion, carbon yield, carbon fraction, first-order rate constants, and carbon and phosphorus balances could be determined. Additionally, the uncertainty in all of the calculated values could be calculated. The uncertainties in all measured quantities were determined from the reproducibility error of the instrument and the precision error from multiple measurements of each quantity. The uncertainty in all other reported values was propagated using the differential method.

*Reactor Concentrations*

To calculate the MPA and $O_2$ concentrations in the reactor inlet, the volumetric flowrate of the individual MPA and $O_2$ feed streams ($F_{MPA}$ and $F_{O2}$), the total measured volumetric flowrate ($F_{TOTAL}$), the ambient MPA and $H_2O_2$ feed concentrations ($[MPA]_{0,AMB}$ and $[H_2O_2]_{0,AMB}$), and the ambient and supercritical water densities ($\rho_{AMB}$ and $\rho_{SCW}$) were required. The inlet MPA and $O_2$ reactor concentrations were calculated from Eqs. (3-1) and (3-2) below.

$$[MPA]_{0,SCW} = \frac{[MPA]_{0,AMB} F_{MPA} \rho_{SCW}}{F_{TOTAL} \rho_{AMB}} \tag{3-1}$$

$$[O_2]_{0,SCW} = \frac{[H_2O_2]_{0,AMB} F_{O2} \rho_{SCW}}{2F_{TOTAL} \rho_{AMB}} \quad (3\text{-}2)$$

The volumetric flowrates of the individual streams were not measured in this system; only the total volumetric flowrate was directly measured so that the split between the two feed streams must be estimated. As discussed in Section 3.1.1, the flowrates delivered by the HPLC pumps were typically higher than the pump setpoints and pump calibrations were regressed for the flowrate from each pump. For the analysis, the flowrate of the $O_2$ feed stream ($F_{O2}$) was determined by the $O_2$ pump calibration and the MPA feed flowrate ($F_{MPA}$) was the difference of the measured total volumetric flowrate and the $O_2$ feed flowrate. The steam tables were used to calculate the supercritical water density at the measured reactor temperature and pressure and the ambient water density at the measured ambient temperature and pressure (Haar *et al.*, 1984). The outlet reactor concentrations of the liquid-phase products, MPA and phosphoric acid, were calculated using Eq. (3-3) (shown below for MPA) where $[MPA]_{AMB}$ is the ambient outlet concentration of MPA.

$$[MPA]_{SCW} = \frac{[MPA]_{AMB} \rho_{SCW}}{\rho_{AMB}} \quad (3\text{-}3)$$

To calculate the outlet reactor concentrations for the gas-phase products, the concentrations of the gases in both the vapor and liquid effluent had to be determined. The concentration in the vapor effluent was measured by the gas chromatograph, while the concentration in the liquid effluent was calculated from Henry's Law:

$$y_i \hat{\phi}_i(T,P,y_i)P = x_i H_{i,H_2O}(T,P) \quad (3\text{-}4)$$

In this equation, $y_i$ is the gas-phase mole fraction of component i, $\hat{\phi}_i$ is the gas-phase fugacity coefficient, $P$ is the pressure, $x_i$ is the liquid-phase mole fraction, and $H_{i,H2O}$ is the Henry's Law coefficient. Since the gas/liquid separator was at ambient conditions, the fugacity coefficients

for each component were assumed equal to one. The Henry's Law constants as a function of temperature were taken from the literature for $O_2$ (Benson *et al.*, 1979), CO (Rettich *et al.*, 1982), $H_2$, $N_2$, He, and $CO_2$ (Wilhelm *et al.*, 1977), and methane and ethane (Rettich *et al.*, 1981). The liquid-phase concentrations of most of the gases were small compared to the gas-phase concentrations, except for $CO_2$ which had appreciable aqueous solubility. With the mole fractions of each species in the gas and liquid phase effluent, the concentration of each gas-phase species at the reactor outlet could be calculated, with $CO_2$ as an example in Eq. 3-5.

$$[CO_2]_{SCW} = \frac{\left(x_{CO_2} F_L \rho_{L,AMB} + y_{CO_2} F_V \rho_{V,AMB}\right) \rho_{SCW}}{F_L \rho_{L,AMB}} \tag{3-5}$$

In this equation, the vapor phase density ($\rho_{V,AMB}$) is calculated from the ideal gas equation and $F_L$ and $F_V$ are measured liquid and vapor flowrates.

*Residence Time*

The reactor residence time was calculated by dividing the total reactor volume ($V_{rxtr}$) by the volumetric flowrate at supercritical conditions.

$$\tau = \frac{V_{rxtr} \rho_{SCW}}{F_L \rho_{AMB}} \tag{3-6}$$

As discussed in Section 3.1.3, there is a certain amount of uncertainty in the reactor volume due to reaction that can occur in the non-isothermal riser after the reactor outlet. Additionally, Phenix (1998) determined that induction times can exist for oxidation kinetics because there is a certain finite time required for mixing before reaction can occur. For the reported uncertainty in the residence time, the contributions of the precision errors in the temperatures, pressures, and liquid flow rate along with the uncertainty in the reactor volume were included, but the uncertainty due to mixing times was not included. To avoid increased fractional uncertainty due to the mixing times, a minimum residence time of 2 s was set for this experimental apparatus.

*Kinetic Data*

Once the inlet and outlet reactor concentrations were known, the key reaction parameters could be calculated. The MPA conversion was calculated from the inlet and outlet reactor concentrations.

$$X = \frac{[\mathrm{MPA}]_0 - [\mathrm{MPA}]}{[\mathrm{MPA}]_0} \times 100\% \tag{3-7}$$

The fuel equivalence ratio indicates fuel-lean or fuel-rich conditions in the reactor. It is defined as:

$$\Phi \equiv \frac{\left([\mathrm{MPA}]/[\mathrm{O_2}]\right)_0}{\left([\mathrm{MPA}]/[\mathrm{O_2}]\right)_{stoichiometric}} \tag{3-8}$$

The stoichiometric ratio for MPA:$O_2$ is 1:2 for complete conversion of MPA to $H_3PO_4$, $CO_2$, and $H_2O$. As defined, a value of $\Phi>1$ denotes oxygen-lean conditions and $\Phi<1$ denotes oxygen-rich conditions.

Reaction products are typically reported in terms of carbon fraction or carbon yield:

$$\text{Species } (i) \text{ carbon fraction} \equiv \frac{\text{Moles of carbon in product}(i)}{\text{Total moles of carbon fed}} \equiv \frac{[\text{product}]_i}{[\mathrm{MPA}]_0} \tag{3-9}$$

$$\text{Species } (i) \text{ carbon yield} \equiv \frac{\text{Moles of carbon in product}(i)}{\text{Total moles of carbon reacted}} \equiv \frac{[\text{product}]_i}{[\mathrm{MPA}]_0 - [\mathrm{MPA}]} \tag{3-10}$$

The carbon fraction allows one to determine the fate of all the carbon in the system, while the carbon yield allows for analysis of how operating parameters affect the relative reaction rates of different pathways in MPA oxidation. These are convenient parameters for assessing the fate of reacted carbon.

Carbon and phosphorus balances were calculated for all experiments based on measured inlet MPA concentrations and measured outlet product and MPA concentrations.

$$\text{Carbon balance} \equiv \frac{\text{Moles of carbon in effluent}}{\text{Total moles of carbon fed}} \times 100\% \tag{3-11}$$

$$\text{Phosphorus balance} \equiv \frac{\text{Moles of phosphorus in effluent}}{\text{Total moles of phosphorus fed}} \times 100\% \tag{3-12}$$

The carbon and phosphorus balances are key indicators as to the quality of the data. Carbon and phosphorus balances both typically ranged from 95 to 105%, so that almost all of the carbon and phosphorus fed was accounted for in the vapor and liquid phase products or the unreacted MPA. Experiments with carbon or phosphorus balances that were inconsistent with other data indicate that these data may be incorrect due to problems with the analytical measurements, reactor performance, or undetected products.

Apparent first-order rate constants were also calculated for each experiment to compare the oxidation rates at different conditions. The apparent first-order rate constant ($k^*$) was first order in MPA and zeroth order in water and oxygen:

$$-\frac{d[\text{MPA}]}{dt} = k^*[\text{MPA}] \tag{3-13}$$

$$k^* = -\frac{\ln\left(\frac{[\text{MPA}]}{[\text{MPA}]_0}\right)}{\tau} = -\frac{\ln\left(1 - X/100\right)}{\tau} \tag{3-14}$$

*Uncertainty Analysis*

For the uncertainty analysis, the uncertainty in all measured variables (liquid and vapor flowrates, analytical signals for each species from gas chromatogaphy or ion chromatography measurements, reactor temperature and pressure, and ambient temperature and pressure) had to be determined. Then, using standard propagation of error techniques, the uncertainties in all derived quantities, such as reactor concentrations, residence time, and conversion, could be calculated.

For measured variables, there exist two types of uncertainty: precision error and reproducibility error. The precision error is the error resulting from the variance in the repeated measurements of the same value; for example, the standard deviation of the six flowrate measurements or the twelve IC MPA signals that were measured for each experiment. The second error, reproducibility error, is the inherent error in the measurement device; for example, the thermocouples had a reported uncertainty of 3°C, while the pressure transducer for the reactor had an uncertainty of 7.5 psi (Phenix, 1998). For most measurements, the precision error was much larger than the reproducibility error such that the reproducibility error could be ignored. However, for the temperature and pressure measurements, the reproducibility error and the precision error were of the same order of magnitude, such that both sources of uncertainty had to be accounted for.

Confidence intervals of 99% were used to represent the precision error for the measured variables. These confidence intervals were calculated assuming the error on all experimentally measured values was represented by a student's t-distribution. For example, the confidence interval for the experimentally measured variable, $x$, is calculated by:

$$\overline{x} \pm \frac{s \times t_{1-CL}\left((n_{obs}-1)\text{degrees of freedom}\right)}{\sqrt{n_{obs}}} \tag{3-15}$$

Here, $\overline{x}$ is the sample mean, $s$ is the sample standard deviation, $n_{obs}$ is the number of observations and $t_{1-CL}((n_{obs}\text{-}1)$degrees of freedom) is the t-value at the stated confidence level for the given number of measurements ($n_{obs}$). Using Eq. 3-15, the confidence intervals for all measured variables could be estimated.

To calculate the uncertainty in the reactor temperature and pressure, the reproducibility error was also included in the reported uncertainty. For the temperature measurements, at least 360 temperature measurements were logged by Hotmux for each experiment, leading to a

precision error of approximately 0.1 °C for the temperature measurement. However, the inherent uncertainty of the thermocouple used to measure the temperature was 3°C. Thus, the reported uncertainty for the reactor pressure and temperature was calculated as:

$$\text{Uncertainty}=\sqrt{CI^2+\sigma^2_{reproducibility}} \tag{3-16}$$

In this equation, $CI$ is the confidence interval from the precision error while $\sigma_{reproducibility}$ is the reproducibility error, the reported uncertainty of the instrument.

Once the confidence intervals for all the measured variables were determined, the uncertainties were propagated using differential techniques. For quantities that were calculated via calibrations, such as the oxygen stream volumetric flowrate or the ambient concentrations in the vapor and liquid effluent, the uncertainties in the calibration parameters were also included in the error propagation calculations. The uncertainties in all other parameters, such as conversion or carbon yield, were simply calculated by differential techniques.

## 3.3 Experimental Results

A total of 4 MPA hydrolysis and 67 MPA oxidation experiments were conducted at varying temperatures ($T$), residence times ($\tau$), fuel equivalence ratios ($\Phi$), pressures ($P$) or water densities ($\rho$), and initial MPA concentrations ($[MPA]_0$) (see Table 3-1). The bulk of the data were taken at stoichiometric conditions ($\Phi$=1), $P$=246 bar, and $[MPA]_0$=1 mM in an effort to be consistent with previous experiments in our laboratory. Section 8.1 in the Appendix contains all experimental data for the hydrolysis and oxidation experiments.

**Table 3-1: Experimental variables and ranges for MPA study**

| Experimental Variable | Range |
|---|---|
| Temperature ($T$) | 478 – 572 °C |
| Residence time ($\tau$) | 3.0 – 9.5 s |
| Initial MPA concentration $[MPA]_0$ | 0.5 – 1.0 mM |
| Fuel equivalence ratio ($\Phi$) | 0.55 – 1.97 |
| Pressure ($P$) | 138 – 277 bar |
| Water density ($\rho$) | 41 – 95 kg/m$^3$ |

Carbon and phosphorus balances were calculated for all experiments based on measured inlet MPA concentrations and measured outlet product and MPA concentrations. For the phosphorus balance, phosphoric acid was the only detected phosphorus-containing product and the average phosphorus balance was 101±3% at a 99% confidence interval with a range from 95 to 104 %. The detectable carbon-containing products and intermediates were carbon monoxide, methane, and carbon dioxide, all measured in the gas phase. The carbon balances had an average value of 103±3% with a range of 94 to 109%. The larger range of the carbon balances can most likely be attributed to higher uncertainty in the gas phase measurements of these compounds.

### *3.3.1 Hydrolysis*

To determine the level of hydrolysis that occurred in the preheater and the reactor, a set of experiments was performed at $\tau$=7 s for temperatures between 503 and 571 °C in the absence of any added oxygen (or $H_2O_2$). Experimental conversions varied between 3 and 6% with average errors of 3%, in agreement with the earlier study by Bianchetta *et al.* (1999). As a consequence, any conversion due to hydrolysis was ignored during the analysis of MPA oxidation results.

### *3.3.2 Oxidation*

The effects of temperature and residence time on MPA oxidation rates were determined by a set of 36 experiments at $\Phi$=0.98±0.07, $P$=246±1 bar, and $[MPA]_0$=0.99±0.03 mM (see Table 3-1). As seen in Figure 3-2, MPA conversion was fairly low ($X$<30% at $\tau$=8.9 s) at $T \leq$503 °C and conversion was almost complete ($X$>99%) at $\tau$=7.5 s and $T$=571 °C. To gain more insight into the MPA oxidation mechanism, conditions favoring moderate conversions were sought to better quantify the effects of operating variables on MPA oxidation. Given this goal, $\Phi$ and pressure variation experiments were conducted at $T$=527 and 551 °C where MPA conversions range between 25 and 85%.

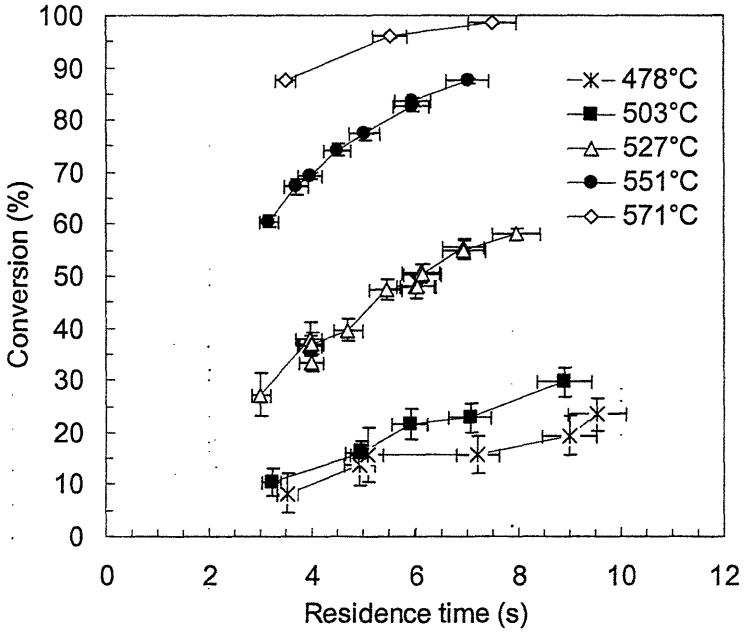


**Figure 3-2: MPA conversion as a function of temperature and residence time**
$\Phi$=0.98±0.07, $[MPA]_0$=0.99±0.03 mM, $P$=246±1 bar

The carbon yields of the intermediates, $CH_4$ and CO, and the final carbon containing product, $CO_2$, are plotted in Figure 3-3 as a function of temperature at $\tau$=5.8±0.4 s. The yields of all carbon-containing products and intermediates should sum to unity assuming mass balance

closure. CO and $CO_2$ were the major MPA oxidation products, while $CH_4$ was a minor product whose yield was always less than 20% at these experimental conditions. In this temperature range, CO was a reactive intermediate whose yield decreased as temperature increased, while $CH_4$ was a refractory intermediate, as its yield increased with temperature. The $CO_2$ yield increased continually over the studied temperature range to a maximum value of almost 0.8 at $T$=571 °C where MPA conversion was 96%.

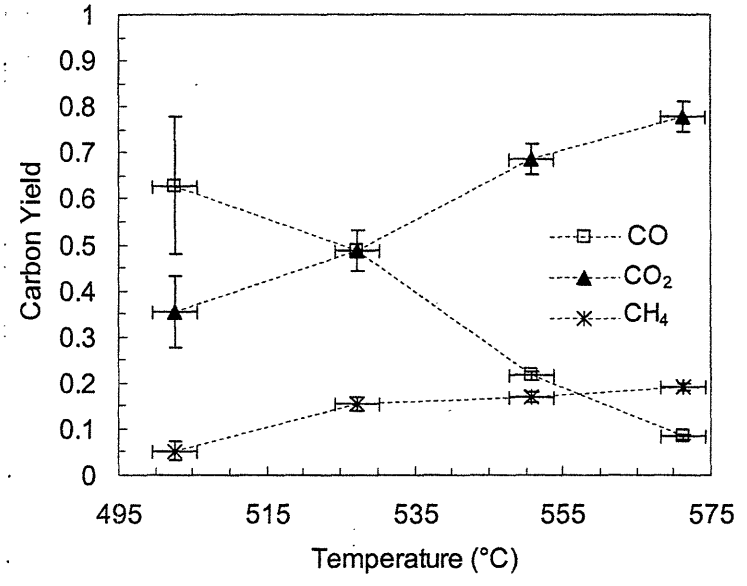


**Figure 3-3: Species carbon yields for the carbon-containing intermediates, CO and $CH_4$, and product, $CO_2$, as a function of temperature**

$\tau$=5.8±0.4 s,$\Phi$=0.98±0.07, $[MPA]_0$=0.99±0.03 mM, $P$=246±1 bar

Since CO is a reactive intermediate in MPA oxidation, MPA and CO oxidation occur on similar reaction time scales. Two previous carbon monoxide oxidation studies have been conducted in our research group (Helling and Tester, 1987; Holgate *et al.*, 1992; Holgate and Tester, 1994a) at similar conditions to the present MPA study ($T$=420 to 571 °C, $\tau$=3.4 to 12.1 s, $P$=118 to 263 bar). CO oxidation rates were comparable to MPA's at these conditions; CO conversion was low ($X$<30%) at $T$=530 °C and $\tau$=5.5 s and high conversions (>90%) occurred at $T$>560 °C and $\tau$=7 s. The relationship between MPA and CO oxidation rates can be seen by

examining the CO carbon fraction at different temperatures and residence times in Figure 3-4. At $T$=503 °C, the CO carbon fraction was relatively low because MPA conversion was low, and it increased with residence time because CO was refractory at this temperature. The CO carbon fraction reached a maximum at $T$=527 °C where MPA conversion was substantial enough to produce a significant amount of CO, but CO oxidation was not yet fast enough to react completely. However, once the temperature reached 571 °C, CO oxidation proceeded rapidly as evidenced by its decreasing fraction with residence time.

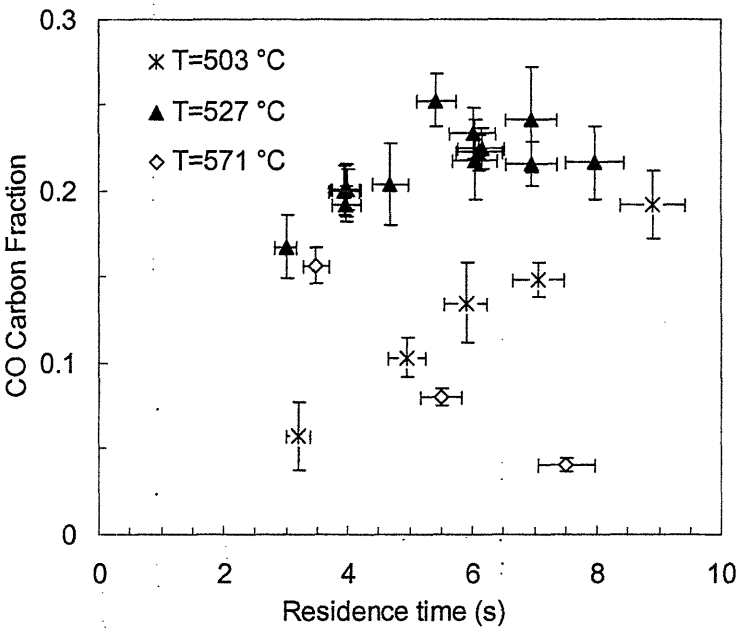


**Figure 3-4: CO carbon fraction as a function of residence time and temperature**
$\Phi$=0.98±0.07, $[MPA]_0$=0.99±0.03 mM, $P$=246±1 bar

The other carbon-containing intermediate, methane, has also been previously studied at SCWO conditions (Webley and Tester, 1991; Savage *et al.*, 1998). As compared to the CO intermediate, $CH_4$ is refractory at the temperature range of the present MPA study. As shown in Figure 3-3, the carbon yield of $CH_4$ increased from 0.05 at 503 °C to 0.19 at 571 °C. Based on previous $CH_4$ oxidation studies, temperatures greater than 600 °C would be required to achieve

appreciable $CH_4$ conversion (>40%) at a residence time of 6 s. Thus, due to the slower $CH_4$ oxidation rates at the temperature range of the MPA study, $CH_4$ accumulation is expected.

Due to the existence of the two intermediates, CO and $CH_4$, Bianchetta *et al.* (1999) hypothesized that two separate pathways for MPA oxidation could exist: a primary reaction pathway through CO ($k_1$) and a minor pathway through $CH_4$ ($k_2$) as illustrated in Figure 3-5. Both of these pathways also form $H_3PO_4$ since it is the only phosphorus-containing product. Once formed, $CH_4$ reacts to CO ($k_4$) and CO is further oxidized to $CO_2$ ($k_3$). Because CO is an intermediate in $CH_4$ oxidation, one could also postulate a different mechanism where MPA reacts by a single pathway from $CH_4$ to CO and then to $CO_2$. However, because the reaction rate of $CH_4$ is not expected to be significant at these temperatures and residence times, the measured concentrations of CO and $CO_2$ cannot result solely from $CH_4$ oxidation and the two pathway mechanism shown in Figure 3-5 is more plausible.

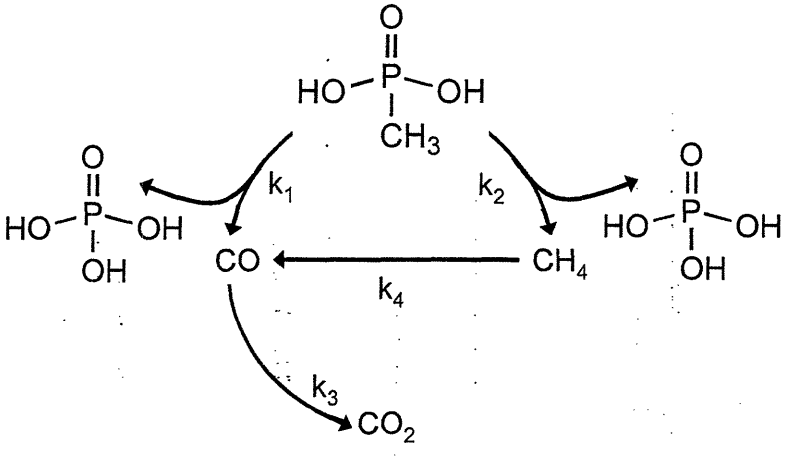


**Figure 3-5: Macroscopic reaction pathway of the fate of carbon and phosphorus in the MPA oxidation system balancing in carbon and phosphorus only**

Note that water and oxygen provide a source for the oxygen and hydrogen necessary to balance stoichiometry. The MPA pathways to form carbon monoxide and methane ($k_1$ and $k_2$ respectively) both form phosphoric acid as the phosphorus-containing product. $CH_4$ oxidizes to CO ($k_4$) and CO reacts with oxygen to form $CO_2$ ($k_3$).

The two-pathway macroscopic mechanism in Figure 3-5 presents a global view for P-C bond cleavage in this system. In an analysis of low pressure combustion mechanisms, only one

MPA bimolecular reaction rate has been estimated (Korobeinichev *et al.*, 2000; Glaude *et al.*, 2000):

$$PO(OH)_2CH_3 + OH^{\bullet} \rightarrow PO(OH)_3 + CH_3^{\bullet} \quad \text{(R2)}$$

In this reaction, an $OH^{\bullet}$ radical adds to the phosphorus center and displaces a $CH_3^{\bullet}$ radical from MPA. This single reaction could possibly account for the two MPA global pathways if the $CH_3$ reacted by two separate pathways to form CO and $CH_4$. However, a preliminary elementary reaction rate model indicates that in SCW at these conditions, the methyl radical primarily reacts with water to form methane with little formation of CO or $CO_2$, unlike experimental results. Given these results, additional P-C bond cleavage pathways for MPA oxidation appear to exist which are explored in more detail in Chapters 4 and 5.

*Effect of Fuel Equivalence Ratio*

To explore the effect of oxygen on MPA conversion and carbon fraction, the fuel equivalence ratio was varied from sub- to superstoichiometric values at temperatures of 503, 527, and 551 °C with $P$=246±1 bar and $[MPA]_0$=1.00±0.03 mM for a set of 13 experiments. The effect of $\Phi$ on carbon fraction at $T$=527±3 °C and $\tau$=6.0±0.4 s is plotted in Figure 3-6 where $\Phi$=0.70 is at 43 % oxygen excess and $\Phi$=2.0 is at 50 % of stoichiometric oxygen. MPA carbon fraction decreased as $\Phi$ decreased (or $[O_2]$ increased), implying that oxygen has a significant role in the formation of radicals in MPA oxidation at SCW conditions.

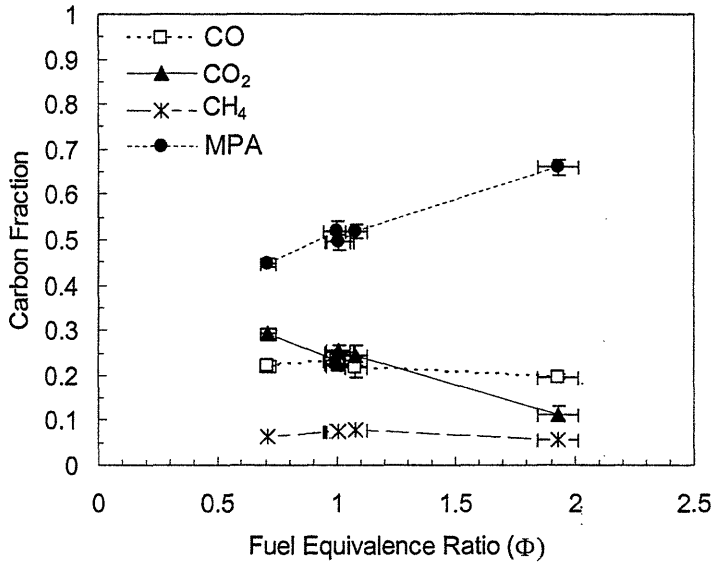


**Figure 3-6: Species carbon fractions as a function of fuel equivalence ratio**
$T$=527±3°C, $\tau$=6.0±0.4 s, $[MPA]_0$=1.00±0.03 mM, $P$=246±1 bar

Carbon dioxide is the only carbon-containing product that was significantly affected by varying Φ at these conditions. The $CO_2$ carbon fraction increased as Φ decreased, while CO and $CH_4$ were generally unaffected by the change in Φ. Similar results were also obtained for the 551°C data. The $CH_4$ carbon fraction's lack of dependence on Φ suggests a non-oxidative formation route for methane from the methyl group of MPA. The oxidation rate of CO to $CO_2$ has an oxygen dependence to the order of 0.3 from previous studies (Holgate *et al.*, 1992; Holgate and Tester, 1994a). Thus, the CO carbon fraction remaining approximately constant as Φ is varied indicates that the rates of CO formation, $k_1[\text{MPA}][O_2]^{b1}$, and CO destruction, $k_3[\text{CO}][O_2]^{b3}$, are approximately in balance and their ratio is essentially independent of oxygen at this residence time. It is somewhat surprising that these reaction rates would exhibit similar oxygen dependence since these macroscopic pathways occur through a series of elementary, radical reactions. Further insight into the relationship between the rates of CO formation and destruction is developed in the major pathways analysis in Section 3.4.2.

*Effect of Pressure (Water Density)*

Previous experimental studies have found that some organic compounds can exhibit a dependence on water density (DiNaro *et al.*, 2000a; Holgate and Tester, 1994a; Koo *et al.*, 1997). Unfortunately, at SCW conditions, the effects of pressure and water density are not easily separated since water density is a function of both pressure and temperature. Also, water's role as a solvent and/or a reactant in SCWO is not very well understood. Koo *et al.* (1997) attempted to decouple the effects of pressure and water density by adding helium, an inert gas, to adjust the system pressure while keeping the water density constant. They demonstrated that a reported increase in phenol conversion was due to an increase in water density. Additionally, analysis of elementary reaction rate models for SCWO indicated that the increase in water density or concentration, rather than the pressure, most likely caused the increase in conversion found experimentally for CO and benzene (Holgate and Tester, 1994b; DiNaro *et al.*, 2000b).

For the present set of experiments, pressures were varied from a subcritical pressure of 138 bar to a supercritical pressure of 277 bar at $T$=527 and 551 °C, $\Phi$=1.01±0.05 and $[MPA]_0$=1.00±0.03 mM for a set of 15 experiments. As shown in Figure 3-7, MPA conversion approximately doubled over the water density range of 41 to 94 kg/m$^3$ at $T$=527 °C. The 551 °C data also showed a strong dependence of MPA conversion on the water density; for example, at $\tau$=5 s, MPA conversion increased from 64±2% at $\rho$=51 kg/m$^3$ ($P$=173 bar) to 77±1% at $\rho$=76 kg/m$^3$ ($P$=246 bar).

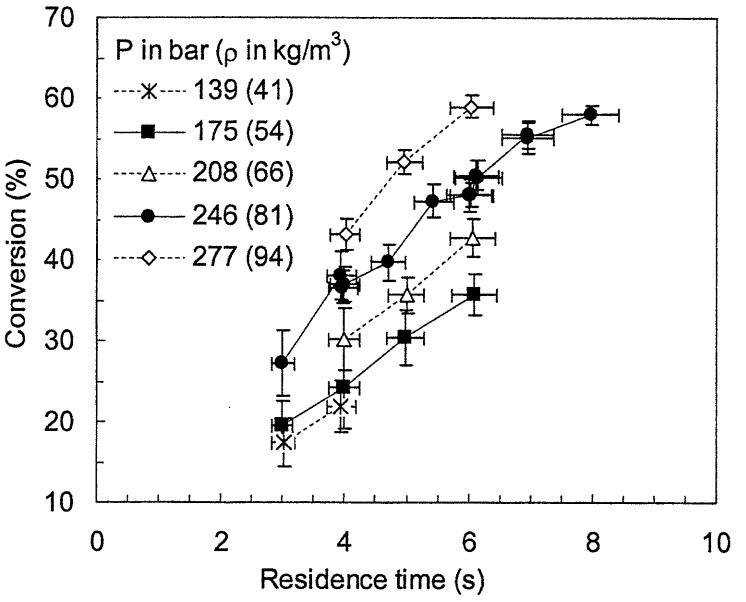


**Figure 3-7: MPA conversion as a function of pressure (water density) and residence time**
$T$=527±3°C, Φ=1.01±0.05, $[MPA]_0$=1.00±0.03 mM

The carbon fractions for the pressure variation experiments at τ=6 s are shown in Figure 3-8. As the MPA conversion increased with increasing water density, the $CO_2$ carbon fraction increased substantially while the $CH_4$ carbon fraction was relatively constant over the water density range. The CO carbon fraction did increase with increasing water density at the lower water densities where the MPA conversion was slow; however, at higher densities and MPA conversions, the CO carbon fraction was approximately constant. Earlier studies of CO oxidation by our group indicated a marked dependence on water density or pressure (Holgate et al, 1994a). Due to the complex role that water plays as a three-body collider and reactant in the free radical dominated networks, it is difficult to explain exactly how water influences MPA oxidation in SCW. Water's role during MPA oxidation in SCW is further explored in the MPA elementary reaction rate model in Chapter 5.

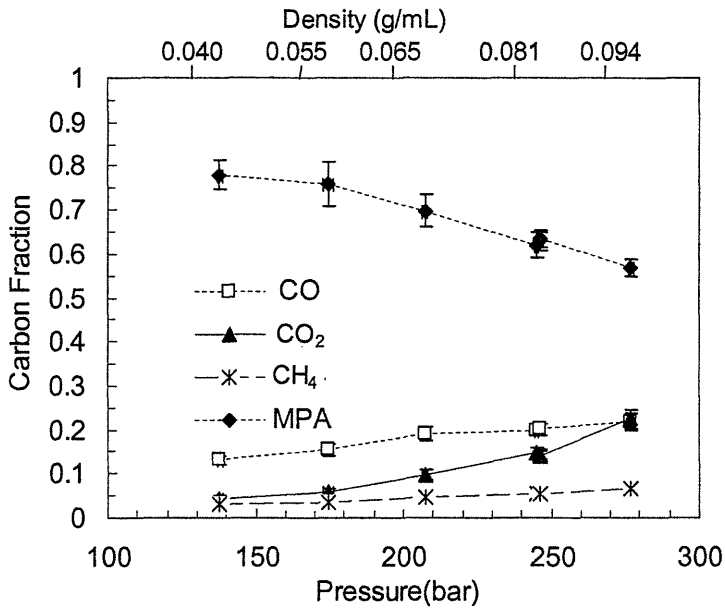


**Figure 3-8: Carbon fraction as a function of pressure (or water density)**
$\tau$=6.1±0.4 s, $T$=527±3°C, $\Phi$=1.01±0.05, $[MPA]_0$=1.00±0.03 mM

*Effect of Initial MPA Concentration*

The final set of experiments was conducted at $\Phi$=1.00±0.06, $P$=246±1 bar, and $T$=527±3°C at $[MPA]_0$=0.5 and 1.0 mM to determine if MPA oxidation rates were dependent on the initial concentration, $[MPA]_0$. Due to the combination of solubility and detection limits, the MPA feed concentrations could only be studied over a limited range. As shown in Figure 3-9, decreasing $[MPA]_0$ by 50% caused a minimal decrease in MPA conversion. These conversion values were approximately equal within experimental error bounds, indicating that MPA conversion was nearly independent of $[MPA]_0$.

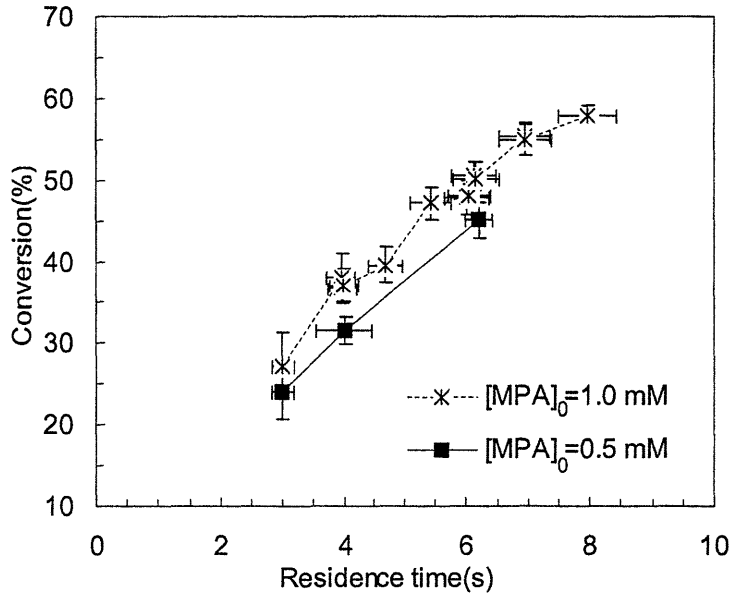


**Figure 3-9: Effect of initial MPA concentration on MPA conversion**
$T$=527±3°C, Φ=1.00±.06, $P$=246±1 bar

A lack of dependence of MPA conversion on initial concentration is consistent with a first-order kinetic behavior. First-order rate constants were calculated from stoichiometric MPA oxidation data at different residence times to determine if they were constant at specified temperatures and pressures ($P$=246 bar). If MPA follows first-order behavior, then a plot of ln(1-conversion) = ln(1-$X$) vs τ, as shown in Figure 3-10, should be linear for each temperature with a slope equal to the apparent first-order rate constant, $-k^*$, as defined in Equations 3-13 and 3-14. The linearity of the data set for each temperature shown in Figure 3-10 verifies first-order dependence, consistent with measured SCWO rates for other organic compounds, including methane and carbon monoxide (Webley and Tester, 1991; Holgate *et al.*, 1992).

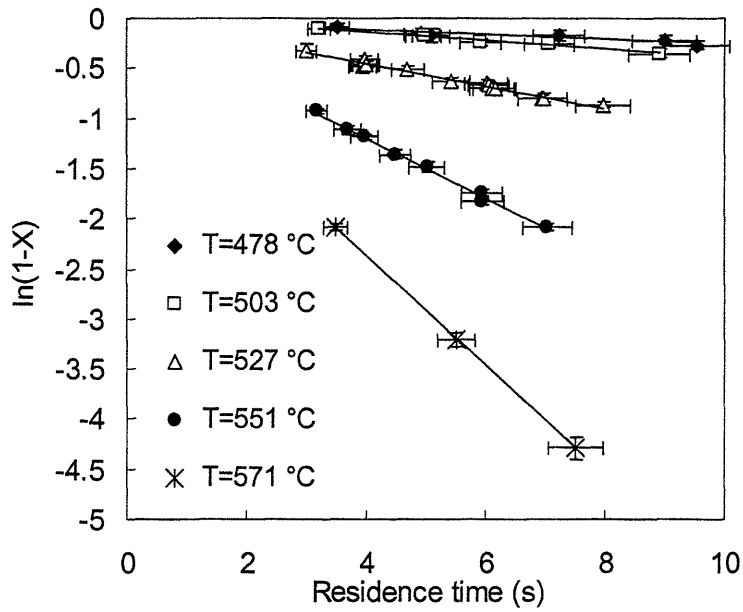


**Figure 3-10: First-order plot of ln(1-*X*) as a function of residence time for five different temperatures**

$\Phi$=0.98±0.07, $[MPA]_0$=0.99±0.03 mM, and $P$=246±1 bar

The slope at each temperature is equal to $-k^*$, the apparent first-order rate constant.

## 3.4 Global Model Regression

The overall goal of the MPA SCWO study was to improve the general understanding of organophosphorus oxidation kinetics using a multi-scale modeling approach from global kinetic correlations to elementary reaction rate models. In this section, the development of an empirical global correlation for the MPA oxidation rate and its dependence on MPA, $O_2$, and $H_2O$ concentrations is presented. Additionally, regression of the macroscopic rate constants in Figure 3-5 is discussed. The estimation of these macroscopic rate constants yields insight into the relative reaction rates of the different pathways in the MPA oxidation system.

### *3.4.1 Global Rate Law*

An empirical global rate law for MPA oxidation was developed as a convenient means for correlating MPA conversion data as a function of $T$, [MPA], $[O_2]$, and $[H_2O]$:

$$-R_{MPA} = -\frac{d[\mathrm{MPA}]}{dt} = A\exp\left(\frac{-E_a}{RT}\right)[\mathrm{MPA}]^a[\mathrm{O_2}]^b[\mathrm{H_2O}]^c \tag{3-17}$$

Here, $A$ is the pre-exponential factor, $E_a$ is the activation energy and $a$, $b$, and $c$ are the reaction orders of MPA, $O_2$, and $H_2O$, respectively. Since the experimental data were measured at varying MPA, $O_2$, and $H_2O$ concentrations, their effects could be quantitatively determined using multiple variable parameter regression. Plug flow behavior in the reactor could be reasonably assumed since all experiments were in the turbulent flow region (Reynolds number >3000). With the plug flow reactor design equation in Eq. 3-18, the global rate law was regressed as:

$$\frac{\tau}{[\mathrm{MPA}]_0} = \int_0^X \frac{dX}{-R_{MPA}} \tag{3-18}$$

In order to integrate Eq. 3-18, the overall rate, $R_{MPA}$, must be expressed in terms of MPA conversion. The water concentration was assumed to be constant and equal to the molar density of pure water at the $T$ and $P$ of each experiment since it is very large and does not change significantly during oxidation. The oxygen concentration was expressed in terms of MPA conversion as:

$$[\mathrm{O_2}] = [\mathrm{MPA}]_0\left(\frac{S}{\Phi} - SX\right) \tag{3-19}$$

where $S$ is the stoichiometric ratio of $O_2$:MPA. If $S$ is set to 2, this is equivalent to assuming complete oxidation of the carbon in MPA to $CO_2$. But, at the conditions studied, MPA also reacted to the intermediates, CO and $CH_4$, which accumulated to finite values, causing $S$ to be less than 2. By comparing measured $O_2$ and MPA conversions, a stoichiometric ratio of 1.3 would be more appropriate for the conditions studied. However, setting $S$=1.3 did not improve the regression predictions and did not change the fitted parameters outside the 95% confidence interval. Thus, we set $S$=2 for all global regressions as the carbon product distribution would not be known *a priori* to assign a best fit value of the stoichiometric ratio.

The nonlinear regression was calculated in MATLAB using the Marquardt method from a published algorithm (Constantinides and Mostoufi, 1999). For each data point in the program, the dependent variable was temperature, the independent variable was MPA conversion, and $\Phi$, $[MPA]_0$, $[H_2O]$, and $\tau$ were input parameters. The 95% confidence intervals for each parameter were also calculated. In an effort to decrease the number of fit parameters, first-order dependence for MPA was assumed, i.e. $a$=1, since the experimental data indicate such behavior based on the linear data in Figure 3-10. An attempt was made to regress the reaction order of MPA and a value of $a$=0.55±0.14 was estimated. However, when the goodness of the overall fit of this rate law was compared with the expression with $a$=1, no significant difference was found. Thus, we chose to retain the value of $a$=1 for the global rate law based on the experimental evidence. The resulting global rate law is shown below with 95% confidence intervals for each parameter.

$$\frac{-d[\mathrm{MPA}]}{dt} = 10^{14.0\pm1.6} \exp\left(\frac{-(228\pm22)\mathrm{x}10^3}{RT}\right)[\mathrm{MPA}][\mathrm{O_2}]^{0.30\pm0.18}[\mathrm{H_2O}]^{1.17\pm0.30} \qquad (3\text{-}20)$$

The activation energy of 228±22x$10^3$ is in J/mol and all concentrations are in mol/L. Consistent with experimental results, the MPA oxidation rate exhibits a dependence on MPA, $O_2$, and $H_2O$ concentrations.

Bianchetta *et al.* (1999) also developed two global rate laws for MPA oxidation. They did not adjust the water concentration experimentally, so they did not include water concentration in their regression. Also, since the majority of the data were taken at 200% excess oxygen, the oxygen concentration was assumed constant in their rate laws. The first global rate law regressed from 17 data points with conversions greater than 92% assumed first-order MPA dependence and predicted first-order $O_2$ dependence as shown in Eq. 3-21.

$$\frac{-d[\mathrm{MPA}]}{dt} = 10^{14.09\pm9.11} \exp\left(\frac{-(186\pm36)\times10^3}{RT}\right)[\mathrm{MPA}][\mathrm{O_2}]^{1.01\pm0.65} \tag{3-21}$$

The activation energy is J/mol and the concentrations are in mol/L. A second global rate law was developed from all 43 data points with an assumed first-order MPA dependence and 0.33 order $O_2$ dependence in Eq. 3-22.

$$\frac{-d[\mathrm{MPA}]}{dt} = 10^{12.57\pm8.13} \exp\left(\frac{-(186\pm36)\times10^3}{RT}\right)[\mathrm{MPA}][\mathrm{O_2}]^{0.33} \tag{3-22}$$

The first global rate law in Eq. 3-21 provides an accurate global rate law for high conversion conditions for more practical applications, while the rate law in Eq. 3-22 is a correlation of all of the data collected in their study at both low and high conversions.

To determine how well each global rate law represents its corresponding data set, conversions were predicted by integrating Eqs. (3-20) to (3-22) and compared to measured experimental conversions. In Figure 3-11, predicted conversions for the experimental data from this study are shown with a 45° line and ±5% conversion dotted lines to illustrate the accuracy of the predicted conversions from Eq. 3-20. The predicted conversions for the Bianchetta *et al.* data from the global rate laws in Eqs. (3-21) and (3-22) are also included for comparison. To better represent Bianchetta *et al.*'s high conversion data, a magnified plot for $X$>90% was included in Figure 3-11. For the present MPA study, the majority of the data are predicted within ±5% conversion by the regressed global rate law. As expected, the high and low conversion data predictions contain the largest uncertainty. Predicted conversions from Eqs. (3-21) and (3-22) also agree reasonably well with their corresponding data sets.

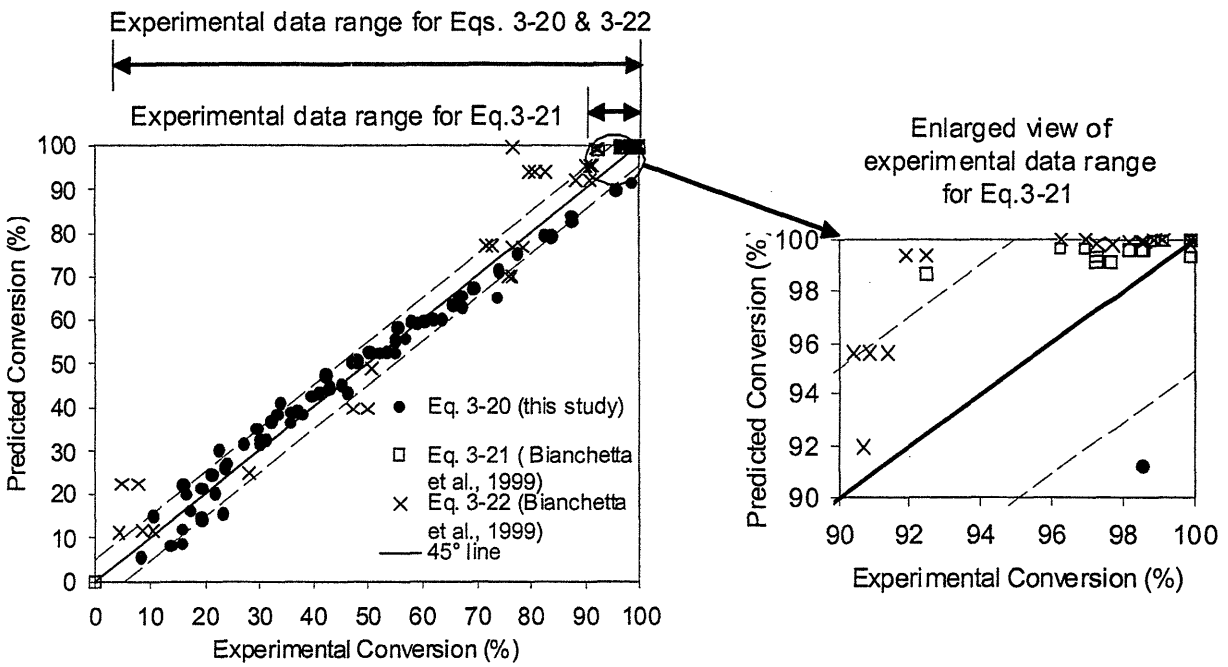


**Figure 3-11: Predicted conversions compared to experimental conversions for the three global rate laws (Eqs. (3-20) to (3-22)) using their respective data sets**

The data ranges for each equation are shown at the top of the figure. The dashed lines represent ± 5% uncertainty in conversion predictions to demonstrate the accuracy of each global rate law.

Given the three global rate laws in Eqs. (3-20) to (3-22), we wanted to determine how well each expression predicts the present MPA oxidation data. The integration of each equation was performed with their limiting assumptions, i.e. constant $[O_2]$ was assumed for the integration of Eqs. (3-21) and (3-22), and the calculated results are presented in Figure 3-12. The global rate law from (3-20) agrees with experimental results satisfactorily while the other two global rate laws predict substantially higher conversions. The predicted rate constants from Eq. (3-22) are almost twice as large as those from Eq. (3-21) because of the different oxygen orders in the two equations. The limiting assumption of constant excess oxygen leads to an effective pre-exponential factor of $A^*[O_2]_0^b$ equal to $10^{14.09\pm9.11}[O_2]_0^{1.01\pm0.65}$ in Eq. (3-21) and $10^{12.57\pm8.13}[O_2]_0^{0.3}$ in Eq. (3-22). At the average oxygen concentrations examined in the present study ($[O_2]_0 \approx 2$ mM), the effective pre-exponential factor almost doubles from $2.5\text{x}10^{11}$ for Eq. (3-21) to

$4.8x10^{11}$ for Eq. (3-22). However, for the Bianchetta *et al.* data from which these rate parameters were regressed, $[O_2]_0$ is approximately equal to 4 mM, increasing the effective pre-exponential factor slightly from $4.9x10^{11}$ to $6.0x10^{11}$ between the two equations. This indicates that the global rate laws in Eqs. (3-21) and (3-22) may not be appropriate for lower oxygen concentrations ($\Phi>1$) since they were developed with the limiting assumption of constant excess oxygen concentration conditions ($\Phi<0.5$).

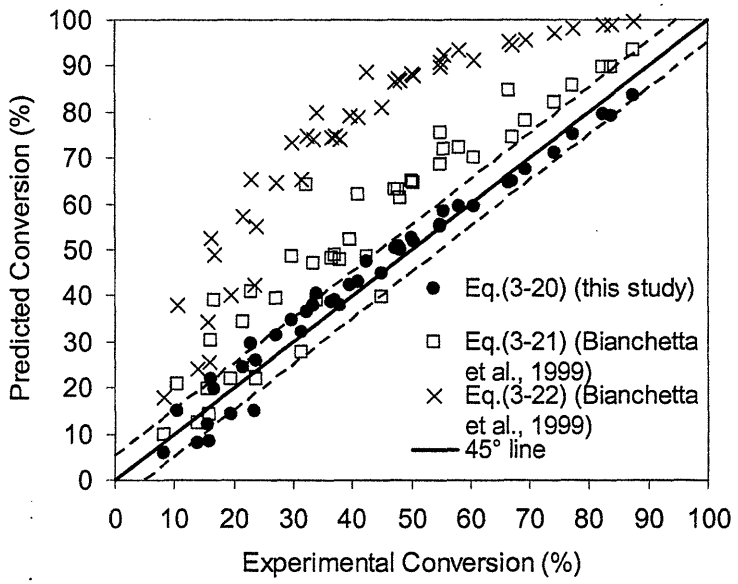


**Figure 3-12: Predicted conversions compared to experimental conversions for the three different global rate laws (Eqs. (3-20) to (3-22)) for the data from the present MPA experiments**

The dashed lines represent ± 5% uncertainty in conversion predictions to demonstrate the accuracy of each global rate law.

### *3.4.2 Macroscopic Pathways Analysis*

To estimate the relative reaction rates of the major carbon pathways in MPA oxidation, a model was developed using the four pathway mechanism hypothesized in Figure 3-5. The relevant set of ordinary differential equations for this model is given by:

$$\frac{d[\mathrm{MPA}]}{dt} = -k_1[\mathrm{MPA}][\mathrm{O_2}]^{b_1} - k_2[\mathrm{MPA}][\mathrm{O_2}]^{b_2} \tag{3-23}$$

$$\frac{d[\mathrm{CO}]}{dt} = k_1[\mathrm{MPA}][\mathrm{O_2}]^{b_1} + k_4[\mathrm{CH_4}][\mathrm{O_2}]^{b_4} - k_3[\mathrm{CO}][\mathrm{O_2}]^{b_3} \tag{3-24}$$

$$\frac{d[\mathrm{CH_4}]}{dt} = k_2[\mathrm{MPA}][\mathrm{O_2}]^{b_2} - k_4[\mathrm{CH_4}][\mathrm{O_2}]^{b_4} \tag{3-25}$$

$$\frac{d[\mathrm{CO_2}]}{dt} = k_3[\mathrm{CO}][\mathrm{O_2}]^{b_3} \tag{3-26}$$

$$\frac{d[\mathrm{O_2}]}{dt} = -k_1[\mathrm{MPA}][\mathrm{O_2}]^{b_1} - k_2[\mathrm{MPA}][\mathrm{O_2}]^{b_2} - k_3[\mathrm{CO}][\mathrm{O_2}]^{b_3} - k_4[\mathrm{CH_4}][\mathrm{O_2}]^{b_4} \tag{3-27}$$

$$k_i = A_i \exp\left(\frac{-E_{a,i}}{RT}\right) \text{ for i=1:4} \tag{3-28}$$

Using these equations, the parameters, $A_i$, $E_{a,i}$, and $b_i$, were regressed for each reaction pathway in MATLAB using the Marquardt algorithm and the MATLAB function, "ode23", to solve the differential equations (Constantinides and Mostoufi, 1999). All pathways were assumed to follow first-order behavior with respect to MPA, CO, and $CH_4$ since the global rate laws for each of these compounds also predict first-order behavior (Holgate *et al.*, 1992; Webley and Tester, 1991). The water density variation data were excluded from the regression since an explicit dependence on water is not included in these rate constants. All data used in these regressions were at a constant pressure of 246 bar, in a water concentration range from 4.1 to 5.2 M or a density range of 73 to 93 kg/m$^3$.

The macroscopic reaction rates are shown in Table 3-2, which also includes parameters from the pure CO and $CH_4$ oxidation rates in the literature for comparison (Webley and Tester, 1991; Holgate *et al.*, 1992). Pseudo first-order rate constants are included as a means of comparison between the different reaction rates. To calculate these rate constant values, $[O_2]$ is assumed to be constant at 2 mM, the initial concentration of $O_2$ in most of the MPA experiments.

The regressed reaction rate for $CH_4$ reaction to CO, $k_4$, is not included in Table 3-2 because the reaction rate for $CH_4$ to CO oxidation was estimated to not be statistically different than zero from the regression results. Since the $CH_4$ concentration in the system is very low, it was difficult to estimate both the $CH_4$ production ($k_2$) and oxidation ($k_4$) rates with any confidence. The $CH_4$ oxidation rate from Webley and Tester (1991) is slower than the rate of $CH_4$ production ($k_2$) at all temperatures, leading to $CH_4$ accumulation during MPA oxidation. The formation reaction rate expression for $CH_4$ is independent of $O_2$ concentration with $b_2$=0.03±0.03 or $b_2 \approx 0$ because the reaction pathway from MPA to $CH_4$ occurs by reduction, not oxidation.

**Table 3-2: Reaction rate parameters for the macroscopic reaction rates in MPA oxidation based on the model of Eqs. (3-23) to (3-28)**

The subscripts for the MPA and CO rates refer to the pathways in Figure 3-5. Global rates for CO and $CH_4$ oxidation from Eq. 22 in Holgate *et al.* (1992) and Eq. 4 in Webley and Tester (1991) are also included, along with pseudo first-order rate constants, assuming $[O_2]$=2 mM, for each reaction rate.

| Parameter | $\left(\frac{d[\text{MPA}]}{dt}\right)_1$ | $\left(\frac{d[\text{MPA}]}{dt}\right)_2$ | $\left(\frac{d[\text{CO}]}{dt}\right)_3$ | $\left(\frac{d[\text{CO}]}{dt}\right)_{lit}$ | $\left(\frac{d[\text{CH}_4]}{dt}\right)_{lit}$ |
|---|---|---|---|---|---|
| $\log_{10}(A)$ | 11.3±0.1 | 12.5±0.5 | 9.8±0.2 | 8.5±3.3 | 11.4±1.1 |
| $E_a$(kJ/mol) | 176±2 | 218±10 | 146±3 | 134±32 | 179±18 |
| $b$ | 0.28±.05 | 0.03±.03 | 0.31±.06 | 0.34±0.24 | 0.66±0.14 |
| $T$(°C) | $k_1(M^{0.28}s)^{-1}$ | $k_2(s^{-1})$ | $k_3(M^{0.31}s)^{-1}$ | $k_3$(lit) $(M^{0.34}s)^{-1}$ | $k_4$(lit) $(M^{0.66}s)^{-1}$ |
| 478 | $1.9\times10^{-02}$ | $2.0\times10^{-03}$ | $6.1\times10^{-02}$ | $1.8\times10^{-02}$ | $1.5\times10^{-03}$ |
| 503 | $4.8\times10^{-02}$ | $6.1\times10^{-03}$ | $1.3\times10^{-01}$ | $3.7\times10^{-02}$ | $3.7\times10^{-03}$ |
| 527 | $1.1\times10^{-01}$ | $1.8\times10^{-02}$ | $2.6\times10^{-01}$ | $7.0\times10^{-02}$ | $8.9\times10^{-03}$ |
| 551 | $2.3\times10^{-01}$ | $4.4\times10^{-02}$ | $4.8\times10^{-01}$ | $1.2\times10^{-01}$ | $1.9\times10^{-02}$ |
| 571 | $4.3\times10^{-01}$ | $9.3\times10^{-02}$ | $8.0\times10^{-01}$ | $1.9\times10^{-01}$ | $3.5\times10^{-02}$ |

The CO oxidation rate constant to form $CO_2$, $k_3$, is compared to an experimental value determined earlier in Holgate *et al.* (1992) (see Table 3-2). The estimated value for $k_3$ from the MPA regression is approximately three to four times larger than the rate constant from the earlier pure CO experiments. An initial attempt was made to include the CO literature parameters in the regression of Eqs. (3-23) to (3-28); however, this CO oxidation rate was too slow at all conditions, so the CO oxidation rate, $k_3$, was regressed from the MPA oxidation data. The CO

oxidation rates could be faster during MPA oxidation than for pure CO oxidation due to co-oxidation effects (Savage *et al.*, 2000). CO oxidation to $CO_2$ is primarily dependent on the OH radical. If the OH radical concentration is higher during pure MPA oxidation than for CO oxidation, CO would react faster in the MPA system.

The MPA oxidation rates, $k_1$ and $k_2$, are also estimated in Table 3-2. The branching between the two MPA pathways is the ratio of $k_1$:$k_2$, which decreases from 10 at $T$=478 °C to 5 at $T$=571°C. This indicates that the second, slower pathway to $CH_4$ becomes more significant as the temperature increases. Experimentally, the methane yield increased from 0.05 at $T$=503 °C to 0.19 at $T$=571 °C in Figure 3-3 showing that the methane pathway does become more important at higher temperatures. However, $k_1$, the oxidation rate for MPA to CO formation remains the dominant reaction rate at all temperatures.

Finally, we return to the experimental observation that $k_1$, the reaction rate of MPA to CO, and $k_3$, the reaction rate of CO to $CO_2$, have similar time scales leading to accumulation of the CO intermediate at lower temperatures. These two rates, $k_1$ and $k_3$, shown in Table 3-2 are within a factor of 2 or 3 of each other, indicating that oxidation of MPA and CO are indeed occurring at comparable rates. Also, the oxygen orders of both reactions were estimated in Table 3-2 to be about 0.3, the same as the $O_2$ order in the MPA global rate laws in Eqs. (3-20) and (3-22) and in the CO global rate law from literature (Holgate *et al.*, 1992). From the independence of CO carbon fraction on $O_2$ concentration, similar oxygen orders for $k_1$ and $k_3$ would be expected. However, it is difficult to speculate on what a global $O_2$ order of 0.3 implies mechanistically. A full elementary reaction rate model has been developed to quantify this effect as discussed in Chapter 5.

## 3.5 Co-oxidation Experiments with MPA and Ethanol

As a continuation of the MPA experimental study, we have also begun a co-oxidation study with the labile model compound, ethanol, and the refractory model compound, MPA, to quantify co-oxidation effects in SCW. The goal of the co-oxidation study is to experimentally determine if the addition of ethanol increases MPA oxidation rates and to quantify the effects of different operating variables on co-oxidation rates. Additionally, we are developing a co-oxidation elementary reaction rate model with MPA and ethanol to determine how co-oxidation conditions affects radical concentrations and oxidation rates. The co-oxidation study is being completed in conjunction with Jason Ploeger and will be presented completely in an upcoming paper. The background and approach that we have chosen to assess this problem are briefly summarized below.

For real SCWO processes, the feed streams would contain multiple compounds that need to be remediated. Simultaneous oxidation of compounds could influence the oxidation rates of the individual compounds because the radical concentrations could change significantly. Thus, global rate laws that are developed from single-component oxidation studies, such as the MPA global rate law in Eq. (3-20), may not properly predict the oxidation rates of a model compound in a mixed waste stream. In single component waste streams, the radical concentrations increase significantly only as the model compound begins to oxidize. So, for a refractory compound, like MPA, radical concentrations would only increase after significant conversion begins to occur. If a more labile compound is also included in the waste stream, the labile compound would undergo oxidation and generate higher radical concentrations at lower temperatures. At lower temperatures, the increased radical concentrations could possibly increase the oxidation rate of the refractory compound. Increasing oxidation rates of refractory compounds by co-oxidation

with a more labile compounds has been demonstrated, but has not been studied in a well-defined manner previously (Savage *et al.*, 2000). To properly assess co-oxidation effects, single component oxidation kinetics for a refractory and a labile compound along with the oxidation kinetics of each compound in a mixed feed would be required at varying organic and oxidant concentrations.

In this thesis, the oxidation kinetics of the refractory compound, MPA were thoroughly examined. The oxidation kinetics of ethanol, a more labile compound, were also recently studied in our laboratory (Schanzenbacher, 2002). Ethanol oxidation rates were measured in a temperature range of 433 to 494 °C and a residence time range of 2 to 12 s, at a constant pressure (246 bar), initial ethanol concentration (1 mM), and stoichiometric conditions ($\Phi$=1). Conversion due to hydrolysis was minimal with a measured range of 1.9 to 7.4%. Oxidation rates were very rapid with essentially complete ethanol conversion measured at 490 °C and 6 s residence time. Ethanol oxidation rates were found to be oxygen dependent from a set of experiments varying the fuel equivalence ratio from 0.5 to 1.9 at 470 °C, 246 bar, and $[EtOH]_0$=1 mM. From this data, the global rate expression to a 95% statistical confidence level was regressed as:

$$-\frac{d[\mathrm{EtOH}]}{dt} = 10^{17.23\pm1.65}\exp\left(\frac{-(213.9\pm18.3)\times10^3}{RT}\right)[\mathrm{EtOH}]^{1.34\pm0.11}[\mathrm{O_2}]^{0.55\pm0.19} \qquad (3\text{-}29)$$

From this experimental study, ethanol oxidation rates are much faster than the MPA oxidation rates reported presently at $T$<500 °C.

Co-oxidation of MPA and ethanol would provide an ideal, model system from which an improved understanding of co-oxidation effects in SCW could be gained. At $T$<500 °C, MPA oxidation rates are very slow with MPA conversions less than 30% after a residence time of 8 s. However, at $T$=490°C and $\tau$=6 s, ethanol conversion is almost complete. First-order rate

constants for MPA and ethanol are shown in Figure 3-13 to demonstrate how the global rate constants for both compounds differ over the temperature range of 400 to 600 °C. At temperatures between 450 and 500 °C, the ethanol oxidation rates are fast enough to significantly increase radical concentrations which could possibly increase MPA oxidation rates at these conditions. We chose the temperature range of 450 °C to 500 °C to be the optimal area in which to experimentally measure increased MPA oxidation rates due to co-oxidation effects.

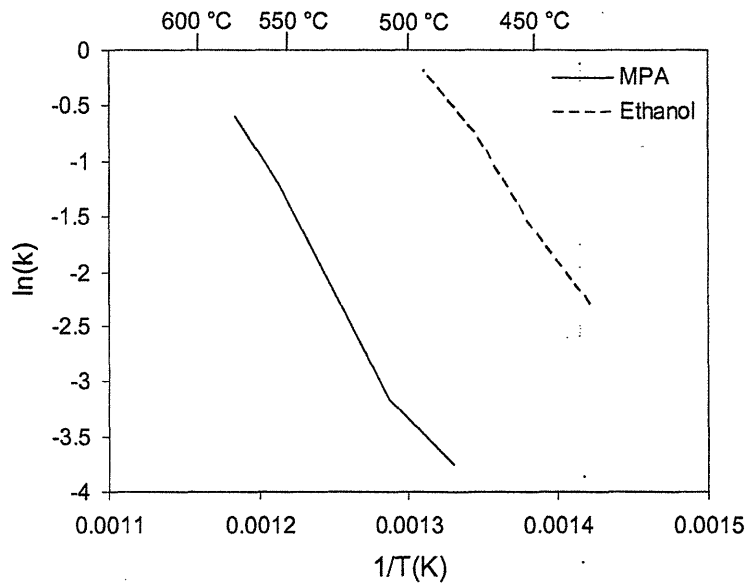


**Figure 3-13: Arrhenius plot of first-order rate constants for MPA and ethanol**

For the experimental measurements, the organic feed stream contains both ethanol and MPA since neither of these compounds undergo extensive hydrolysis at sub- and supercritical temperatures. To assess co-oxidation effects, we have chosen to vary the MPA concentration from 0.1 to 1.0 mM and the ethanol concentration from 0.1 to 3.0 mM at $T$=473 °C, $\Phi$=1, and $P$=246 bar. To determine that increased MPA oxidation rates are not due to the increased oxygen concentrations for the co-oxidation study, MPA conversions are also measured in a single component MPA feed stream at higher co-oxidation oxygen concentrations.

Preliminary data from these co-oxidation experiments indicate that MPA conversion increases significantly with the addition of ethanol as a co-oxidant. To assess the co-oxidation experimental data, an SCWO ethanol model is being added to the MPA elementary reaction rate model developed in Chapter 5. With the combined MPA and ethanol model, the factors responsible for increased MPA oxidation rates during co-oxidation can be determined. For this co-oxidation study, we are gaining a better, quantitative understanding of how co-oxidation of a labile and a refractory compound affects reaction rates.

## 3.6 CONCLUSIONS

An experimental study of MPA hydrolysis and oxidation in SCW was completed that systematically explored the effects of temperature, residence time, oxygen concentration, MPA concentration, and pressure (or water density) on MPA conversion and on its product distribution. Conversion due to hydrolysis was less than 6% after $\tau$=7 s at all temperatures studied. Minimal conversion ($X$<30% at $\tau$=10 s) was measured at $T$<503 °C, while almost complete conversion ($X$=99%) was measured at $T$=571 °C and $\tau$=7 s at stoichiometric conditions and $P$=246 bar. MPA oxidation rates exhibited a dependence on both oxygen concentration and pressure (or water density), but were relatively independent of initial MPA concentration. A global rate law was also developed with a first-order dependence on MPA and a non-zero dependence on both oxygen and water concentrations.

MPA oxidation occurs by two pathways to the carbon-containing intermediates, CO and $CH_4$. The dominant pathway is through the CO intermediate to the final carbon-containing product, $CO_2$. A macroscopic model was developed to estimate the relative reaction rates of these major pathways in MPA oxidation. The model predicted that the branching ratio of CO to $CH_4$ production was approximately 10:1 at lower temperatures and decreased to 5:1 at $T$=571°C

as the methane pathway became more important. The reaction rate constants for oxidation of MPA to CO, $k_1$, and CO to $CO_2$, $k_3$, were of the same order of magnitude indicating that these rates occur on similar time scales. For the CO and $CH_4$ intermediates, $CH_4$ was unreactive during MPA oxidation while CO oxidation occurred more quickly during MPA oxidation than during pure CO oxidation due to co-oxidation effects.

## 3.7 REFERENCES

Benson, B. B., D. Krause and M. A. Peterson, "The solubility and isotopic fractionation of gases in dilute aqueous solution. I. Oxygen." *J. Sol. Chem.* **8**(9), 655-690 (1979).

Bianchetta, S., L. Li and E. F. Gloyna, "Supercritical water oxidation of methylphosphonic acid." *Ind. Eng. Chem. Res.* **38**, 2902-2910 (1999).

Constantinides, A. and N. Mostoufi, *Numerical Methods for Chemical Engineers with Matlab Applications*. Prentice Hall PTR, Upper Saddle River, NJ (1999).

DiNaro, J. L., "Oxidation of benzene in supercritical water: Experimental measurements and development of an elementary reaction mechanism." PhD Thesis, Department of Chemical Engineering, Massachusetts Institute of Technology, Cambridge, MA, (1999).

DiNaro, J., J. Tester, J. Howard and K. Swallow, "Experimental measurements of benzene oxidation in supercritical water." *AICHE J.* **46**(11), 2274-2284 (2000a).

DiNaro, J., J. Howard, W. Green, J. W. Tester and J. Bozzelli, "Elementary reaction mechanism for benzene oxidation in supercritical water." *J. Phys. Chem. A* **104**(45), 10576-10586 (2000b).

Glaude, P. A., H. J. Curran, W. J. Pitz and C. K. Westbrook, "Kinetic study of the combustion of organophosphorus compounds." *Proceedings of the Combustion Institute* **28**, 1749-1756 (2000).

Haar, L., J. S. Gallagher and G. S. Kell, *NBS/NRC Steam Tables*. Hemisphere Publishing Corp., New York (1984).

Helling, R. K. and J. W. Tester, "Oxidation kinetics of carbon monoxide in supercritical water." *Energy Fuels* **1**(5), 417-423 (1987).

Holgate, H. R., P. A. Webley, J. W. Tester and R. K. Helling, "Carbon monoxide oxidation in supercritical water: the effects of heat transfer and the water-gas shift reaction on observed kinetics." *Energy Fuels* **6**(5), 586-597 (1992).

Holgate, H. R., "Oxidation chemistry and kinetics in supercritical water: Hydrogen, carbon monoxide, and glucose." PhD Thesis, Department of Chemical Engineering, Massachusetts Institute of Technology, Cambridge, MA, (1993).

Holgate, H. R. and J. W. Tester, "Oxidation of hydrogen and carbon monoxide in sub- and supercritical water: reaction kinetics, pathways, and water-density effects. 1. Experimental results." *J. Phys. Chem.* **98**(3), 800-809 (1994a).

Holgate, H. R. and J. W. Tester, "Oxidation of hydrogen and carbon monoxide in sub- and supercritical water: reaction kinetics, pathways, and water-density effects. 2. Elementary reaction rate modeling." *J. Phys. Chem.* **98**(3), 810-822 (1994b).

Koo, M., W. K. Lee and C. H. Lee, "New reactor system for supercritical water oxidation and its application on phenol destruction." *Chem. Eng. Sci.* **52**(7), 1201-1214 (1997).

Korobeinichev, O. P., S. B. Ilyin, T. A. Boshova, V. M. Shvartsberg and A. A. Chernov, "The chemistry of the destruction of organophosphorus compounds in flames -III: The destruction of DMMP and TMP in a flame of hydrogen and oxygen." *Combust. Flame* **121**(4), 593-609 (2000).

Phenix, B., "Hydrothermal oxidation of simple organic compounds." PhD Thesis, Department of Chemical Engineering, Massachusetts Institute of Technology, Cambridge, MA, (1998).

Rettich, T. R., Y. P. Handa, R. Battino and E. Wilhelm, "Solubility of gases in liquids. 13. High-precision determination of Henry's constants for methane and ethane in liquid water at 278 to 328 K." *J. Phys. Chem.* **85**, 3230 (1981).

Rettich, T. R., R. Battino and E. Wilhelm, "Solubility of gases in liquids. 15. High-precision determination of Henry's coefficients for carbon monoxide in water at 278 to 323K." *Berichte Bunsengeschlaftt fur Physiche Chemie* **86**, 1128-1132 (1982).

Savage, P., J. Yu, N. Stylski and E. Brock, "Kinetics and mechanism of methane oxidation in supercritical water." *J. Supercrit. Fluids* **12**, 141-153 (1998).

Savage, P., J. Rovira, N. Stylski and C. Martino, "Oxidation kinetics for methane/methanol mixtures in supercritical water." *J. Supercrit. Fluids* **17**, 155-170 (2000).

Schanzenbacher, J., J. D. Taylor and J. W. Tester, "Ethanol oxidation and hydrolysis rates in supercritical water." *J. Supercrit. Fluid* **22**(2), 139-147 (2002).

Webley, P. A. and J. W. Tester, "Fundamental kinetics of methane oxidation in supercritical water." *Energy and Fuels* **5**, 411-419 (1991).

Wilhelm, E., R. Battino and R. J. Wilcock, "Low-pressure solubility of gases in liquid water." *Chem. Rev.* **77**(2), 219-262 (1977).

# 4 *Ab initio* Calculations of Organophosphorus Combustion Chemistry

For the MPA SCWO elementary reaction rate model developed in Chapter 5, reliable organophosphorus thermochemistry and reaction rates were needed. In the absence of experimental data, *ab initio* calculations are one of the best methods to estimate thermochemistry and reaction rates. In this chapter, the equations needed to calculate thermochemistry and transition state theory rate constants from *ab initio* results are presented. The predicted organophosphorus thermochemistry is discussed and compared to literature values, when available. Transition state theory rate constants for fourteen reaction pathways in the MPA SCWO model are presented and assessed. For some of these reaction rates, previous estimates available from organophosphorus combustion mechanisms were compared to the calculated transition state theory rates to estimate the accuracy of rate estimation methods for organophosphorus chemistry.

## 4.1 Motivation and Introduction

Typically, SCWO elementary reaction rate models for a model compound are adapted from well-defined combustion models to the lower temperature, higher pressure conditions of SCW. However, organophosphorus combustion chemistry has not been extensively studied. A few models have been developed for DMMP combustion that contain only estimated organophosphorus reaction rates. No organophosphorus elementary reaction rates have experimentally measured and few detailed *ab initio* transition state rate constants have been calculated for this chemistry. Additionally, MPA is only a minor intermediate during DMMP combustion so only three reaction rates involving MPA have been included in previous DMMP

models. This *ab initio* study was motivated by the large amount of uncertainty that currently exists for organophosphorus combustion chemistry to improve the overall understanding of organophosphorus kinetics and to determine additional reactions that could be important during MPA oxidation.

### *4.1.1 Previous Organophosphorus Combustion Models*

Organophosphorus combustion chemistry has important applications in flame retardation and incineration of organophosphorus chemical warfare agents (Werner and Cool, 1999; Korobeinichev *et al.*, 1999, 2000, 2001; MacDonald *et al.*, 2001; Nogueira and Fisher, 2003). Experimental pyrolysis studies in flow reactors and oxidation studies in flames have measured temperature and species concentration profiles for organophosphorus simulants such as dimethyl methylphosphonate (DMMP, $PO(OCH_3)_2CH_3$), diethyl methylphosphonate (DEMP, $PO(OCH_2CH_3)_2CH_3$), di-isopropyl methylphosphonate (DIMP, $PO(OCH(CH_3)_2)_2CH_3$), trimethylphosphate (TMP, $PO(OCH_3)_3$), and triethylphosphate (TEP, $PO(OC_2H_5)_3$) (Zegers and Fisher, 1996, 1998a, 1998b; Werner and Cool, 1999; Korobeinichev *et al.*, 2000). By identifying important intermediates, these experimental studies have helped to elucidate global mechanistic pathways and have fostered a series of kinetic mechanisms for DMMP oxidation (Werner and Cool, 1999; Korobeinichev *et al.*, 2000; Glaude *et al.*, 2000). Since no direct measurements for individual organophosphorus rate constants exist, most rate constants in these mechanisms have been estimated with a high degree of uncertainty.

The first model developed for phosphorus-containing chemistry was a phosphine ($PH_3$) combustion model in a $H_2/O_2$ flame by Twarowski (1995). This model did not contain any organic compounds, but the P/O reaction set and the estimation methodology from this model were used in later organophosphorus models. By accounting for all possible reaction

intermediate pathways, Twarowski developed a model with 17 phosphorus-containing species and 162 reactions. All rate constants were estimated using rate estimation rules established by Benson (1976). For the Arrhenius expression of these reactions, the pre-exponential factor was determined based on the type of reaction, such as recombination, atom metathesis, or bimolecular exchange, and the activation energy was calculated from the heat of reaction and electron affinities. After a sensitivity analysis, this model was reduced to a reaction set of 39 reactions that was able to adequately predict the reaction kinetics of phosphine combustion. This study developed the first phosphorus-containing combustion model.

Werner and Cool (1999) conducted experiments on the combustion of DMMP in a $H_2/O_2$ flame and measured the rate of disappearance of DMMP and also the formation of reaction intermediates, such as $CH_3PO_2$ and $CH_3OPO_2$, using laser-ionization mass spectrometry. To model their experimental results, a DMMP combustion model was developed with 20 organophosphorus reactions and 10 organophosphorus species. Four unimolecular decomposition rates were estimated from transtition state energies that had been calculated by Melius using the *ab initio* method, BAC-MP4. The other organophosphorus rate constants were estimated from heats of reaction, structural considerations, and estimated barrier heights. Some of the pre-exponential factors for the organophosphorus reactions were adjusted to achieve better agreement between model predictions and experimental concentration profiles. The model included 11 of Twarowski's P/O reactions along with 31 $H_2/O_2$ and 66 C/H/O reactions from several different combustion models. Predicted results from this model did correctly predict the concentration profiles of some compounds, but also were in poor agreement with other measured intermediates and products.

Korobeinichev *et al.* published a series of papers on both the experimental and modeling results of the combustion of DMMP and TMP in a $H_2/O_2$ flame using molecular-beam mass spectrometry (1999, 2000, 2001). Korobeinichev *et al.* (2000) used the Werner and Cool (1999) DMMP model as a basis for their new DMMP model. To include previously unidentified intermediates, such as MPA and phosphoric acid, Korobeinichev *et al.* (2000) added nine organophosphorus reaction pathways to the DMMP model. Rate constants for the nine new reactions were estimated by comparing these reactions to similar ones from the Werner and Cool study. This DMMP reaction mechanism contained 26 organophosphorus reactions, 15 P/O reactions from Twarowski (1995), and 23 $H_2/O_2$ and 36 H/C/O reactions from Werner and Cool's (1999) DMMP model. To obtain agreement with their data, Korobeinichev *et al.* adjusted pre-exponential factors for 12 of the P/O reactions and 4 of the organophosphorus reactions. The model predicted the experimental concentration profiles well for most of the measured species by the addition of new reaction intermediates and pathways and the adjustment of sensitive rate constants.

Glaude *et al.* (2000) also developed a DMMP and TMP combustion model. In this study, models were developed to predict the results from pyrolysis experiments of DEMP, TEP, and DIMP by Zegers and Fisher (1996, 1998a, 1998b) and from combustion experiments of DMMP and TMP by Korobeinichev *et al.* (2000). Fifteen unimolecular reaction rates were estimated for the pyrolysis of DEMP, TEP, and DIMP. Rate constants for six-centered unimolecular decomposition of these compounds to form alkenes were calculated from experimental data (Zegers and Fisher, 1996, 1998a, 1998b). Four-centered decomposition reactions were also included; these rate constants were estimated from comparison with known rates for similar

carbon-containing compounds. Results from the pyrolysis model predicted experimental concentration profiles of both products and reactants well.

To develop the DMMP and TMP combustion model, Glaude *et al.* (2000) attempted to account for all possible organophosphorus reaction pathways leading to a larger model with 41 phosphorus-containing species and 202 reactions. Phosphorus-containing rate constants were estimated by comparison to similar carbon- or nitrogen-containing chemistry. This model also included 263 reactions from an available dimethyl ether mechanism for the C/H/O and $H_2/O_2$ reactions (Kaiser *et al.*, 2000). The modeling results were able to predict much of the experimental DMMP and TMP data from Korobeinichev *et al.* (2000) correctly, which could be due in part to the inclusion of the much larger reaction set.

### *4.1.2 Previous Ab initio Phosphorus Oxide Studies*

In an effort to calculate accurate thermochemistry and reaction rates for phosphorus-containing compounds, a series of *ab initio* studies has been recently conducted for phosphorus oxide species (Haworth *et al.*, 2002; Mackie *et al.*, 2002; Haworth and Backsay, 2002). Haworth *et al.* (2002) calculated heats of formation for 17 phosphorus-containing compounds using the Gaussian compound methods, G2, G3, G3X, and G3X2. The G3X2 method predicted heats of formation accurately for most of the phosphorus-containing compounds when results were compared to experimental data or computed CBS values from Bauschlicher (1999). Haworth *et al.* (2002) also calculated transition state theory and RRKM rate constants for four $PO_2$ reactions in Twarowski's (1995) phosphorus oxide model. Rate constants were either calculated using classical transition state theory for reactions with a well-defined transition state or were calculated using variational transition state theory for barrierless reactions. The authors treated all torsional vibrations as vibrational frequencies after determining that use of the hindered rotor

correction would result in negligible changes to the partition functions. For dissociation rate constants, the pressure dependence was calculated using the RRKM model. Haworth *et al.* (2002) found that rate constants from Twarowski (1995) were overestimated by several orders of magnitude, while the estimated Korobeinichev *et al.* (2001) rate constants agreed within an order of magnitude of all four calculated TST rate constants.

Mackie *et al.* (2002) calculated rate constants for four phosphorus oxide reactions that occur through stabilized adducts and subsequently decompose by water elimination. These reaction rates were calculated using the G3X and G3X2 methods in Gaussian 98. The rate constant for one reaction, $PO_2OH$ and $H^{\bullet}$ to form $H_2O$ and $P^{\bullet}O_2$, was previously calculated by Haworth *et al.* (2002) through a different pathway involving direct abstraction of the OH group by the H radical. For this reaction, Mackie *et al.* (2002) determined that the rate constant through the stabilized adduct, $P^{\bullet}O(OH)_2$, was three orders of magnitude greater at $T$=1000 K than the direct abstraction rate constant calculated by Haworth *et al.* (2002). With the faster reaction pathway, Mackie *et al.*'s rate constant for this reaction agreed within an order of magnitude with Twarowski's estimated reaction rate for this pathway, while the Korobeinichev *et al.* (2001) rate constant was underestimated by two orders of magnitude. Two other rate constants calculated by Mackie *et al.* (2002) agreed well with the Twarowski (1995) reaction rates and were 1 to 2 orders of magnitude greater than the Korobeinichev *et al.* (2001) reaction rates. Mackie *et al.* (2002) determined that reaction rates through two-step pathways could be faster than direct abstraction pathways for certain reactions. Also, these results indicate that phosphorus-containing reaction rates from Twarowski (1995) may be more accurate than those from Korobeinichev *et al.* (2001), contrary to the conclusions developed by Haworth *et al.* (2002).

These *ab initio* studies demonstrate the high uncertainty in phosphorus-containing reaction rates prevalent in organophosphorus combustion mechanisms. Mackie *et al.* (2002) proposed new pathways through stabilized intermediates that appear to be faster than the direct abstraction pathways. After examining multiple reaction pathways, these authors concluded that the rate constants from Twarowski's (1995) mechanism appear to be more accurate than estimated reaction rates from Korobeinichev *et al.* (2001). Many of Korobeinichev *et al*'s rates were taken from Twarowski's (1995) $PH_3$ mechanism and adjusted to achieve better agreement with measured concentration profiles of $P^{\bullet}O(OH)_2$, $PO_2OH$, and HOPO. These results indicate that perhaps Korobeinichev *et al.* were missing reaction pathways or had incorrectly estimated other reaction rates that could improve their model predictions. Without experimental measurement of individual reaction rates or *ab initio* calculation of transition state theory rate constants, it is difficult to determine which estimated reaction rates in the organophosphorus combustion mechanisms are the most accurate. The results from these studies demonstrate the increased insight that *ab initio* calculations can provide for reaction rates in phosphorus-containing chemistry.

### *4.1.3 Research Needs for MPA SCWO Model Development*

In the initial development of the MPA SCWO model, all MPA reactions from the DMMP combustion models were examined (Korobeinichev *et al.*, 2000; Glaude *et al.*, 2000). MPA is a minor intermediate in DMMP oxidation at combustion conditions and its reaction pathways have not been extensively studied. The three MPA reaction rates (R1a to R3a) from Glaude *et al.* (2000) and Korobeinichev *et al.* (2000) are shown below in Table 4-1. Glaude *et al* estimated the MPA rate constants by comparisons to similar carbon- or nitrogen-containing reactions.

Korobeinichev *et al* estimated the bimolecular MPA reaction rate (R3a) to be equal to the rate for DMMP and $OH^{\bullet}$ (R4a) from Werner and Cool (1999).

$$PO(OCH_3)_2CH_3 + OH^{\bullet} = PO(OCH_3)_2OH + CH_3^{\bullet} \quad \text{(R4a)}$$

$$PO(OCH_3)_2CH_3 + OH^{\bullet} = PO(OCH_3)(OH)CH_3 + OCH_3^{\bullet} \quad \text{(R5a)}$$

In their mechanism, Werner and Cool also estimated that OH substitution of DMMP's $OCH_3$ group (R5a) would have the same reaction rate as OH substitution of DMMP's $CH_3$ group. The estimated reaction rates for reactions (4a and 5a) could be in error because these reactions would occur by different transition states and would not be expected to have the same reaction rates.

**Table 4-1: MPA rate constants from Glaude *et al.* (2000) and Korobeinichev *et al.* (2000)**
Two of the rate constants were not included in Korobeinichev *et al.*'s mechanism, as noted by *NA* below. The rate constants ($k$) and the pre-exponential factors ($A$) are in $s^{-1}$ for reactions (R1a) and (R2a) and are in mol $(cm^3s)^{-1}$ for reaction (R3a).

| Reaction | Glaude *et al.* (2000) | | | | Korobeinichev *et al.* (2000) | | | |
|---|---|---|---|---|---|---|---|---|
| | $A$ | $E_a$ (kcal/mol) | $k$ 800 K | $k$ 1500 K | $A$ | $E_a$ (kcal/mol) | $k$ 800 K | $k$ 1500 K |
| (R1a) MPA= $PO_2CH_3+H_2O$ | $5.0x10^{13}$ | 39.0 | $1.1x10^{03}$ | $1.0x10^{08}$ | *NA* | *NA* | *NA* | *NA* |
| (R2a) MPA= $PO_2OH+CH_4$ | $6.0x10^{11}$ | 61.0 | $1.3x10^{-05}$ | $7.8x10^{02}$ | *NA* | *NA* | *NA* | *NA* |
| (R3a) MPA+$OH^{\bullet}$= $PO(OH)_3+CH_3^{\bullet}$ | $1.0x10^{12}$ | 2.0 | $2.8x10^{11}$ | $5.1x10^{11}$ | $1.0x10^{13}$ | 4.0 | $8.1x10^{11}$ | $2.6x10^{12}$ |

To assess the MPA reactions in Table 4-1, we wanted to determine how well these reactions could predict MPA SCWO kinetic data. These two sets of MPA reactions were each added to a C-1 SCWO model that was developed from Hughes *et al.*'s (2001) methane combustion mechanism. Both the Korobeinichev *et al.* (2000) and Glaude *et al.* (2000) MPA models were compared to MPA SCWO experimental data at $T$=527 °C, $P$=246 bar, $[MPA]_0$=1 mM, and $\Phi$=1.0, as shown in Figure 4-1. The unimolecular rates from Glaude *et al.* (2000) in Table 4-1 were included in these predictions, but the MPA reaction flux did not proceed through the unimolecular reactions. So, the differences between the model predictions in Figure 4-1 are solely due to the different MPA + $OH^{\bullet}$ bimolecular rate constants in Table 4-1.

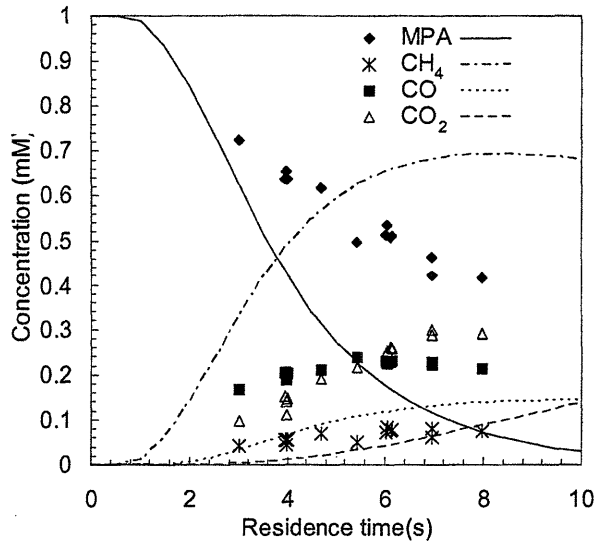


**Figure 4-1a: Korobeinichev *et al.* predictions**

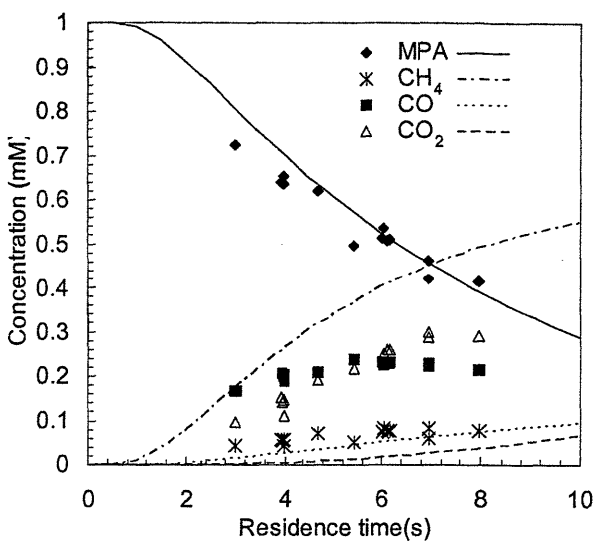


**Figure 4-1b: Glaude *et al.* predictions**

**Figure 4-1: Comparison of predicted concentration profiles from Korobeinichev *et al.* or Glaude *et al.* MPA rate constants and MPA SCWO experimental data at $T$=527 °C**

The MPA rate constants from both models were added to a C-1 SCWO model developed during the present study that was modified from a methane combustion model by Hughes *et al.* (2001). The conditions shown here are at $P$=246 bar, $[MPA]_0$ =1 mM, and $\Phi$=1.

From Figure 4-1a, the Korobeinichev *et al.* (2000) reaction rate overpredicts the MPA oxidation rate and incorrectly predicts that the methane carbon yield is 80 to 90%. With the Glaude *et al.* (2000) MPA rate constant, the MPA oxidation rate is correctly predicted, but the carbon product distribution is still incorrect. Due to the large water concentration in the system, the $CH_3^{\bullet}$ radical primarily reacts with water to form methane and the $OH^{\bullet}$ radical. Once formed, methane is refractory at $T$<600 °C in SCW and little reaction to CO or $CO_2$ is predicted by the model (Webley and Tester, 1991). These results indicate that additional pathways for a more direct route to carbon monoxide formation may be missing from the current models, ignored previously due to the different operating parameters in DMMP combustion such as smaller MPA concentrations, higher temperatures, and lower pressures (Korobeinichev *et al.*, 2000).

To better estimate MPA combustion chemistry, an *ab initio* study was conducted to determine key reaction rates and thermochemistry for MPA oxidation. Reaction rates that are estimated from *ab initio* calculations are expected to contain less uncertainty than those estimated from analogy to hydrocarbons. The goals of this study were (1) to determine the thermochemistry of MPA and its organophosphorus intermediates, (2) to estimate the accuracy of phosphorus-containing rate constants that could be important during MPA oxidation, and (3) to identify and calculate rate constants for new organophosphorus reaction pathways using transition state theory. Because organophosphorus group additivity values (Glaude *et al.*, 2000) do not exist for all molecular subgroups that are required to estimate the thermochemistry for the compounds identified during this study, thermochemistry values were calculated using *ab initio* methods and compared to literature values, when available. Chosen reaction pathways were MPA unimolecular reactions, MPA reactions with an $OH^{\bullet}$ radical, and $PO(OH)_3$ and $P^{\bullet}O(OH)_2$ reactions that could be important in the MPA reaction network. All reaction pathways examined in this study are listed below.

$$PO(OH)_2CH_3 \rightarrow [TS_1]^{\dagger} \rightarrow PO_2CH_3+H_2O \quad (R1)$$

$$PO(OH)_2CH_3 \rightarrow [TS_2]^{\dagger} \rightarrow PO_2OH+CH_4 \quad (R2)$$

$$PO(OH)_2CH_3 \rightarrow [TS_3]^{\dagger} \rightarrow PO(OH)CH_2+H_2O \quad (R3)$$

$$PO(OH)_2CH_3 \rightarrow [TS_4]^{\dagger} \rightarrow PO(OH)+CH_3OH \quad (R4)$$

$$PO(OH)_2CH_3+OH^{\bullet} \rightarrow [TS_5]^{\dagger} \rightarrow PO(OH)_2CH_2^{\bullet}+H_2O \quad (R5)$$

$$PO(OH)_2CH_3+OH^{\bullet} \rightarrow [TS_6]^{\dagger} \rightarrow PO(O^{\bullet})OHCH_3+H_2O \quad (R6)$$

$$PO(OH)_2CH_3+OH^{\bullet} \rightarrow [TS_7]^{\dagger} \rightarrow PO^{\bullet}(OH)_3CH_3 \quad (R7)$$

$$PO^{\bullet}(OH)_3CH_3 \rightarrow [TS_8]^{\dagger} \rightarrow PO(OH)_3+CH_3^{\bullet} \quad (R8)$$

$$PO(OH)_3 \rightarrow [TS_9] \rightarrow PO_2OH+H_2O \quad (R9)$$

$$PO(OH)_3+H^{\bullet} \rightarrow [TS_{10}]^{\dagger} \rightarrow P^{\bullet}O(OH)_2+H_2O \quad (R10)$$

$$PO(OH)_3+H^{\bullet} \rightarrow [TS_{11}]^{\dagger} \rightarrow P^{\bullet}(OH)_4 \quad (R11)$$

$$P^{\bullet}(OH)_4 \rightarrow [TS_{12}]^{\dagger} \rightarrow P^{\bullet}O(OH)_2+H_2O \quad (R12)$$

$$PO_2OH+H^{\bullet} \rightarrow [TS_{13}]^{\dagger} \rightarrow P^{\bullet}O(OH)_2 \quad (R13)$$

$$P^{\bullet}O(OH)_2 + O_2 \rightarrow [TS_{14}]^{\dagger} \rightarrow PO_2OH + HO_2^{\bullet} \qquad \text{(R14)}$$

These fourteen reactions were chosen either to evaluate their possible importance in the MPA oxidation mechanism or to compare predicted TST rate constants to available estimated rate constants from literature. Many of these reactions involve new pathways and intermediates that have not been previously examined in the literature, including the $PO(OH)_2CH_2^{\bullet}$ and $PO(O^{\bullet})OHCH_3$ intermediates.

## 4.2 Method Choice and Calculations

All *ab initio* molecular orbital theory calculations were performed using Gaussian 98 software (Frisch *et al.*, 1998). The energies of the reactants, products and transition states were calculated using the CBS-Q method (Montgomery *et al.*, 1994; Ochterski *et al.*, 1996). The CBS-Q method was chosen because it is one of the most accurate compound methods which is aimed to predict reasonably accurate atomization energies of molecules. Petersson *et al.* (1998) compared the deviations of model predictions for heats of formation and found that the CBS-Q method had the lowest root mean square deviation of all the methods compared, including the G2, MP2, and CBS-4 methods. In the CBS-Q method, geometries were first optimized and were characterized at the HF/6-31g(d') level using their vibrational frequencies and rotational constants. Geometries were then reoptimized at the MP2/6-31g(d') level. The base energy in the CBS-Q method was calculated at the MP2 level with a large basis set and energy corrections were done at varying levels (MP3, MP4, QCISD(T)) using relatively smaller basis sets to account for higher order correlation effects and were extrapolated to obtain the complete basis set limit (Foresman and Frisch, 1996). For comparison, computations were also made for MPA, phosphoric acid, and $PO^{\bullet}(OH)_3CH_3$ using the CBS-QB3 method which optimizes the geometries

at the density functional theory level (B3LYP/CBSB7) and the higher order correlation energy was computed using the coupled cluster methodology rather than QCISD(T).

Thermochemical values for all stable structures and transition states were calculated and compared to literature values, when available. Heats of formation ($\Delta H_f^o$) were calculated by the standard atomization method of Nicolaides *et al.* (1996). The equation used to calculate $\Delta H_f^o$(0 K) for MPA is shown below as an example.

$$\begin{aligned}&\Delta H_f^o(\mathrm{PO(OH)_2CH_3},0\mathrm{K}) = \Delta H_{f,\exp}^o(\mathrm{P},0\mathrm{K}) + \Delta H_{f,\exp}^o(\mathrm{C},0\mathrm{K}) \\ &+3\Delta H_{f,\exp}^o(\mathrm{O},0\mathrm{K}) + 5\Delta H_{f,\exp}^o(\mathrm{H},0\mathrm{K}) + \\ &\left[\begin{array}{l}\mathrm{CBS\text{-}Q_0(PO(OH)_2CH_3)} - \mathrm{CBS\text{-}Q_0(P)} \\ -\mathrm{CBS\text{-}Q_0(C)} - 3\mathrm{CBS\text{-}Q_0(O)} - 5\mathrm{CBS\text{-}Q_0(H)}\end{array}\right] \times 627.5095\end{aligned} \tag{4-1}$$

The $\Delta H_{f,exp}^o$(0 K) values for the atoms in kcal/mol were taken from the JANAF thermochemical tables (Chase *et al.*, 1985a, 1985b). The CBS-$Q_0$ energies for the atoms and MPA were calculated at 0 K in hartree/particle, so the conversion factor of 627.5095 kcal/mol/hartree was included. To calculate the $\Delta H_f^o$(298 K), the following equation was used that includes the thermal corrections.

$$\begin{aligned}&\Delta H_f^o(\mathrm{PO(OH)_2CH_3},298\mathrm{K}) = \Delta H_f^o(\mathrm{PO(OH)_2CH_3},0\mathrm{K}) \\ &+ \int_{0K}^{298K} Cp^o(\mathrm{PO(OH)_2CH_3})dT + \left(H_0 - H_{298}\right)_{\exp,P} + \left(H_0 - H_{298}\right)_{\exp,C} \\ &+3\left(H_0 - H_{298}\right)_{\exp,O} + 5\left(H_0 - H_{298}\right)_{\exp,H} + \sum_i SOC_i + \sum_j BAC_j\end{aligned} \tag{4-2}$$

The experimental thermal corrections for the atoms, $(H_0\text{-}H_{298})_{exp}$, were taken from the JANAF thermochemical tables (Chase *et al.*, 1985a, 1985b). The ideal gas heat capacity ($C_p^o$) for MPA was calculated using the equations from Lay *et al.* (1995) as detailed below in Equations 4-7 to 4-11. To provide a more accurate estimate of $\Delta H_f^o$(298 K), spin-orbit interactions (SOC) for the atoms and bond additivity corrections (BAC) were included from Petersson *et al.* (1998). The spin-orbit atomic lowerings were 0.0847 for carbon and 0.2230 kcal/mol for oxygen. The bond

additivity corrections used for the compounds in these calculations were -0.11 kcal/mol for C-H bonds, 0.02 kcal/mol for O-H bonds, 0.33 kcal/mol for C-O bonds, and 0.55 kcal/mol for C=O bonds (Petersson *et al.*, 1998). Due to the limited benchmark calculations on phosphorus-containing compounds using the CBS-Q method, bond additivity corrections for P-O and P-C bonds could not be included.

The ideal gas state entropies ($S^o(T)$) and heat capacities ($C_p^o(T)$) were calculated within the rigid rotor harmonic oscillator approximation using the equations from Lay *et al.* (1995) shown below for stable molecules.

$$S^o(T) = S^o(\text{trans}) + S^o(\text{ext-rot}) + \sum_{j=1}^{s} S_j^o(\text{vib}) + \sum_{n=1}^{r} S_n^o(\text{int-rot}) \tag{4-3}$$

$$S^o(\text{trans}) = \frac{5}{2}R + R\ln\left[\left(\frac{2\pi m k_B T}{h^2}\right)^{3/2}\left(\frac{RT}{p^o N_A}\right)\right] \tag{4-4}$$

$$S^o(\text{ext-rot}) = \frac{3}{2}R + R\ln\left[\left(\frac{\pi^{1/2}}{\sigma_{ext}}\right)\left(\frac{8\pi^2 k_B T}{h^2}\right)^{3/2}\left(I_x I_y I_z\right)^{1/2}\right] \tag{4-5}$$

$$S_j^o(\text{vib}) = \frac{\left[\left(\frac{RTu_j}{\exp(u_j)-1}\right) + RT\ln\left(\frac{1}{1-\exp(-u_j)}\right)\right]}{T} \tag{4-6}$$

$$u_j = \frac{ch\nu_j}{k_B T} \tag{4-7}$$

$$C_p^o(T) = C_p^o(\text{trans}) + C_p^o(\text{ext-rot}) + \sum_{j=1}^{s} C_{p,j}^o(\text{vib}) + \sum_{n=1}^{r} C_{p,n}^o(\text{int-rot}) \tag{4-8}$$

$$C_p^o(\text{trans}) = \tfrac{5}{2}R \tag{4-9}$$

$$C_p^o(\text{ext-rot}) = \tfrac{3}{2}R \tag{4-10}$$

$$C_{p,j}^o(\text{vib}) = \frac{Ru_j^2 \exp(u_j)}{\left(\exp(u_j)-1\right)^2} \tag{4-11}$$

In these equations, $R$ is the ideal gas constant in cal/mol K, $m$ is the molecular mass, $k_B$ is Boltzmann's constant, $h$ is Planck's constant, $T$ is the temperature, $p^o$ is the standard pressure, $N_A$ is Avogadro's number, $\sigma_{ext}$ is the external rotational symmetry of the molecule, $I_x$, $I_y$, and $I_z$ are the principal moments of inertia, $\nu_j$ is the vibrational frequency, and $c$ is the speed of light. For linear molecules, the $C_p^o$(ext-rot) value is only equal to $R$. For radical species, there is an additional spin degeneracy contribution equal to $R\ln(g_i)$ added to the entropy, where $g_i$ is the degeneracy or multiplicity of the radical (typically equal to 2). The entropies and heat capacities were calculated using the scaled (0.91844) harmonic vibrational frequencies and the rotational constants that were both calculated at the HF/6-31g(d') level in the CBS-Q calculation.

For the internal rotation component of the heat capacity and entropy, the torsional motion around single bonds between non-hydrogen atoms was treated as a hindered rotation. In the Gaussian output, these hindered rotors were identified as low frequency harmonic vibrations. Upon visual examination of the low vibrational frequencies, the hindered rotors were identified and these vibrational frequencies were removed from the calculations and replaced as hindered internal rotations. For example, MPA had three internal rotors, two OH rotors and one $CH_3$ rotor. To calculate the internal rotation contributions to the heat capacity and entropy, the hindrance potential and the reduced moment of inertia of the rotor were required. The reduced moment of inertia of the rotor was estimated from the moment of the two groups about the axis that passes through the center of gravity of both the rotating groups. The hindrance potential was calculated by varying the specific dihedral angle from 0 to 360° in increments of 30° while optimizing the remaining geometric parameters at every point along the potential energy surface at the HF/6-31g(d') level. Hindrance potentials thus calculated for OH rotations were then fit to 5$^{th}$ order Fourier series and the hindered rotor contribution to the heat capacity and entropy was

obtained using the procedure of Sumathi *et al.* (2001). For the $CH_3$ internal rotations, the entropies and heat capacities were extrapolated from the Pitzer-Gwinn tables using the calculated hindrance potential and reduced moment of inertia (Pitzer and Gwinn, 1942). With these equations, the thermochemistry for all compounds could be calculated at different temperatures.

The reaction rate constants for reactions (R1) to (R14) were calculated using conventional transition state theory (TST). Transition state theory postulates that a transition state intermediate exists along a reaction coordinate that has a potential energy barrier that must be crossed for reaction to occur. Once a reactant crosses the transition state to form the products, it is assumed that it cannot cross back to reform the reactants. Also, it is assumed that the motion of the transition state along the reaction coordinate can be separated from other motions and treated as a translation.

From these assumptions, the TST rate expression is derived as detailed in Steinfeld *et al.* (1999). The rate expression is shown below for a bimolecular reaction.

$$k_\infty(T) = \alpha\kappa(T)\frac{N_A k_B T}{h}\frac{\left(Q/V\right)^{\dagger}}{\left(Q/V\right)_A\left(Q/V\right)_B}\exp\left(-E_0/k_B T\right) \qquad (4\text{-}12)$$

In the TST rate expression, $k_\infty$ is the TST rate constant, $k_B$ is the Boltzmann constant, $h$ is Planck's constant, $Q_A$, $Q_B$, and $Q^+$ are the partition functions for the reactants (A and B) and the transition state, $V$ is the volume per molecule, $N_A$ is Avogadro's number, $T$ is the temperature, $\kappa(T)$ is the transmission coefficient, $\alpha$ is the reaction path degeneracy, and $E_o$ is the difference in zero point energies between the transition state and the reactants in cal/molecule. To calculate the rate expression, the partition functions for the reactants and the transition state, the barrier height, $E_o$, the transmission coefficient, $\kappa(T)$, and the reaction path degeneracy are required. Since the CBS-Q energy from the Gaussian calculations already includes the zero-point energy,

the barrier height, $E_o$, is the difference in CBS-Q(0 K) energies of the reactants and the transition state.

The partition functions are separated into translational, rotational, vibrational, internal rotational, and electronic energies, as shown below.

$$Q = Q_{\text{rot}} Q_{\text{vib}} Q_{\text{elec}} Q_{\text{trans}} Q_{\text{int-rot}} \tag{4-13}$$

$$Q_{\text{rot}} = \left(\frac{\pi^{1/2}}{\sigma_{ext}}\right)\left(\frac{8\pi^2 k_B T}{h^2}\right)^{3/2} \left(I_x I_y I_z\right)^{1/2} \tag{4-14}$$

$$Q_{\text{vib}} = \prod_{j=1}^{s} \frac{1}{1-\exp(-{}^{hc\nu_j}/_{k_B T})} \tag{4-15}$$

$$\frac{Q_{\text{trans}}}{V} = \left(\frac{2\pi m k_B T}{h^2}\right)^{3/2} \tag{4-16}$$

The electronic partition function was estimated to be equal to $g_i$, the degeneracy of the molecule or transition state. For linear molecules, the rotational partition function has a simpler form that is available in Steinfeld *et al.*, 1999. The internal rotational partition was calculated from the torsional potential and reduced moment of inertia using the method of Sumathi *et al.* (2001) for OH rotors and the Pitzer-Gwinn tables for $CH_3$ rotors. All information required for calculating these partition functions from the *ab initio* calculations are included in Section 8.2 in the Appendix.

The transmission coefficient, $\kappa(T)$, was included to account for quantum mechanical tunneling effects. Tunneling effects are most important for hydrogen transfer reaction where reaction could possibly occur at energies less than the barrier height, $E_o$. The transmission coefficient was calculated using the Wigner correction shown below.

$$\kappa(T) = 1 + \frac{1}{24}\left(1.44\frac{\nu_i}{T}\right)^2 \tag{4-17}$$

Here, $\nu_i$ is the magnitude of the imaginary frequency in wavenumbers corresponding to the reaction coordinate of the transition state, calculated at the HF/6-31g(d') level and scaled by 0.8929 (Hirschfelder, 1939).

TST rate constants were calculated from Equation 4-11 at 100 K intervals from 300 to 1500 K. For the effective use of the computed TST rate constants in the MPA SCWO elementary reaction rate model developed in Chapter 5, the calculated rate constants were fit to the modified Arrhenius equation below.

$$k_\infty(T) = AT^n \exp\left(-E_a/RT\right) \tag{4-18}$$

Here, $A$ is the pre-exponential factor, $E_a$ is the activation energy in cal/mol, $n$ is an exponential parameter for the temperature to account for non-Arrhenius behavior, and $R$ is the gas constant in cal/mol K. To calculate the Arrhenius parameters, the logarithm of Equation 4-18 was employed to linearize it with respect to ln($A$), $n$ and $E_a/R$. In this form, the parameters could be regressed using the linear least squares method.

## 4.3 THERMOCHEMISTRY RESULTS

The thermochemistry of all species included in the 14 reactions studied here was determined at the CBS-Q level (see Table 4-2). All information required to calculate these thermochemical values is in Section 8.2 in the Appendix. In addition, the thermochemistry for several new species that are introduced in the new MPA SCWO mechanism in Chapter 5 are also shown in the table. The MP2/6-31g(d') geometries for the phosphorus-containing compounds in reactions R1 to R14 are displayed in Figure 4-2. The geometries for $PO^{\bullet}(OH)_3CH_3$ are presented later in Figure 4-6.

## Table 4-2: Thermochemistry calculated at the CBS-Q level

The conversion for hartree/particle to kcal/mol is 627.5095. The entropy ($S^o$) and heat capacity ($C_p^o$) are ideal gas state values. The thermochemistry for $PO^{\bullet}(OH)_3CH_3$ was calculated from CBS-QB3 energies.

| Species | $E_0$(0 K) (hartree) | $\Delta H_f^o$(298 K) (kcal/mol) | $S^o$(298 K) (cal/mol) | $C_p^o$(298 K) (cal/mol K) | $\Delta H_f^o$(298 K) (kcal/mol) Literature |
|---|---|---|---|---|---|
| $PO(OH)_2CH_3$ | -607.486491 | -217.5 | 80.0 | 25.8 | -215.9[a] |
| $PO(OH)_3$ | -643.436118 | -271.7 | 80.6 | 21.9 | -272.5[a], -283.5[b] |
| $PO(OH)_2CH_2^{\bullet}$ | -606.822611 | -165.0 | 82.4 | 25.4 | |
| $PO(O^{\bullet})OHCH_3$ | -606.798947 | -150.7 | 78.8 | 23.6 | |
| $PO^{\bullet}(OH)_3CH_3$ | -683.141469 | -212.2 | 88.5 | 31.6 | |
| $PO_2CH_3$ | -531.085522 | -118.4 | 69.8 | 15.9 | -117.9[c] |
| PO(OH) | -491.856476 | -111.1 | 62.4 | 11.6 | -110.6[d], -110.3[e] |
| $P^{\bullet}O(OH)_2$ | -567.591649 | -157.0 | 74.4 | 17.3 | -156.4[f], -158.8[g] |
| $PO_2OH$ | -567.028186 | -168.5 | 66.6 | 14.4 | -168.8[d], -167.4[e] |
| $PO(OH)_2CH_2O^{\bullet}$ | -681.944403 | -190.5 | 87.1 | 28.2 | |
| $PO(OH)_2CH_2OH$ | -682.616871 | -248.4 | 84.7 | 28.2 | |
| $PO(OH)_2CHO$ | -681.411227 | -220.1 | 88.1 | 26.0 | |
| $PO(OH)_2C^{\bullet}HOH$ | -681.976329 | -210.9 | 85.9 | 28.3 | |
| $PO(OH)_2C^{\bullet}O$ | -680.775828 | -185.4 | 88.2 | 25.7 | |
| $PO(O^{\bullet})OHCH_2OH$ | -681.900453 | -163.3 | 84.3 | 26.4 | |
| $PO(OH)CH_2$ | -531.041707 | -90.6 | 71.1 | 18.4 | -93.7[c] |
| $P^{\bullet}(OH)_4$ | -643.930739 | -217.6 | 81.2 | 25.9 | |
| $CH_4$ | -40.409579 | -18.0 | 44.4 | 8.4 | -17.9[h] |
| $CH_3^{\bullet}$ | -39.745169 | 35.0 | 56.7 | 9.9 | 35.1[h] |
| $CH_3OH$ | -115.538269 | -48.3 | 54.6 | 10.7 | -48.0[h] |
| $H_2O$ | -76.336487 | -57.7 | 44.9 | 8.0 | -57.8[h] |
| $O_2$ | -150.162728 | 0.0 | 48.8 | 7.0 | 0.0 |
| $OH^{\bullet}$ | -75.648873 | 9.2 | 42.5 | 7.0 | 8.9[h] |
| $HO_2^{\bullet}$ | -150.738149 | 3.5 | 54.5 | 8.3 | 3.0[h] |
| $H^{\bullet}$ | 0.499818 | 52.1 | 27.4 | 5.0 | 52.1[h] |

a) Melius (1997) BAC-MP4 calculations b) estimated this study from $H_3PO_4$ $\Delta H_f^{\circ}$(298K, liquid) from Chase *et al.* (1985b) and estimated $\Delta H_{vap}$(298K) from AspenPlus calculations c) Heydorn *et al.* (2003) d) Hildenbrand and Lau (1994) e) Haworth *et al.* (2002) G3X Method f) Mackie *et al.* (2002) G3X Method g) Mackie *et al.* (2002) G3X2 Method h) Burcat (2003)

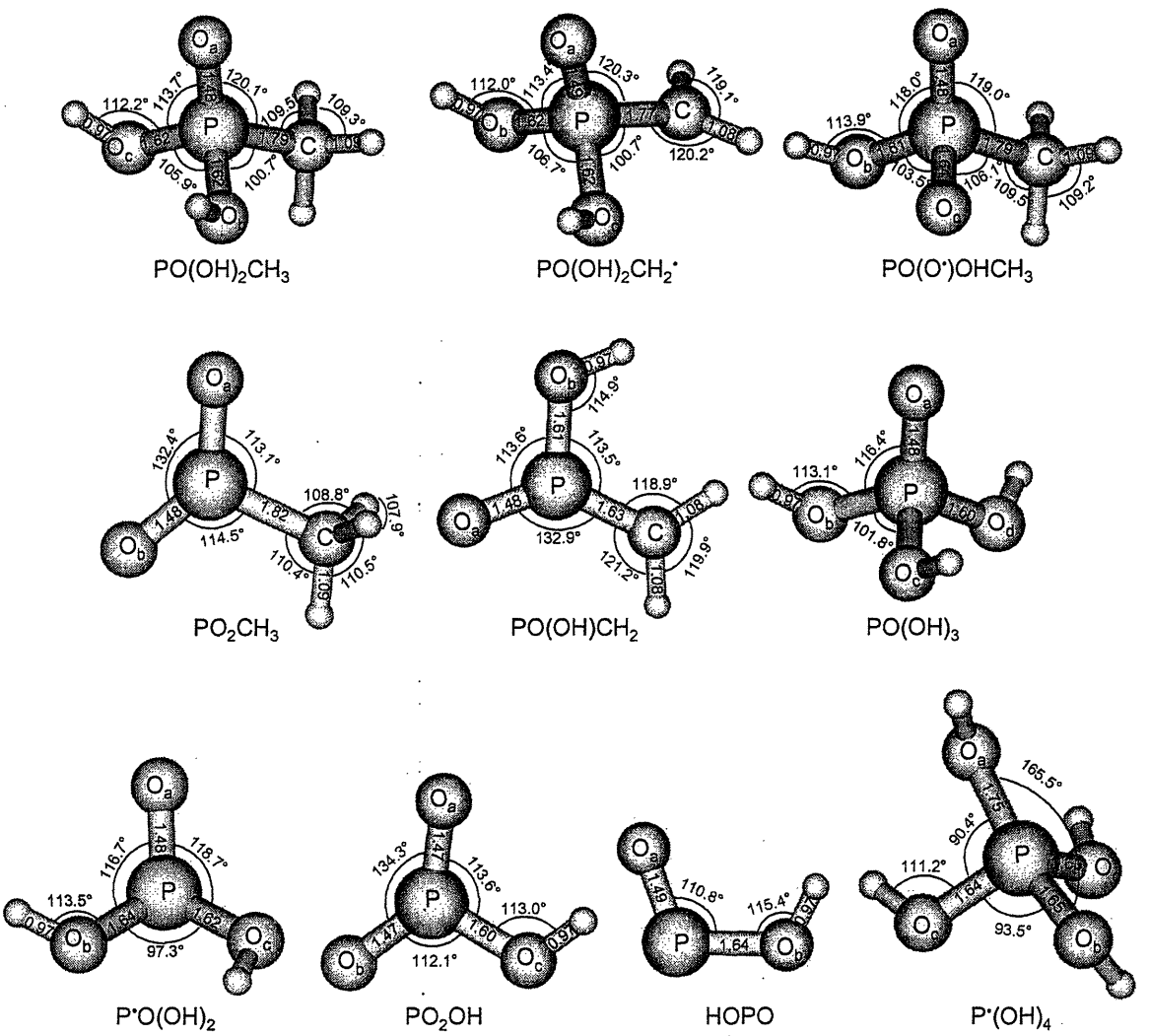


**Figure 4-2: CBS-Q optimized geometries at the MP2/6-31g(d') level for the intermediate structures included in reactions (R1) through (R14)**

The structure for $PO^{\cdot}(OH)_3CH_3$ is include in Figures 4-5 and 4-6

Thermochemical calculations were performed for several reasons. Organophosphorus gas-phase thermochemistry values have not been experimentally measured for these compounds. The most accurately predicted values available are from BAC-MP4 *ab initio* calculations by Melius performed more than five years ago (Melius, 1997). *Ab initio* thermochemistry calculations using a higher method would provide an estimate of the uncertainty in the current predicted values. Furthermore, many new organophosphorus species are introduced in the reactions presented here and in the new MPA SCWO mechanism whose thermochemistry cannot

be estimated from the group additivity values in Glaude *et al.* (2000). Additionally, comparison of the predicted CBS-Q $\Delta H_f^o$(298 K) values with those from literature can help to assess the accuracy of the CBS-Q calculation method for predicting the atomization energies of phosphorus-containing compounds.

The CBS-Q $\Delta H_f^o$(298 K) for MPA is compared with the BAC-MP4 value from Melius in Table 4-2 (Melius, 1997). The CBS-Q heat of formation is 1.6 kcal/mol less than the BAC-MP4 value, well within the calculation error of these two methods. The vapor phase $\Delta H_f^o$(298 K) values for phosphoric acid calculated from CBS-Q and BAC-MP4 methods agree within 1 kcal/mol of each other, showing good agreement between the BAC-MP4 and CBS-Q calculations. The $\Delta H_f^o$(298 K) for phosphoric acid has been measured in the liquid phase to be -303.7 kcal/mol, 32 kcal/mol less than the calculated gas phase $\Delta H_f^o$(298 K) value (Chase *et al.*, 1984). Adding an estimated heat of vaporization for phosphoric acid of 22 kcal/mol to the experimental liquid-phase $\Delta H_f^o$(298 K) value results in an estimated gas phase $\Delta H_f^o$(298 K) of -283.5 kcal/mol, in much closer agreement with the calculated CBS-Q gas phase value. In addition to Melius' BAC-MP4 calculations, many other calculated gas-phase $\Delta H_f^o$(298 K) values for phosphoric acid presented by Glaude *et al.* (2000) agree with the CBS-Q value.

The CBS-QB3 method was used to calculate $\Delta H_f^o$(298 K) values for MPA and phosphoric acid and compared to values generated by CBS-Q calculations. The CBS-QB3 $\Delta H_f^o$(298 K) value for MPA is -218.9 kcal/mol, compared to -217.5 kcal/mol for CBS-Q; and the phosphoric acid CBS-QB3 $\Delta H_f^o$(298 K) value is -273.2 kcal/mol, as compared to -271.7 kcal/mol from CBS-Q. Both differ by approximately 1.5 kcal/mol from each other, suggesting the extent of uncertainty associated with these numbers.

In their *ab initio* study on phosphorus oxides, Mackie *et al.* (2002) and Haworth *et al.* (2002) calculated thermochemical values for many phosphorus-containing compounds using another family of compounds methods, namely G3X and G3X2. Comparison of their calculated values with our CBS-Q $\Delta H_f^o$(298 K) values for $P^{\bullet}O(OH)_2$, PO(OH), and $PO_2OH$ shows excellent agreement within < 1 kcal/mol (Table 4-2).

Given the strong agreement between estimated $\Delta H_f^o$(298 K) values from the CBS-Q method and the available heats of formation for both organophosphorus and phosphorus oxide chemistry from the literature, the CBS-Q method appears to be an appropriate choice to calculate the geometries and energies of phosphorus-containing species.

Bond dissociation energies (BDE) were calculated at 298 K for four bond types in the MPA molecule, C-H, O-H, P-$CH_3$, and P-OH and compared to similar bond types (Table 4-3). Knowledge of MPA bond energies provides insight into selecting similar chemistry from which to estimate MPA reaction rates. Bond dissocation energies were calculated using the following equation.

$$BDE(298\text{ K,X-Y}) = \Delta H_f^o(298\text{ K,X}^{\bullet}) + \Delta H_f^o(298\text{ K,Y}^{\bullet}) - \Delta H_f^o(298\text{ K,XY}) \qquad (4\text{-}19)$$

In MPA, the O-H bond strength is 14.3 kcal/mol stronger than that of the C-H bond. The C-H bond strength for MPA is similar to those for other hydrocarbons in the literature, such as methanol and methane. The calculated MPA C-H bond strength is also equal to the DMMP C-H bond strength of -104.6 kcal/mol calculated by Glaude *et al.* (2002). The O-H bond strength in MPA is much higher than that of most organic alcohol compounds; its value is closer to the O-H bond strength in water. These results indicate that H abstraction from the $CH_3$ group would be energetically preferred over the OH group in MPA during oxidation.

**Table 4-3: Bond dissociation energies in kcal/mol for MPA at 298 K from CBS-Q $\Delta H_f^o$(298 K) values**

The other bond dissociation energies are from $\Delta H_f^o$(298 K) values in Burcat's thermodynamic database and the C-C bond energy for acetic acid was taken from CBS-Q calculations. Compounds with similar bond dissociation energies are italicized accordingly.

| Bond Cleavage | Energy (kcal/mol) | Bond Cleavage | Energy (kcal/mol) |
|---|---|---|---|
| **$PO(OH)_2CH_2$--H** | **104.6** | **$PO(OH)(CH_3)O$--H** | **118.9** |
| $CH(O)CH_2$--H | 97.8 | $NO_2O$--H | 101.1 |
| $CH_3CH_2$--H | 100.5 | $C_2H_5O$--H | 105.0 |
| *$(HO)CH_2$--H* | *104.1* | $CH_3O$--H | 105.1 |
| *$CH_3$--H* | *105.1* | CH(O)O--H | 106.6 |
| $NO_2CH_2$--H | 107.8 | *HO--H* | *118.8* |
| **$PO(OH)_2$--$CH_3$** | **95.5** | **$PO(OH)(CH_3)$--OH** | **120.0** |
| $NO_2$--$CH_3$ | 62.5 | $NO_2$--OH | 49.1 |
| SH--$CH_3$ | 74.4 | $CH_3$--OH | 92.0 |
| $NH_2$--$CH_3$ | 85.1 | $SO_2(OH)$--OH | 92.0 |
| $CH_3$--$CH_3$ | 90.2 | CH(O)--OH | 109.5 |
| *$C(OH)(O)$--$CH_3$* | *96.5* | $CH_3C(O)$--OH | 109.8 |

From previous organophosphorus studies, the P-C bond is very strong, being inert to acidic and basic hydrolysis with bond cleavage occuring primarily through radical mediated pathways (Cordeiro *et al.*, 1986; Schowanek and Verstraete, 1991). However, the P-C bond strength in organophosphorus compounds has not been reported in the literature. In MPA, the P-C bond strength is 95.5 kcal/mol, while the P-O bond is 24.5 kcal/mol stronger at 120.0 kcal/mol. The P-C bond strength is higher than for most other carbon containing bonds, with a bond strength almost equal to that of the C-C bond in acetic acid. The P-O bond is much stronger than other X-O bonds, such as C-O, N-O, and S-O bonds, which have bond energies ranging from 49.1 to 109.8 kcal/mol, at least 10 kcal/mol less than the P-O bond strength. It appears that the low reactivity of P-C bonds is due to factors more subtle than just the bond strength.

## 4.4 Reaction Rate Results

Reaction rate constants were calculated for reactions (R1) to (R14) using transition state theory. These reactions are grouped into three sets: set (1) for MPA unimolecular reactions (R1

to R4), set (2) for reactions on the MPA + $OH^{\bullet}$ potential surface (R5 to R8), and set (3) for reactions involving $PO(OH)_3$ and $P^{\bullet}O(OH)_2$ (R9 to R14). These three reaction sets are discussed in detail in the following separate sections.

### *4.4.1 Set 1: MPA Unimolecular Reactions*

Four different MPA unimolecular reaction pathways to stable products are presented in Figure 4-3: 1,2-elimination of water involving two OH groups ($TS_1$), 1,2-elimination of methane involving $CH_3$ and OH groups ($TS_2$), 1,2-elimination of water involving $CH_3$ and OH groups ($TS_3$), and 1,1-elimination of methanol ($TS_4$). These endothermic reactions do not form radicals, only stable products. Consequently, they would not be expected to play a significant role in radical reaction networks. However, the rate constants for reactions (R1) and (R2) have been estimated by Glaude *et al.* (2000) and calculating these rate constants could help to assess the accuracy of employing general rate estimation methods for organophophosphorus reactions.

The transition state energy, rotational constants, and vibrational frequencies along with the energy barrier and heat of reaction at $T$=0 K for each unimolecular reaction are shown in Table 4-4. Information on the internal rotation calculations for each transition state is included in Section 8.2 in the Appendix. The geometries for each transition state are shown in Figure 4-3, with the reaction coordinate being highlighted. Additionally, the modified Arrhenius parameters from the calculated TST rate constants are included in Table 4-5 along with rate constant values at typical SCW temperatures (800 K) and combustion temperatures (1500 K). The Arrhenius parameters and rate constants from Glaude *et al.* (2000) for reactions (R1) and (R2) are also included for comparison.

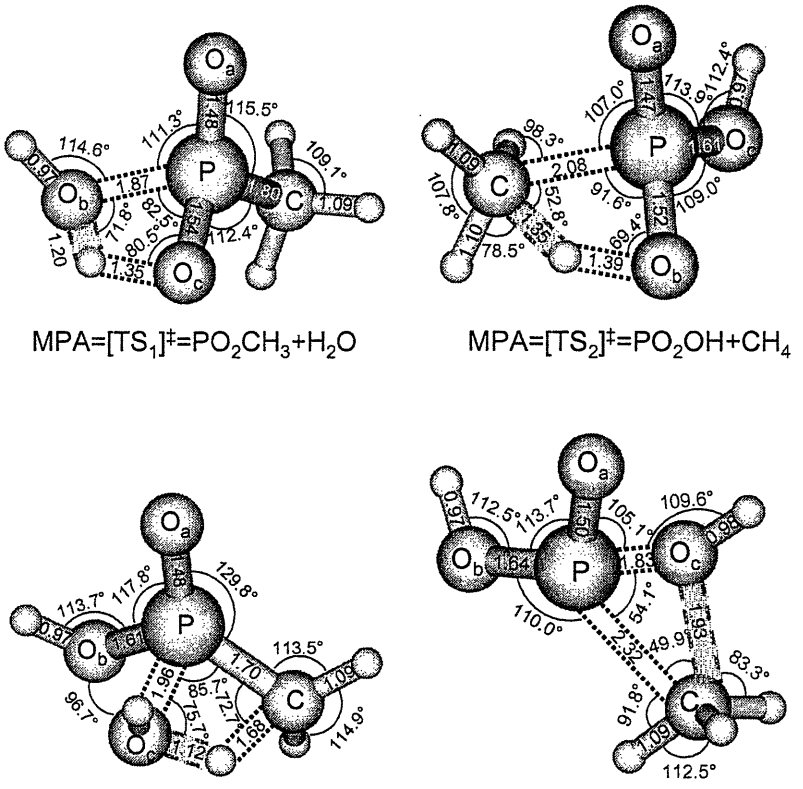


**Figure 4-3: Transition state geometries for the MPA unimolecular reaction set**
Bond lengths are in angstroms and bond angles are in degrees, optimized at the MP2/6-31g(d') level. Breaking bonds are indicated by dotted lines, while forming bonds are shown by dashed lines and the shaded area.

**Table 4-4: Transition state information for MPA unimolecular reactions**

Note: Calculated vibrational frequencies that were replaced with internal rotational values are italicized.

| Reaction | $E_{TS}$(0 K) (hartree) | $E_0$(0 K) (kcal/mol) | $\Delta H_r^\circ$(0 K) (kcal/mol) | Vibrational frequencies ($cm^{-1}$) | Rotational constants ($cm^{-1}$) |
|---|---|---|---|---|---|
| (R1) MPA=$TS_1$= $PO_2CH_3$+$H_2O$ | -607.418710 | 43.1 | 40.5 | 2016.7*i*, *151.2*, 239.2, 310.7, 369.6, 473.5, 572.7, 584.6, 754.0, 824.4, 964.5, 988.2, 1023.7, 1165.9, 1398.4, 1458.4, 1495.4, 1587.4, 1589.2, 2158.6, 3213.4, 3298.8, 3322.4, 4076.8 | 0.160<br>0.140<br>0.122 |
| (R2) MPA=$TS_2$= $PO_2OH$+$CH_4$ | -607.382463 | 65.3 | 30.6 | 1992.9*i*, *130.5*, 259.4, 347.8, 406.6, *466.8*, 479.3, 566.2, 592.8, 675.7, 838.1, 957.0, 1124.3, 1219.4, 1281.4, 1379.4, 1495.5, 1554.5, 1568.4, 1897.5, 3126.9, 3280.3, 3359.0, 4078.9 | 0.158<br>0.131<br>0.129 |
| (R3) MPA=$TS_3$= $PO(OH)CH_2$+$H_2O$ | -607.367466 | 74.7 | 68.0 | 1564.3*i*, 243.0, *278.5*, 305.1, 360.7, 401.3, 438.4, 539.4, 570.3, 710.5, 827.9, 902.0, 964.5, 970.5, 1059.8, 1134.7, 1417.2, 1493.7, 1535.5, 2147.0, 3284.3, 3367.5, 4053.8, 4080.8 | 0.154<br>0.135<br>0.129 |
| (R4) MPA=$TS_4$= $POOH$+$CH_3OH$ | -607.318267 | 105.6 | 57.6 | 754.4*i*, 86.5, 127.2, 208.4, 329.3, 409.9, 462.8, 566.7, 722.5, 824.4, 847.2, 923.3, 1087.2, 1120.9, 1314.1, 1344.5, 1546.2, 1586.4, 3332.2, 3516.4, 3532.7, 3951.5, 4061.4 | 0.213<br>0.104<br>0.089 |

**Table 4-5: MPA unimolecular reaction rate constants**

Estimated rate constants and parameters from Glaude *et al.* (2000) are included for comparison, denoted by lit. In the table, $A$ is in $s^{-1}$ and $E_a$ is in kcal/mol.

| Reaction | $A$ | $n$ | $E_a$ | $k_{TST}$($s^{-1}$) | | $A_{lit}$ | $E_{a,lit}$ | $k_{lit}$($s^{-1}$) | |
|---|---|---|---|---|---|---|---|---|---|
| | | | | 800 K | 1500 K | | | 800 K | 1500 K |
| (R1) $PO(OH)_2CH_3$= $PO_2CH_3$+$H_2O$ | $2.3\times10^{12}$ | 0.04 | 41.9 | $1.0\times10^{01}$ | $2.3\times10^{06}$ | $5.0\times10^{13}$ | 39.0 | $1.1\times10^{03}$ | $1.0\times10^{08}$ |
| (R2) $PO(OH)_2CH_3$= $PO_2OH$+$CH_4$ | $6.3\times10^{11}$ | 0.41 | 64.1 | $3.0\times10^{-05}$ | $5.9\times10^{03}$ | $6.0\times10^{11}$ | 61.0 | $1.3\times10^{-05}$ | $7.8\times10^{02}$ |
| (R3) $PO(OH)_2CH_3$= $PO(OH)CH_2$+$H_2O$ | $2.6\times10^{09}$ | 1.31 | 73.0 | $1.8\times10^{-07}$ | $8.5\times10^{02}$ | | | | |
| (R4) $PO(OH)_2CH_3$= $POOH$+$CH_3OH$ | $5.1\times10^{11}$ | 0.73 | 105.1 | $1.3\times10^{-15}$ | $5.1\times10^{-02}$ | | | | |

Reaction (R1) has the lowest energy barrier of the MPA unimolecular reactions listed in Table 4-4:

$$PO(OH)_2CH_3 \rightarrow [TS_1]^{\dagger} \rightarrow PO_2CH_3 + H_2O \quad (R1)$$

For this transition state, the dihedral angle of $O_bH$ ($O_aPO_bH$) changes from 21.3° in MPA to 106.5° in $TS_1$, resulting in a 90° difference to form the transition state. The reaction coordinate vector for the $TS_1$ transition state was identified as

$$0.26r_{P..Ob} - 0.61r_{Ob..H} + 0.70r_{Oc..H}$$

where the reaction coordinate involves the simultaneous cleavage of the P-$O_b$ and $O_c$-H bonds together with the formation of the $O_b$-H bond. The P-$O_b$ bond length increases from 1.62 Å in MPA to 1.87 Å in $TS_1$, while the $O_c$-H bond length increases to 1.35 Å and the $O_b$-H bond is calculated to be 1.20 Å. Additionally, the P-$O_c$ bond length decreases from 1.62 Å to 1.54 Å since this bond acquires a double bond character during the course of this reaction.

Transition state theory rate constants were calculated and compared to estimated rate constants from Glaude *et al.* (2000) (see Table 4-5). Glaude *et al.* estimated this rate constant by comparison to water elimination from an organic compound through a four-centered transition state (Benson, 1976). Glaude *et al.*'s estimated rate constant is a factor of approximately 50 to 100 times larger than the rate constant calculated presently. Their activation energy was estimated by assuming it was equal to the heat of reaction, which appears to be an accurate assumption for this reaction given that the calculated energy barrier, $E_0$, is 43.1 kcal/mol and the $\Delta H_r^o$(0 K) is 40.5 kcal/mol for this reaction. However, the estimated pre-exponential factor is ~20 times higher than for our computed TST rate constant. The pre-exponential factor captures the entropy change between the reactant and transition state, which differs between a five-centered phosphorus compound and a four-centered carbon compound. These results indicate that pre-exponential factors from carbon compounds are probably not suitable for estimating rate constants for organophosphorus elimination reactions.

The second MPA unimolecular reaction (R2) has the lowest heat of reaction of the unimolecular reaction set due to the stability of its products; however, its activation barrier is higher than that for $TS_1$ (see Table 4-4).

$$PO(OH)_2CH_3 \rightarrow [TS_2]^{\dagger} \rightarrow PO_2OH+CH_4 \qquad (R2)$$

The higher activation barrier implies that the reverse reaction also has a substantial barrier of ~30 kcal/mol, as compared to reaction (R1) in Table 4-4 where the reverse reaction has a very small barrier. This higher activation barrier is primarily due to the difference between the O-H and C-H bond strengths. The reaction coordinate vector for this transition state was

$$0.39r_{P..C} + 0.60r_{Ob..H} - 0.34r_{C..H}$$

For this transition state, P-C bond cleavage occurs as the hydrogen is abstracted from the $O_bH$ group by the $CH_3$ group. The P-C bond length increases from 1.79 Å to 2.08 Å, while the $O_b$-H bond length increases to 1.39 Å and the forming C-H bond length is 1.35 Å.

The calculated reaction rate constant is shown in Table 4-5 and is about 3 to 6 orders of magnitude less than $k_1$ in this temperature range, due to both a lower pre-exponential factor and a higher activation energy. The calculated rate constant agrees with Glaude *et al.*'s estimated rate constant for this reaction to within a multiple of 2 to 8, well within the uncertainties of these values. The close agreement between the calculated and estimated rate constants for this reaction does show that estimation of organophosphorus rate constants can provide precise predictions; however, the difficulty is knowing *a priori* which estimated rate constants are correct in the organophosphorus combustion mechanisms.

In the MPA unimolecular reaction (R3), the transition state ($TS_3$) is formed by abstracting a hydrogen from the $CH_3$ group by the $O_cH$ substituent (see Figure 4-3).

$$PO(OH)_2CH_3 \rightarrow [TS_3]^{\dagger} \rightarrow PO(OH)CH_2+H_2O \qquad (R3)$$

From the values in Table 4-4, reaction (R3) is highly endothermic with a $\Delta H_r^o$(0 K) of 68 kcal/mol and has an activation barrier of 74.7 kcal/mol. This reaction is more endothermic due to the P=$CH_2$ double bond being less stable than the P=O double bond that is formed in $TS_1$ and $TS_2$. The reaction coordinate vector for this transition state is:

$$0.38r_{P..Oc} + 0.70r_{C..H} - 0.51r_{Oc..H}$$

where the P-$O_c$ bond length increases to 1.96 Å, while the C-H bond length increases to 1.68 Å and the $O_c$-H bond length becomes 1.12 Å. The reaction rate constant for (R3) is shown in Table 4-5 and is 3 to 8 orders of magnitude less than $k_1$, where dehydration occurs by hydrogen abstraction between the two OH's. Experimental evidence of the existence of the $PO(OH)CH_2$ intermediate has been recently reported from an MPA precursor by Heydorn *et al.* (2003).

The fourth MPA unimolecular reaction (R4) is simultaneous cleavage of the P-C and P-O bonds to form methanol and would be expected to proceed slowly.

$$PO(OH)_2CH_3 \rightarrow [TS_4]^{\dagger} \rightarrow PO(OH) + CH_3OH \qquad \text{(R4)}$$

From Table 4-4, the $\Delta H_r^o$(0 K) for this reaction is 57.6 kcal/mol and the activation barrier is very high at 105.6 kcal/mol. Thus, the reaction has large activation barriers (greater than 48 kcal/mol) in both the forward and reverse directions. The geometry for $TS_4$ is shown in Figure 4-3 and the reaction coordinate vector was identified as

$$-0.20r_{P..Oc} - 0.38r_{P..C} + 0.60r_{C..Oc}$$

The rate constant parameters for (R4) are shown in Table 4-5 and are much lower than those for the other MPA unimolecular reactions, as expected. The reaction involving a constrained three-centered transition state is both energetically and entropically unfavorable and is expected to proceed slower than the reactions, (R1) to (R3), involving a four-centered transition state.

### *4.4.2 Set 2: Reactions on the MPA + OH• Potential Surface*

A key goal in examining reaction set 2 was to establish possible reaction pathways for MPA with the OH• radical. To accomplish this, the accuracy of the MPA + OH• rate constants for reaction (3a) from Glaude *et al.* (2000) and Korobeinichev *et al.* (2000) were examined and additional pathways on the MPA + OH• potential surface were explored. Three different reaction pathways between MPA and OH• were studied: hydrogen abstraction from MPA's $CH_3$ group by an OH• (R5), hydrogen abstraction from MPA's OH group by an OH• (R6), or direct addition of an OH• to the phosphorus center to form a five-centered intermediate ($PO^{\bullet}(OH)_3CH_3$) (R7). Additionally, once $PO^{\bullet}(OH)_3CH_3$ is formed, it dissociates to $PO(OH)_3$ and $CH_3^{\bullet}$ (R8). The geometries for the hydrogen abstraction transition states are shown in Figure 4-4 and the energy, vibrational frequencies, and rotational constants for these two transition states are in Table 4-6 along with the activation barrier and heat of reaction. The calculated rate constants and modified Arrhenius parameters for the hydrogen abstraction reactions are included in Table 4-7. Discussion of the transition states for reactions (R7) and (R8) through the $PO^{\bullet}(OH)_3CH_3$ is presented separately.

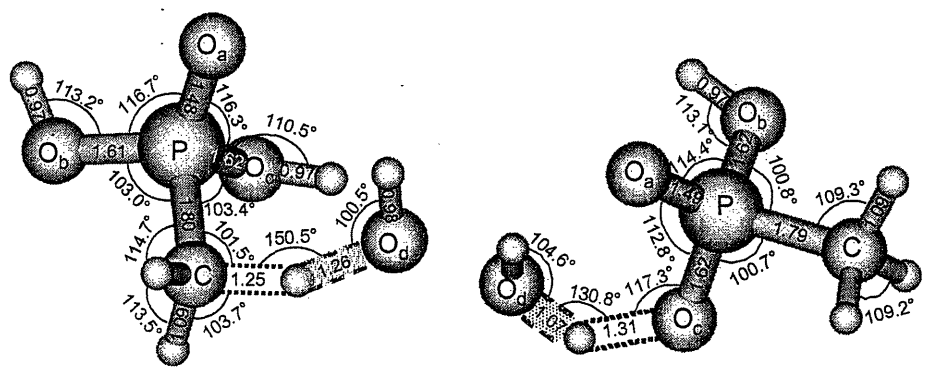


**Figure 4-4: Transition state geometries for the MPA + OH hydrogen abstraction reactions**
Bond lengths are in angstroms and bond angles are in degrees, optimized at the MP2/6-31g(d') level. Breaking bonds are indicated by dotted lines, while forming bonds are shown by dashed lines and the shaded area.

**Table 4-6: Transition state information for MPA + OH hydrogen abstraction reactions**
Calculated vibrational frequencies that were replaced with internal rotational values are italicized.

| Reaction | $E_{TS}$ (0 K) (hartree) | $E_0$ (0 K) (kcal/mol) | $\Delta H_r^o$(0 K) (kcal/mol) | Vibrational frequencies ($cm^{-1}$) | Rotational constants ($cm^{-1}$) |
|---|---|---|---|---|---|
| (R5) MPA+OH$^{\bullet}$=TS$_5$= PO(OH)$_2$CH$_2^{\bullet}$+H$_2$O | -683.133610 | 1.1 | -14.9 | 3277.5i, *34.0*, 103.5, *187.7*, *246.2*, 304.6, *314.1*, 388.9, 428.2, 442.2, 484.3, 488.5, 593.0, 790.9, 877.2, 939.6, 954.5, 1024.4, 1083.8, 1110.5, 1128.3, 1240.1, 1387.1, 1542.6, 1652.0, 3282.2, 3375.8, 4016.0, 4081.7, 4090.3 | 0.142<br>0.064<br>0.062 |
| (R6) MPA+OH$^{\bullet}$=TS$_6$= PO(O$^{\bullet}$)OHCH$_3$+H$_2$O | -683.130444 | 3.1 | 0.0 | 5440*i*, *54.2*, 168.6, *186.8*, *236.4*, 283.1, 298.7, 399.4, 441.6, 455.4, 480.8, 583.9, 682.4, 791.7, 906.3, 949.6, 1011.1, 1040.5, 1092.1, 1118.2, 1363.6, 1498.4, 1587.7, 1589.0, 1697.3, 3215.9, 3307.9, 3314.2, 3970.9, 4084.1 | 0.145<br>0.068<br>0.065 |

**Table 4-7: Rate constants for MPA + OH hydrogen abstraction reactions**

| Reaction | $A$ ($cm^3(mol\ s)^{-1}$) | $n$ | $E_a$ (kcal/mol) | $k_{TST}$($cm^3(mol\ s)^{-1}$) 800 K | 1500 K |
|---|---|---|---|---|---|
| (R5) PO(OH)$_2$CH$_3$+OH$^{\bullet}$= PO(OH)$_2$CH$_2^{\bullet}$+H$_2$O | $1.0\times10^{06}$ | 2.39 | -1.14 | $1.8\times10^{13}$ | $5.8\times10^{13}$ |
| (R6) PO(OH)$_2$CH$_3$+OH$^{\bullet}$= PO(O$^{\bullet}$)OHCH$_3$+H$_2$O | $2.1\times10^{04}$ | 2.40 | 0.20 | $1.8\times10^{11}$ | $8.4\times10^{11}$ |

Hydrogen abstraction from MPA's $CH_3$ group by an $OH^{\bullet}$ to form $PO(OH)_2CH_2^{\bullet}$ and water via reaction (R5) is exothermic with a $\Delta H_r^o$(0 K) of -14.9 kcal/mol and has a low activation barrier of 1.1 kcal/mol.

$$PO(OH)_2CH_3 + OH^{\bullet} \rightarrow [TS_5]^{\dagger} \rightarrow PO(OH)_2CH_2^{\bullet} + H_2O \qquad \text{(R5)}$$

Reaction (R5) would proceed quite rapidly with its importance in an organophosphorus radical network dependent on the reactivity of the $PO(OH)_2CH_2^{\bullet}$ intermediate. The reaction coordinate vector for this transition state was identified as

$$-0.58r_{C..H} + 0.80r_{Od..H}$$

For $TS_5$, the C-H bond length increases to 1.25 Å and the $O_d$-H bond length becomes 1.26 Å. The P-C bond length is unchanged since the phosphorus center still has 5 bonds in the product, $PO(OH)_2CH_2^{\bullet}$. From the $PO(OH)_2CH_2^{\bullet}$ and $PO(OH)_2CH_3$ geometries in Figure 4-2, the P-$CH_2$ and P-$CH_3$ bond lengths are approximately equal.

The calculated rate constant for $TS_5$ is $1.8 \times 10^{13}$ $cm^3(mol\ s)^{-1}$ at $T$=800 K, shown in Table 4-7. The activation energy, $E_a$, is negative in Table 4-7 because of the three parameter fit for this rate constant; however, this reaction does have a positive activation barrier of 1.1 kcal/mol (Table 4-6). Although this reaction rate has not been previously estimated, the hydrogen abstraction rate from DMMP's methyl group by an $OH^{\bullet}$ was estimated by Glaude *et al.* (2000).

$$PO(OCH_3)_2CH_3 + OH^{\bullet} \rightarrow PO(OCH_3)_2CH_2^{\bullet} + H_2O \qquad \text{(R6a)}$$

The estimated parameters for the DMMP rate constant are $A$=$3.6 \times 10^6$, $n$=2, and $E_a$=3.45 kcal/mol giving a value of $2.6 \times 10^{11}$ $cm^3(mol\ s)^{-1}$ at 800 K, seventy times slower than the rate constant calculated presently. Information on how this rate constant was estimated by Glaude *et al.* (2000) was unavailable.

Hydrogen abstraction from MPA's $O_cH$ group via reaction (R6) was also examined to determine if this reaction would be competitive with hydrogen abstraction from the $CH_3$ group (R5).

$$PO(OH)_2CH_3 + OH^{\bullet} \rightarrow [TS_6]^{\dagger} \rightarrow PO(O^{\bullet})OHCH_3 + H_2O \qquad \text{(R6)}$$

Reaction (R6) has a $\Delta H_r^o$(0 K)=0 kcal/mol since the O-H bond strengths in MPA and water are approximately equal, as shown in Table 4-3. The heat of reaction being zero, along with no significant change in the entropy between the reactants and products, leads to this reversible reaction having an equilibrium constant approximately equal to one. This reaction has an

activation barrier of 3.1 kcal/mol, 2 kcal/mol higher than that for $TS_5$, but still relatively small. The reaction coordinate vector for this transition state is

$$0.72r_{Oc..H} - 0.57r_{Od..H}$$

This reaction coordinate involves the stretching of the $O_c$-H bond to 1.31 Å and the formation of the $O_d$-H bond at 1.07 Å. The imaginary frequency was overestimated to be 5440*i* $cm^{-1}$ for this transition state (Table 4-6). To better estimate the tunneling correction, a more reasonable imaginary frequency (4642*i* $cm^{-1}$) from the CBS-Q calculations of a similar transition state for the reaction, $H_2O + OH^{\bullet}$ to form $OH^{\bullet}$ and $H_2O$, was used. Since the O-H bond strength in water and MPA are approximately equal, this is an appropriate choice for a similar transition state. At 800 K, the tunneling correction is 2.15 using the 4642 $cm^{-1}$ imaginary frequency, while it would be 3.32 with the 5440 $cm^{-1}$ imaginary frequency.

The rate constant parameters for (R6) are shown in Table 4-7 with $k_6$(800 K)=1.8x$10^{11}$ $cm^3(mol\ s)^{-1}$, as compared to $k_5$(800 K)=1.8x$10^{13}$ $cm^3(mol\ s)^{-1}$ for hydrogen abstraction from the methyl group. The branching between reactions 5 and 6 at 800 K was 100:1 with reaction 6 being a minor pathway. In supercritical water, both reactions (R5) and (R6) achieve equilibrium due to the high water concentrations (approximately 4 to 5 M) and the fast reaction rates. Reaction through these two pathways would depend on the reactivities of the two intermediates, $PO(OH)_2CH_2^{\bullet}$ and $PO(O^{\bullet})OHCH_3$.

The final two reactions in the MPA + $OH^{\bullet}$ reaction set were examined in an effort to calculate the rate constant for the only bimolecular MPA reaction in the the DMMP combustion mechanisms (Korobeinichev *et al.*, 2000 and Glaude *et al.*, 2000).

$$PO(OH)_2CH_3 + OH^{\bullet} \rightarrow PO(OH)_3 + CH_3^{\bullet} \qquad \text{(R3a)}$$

The transition state for reaction (R3a) would concurrently form a P-O bond and cleave a P-C bond. All attempts to find a transition state involving simultaneous P-O bond formation and P-C

bond cleavage proved futile. Instead, a five-centered intermediate ($PO^{\bullet}(OH)_3CH_3$) was identified through which reactions (R7) and (R8) could occur to react through the same overall pathway as reaction (R3a).

$$PO(OH)_2CH_3 + OH^{\bullet} \rightarrow [TS_7]^{\dagger} \rightarrow PO^{\bullet}(OH)_3CH_3 \quad (R7)$$

$$PO^{\bullet}(OH)_3CH_3 \rightarrow [TS_8]^{\dagger} \rightarrow PO(OH)_3 + CH_3^{\bullet} \quad (R8)$$

To calculate rate constants for reactions (R7) and (R8), the lowest energy conformation for $PO^{\bullet}(OH)_3CH_3$ was chosen. Four different trigonal bipyramidal conformations for the $PO^{\bullet}(OH)_3CH_3$ intermediate were identified with two apical bonds and three equatorial bonds each, as shown in Figure 4-5. The apical bonds are longer than the equatorial bonds, indicating that these bonds are weaker than the equatorial bonds, as found in previous organophosphorus studies (Quin, 2000). When the $PO^{\bullet}(OH)_3CH_3$ structure is formed, the P=O bond in MPA becomes a P-O$^{\bullet}$ bond which destabilizes this very strong bond, while an additional P-OH bond is formed which would stabilize this compound. The $PO^{\bullet}(OH)_3CH_3$ energy depends on the stability and location of the P-O$^{\bullet}$ and P-OH bonds.

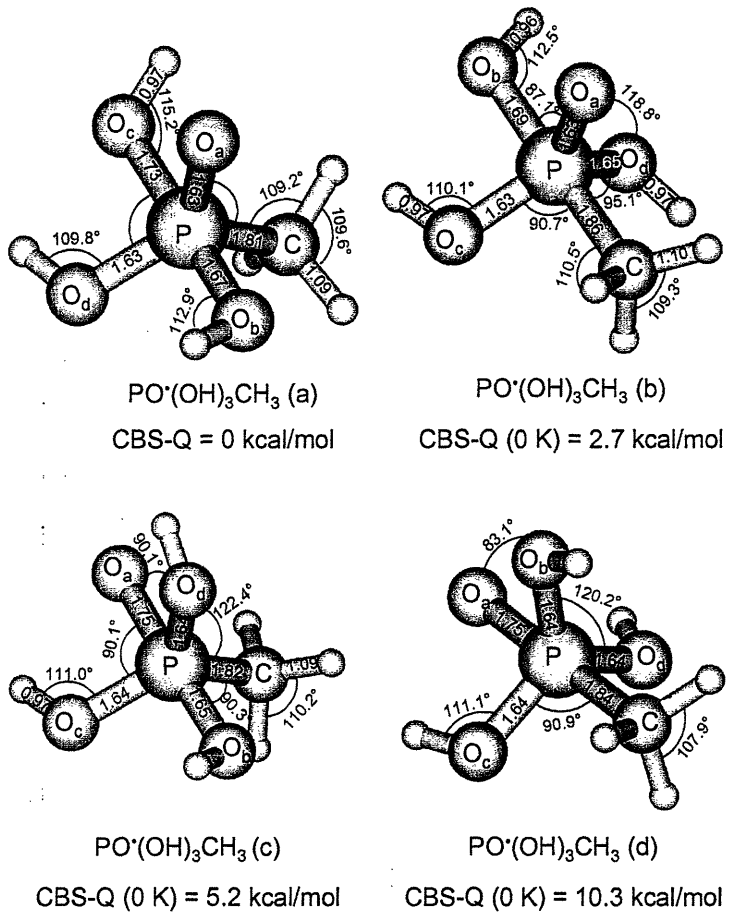


**Figure 4-5: Optimized geometries for four conformations of $PO^{\bullet}(OH)_3CH_3$ intermediate**
The CBS-Q (0 K) energies are normalized to the minimum energy conformation, $PO^{\bullet}(OH)_3CH_3$ (a). The CBS-Q (0 K) energy for $PO^{\bullet}(OH)_3CH_3$ (a) is -683.134384 hartree/particle.

As shown in Figure 4-5, the structure, $PO^{\bullet}(OH)_3CH_3$ (a), has the lowest energy with the other three conformations having energies 2 to 10 kcal/mol higher at $T$=0 K. $PO^{\bullet}(OH)_3CH_3$(a) has the lowest energy conformation because the apical bonds are two P-OH bonds and the equatorial bonds are P-O$^{\bullet}$, P-OH, and P-$CH_3$. The two lowest energy conformations, $PO^{\bullet}(OH)_3CH_3$ (a) and (b), have the P-O$^{\bullet}$ bond with the odd electron in the equatorial position, while the higher energy conformations have the odd electron in the axial position. The position of the P-O$^{\bullet}$ bond is important because the P=O bond is the strongest bond in this structure and thus, the lowest energy conformation would have a shorter, stronger P-O$^{\bullet}$ bond.

$PO^{\bullet}(OH)_3CH_3$(a) is more stable than $PO^{\bullet}(OH)_3CH_3$ (b) because the more electronegative substituent is favored for the apical bond due to the polarizability of the apical site (Quin, 2000).

Two transition states, $TS_7$ and $TS_8$, were identified along this reaction coordinate with bond cleavage/formation occuring at the weaker, apical bonds, as shown in Figure 4-6 from calculations using both the CBS-Q and CBS-QB3 methods. From Table 4-8 and Figure 4-7, the CBS-Q energies along this reaction coordinate for MPA+$OH^{\bullet}$, $TS_7$, $PO^{\bullet}(OH)_3CH_3$, and $TS_8$ are all within 1 kcal/mol of each other. However, the P-O and P-C bond lengths, and consequently, their bond strengths and stabilization vary a lot among the structures, suggesting some unusual energetics. In Figure 4-6, the CBS-Q P-$O^{\bullet}$ bond length in both transition states is approximately 1.55 Å, but it is 1.63 Å in the $PO^{\bullet}(OH)_3CH_3$ structure. Also, from the potential energy surface in Figure 4-7, both $TS_7$ and $TS_8$ have lower CBS-Q energies than $PO^{\bullet}(OH)_3CH_3$, leading to negative energy barriers. Interestingly, comparison of the relative energetics of $TS_7$, $PO^{\bullet}(OH)_3CH_3$, and $TS_8$ at various component levels of CBS-Q methodology viz., QCISD(T)/6-31+g(d'), MP4SDQ/CBSB4, and MP2/CBSB3 reveals that $PO^{\bullet}(OH)_3CH_3$ is energetically lower than $TS_7$ and $TS_8$ at each of these levels (Table 4-8).

Not only does the $PO^{\bullet}(OH)_3CH_3$ intermediate have a higher energy than the two transition states, $TS_7$ and $TS_8$, but it also has a higher energy than MPA + $OH^{\bullet}$ at the CBS-Q level. For reaction to occur through this intermediate, the $PO^{\bullet}(OH)_3CH_3$ energy would be expected to be stabilized as compared to the MPA + $OH^{\bullet}$ energy due to the large decrease in entropy upon formation of $PO^{\bullet}(OH)_3CH_3$. If the reaction is endothermic and the entropy decreases upon reaction, the Gibbs free energy of reaction is positive and the equilibrium constant favors the reactants, MPA and $OH^{\bullet}$. Due to the negative transition state barriers and

$PO^{\bullet}(OH)_3CH_3$ not being stabilized, rate constants using the CBS-Q calculations were not calculated for reactions (R7) and (R8).

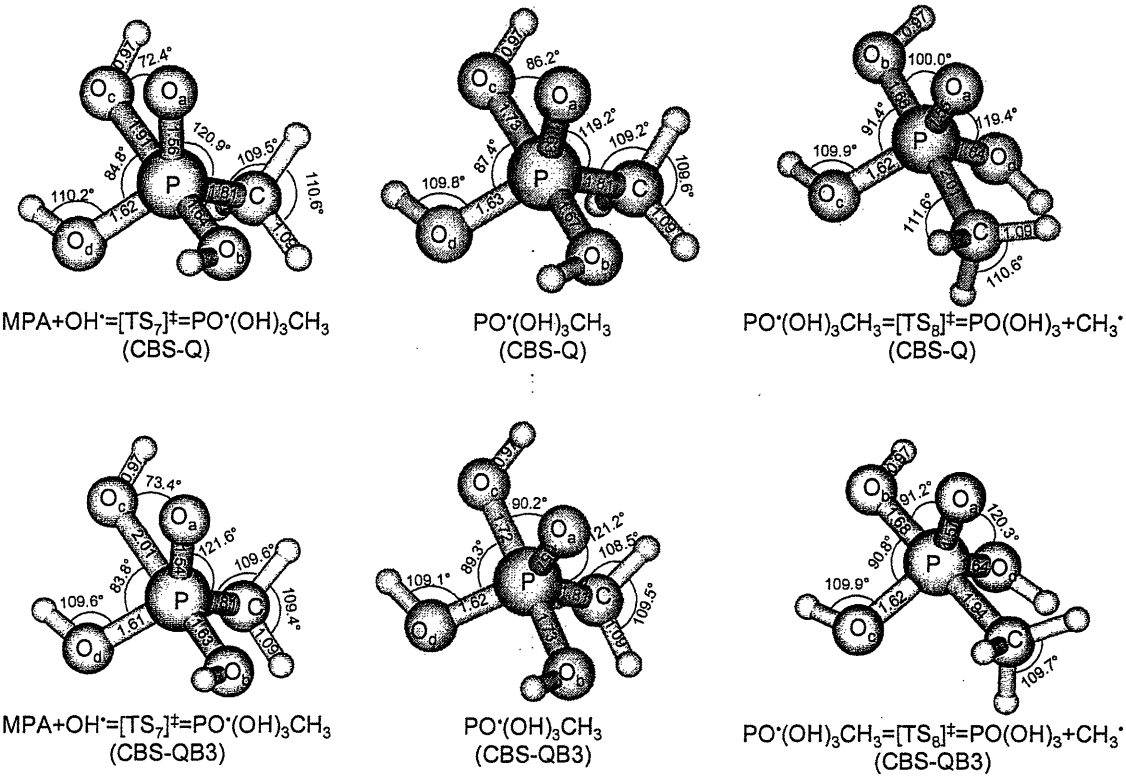


**Figure 4-6: Optimized geometries for $PO^{\bullet}(OH)_3CH_3$, $TS_7$ and $TS_8$ from CBS-Q and CBS-QB3 calculations**

CBS-Q geometries are optimized at the MP2/6-31g(d') level and CBS-QB3 geometries are optimized at the B3LYP/CBSB7 level

**Table 4-8: CBS-Q and CBS-QB3 energies for MPA and $OH^{\bullet}$ reaction to form $PO(OH)_3$ and $CH_3^{\bullet}$ via $PO^{\bullet}(OH)_3CH_3$**

| Energies | MPA+$OH^{\bullet}$ | $TS_7$ | $PO^{\bullet}(OH)_3CH_3$ | $TS_8$ | $PO(OH)_3+CH_3^{\bullet}$ |
|---|---|---|---|---|---|
| CBS-Q (hartree/particle) | -683.135367 | -683.135456 | -683.134384 | -683.135206 | -683.181289 |
| CBS-Q (kcal/mol) | 0 | -0.06 | 0.62 | 0.10 | -28.82 |
| CBS-QB3 (hartree/particle) | -683.140662 | -683.136460 | -683.141469 | -683.136649 | -683.185602 |
| CBS-QB3 (kcal/mol) | 0 | 2.64 | -0.51 | 2.52 | -28.20 |
| CBS-Q Component Energies | MPA+$OH^{\bullet}$ | $TS_7$ | $PO^{\bullet}(OH)_3CH_3$ | $TS_8$ | $PO(OH)_3+CH_3^{\bullet}$ |
| QCISD(T)/ (hartree/particle) | -682.580027 | -682.576773 | -682.581245 | -682.573001 | -682.609102 |
| 6-31+g(d') (kcal/mol) | 0 | 2.04 | -0.76 | 4.41 | -18.24 |
| MP4SDQ/ (hartree/particle) | -682.679383 | -682.670382 | -682.680034 | -682.671785 | -682.717409 |
| CBSB4 (kcal/mol) | 0.0 | 5.65 | -0.41 | 4.77 | -23.86 |
| MP2/ (hartree/particle) | -682.996472 | -682.989486 | -682.995924 | -682.992667 | -683.045763 |
| CBSB3 (kcal/mol) | 0.0 | 4.38 | 0.34 | 2.39 | -30.93 |

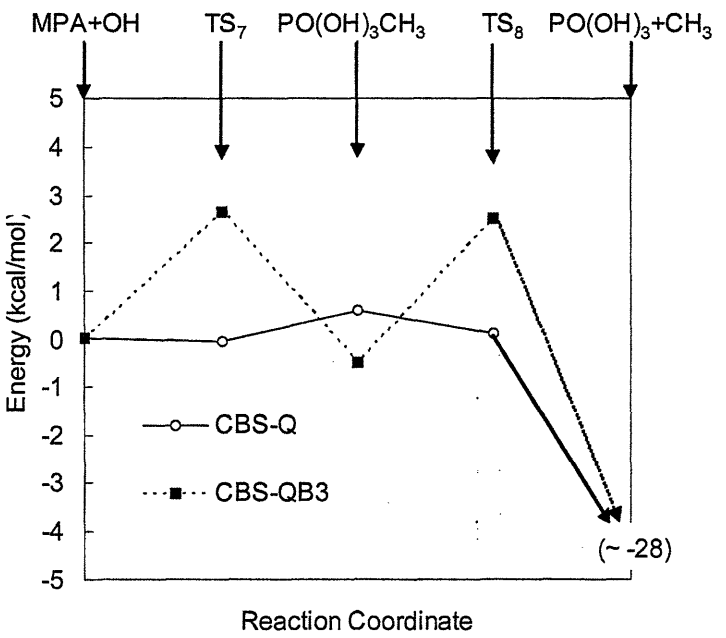


**Figure 4-7: Potential Energy Surface for MPA+OH Reaction to $PO(OH)_3$ and $CH_3$ from CBS-Q and CBS-QB3 Calculations**

The energies on this potentiall energy surface are relative to the CBS-Q and CBS-QB3 MPA + $OH^{\bullet}$ energies at 0 K. For both calculation methods, the energy of $PO(OH)_3$ + $CH_3^{\bullet}$ is ~ -28 kcal/mol.

In order to check the accuracy of the energetics and the effect of the optimized geometry on the energetics, we performed a set of calculations at the CBS-QB3 level. The energies for the CBS-QB3 calculations are included in Table 4-8 and the optimized geometries are shown in Figure 4-6. The potential energy surface from the CBS-QB3 calculations appears to provide a more reasonable estimate for this reaction pathway (see Figure 4-7). The $PO^{\bullet}(OH)_3CH_3$ energy is slightly stabilized as compared to the MPA + $OH^{\bullet}$ energy and the transition state energies are approximately 2 kcal/mol higher than the MPA + $OH^{\bullet}$ energy. The CBS-QB3 potential energy surface is different because the B3LYP/CBSB7 optimized geometries from the CBS-QB3 method are significantly different than the MP2/6-31g(d') geometries from the CBS-Q method (Figure 4-6).

The energy of the $PO^{\bullet}(OH)_3CH_3$ structure being stabilized as compared to MPA + $OH^{\bullet}$ is dependent on the concurrent weakening of the P=O bond and forming of the P-OH bond. In the CBS-Q structure, the P-$O^{\bullet}$ bond length increases from 1.48 Å in MPA to 1.63 Å in $PO^{\bullet}(OH)_3CH_3$ to the bond length of a P-OH bond. Also, the two CBS-Q apical bonds increase from the MPA P-OH bond lengths of 1.62 Å to 1.73 and 1.67 Å. In the CBS-QB3 structure, the P-$O^{\bullet}$ bond length increases from an MPA bond length of 1.47 Å to a bond length of 1.58 Å, while the two apical P-OH bond lengths increase to 1.72 and 1.73 Å. Thus, in the CBS-QB3 geometry, the much stronger P-$O^{\bullet}$ bond retains more of its double bond character with a shorter bond length of 1.58 Å, while the bond strengths of the weaker apical OH bonds decrease. These results reveal that stabilization of the P-$O^{\bullet}$ bond with the odd electron is more important than stabilization of the P-OH bond. Unfortunately, with the available computational resources, we could not perform an MP2 optimization with a larger basis set (CBSB7) and so it is difficult to estimate how this basis set affects the calculations.

The relative transition state energies are also different between the two optimization methods, CBS-Q and CBS-QB3 (Table 4-8). The primary difference between the geometries for both transition states are the bond lengths of the apical bonds (shown in Figure 4-6). For $TS_7$ where the P-OH bond is formed, the CBS-Q P-OH bond length is 1.91 Å while the CBS-QB3 bond length is 2.01 Å. The longer P-OH bond length in the CBS-QB3 method is closer to the structure of the reactant which would be expected for the exothermic reaction, leading to a better estimate of the transition state barrier for this pathway. Likewise, for $TS_8$, the CBS-Q P-$CH_3$ bond length is 2.01 Å while the CBS-QB3 P-$CH_3$ bond length is 1.94 Å. This is a highly exothermic reaction and the transition state would be expected to have a geometry closer to that of $PO^{\bullet}(OH)_3CH_3$ than the products, as observed in the CBS-QB3 calculation.

These results suggest that the optimization using a smaller basis set in the CBS-Q method is likely not appropriate for pentavalent organophosphorus intermediates. However, additional crystallographic data on pentavalent organophosphorus compounds are needed to establish this firmly. The nature of the P=O bond in the 5-coordinate state of phosphorus and the role that the phosphorus d-orbitals play in bonding are not well understood in organophosphorus chemistry (Quin, 2000). For the four-coordinate phosphorus compounds that are examined in the rest of this study, the CBS-Q method does calculate the geometries and energies as well as the CBS-QB3 method does. As described in the thermochemistry section, $\Delta H_f^o$(298 K) values calculated from both methods agree with each other within 1.5 kcal/mol. Also, the bond lengths in the optimized geometries from both the CBS-Q and CBS-QB3 methods agree within ±0.01 Å of each other. The CBS-Q method seems to have problems with five-centered intermediates due to its inability to properly optimize the geometries of the P-O and P-OH bonds in the structure, $PO^{\bullet}(OH)_3CH_3$.

Since the CBS-QB3 results provide a more reasonable potential energy surface for the reactions through the $PO^{\bullet}(OH)_3CH_3$ intermediate, the rate constants for reactions (R7) and (R8) were calculated using the CBS-QB3 transition state results in Table 4-9. The rate constants for reactions (R7) and (R8) are included in Table 4-10. To compare our rate constants with the estimated rate constants for overall reaction of MPA + $OH^{\bullet}$ to $PO(OH)_3$ and $CH_3^{\bullet}$ from Korobeinichev *et al.* (2000) and Glaude *et al.* (2000) in Table 4-1, the effective reaction rate through reactions (R7) and (R8) needs to be calculated. Assuming pseudo steady state behavior for the $PO^{\bullet}(OH)_3CH_3$ intermediate and assuming that the reverse reaction flux for reaction (R8) is approximately zero because this reaction is highly exothermic, the effective rate constant for reaction of MPA and OH to form $PO(OH)_3$ and $CH_3^{\bullet}$ is derived as shown below.

$$\frac{d[\mathrm{MPA}]}{dt} = -k_7[\mathrm{MPA}][\mathrm{OH}^\bullet] + k_{-7}[\mathrm{PO}^\bullet(\mathrm{OH})_3\mathrm{CH}_3] \quad (4\text{-}20)$$

$$\frac{d[\mathrm{PO}^\bullet(\mathrm{OH})_3\mathrm{CH}_3]}{dt} = k_7[\mathrm{MPA}][\mathrm{OH}^\bullet] - k_{-7}[\mathrm{PO}^\bullet(\mathrm{OH})_3\mathrm{CH}_3] - k_8[\mathrm{PO}^\bullet(\mathrm{OH})_3\mathrm{CH}_3] \approx 0 \quad (4\text{-}21)$$

$$[\mathrm{PO}^\bullet(\mathrm{OH})_3\mathrm{CH}_3] = \frac{k_7}{k_{-7}+k_8}[\mathrm{MPA}][\mathrm{OH}] \quad (4\text{-}22)$$

$$\frac{d[\mathrm{MPA}]}{dt} = \left(-k_7 + \frac{k_{-7}k_7}{k_{-7}+k_8}\right)[\mathrm{MPA}][\mathrm{OH}^\bullet] = -k_{eff}[\mathrm{MPA}][\mathrm{OH}^\bullet] \quad (4\text{-}23)$$

$$k_{eff} = \frac{k_8 k_7}{k_{-7}+k_8} \quad (4\text{-}24)$$

In Equation 4-24, the reverse rate constant can be calculated from the equilibrium constant with the thermodynamic information in Table 4-2. At 800 K, the Korobeinichev *et al.* rate is $8.1\text{x}10^{11}$ $\mathrm{cm}^3(\mathrm{mol\ s})^{-1}$ and the Glaude *et al.* rate is $2.8\text{x}10^{11}$ $\mathrm{cm}^3(\mathrm{mol\ s})^{-1}$, while the calculated rate constant from Equation (4-24) is $1.10\text{x}10^{09}$ $\mathrm{cm}^3(\mathrm{mol\ s})^{-1}$ at 800 K.. From these results, the Korobeinichev *et al.* and Glaude *et al.* rates appear to be overestimated for this reaction pathway.

**Table 4-9: Transition state information for $PO^\bullet(OH)_3CH_3$ reactions from the CBS-QB3 method**

| Reaction | $E_{TS}$(0 K) (hartree) | $E_0$(0 K) (kcal/mol) | $\Delta H_r^\circ$(0 K) (kcal/mol) | Vibrational frequencies ($cm^{-1}$) | Rotational constants ($cm^{-1}$) |
|---|---|---|---|---|---|
| (R7) MPA+$OH^\bullet$=$TS_7$ =$PO^\bullet(OH)_3CH_3$ | -683.136460 | 2.6 | -0.5 | 174.0*i*, 104.8, 197.4, 228.5, 293.9, 319.8, 346.7, 402.4, 437.2, 451.0, 489.4, 558.7, 704.5, 789.3, 819.3, 873.2, 921.0, 946.4, 1036.2, 1065.3, 1148.8, 1350.4, 1462.6, 1471.7, 3062.6, 3141.3, 3166.6, 3789.6, 3825.9, 3830.7 | 0.124<br>0.093<br>0.088 |
| (R8) $PO^\bullet(OH)_3CH_3$=$TS_8$ =$PO(OH)_3$+$CH_3^\bullet$ | -683.136649 | 3.0 | -27.7 | 197.5*i*, 192.4, 208.6, 226.6, 296.0, 378.6, 381.2, 448.5, 468.7, 474.1, 488.9, 545.9, 677.7, 736.1, 830.0, 848.4, 904.6, 971.2, 1076.6, 1098.5, 1134.8, 1269.5, 1446..4, 1481.9, 3030.1, 3125.4, 3165.3, 3811.3, 3850.1 | 0.124<br>0.095<br>0.093 |

**Table 4-10: Rate constants for $PO^{\bullet}(OH)_3CH_3$ reactions from the CBS-QB3 method**
Comparisons with MPA+OH rates from Glaude *et al.* (2000) and Korobeinichev *et al.* (2000) are discussed in the text. For R7, $A$ and $k$ have units of $cm^3$ $(mol\ s)^{-1}$. For R8, $A$ and $k$ have units of $s^{-1}$.

| Reaction | $A$ | $n$ | $E_a$ (kcal/mol) | $k_{TST}$ 800 K | $k_{TST}$ 1500 K |
|---|---|---|---|---|---|
| (R7) $PO(OH)_2CH_3+OH^{\bullet}=P^{\bullet}O(OH)_3CH_3$ | $5.3x10^{03}$ | 2.01 | 0.84 | $2.2x10^{09}$ | $9.7x10^{09}$ |
| (R8) $P^{\bullet}O(OH)_3CH_3=PO(OH)_3+CH_3^{\bullet}$ | $7.4x10^{11}$ | 0.05 | 2.94 | $1.6x10^{11}$ | $4.0x10^{11}$ |

From the MPA + $OH^{\bullet}$ reactions calculated in Tables 4-7 and 4-10, the hydrogen abstraction reactions (R5) and (R6) appear to be the dominant MPA reactions. The two hydrogen abstraction rate constants are two to four orders of magnitude faster than reaction through the $PO^{\bullet}(OH)_3CH_3$ intermediate to form $PO(OH)_3$ and $CH_3^{\bullet}$ in reactions (R7) and (R8). Previously, Korobeinichev *et al.* (2000) and Glaude *et al.* (2000) had only proposed the reaction pathway of MPA + $OH^{\bullet}$ to form $PO(OH)_3$ and $CH_3^{\bullet}$. The rate constants that they estimated for this reaction pathway are on the same order of magnitude or slower than the hydrogen abstraction rates for reactions (R5) and (R6). The MPA + $OH^{\bullet}$ rate constants from these two studies could possibly have been overestimated to achieve sufficient reaction of the MPA because the hydrogen abstraction pathways were not included. From these results, the hydrogen abstraction pathways are important reactions that need to be included for MPA oxidation.

### *4.4.3 Set 3: Reactions Involving $PO(OH)_3$ and $P^{\bullet}O(OH)_2$*

The final set of reaction rates was calculated for $PO(OH)_3$ and $P^{\bullet}O(OH)_2$ reactions included in the MPA SCWO model in Chapter 5. At higher combustion temperatures ($T$>1000 K), identified phosphorus oxide species typically are $PO^{\bullet}$, $P^{\bullet}O_2$, HOPO, $P^{\bullet}O(OH)_2$, and $PO_2OH$. As discussed in Section 4.1.2, previous *ab initio* papers on phosphorus oxide chemistry have studied rate constants for these smaller compounds (Mackie *et al.*, 2002; Haworth *et al.*, 2002). However, at SCW temperatures and pressures ($T$ <873 K, $P$>221 bar), the final phosphorus-

containing product is $PO(OH)_3$, which is a minor intermediate in organophosphorus combustion experiments, being detected only at lower temperatures near the burner (Korobeinichev *et al.*, 2000). In the MPA SCWO mechanism, the intermediates, $P^{\bullet}O(OH)_2$ and $PO_2OH$, are formed by separate pathways and react further to form the final phosphorus-containing product, $PO(OH)_3$. The reaction rates and pathways for phosphoric acid have not been examined in as much detail as have the rates for smaller phosphorus oxide compounds. Thus, we chose to study six key reaction pathways with $P^{\bullet}O(OH)_2$, $PO_2OH$, and $PO(OH)_3$ to more accurately determine the reaction kinetics for these compounds. Transition state geometries for this reaction set are in Figure 4-8 along with the calculated information for each transition state in Table 4-11 and calculated rate constants in Table 4-12.

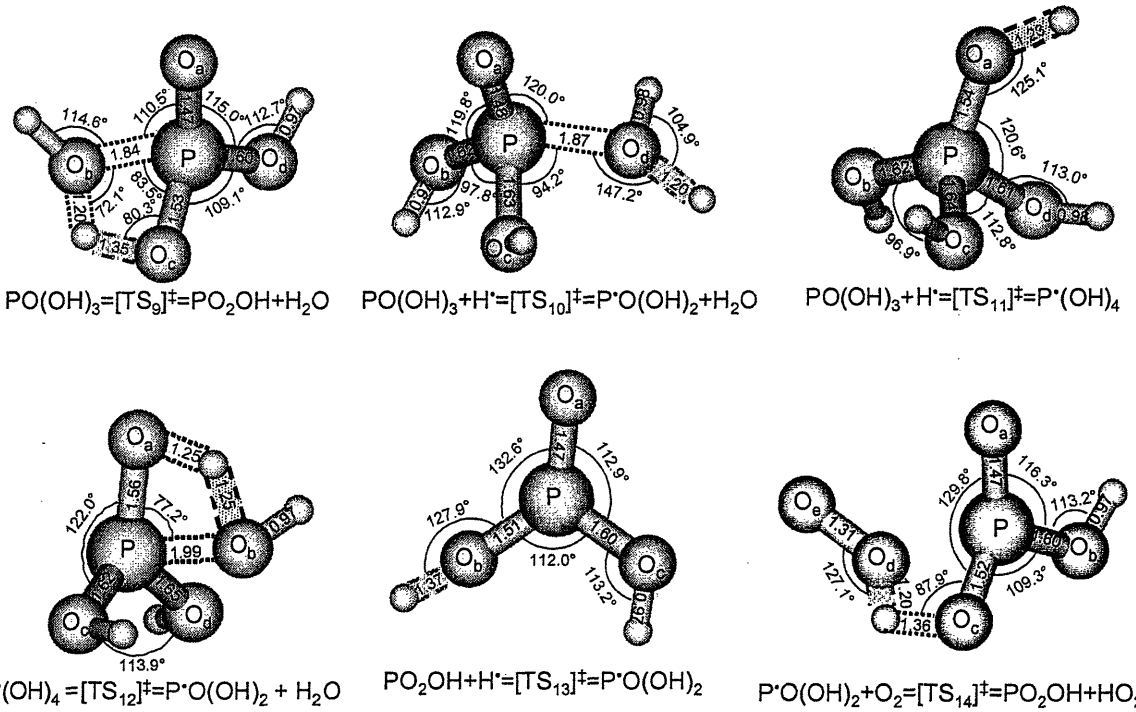


**Figure 4-8: Transition state geometries for reactions involving $PO(OH)_3$ and $P^{\bullet}O(OH)_2$**
Bond lengths are in angstroms and bond angles are in degrees, optimized at the MP2/6-31g(d') level. Breaking bonds are indicated by dotted lines, while forming bonds are shown by dashed lines and the shaded area.

**Table 4-11: Transition state information for reactions involving $PO(OH)_3$ and $P^{\bullet}O(OH)_2$**

Calculated vibrational frequencies that were replaced with internal rotational values are italicized.

| Reaction | $E_{TS}$ (0 K) (hartree) | $E_0$ (0 K) (kcal/mol) | $\Delta H_r^o$ (0 K) (kcal/mol) | Vibrational frequencies ($cm^{-1}$) | Rotational constants ($cm^{-1}$) |
|---|---|---|---|---|---|
| (R9) $PO(OH)_3$= $TS_9$= $PO_2OH+H_2O$ | -643.365360 | 44.4 | 44.8 | 2039.8*i*, 277.5, *357.0*, 424.5, 459.4, 486.7, 565.4, 655.0, 800.0, 965.2, 1006.6, 1119.5, 1214.3, 1376.6, 1488.7, 2183.2, 4077.8, 4087.6 | 0.177<br>0.147<br>0.133 |
| (R10) $PO(OH)_3+H^{\bullet}$= $TS_{10}=P^{\bullet}O(OH)_2+H_2O$ | -643.872991 | 39.5 | 4.9 | 2467.9*i*, *109.2*, 134.1, *187.6*, *236.7*, 302.0, 371.5, 422.9, 496.7, 587.8, 630.6, 751.5, 915.5, 969.7, 1089.4, 1122.0, 1389.8, 1525.3, 4010.7, 4061.5, 4098.9 | 0.152<br>0.124<br>0.117 |
| (R11) $PO(OH)_3+H^{\bullet}$= $TS_{11}=P^{\bullet}(OH)_4$ | -643.897597 | 24.1 | 3.3 | 2930.4*i*, *81.2*, *250.5*, *279.6*, *306.9*, 424.9, 505.4, 512.9, 571.0, 741.2, 876.4, 939.8, 983.4, 1106.4, 1124.3, 1167.9, 1214.5, 3994.0, 4100.1, 4119.3 | 0.155<br>0.144<br>0.129 |
| (R12) $P^{\bullet}(OH)_4$= $TS_{12}=P^{\bullet}O(OH)_2+H_2O$ | -643.884832 | 28.8 | 1.6 | 1898.5*i*, 208.5, 306.6, 325.6, *339.4*, 413.8, 436.1, 557.3, 674.8, 772.9, 812.2, 874.3, 1016.4, 1129.7, 1181.5, 1226.0, 1436.2, 2072.3, 3987.3, 4080.3, 4158.2 | 0.149<br>0.140<br>0.127 |
| (R13) $PO_2OH+H^{\bullet}$= $TS_{13}=P^{\bullet}O(OH)_2$ | -567.515210 | 8.0 | -39.9 | 2223.9i, 271.9, 398.3, 443.7, 478.7, 513.2, 626.8, 943.6, 1102.5, 1139.4, 1486.0, 4077.7 | 0.298<br>0.265<br>0.147 |
| (R14) $P^{\bullet}O(OH)_2+O_2$= $TS_{14}=PO_2OH+HO_2^{\bullet}$ | -717.749182 | 3.3 | -7.5 | 2037.3i, 115.1, 199.9, 273.8, 384.7, 460.5, 472.3, 552.1, 603.6, 659.3, 975.7, 1110.9, 1164.0, 1236.9, 1301.8, 1511.5, 2197.9, 4073.5 | 0.151<br>0.083<br>0.078 |

**Table 4-12: Rate constants for reactions involving $PO(OH)_3$ and $P^{\bullet}O(OH)_2$**
Comparisons with rate constants from Glaude *et al.* (2000) and Korobeinichev *et al.* (2000) are included. Rate constants have units of $s^{-1}$ or $cm^3$ $(mol\ s)^{-1}$.

| Reaction | $A$ | $n$ | $E_a$ | $k_{TST}$ | | $k_{Korobeinichev}$ | | $k_{Glaude}$ | |
|---|---|---|---|---|---|---|---|---|---|
| | | | | 800 K | 1500 K | 800 K | 1500 K | 800 K | 1500 K |
| (R9) $PO(OH)_3 = PO_2OH+H_2O$ | $2.1x10^{07}$ | 1.46 | 42.12 | $1.1x10^{00}$ | $6.5x10^{05}$ | $2.1x10^{-2}$ | $5.1x10^{04}$ | $4.1x10^{01}$ | $3.0x10^{07}$ |
| (R10) $PO(OH)_3+H^{\bullet} = P^{\bullet}O(OH)_2+H_2O$ | $4.7x10^{08}$ | 1.69 | 37.89 | $1.6x10^{03}$ | $3.3x10^{08}$ | $6.5x10^{09}$ | $6.8x10^{10}$ | | |
| (R11) $PO(OH)_3+H^{\bullet} = P^{\bullet}(OH)_4$ | $4.9x10^{06}$ | 2.07 | 21.77 | $5.8x10^{06}$ | $1.3x10^{10}$ | | | | |
| (R12) $P^{\bullet}(OH)_4 = P^{\bullet}O(OH)_2+H_2O$ | $1.6x10^{09}$ | 0.91 | 26.89 | $3.0x10^{04}$ | $1.4x10^{08}$ | | | | |
| (R13) $PO_2OH+H^{\bullet} = P^{\bullet}O(OH)_2$ | $3.1x10^{08}$ | 1.58 | 6.19 | $2.4x10^{11}$ | $4.0x10^{12}$ | | | $2.2x10^{11}$ | $9.3x10^{11}$ |
| (R14) $P^{\bullet}O(OH)_2+O_2 = PO_2OH+HO_2^{\bullet}$ | $1.3x10^{02}$ | 2.40 | 0.42 | $9.3x10^{08}$ | $4.7x10^{09}$ | | | | |

Unimolecular decomposition of phosphoric acid to form $PO_2OH$ and water:

$$PO(OH)_3 \rightarrow [TS_9] \rightarrow PO_2OH + H_2O \qquad \text{(R9)}$$

occurs by the simultaneous cleavage of the P-$O_b$ and the $O_c$-H bond, as shown in Figure 4-8. This reaction was included in both the Glaude *et al.* (2000) and Korobeinichev *et al.* (2000) mechanisms, but their rates differ by approximately three orders of magnitude from each other as shown in Table 4-12. For example, at $T$=800 K, the two rate constants are $2.1x10^{-02}$ and $4.1x10^{01}$ $s^{-1}$. For these two rate constants, the pre-exponential factors differ by two orders of magnitude, i.e. from Glaude *et al.*, $A$=$1.5x10^{14}$ $s^{-1}$ and $E_a$=46 kcal/mol and from Korobeinichev *et al.*, $A$=$1.0x10^{12}$ $s^{-1}$ and $E_a$=50 kcal/mol. Given the wide discrepancy between these two rate constants, a more accurate estimate for this rate constant was desired.

The unimolecular dehydration of $PO(OH)_3$ in reaction (R9) is highly endothermic with a $\Delta H_r^o$(0 K) of 44.8 kcal/mol and an activation barrier at 0 K of 44.4 kcal/mol at CBS-Q level (see Table 4-11). The geometry for the transition state is displayed in Figure 4-8 and the reaction coordinate vector for the transition state was identified as

$$0.70r_{Oc..H} + 0.24r_{P..Ob} - 0.11r_{P..Oc}$$

In this reaction coordinate, the P-$O_c$ bond length decreases to 1.53 Å as the bond nature changes from a double to a single bond, while the P-$O_b$ bond length increases to 1.84 Å as this bond gets broken. Also, the $O_c$-H bond length increases to 1.35 Å, while the $O_b$-H bond is formed with a bond length of 1.20 Å.

The calculated rate constants are shown in Table 4-12 and compared to those from Korobeinichev *et al.* (2000) and Glaude *et al.* (2000). The calculated rate constant is 1.1 $s^{-1}$ at $T$=800 K, 40 times slower than the Glaude *et al.* rate and 50 times faster than the Korobeinichev *et al.* rate estimates. These results indicate that both estimated rate constants from the literature may be in error by approximately one order of magnitude. As found in the MPA unimolecular reaction set, it can be difficult to accurately estimate unimolecular reaction rates for five-centered compounds from four-centered carbon chemistry. The entropy change would differ for these structure types, leading to different pre-exponential factors for these reaction rates.

In reaction (R10), a hydrogen atom abstracts an OH group from phosphoric acid to form $P^{\bullet}O(OH)_2$ and water.

$$PO(OH)_3 + H^{\bullet} \rightarrow [TS_{10}]^{\dagger} \rightarrow P^{\bullet}O(OH)_2 + H_2O \qquad \text{(R10)}$$

Reaction 10 is slightly endothermic with a $\Delta H_r^o$(0 K) of 4.9 kcal/mol, but it has a high activation barrier of 39.5 kcal/mol, indicating that reactions in both the forward and reverse direction encounter a significant reaction barrier. The reaction coordinate vector for the transition state is:

$$0.71 r_{Od..H} - 0.64 r_{P..Od}$$

In this reaction coordinate, the P-$O_d$ bond length increases to 1.87 Å as this bond is broken, while the $O_d$-H bond length becomes 1.20 Å as this bond is formed.

The calculated rate constants are shown in Table 4-12 along with the estimated rate constants from Korobeinichev *et al.* (2000). At lower temperatures ($T$=800 K), the

Korobeinichev *et al.* (2000) rate constant is six orders of magnitude faster than the TST rate constant because its activation energy is underestimated to be 8 kcal/mol. However, at $T$=1500 K, the two rate constants differ by two orders of magnitude, as compared to six orders of magnitude at 800 K. Korobeinichev *et al.* (2000) estimated the rate constant for combustion temperatures between 800 and 2400 K; at these higher average temperatures, the error in underestimating the activation energy is not as significant. However, when this rate constant is used at lower SCW temperatures, it is overestimated by several orders of magnitude due to the underestimated activation energy.

Recently, Mackie *et al.* (2002) examined a similar reaction for $PO_2OH$ chemistry

$$PO_2OH + H^\bullet \rightarrow P^\bullet O(OH)_2 \rightarrow P^\bullet O_2 + H_2O \qquad \text{(R7a)}$$

They found that the overall rate constant for formation of $P^\bullet O_2$ and water was faster if the transition state occurred through a two-step process: first, addition of the hydrogen atom to a P=O bond to form the stabilized intermediate, $P^\bullet O(OH)_2$, followed by unimolecular decomposition to eliminate water. At higher combustion temperatures, the $P^\bullet O(OH)_2$ intermediate does not have a significant lifetime as the water elimination reaction proceeds rapidly. Mackie *et al.* (2002) determined the two-step addition and water elimination mechanism had a reaction rate at least an order of magnitude higher than for the single-step hydrogen abstraction of a hydroxyl group.

Reactions (R11) and (R12) represent a two-step pathway for the overall reaction, (R10), through the $P^\bullet(OH)_4$ intermediate.

$$PO(OH)_3 + H^\bullet \rightarrow [TS_{11}]^\dagger \rightarrow P^\bullet(OH)_4 \qquad \text{(R11)}$$

$$P^\bullet(OH)_4 \rightarrow [TS_{12}]^\dagger \rightarrow P^\bullet O(OH)_2 + H_2O \qquad \text{(R12)}$$

The $P^{\bullet}(OH)_4$ energy lies between the energies of the reactants and products, such that reactions (R11) and (R12) are both endothermic reactions. As shown in Table 4-11, the barrier heights for these reactions are 24.1 and 28.8 kcal/mol, while the barrier height for the direct pathway via reaction (R10) is 39.5 kcal/mol. While the lower activation barriers would increase reaction reaction rates, there will also be an entropy loss in the concerted two-step mechanism that will result in a lower pre-exponential factor than for the direct abstraction pathway. The overall reaction rate would be affected by the competing effects of a decreased pre-exponential factor and decreased activation barrier.

The transition states for these two reactions are shown in Figure 4-7. In $TS_{11}$, the reaction coordinate vector involves forming the O-H bond and extending the P-O bond.

$$0.82r_{O..H} - 0.24r_{P..O}$$

The P-O bond length increases to 1.54 Å as it loses its double bond character, while the O-H bond length decreases to 1.23 Å as this bond gets formed. For the unimolecular dissociation of the $P^{\bullet}(OH)_4$ intermediate to form $P^{\bullet}O(OH)_2$ and $H_2O$, the reaction vector is

$$0.67r_{O..H} - 0.62r_{O..H} + 0.29r_{P..O}$$

In $TS_{12}$, the $O_bH$ bond is formed at a bond length 1.25 Å, while the $O_aH$ bond is broken with a bond length of 1.25 Å. Also, the P-$O_b$ bond length increases to 1.99 Å as this bond is broken to form water.

The rate constants for reactions (R11) and (R12) are shown in Table 4-12 and are compared to the rate constant for the competing, direct reaction pathway (R10). The rate constant for formation of the $P^{\bullet}(OH)_4$ intermediate through reaction (R11) is 3 orders of magnitude higher at $T$=800 K than the rate constant through the competing pathway (R10). The reaction flux through reactions (R11) and (R12) depends on the competing reactions of $P^{\bullet}(OH)_4$

to reform $PO(OH)_3$ and $H^\bullet$ or to react further to form $P^\bullet O(OH)_2$ and $H_2O$. The rate constant for the reverse reaction of (R11) was calculated to be $1.3x10^{08}$ $s^{-1}$ at 800 K and $1.1x10^{11}$ $s^{-1}$ at 1500 K. The $P^\bullet(OH)_4$ intermediate will predominantly reform $PO(OH)_3$ and $H^\bullet$ through reaction (R-11) since the rate constant for this pathway is three to four orders of magnitude higher than the rate constant for reaction (R12). Thus, reaction of $PO(OH)_3$ and $H^\bullet$ to form $P^\bullet O(OH)_2$ and $H_2O$ will proceed through reaction (R10) at these conditions because the $P^\bullet(OH)_4$ intermediate primarily dissociates to reform $PO(OH)_3$ and the $H^\bullet$ radical.

The next reaction that was examined was hydrogen atom addition to the P=O bond in $PO_2OH$ to form $P^\bullet O(OH)_2$ in reaction (R13).

$$PO_2OH + H^\bullet \rightarrow [TS_{13}]^\dagger \rightarrow P^\bullet O(OH)_2 \qquad \text{(R13)}$$

In Table 4-11, we calculated the CBS-Q activation barrier to be $E_0$=8.0 kcal/mol with $\Delta H_r$=-39.9 kcal/mol. The geometry for the $TS_{13}$ transition state is included in Figure 4-7, where the reaction coordinate vector for this transition state is

$$0.76r_{Ob..H} - 0.37r_{P..Ob}$$

In $TS_{13}$, the P-$O_b$ bond length increases slightly as the $O_b$-H bond is formed. For the TST rate calculation, the reaction rate in Table 4-12 is $k_{13}$(800 K)=$2.4x10^{11}$ $cm^3(mol\ s)^{-1}$, in excellent agreement with the Glaude *et al.*'s estimated rate constant, $k_{13}$(800 K)=$2.2x10^{11}$ $cm^3(mol\ s)^{-1}$. Due to Glaude *et al.*'s lower activation energy ($E_a$=5.0 kcal/mol), the difference between the predicted rate constants does increase at higher temperatures. For example, at 1500 K, Glaude *et al.*'s rate constant is $k_{13}$=$9.3x10^{11}$ $cm^3(mol\ s)^{-1}$ and the TST rate constant is $k_{13}$=$4.0x10^{12}$ $cm^3(mol\ s)^{-1}$. However, from 300 to 1500 K, the two rate constants do agree within an order of magnitude with each other, showing that Glaude *et al.*'s estimated rate constant appears to be accurate for this reaction.

The reaction of $P^{\bullet}O(OH)_2$ with molecular oxygen was not included in earlier organophosphorus combustion mechanisms; however, this reaction is a possible pathway for $P^{\bullet}O(OH)_2$ reaction to form $PO_2OH$ and eventually $PO(OH)_3$ at SCW temperatures.

$$P^{\bullet}O(OH)_2 + O_2 \rightarrow [TS_{14}]^{\dagger} \rightarrow PO_2OH + HO_2^{\bullet} \qquad \text{(R14)}$$

Due to the high activation barrier for $P^{\bullet}O(OH)_2$ and $H_2O$ to form $PO(OH)_3$ in reactions R10 through R12, the termination reaction of $P^{\bullet}O(OH)_2$ with $OH^{\bullet}$ to form $PO(OH)_3$ dominates and decreases MPA oxidation rates considerably. An alternative reaction pathway for $P^{\bullet}O(OH)_2$ to form $PO(OH)_3$ would be to react first to $PO_2OH$, which once formed, reacts quickly with water to form $PO(OH)_3$ in SCW. Given the high concentrations of $O_2$ at SCWO conditions, the reaction between $P^{\bullet}O(OH)_2$ and $O_2$ was examined as a feasible pathway for formation of $PO_2OH$.

From the $TS_{14}$ *ab initio* calculations in Table 4-11, this reaction is exothermic with a $\Delta H_r^o$(0 K) of -7.5 kcal/mol and has a low activation barrier of 3.3 kcal/mol. The geometry for $TS_{14}$ is shown in Figure 4-8 and the reaction coordinate vector is included below:

$$0.67r_{Oc..H} - 0.59r_{Od..H} - 0.34\theta_{HOeOd}$$

In this reaction coordinate, the $O_c$-H bond length increases to 1.36 Å as this bond is broken, while the $O_d$-H bond length becomes 1.20 Å as it is formed. Additionally, the $HO_2^{\bullet}$ bond angle becomes 127° as the $HO_2^{\bullet}$ radical is formed. The transition state energy is stabilized by the $O_2$ molecule aligning itself with respect to the radical phosphorus center of $P^{\bullet}O(OH)_2$ at a distance of 1.97 Å. The calculated rate constant and parameters in Table 4-12 result in $k_{14}$=9.3x10$^8$ cm$^3$(mol s)$^{-1}$ at $T$=800 K. Though this rate constant is not very large, it is an important pathway because $O_2$ concentrations are on the order of 1 mM at SCWO conditions. Inclusion of this rate constant in an organophosphorus mechanism is more important at SCW temperatures where reactions with high activation barriers, such as reaction (R10), are less likely to proceed.

## 4.5 CONCLUSIONS

In this study, the thermochemistry of important organophosphorus intermediates was calculated and several reaction rates that could potentially be important during MPA oxidation were examined for use in an MPA SCWO elementary reaction rate mechanism, developed in Chapter 5. In several cases, our calculations confirm that previous estimates in the literature based on analogies are reasonable. However, for other reactions, our calculations show that the literature estimates are inaccurate by several orders of magnitude. Several reactions were also introduced that are important during MPA oxidiation in supercritical water.

Rate constants for three possible MPA + $OH^{\bullet}$ reactions were calculated since they would probably be important reactions for MPA oxidation in SCW. One pathway, MPA + $OH^{\bullet}$ to form $PO(OH)_3$ and $CH_3^{\bullet}$, was previously estimated by Korobeinichev *et al.* (2000) and Glaude *et al.* (2000). From our calculations, this reaction occurs through a stabilized intermediate, $PO^{\bullet}(OH)_3CH_3$, and is two orders of magnitude slower than estimated by Glaude *et al.* and Korobeinichev *et al.* The other two MPA + $OH^{\bullet}$ reactions were hydrogen abstraction reactions from the $CH_3$ or the OH group. The rate constants for the two hydrogen abstraction pathways are two to four orders of magnitude faster than the rate through the other MPA + $OH^{\bullet}$ pathway. From these results, the MPA + $OH^{\bullet}$ hydrogen abstraction pathways are important reactions for MPA oxidation.

The accuracies of estimated organophosphorus and phosphorus oxide rate constants from current combustion mechanisms were determined. For the cases of unimolecular reaction of MPA to form $PO_2OH$ and $CH_4$ (R2) and bimolecular reaction of $PO_2OH$ and an $H^{\bullet}$ atom to form $P^{\bullet}O(OH)_2$ (R13), the calculated rate constants agreed within one order of magnitude with estimated rate constants from the literature. However, for other reactions, such as (R1), the

unimolecular reaction of MPA to form $PO_2CH_3$ and $H_2O$, (R9), the unimolecular decomposition of $PO(OH)_3$ to form $PO_2OH$ and $H_2O$, and (R10), the bimolecular reaction of $PO(OH)_3$ and an $H^{\bullet}$ atom to form $P^{\bullet}O(OH)_2$ and $H_2O$, the estimated rate constants differed by two orders of magnitude or more from our calculated rate constants. From these results, it appears that reaction rates involving P-O bond cleavage are difficult to estimate from typical rate estimation methods because the P-O bond strength is much higher than X-O bond strengths in other molecules. The calculations reported here are very helpful in constructing the MPA SCWO reaction mechanism, as discussed in Chapter 5.

## 4.6 REFERENCES

Bauschlicher, C. W., "Heats of formation for $PO_n$ and $PO_nH$ (n=1-3)." *J. Phys. Chem. A* **103**(50), 11126-11129 (1999).

Benson, S. W., *Thermochemical Kinetics*. Wiley, New York (1976).

Burcat, A., "Alexander Burcat's Ideal Gas Thermochemical Database." May, 2003 <http://garfield.chem.elte.hu/Burcat/burcat.thr> (2003).

Chase, M. W. J., C. A. Davies, J. Downey, J.R., D. J. Frurip, R. A. McDonald and A. N. Syverud, "JANAF thermochemical tables - 3rd edition .1, Al-Co." *J. Phys. Chem. Ref. Data* **14**(Suppl. 1), 1-962 (1985a).

Chase, M. W. J., C. A. Davies, J. Downey, J.R., D. J. Frurip, R. A. McDonald and A. N. Syverud, "JANAF thermochemical tables - 3rd edition .2." *J. Phys. Chem. Ref. Data* **14**(Suppl. 1), 927-1856 (1985b).

Cordeiro, J. L., D. L. Pompliano and J. W. Frost, "Degradation and detoxification of organophosphonates: Cleavage of the carbon to phosphorus bond." *J. Am. Chem. Soc.* **108**, 332-334 (1986).

Foresman, J. B. and A. Frisch, *Exploring Chemistry with Electronic Structure Methods*. Gaussian, Inc., Pittsburgh, PA (1996).

Frisch, M. J., G. W. Trucks, H. B. Schlegel, G. E. Scuseria, M. A. Robb, J. R. Cheeseman, V. G. Zakrzewski, J. A. Montgomery, R. E. Stratmann, J. C. Burant, S. Dapprich, J. M. Millam, A. D. Daniles, K. N. Kudin, M. C. Strain, O. Farkas, J. Tomasi, V. Barone, M. Cossi, R. Cammir, B. Mennucci, C. Pomelli, C. Adamo, S. Clifford, J. Ochterski, G. A. Petersson, P. Y.

Ayala, Q. Cui, K. Morokuma, D. K. Malick, A. D. Rabuck, K. Raghavachari, J. B. Foresman, J. Cioslowski, J. V. Ortiz, A. G. Baboul, B. B. Stefanov, G. Liu, A. Liashenko, P. Piskorz, I. Komaromi, R. Gomperts, A. Martin, D. J. Fox, T. Keith, M. A. Al-Laham, C. Y. Peng, A. Nanayakkara, M. Challacombe, P. M. W. Gill, B. Johnson, W. Chen, M. W. Wong, J. L. Andres, C. Gonzalez, M. Head-Gordon, E. S. Replogle and J. A. Pople, *Gaussian 98, Revision A.9*. Gaussian, Inc., Pittsburgh, PA (1998).

Glaude, P. A., H. J. Curran, W. J. Pitz and C. K. Westbrook, "Kinetic study of the combustion of organophosphorus compounds." *Proceedings of the Combustion Institute* **28**, 1749-1756 (2000).

Glaude, P. A., C. Melius, W. J. Pitz and C. K. Westbrook, "Detailed chemical kinetic reaction mechanisms for incineration of organophosphorus and fluoro-organophosphorus compounds." *Proceedings of the Combustion Institute* **29**, 2469-2476 (2002).

Haworth, N. L., G. B. Backsay and J. C. Mackie, "The role of phosphorus dioxide in the H + OH recombination reaction: *Ab initio* quantum chemical computation of thermochemical and rate parameters." *J. Phys. Chem. A* **106**(8), 1533-1541 (2002).

Haworth, N. and G. Backsay, "Heats of formation of phosphorus compounds determined by current methods of computational quantum chemistry." *J. Chem. Phys.* **117**(24), 11175-11187 (2002).

Heydorn, L. N., P. C. Burgers, P. J. A. Ruttink and J. K. Terlouw, "Generation of the elusive methyl dioxophosphorane molecule, $CH_3P(=O)_2$, selected by delayed dissociation of precursors." *Chem Phys. Lett.* **368**(5-6), 584-588 (2003).

Hildenbrand, D. L. and K. H. Lau, "Thermochemical properties of gaseous POBr and some H-P-O species." *J. Chem. Phys.* **100**(11), 8373-8376 (1994).

Hirschfelder, J. O. and E. Wigner, "Some quantum mechanical considerations in the theory of reactions involving an activation energy." *J. Chem. Phys.* **7**, 616 (1939).

Hughes, K., T. Turanyi, A. Clague and M. Pilling, "Development and testing of a comprehensive chemical mechanism for the oxidation of methane." *Int. J. Chem. Kinet.* **33**(9), 513-538 (2001).

Kaiser, E. W., T. J. Wallington, M. D. Hurley, J. Platz, H. J. Curran, W. J. Pitz and C. K. Westbrook, "Experimental and modeling study of premixed atmospheric-pressure dimethyl ether-air flames." *J. Phys. Chem. A* **104**(35), 8194-8206 (2000).

Korobeinichev, O. P., S. B. Ilyin, V. M. Shvartsberg and A. A. Chernov, "The destruction chemistry of organophosphorus compounds in flames - I: Quantitative determination of final phosphorus-containing species in hydrogen-oxygen flames." *Combust. Flame* **118**(4), 718-726 (1999).

Korobeinichev, O. P., S. B. Ilyin, T. A. Boshova, V. M. Shvartsberg and A. A. Chernov, "The chemistry of the destruction of organophosphorus compounds in flames -III: The destruction of DMMP and TMP in a flame of hydrogen and oxygen." *Combust. Flame* **121**(4), 593-609 (2000).

Korobeinichev, O. P., T. A. Bolshova, V. M. Shvartsberg and A. A. Chernov, "Inhibition and promotion of combustion by organophosphorus compounds added to flames of CH4 or H-2 in O-2 and Ar." *Combust. Flame* **125**(1-2), 744-751 (2001).

Lay, T. H., J. W. Bozzelli, A. M. Dean and E. R. Ritter, "Hydrogen atom bond increments for calculation of thermodynamic properties of hydrocarbon radical species." *J. Phys. Chem.* **99**(39), 14514-14527 (1995).

Macdonald, M. A., F. C. Gouldin and E. M. Fisher, "Temperature dependence of phosphorus-based flame inhibition." *Combust. Flame* **124**(4), 668-683 (2001).

Mackie, J., G. Backsay and N. Haworth, "Reactions of phosphorus-containing species of importance in the catalytic recombination of H + OH: Quantum chemical and kinetic studies." *J. Phys. Chem. A* **106**(45), 10825-10830 (2002).

Melius, C., "Carl Melius' Home Page." January, 2003 <http://z.ca.sandia.gov/~melius> (1997).

Montgomery, J. A., J. W. Ochterski and G. A. Petersson, "A complete basis set model chemistry .IV. An improved atomic pair natural orbital method." *J. Chem. Phys.* **101**(7), 5900-5909 (1994).

Nicolaides, A., A. Rauk, M. N. Glukhovtsev and L. Radom, "Heats of formation from G2, G2(MP2), and G2(MP2,SVP) total energies." *J. Phys. Chem.* **100**(44), 17460-17464 (1996).

Nogueira, M. F. and E. M. Fisher, "Effects of dimethyl methylphosphonate on premixed methane flames." *Combust. Flame* **132**(3), 352-363 (2003).

Ochterski, J. W., G. A. Petersson and J. A. Montgomery, "A complete basis set model chemistry .5. Extensions to six or more heavy atoms." *J. Chem. Phys.* **104**(7), 2598-2619 (1996).

Petersson, G. A., D. K. Malick, W. G. Wilson, J. W. Ochterski, J. A. Montgomery and M. J. Frisch, "Calibration and comparison of the Gaussian-2, complete basis set, and density functional methods for computational thermochemistry." *J. Chem. Phys.* **109**(24), 10570-10579 (1998).

Pitzer, K. S. and W. D. Gwinn, "Energy levels and thermodynamic functions for molecules with internal rotations I. Rigid frame with attached tops." *J. Phys. Chem.* **1**, 428-440 (1942).

Quin, L. D., *A Guide to Organophosphorus Chemistry*. Wiley-Interscience, New York (2000).

Schowanek, D. and W. Verstraete, "Hydrolysis and free radical mediated degradation of phosphonates." *J. Environ. Qual.* **20**, 769-776 (1991).

Steinfeld, J. I., J. S. Francisco and W. L. Hase, *Chemical Kinetics and Dynamics*. Prentice-Hall, Inc., Upper Saddle River, NJ (1999).

Sumathi, R., H. H. Carstensen and W. H. Green, "Reaction rate prediction via group additivity Part 1: H abstraction from alkanes by H and CH3." *J. Phys. Chem. A* **105**(28), 6910-6925 (2001).

Twarowski, A., "Reduction of a phosphorus oxide and acid reaction set." *Combust. Flame* **102**(1-2), 41-54 (1995).

Webley, P. A. and J. W. Tester, "Fundamental kinetics of methane oxidation in supercritical water." *Energy and Fuels* **5**, 411-419 (1991).

Werner, J. H. and T. A. Cool, "Kinetic model for the decomposition of DMMP in a hydrogen/oxygen flame." *Combust. Flame* **117**(1-2), 78-98 (1999).

Zegers, E. J. and E. M. Fisher, "Gas-phase pyrolysis of diethyl methylphosphonate." *Combust. Sci. Technol.* **116**(1-6), 69-89 (1996).

Zegers, E. J. P. and E. M. Fisher, "Gas-phase pyrolysis of diisopropyl methylphosphonate." *Combust. Flame* **115**(1-2), 230-240 (1998a).

Zegers, E. J. P. and E. M. Fisher, "Pyrolysis of triethyl phosphate." *Combust. Sci. Technol.* **138**(1-6), 85-103 (1998b).

# 5 Elementary Reaction Rate Model for MPA Oxidation in Supercritical Water

In this chapter, the development of the MPA SCWO elementary reaction is presented along with comparisons of the model predictions with MPA SCWO experimental data. Most of the 96 phosphorus-containing reaction rates in this model had to be estimated. The strategy for choosing possible reaction pathways and estimating the reaction rates for different reaction classes is discussed. Major reaction pathways in the MPA SCWO model are presented and the modeling results are compared to the MPA SCWO experimental data at different operating conditions to determine the model's ability to predict the effects of different operating conditions on MPA oxidation rates.

## 5.1 INTRODUCTION

At SCW conditions above 450°C, reactions proceed primarily through radical pathways as compared to liquid water where ionic pathways dominate due to the polar environment. To model SCWO reaction kinetics, elementary reaction rates from combustion mechanisms are typically adapted to SCW conditions. Unlike combustion conditions, where radical concentrations and elementary reaction rates often can be measured directly, only the concentrations of stable intermediates and products are typically quantified at supercritical conditions. Consequently, developing SCWO elementary reaction rate models is a useful tool to infer the identities and concentrations of the radical species and to assess possible reaction pathways in supercritical water.

To develop SCWO models, the primary modifications to combustion models are to extrapolate pressure dependent reactions to the higher pressure conditions of SCWO and to

include stabilized intermediates that may not have finite lifetimes at combustion conditions. Several assumptions are needed to develop and solve the SCWO models. Reaction rates occurring at combustion conditions are assumed to be similar to those in the SCW environment. Also, water solvation effects are ignored in these models; the important roles that water plays are as a reactant and a third body collider. Hundreds of elementary reactions with multiple intermediates are common in free-radical combustion mechanisms of C1 and C2 compounds. For tractable calculation of these large models, the simplifying assumption of ideal gas conditions is made. At combustion conditions, the ideal gas assumption is accurate; however, supercritical water is a dense gas phase environment.combustion conditions. The results of assuming ideal-gas behavior for SCW conditions are discussed below.

In the Chemkin III program, reversible reaction rates are input to the program along with gas-phase thermodynamic data for each species (Kee *et al.*, 1996). The reverse reaction rates are calculated from the equilibrium constant, $K_c$, in concentration units, which is defined below.

$$k_r = \frac{k_f}{K_c} \tag{5-1}$$

$$K_c = \frac{K_a}{K_\phi}\left(\frac{P_{atm}}{ZRT}\right)^{\sum \nu_i} \tag{5-2}$$

$K_a$ is the general equilibrium constant, $K_\Phi$ is the fugacity equilibrium constant, $P_{atm}$ is the standard-state pressure employed to define the standard-state fugacity ($f^0$), $Z$ is the compressibility factor, and $\nu_i$ is the stoichiometric coefficient for each reactant. $K_a$ is defined as written below.

$$K_a = \exp\left(-\Delta G^o/RT\right) = \exp\left(-\Delta H^o/RT + \Delta S^o/R\right) \tag{5-3}$$

$K_a$ is calculated for each reaction from the ideal-gas thermodynamic parameters that are input to the program to calculate the enthalpy, entropy, and heat capacity for each species. The

thermodynamic data that are used to calculate $K_a$ are at a standard-state pressure of 1 bar. To solve the model, the fugacities are equal to one because of the ideal gas assumption. At SCWO conditions ($T$> 450 °C, $P$~250 bar), the fugacity coefficients approach one at higher temperatures and lower densities. To calculate $K_c$, the compressibility factor, $Z$, is also equal to one from ideal-gas assumptions. From the steam tables, the actual value of the compressibility factor of pure water is between 0.78 to 0.9 at the conditions examined in this study (Haar *et al.*, 1984). Assuming this value to be equal to one should not significantly affect the model predictions. Though SCW is a dense vapor phase, it can be closely approximated to an ideal gas at higher temperatures and lower water densities, so that assuming ideal gas behavior to calculate the model equations should not significantly affect the predicted results.

SCWO models have been previously developed for model compounds such as hydrogen, carbon monoxide, methane, methanol, ethanol, and benzene (Holgate and Tester, 1993; Holgate and Tester, 1994; Dagaut *et al.*, 1995; Brock and Savage, 1995; Dagaut *et al.*, 1996; Alkam *et al.*, 1996; Webley and Tester, 1991; Savage *et al.*, 1998; Rice and Croiset, 2001; DiNaro *et al.*, 2000). Given the inherent uncertainties of rate constants and thermochemical values, these models have had varying degrees of success in predicting measured rates and concentration profiles. Nonetheless, they have been useful in validating and identifying important reaction channels and intermediates.

As discussed in Chapter 4, few elementary reaction rate models for organophosphorus combustion are available. The two most detailed combustion mechanisms by Korobeinichev *et al.* (2000) and Glaude *et al.* (2000) are for the model compound, DMMP. In both of these models, most of the reaction rates were estimated because no organophosphorus reaction rates have been measured and only a few DMMP unimolecular rates have been calculated using

transition state theory and BAC-MP4 *ab initio* calculations by Melius (Melius, 1997). In DMMP combustion, MPA is a minor intermediate with only three reaction rates available from two models. However, as shown in Figure 4-1, the MPA rates from these two models could not properly predict the concentration profiles of all carbon-containing species during MPA oxidation. To develop a complete MPA SCWO model, new reaction pathways and intermediates were required.

## 5.2 ORGANOPHOSPHORUS MODEL DEVELOPMENT

In this section, development of an elementary reaction rate model for MPA oxidation in supercritical water is presented. As compared to typical hydrocarbon SCWO model development where the primary steps are to adjust pressure dependent rate constants for the higher pressures and to include stabilized reaction intermediates, the presence of organophospohorus chemistry required generating new reaction pathways for MPA oxidation and estimating reaction rates for these postulated pathways. The accuracy of the MPA model was then determined by comparing model predictions with measured MPA and product concentration profiles from Chapter 3. Results from this model should provide new insight into organophosphorus compound combustion in SCW.

Possible reaction intermediates were identified and the thermochemical values for these intermediates were accurately calculated from CBS-Q *ab initio* calculations in Gaussian 98, as discussed in Chapter 4. By examining different possible reaction types, pathways between the organophosphorus intermediates were proposed and rates were estimated. In addition to developing a new organophosphorus reaction set, an updated C-1 SCWO submechanism was added to the model. The C-1 submechanism reflects the most recent rates available in the

literature and includes pressure corrections and stabilized intermediates (Hughes *et al.*, 2001; Held and Dryer, 1998; Tsang and Hampson, 1986).

From MPA experimental data, the only identified phosphorus-containing compounds for oxidation in SCW were MPA and phosphoric acid ($PO(OH)_3$). The postulated organophosphorus intermediates that could occur between MPA and $PO(OH)_3$ are shown in Table 5-1 along with their thermochemical values. Newly proposed organophosphorus intermediates include the MPA unimolecular reaction product, $PO(OH)CH_2$, MPA hydrogen abstraction products, $PO(OH)_2CH_2^{\bullet}$ and $PO(O^{\bullet})OHCH_3$, and other intermediates, such as $PO(OH)_2CH_2O^{\bullet}$, $PO(OH)_2C^{\bullet}O$, and $PO(OH)_2CH_2O_2^{\bullet}$. The thermochemistry for most of these intermediates was estimated using CBS-Q Gaussian 98 *ab initio* methods from Chapter 4. However, due to practical constraints for calculating CBS-Q energies in Gaussian 98, the thermochemical values for the three larger organophosphorus peroxy compounds in Table 5-1 were not estimated by *ab initio* methods.

## Table 5-1: Thermodynamic values used in the MPA SCWO mechanism

The $\Delta H_f^o$ values are in kcal/mol, $S^o$ and $C_p^o$ are in cal/mol K for ideal gas state reference conditions at the temperatures shown in ( ) and 1.01 bar.

| Compound | $\Delta H_f^o$ (298K) | $S^o$ (298K) | $C_p^o$ (300K) | $C_p^o$ (400K) | $C_p^o$ (500K) | $C_p^o$ (600K) | $C_p^o$ (800K) | $C_p^o$ (1000K) | $C_p^o$ (1500K) | Source |
|---|---|---|---|---|---|---|---|---|---|---|
| O | 59.55 | 38.49 | 5.23 | 5.13 | 5.08 | 5.05 | 5.02 | 5.00 | 4.98 | a |
| $O_2$ | 0.00 | 49.02 | 7.02 | 7.20 | 7.43 | 7.67 | 8.07 | 8.34 | 8.72 | a |
| H | 52.10 | 27.41 | 4.97 | 4.97 | 4.97 | 4.97 | 4.97 | 4.97 | 4.97 | a |
| $H_2$ | 0.00 | 31.23 | 6.89 | 7.00 | 7.00 | 6.99 | 7.08 | 7.21 | 7.73 | a |
| OH | 8.91 | 43.91 | 7.14 | 7.07 | 7.05 | 7.06 | 7.15 | 7.34 | 7.88 | a |
| $H_2O$ | -57.79 | 45.12 | 8.03 | 8.19 | 8.42 | 8.68 | 9.26 | 9.87 | 11.31 | a |
| $HO_2$ | 3.00 | 54.75 | 8.35 | 8.89 | 9.46 | 9.99 | 10.77 | 11.38 | 12.48 | a |
| $H_2O_2$ | -32.58 | 56.04 | 10.15 | 11.08 | 11.98 | 12.78 | 13.98 | 14.93 | 16.58 | a |
| $CH_2$ | 93.49 | 46.46 | 8.37 | 8.73 | 9.07 | 9.39 | 9.97 | 10.59 | 11.77 | a |
| $CH_2$(s) | 102.47 | 45.22 | 8.08 | 8.33 | 8.66 | 9.04 | 9.83 | 10.57 | 11.91 | a |
| $CH_3$ | 35.06 | 46.36 | 9.20 | 9.98 | 10.75 | 11.50 | 12.86 | 14.09 | 16.25 | a |
| $CH_4$ | -17.83 | 44.53 | 8.55 | 9.69 | 11.11 | 12.60 | 15.29 | 17.59 | 21.51 | a |
| CO | -26.42 | 47.23 | 6.96 | 7.02 | 7.12 | 7.27 | 7.62 | 7.93 | 8.40 | a |
| $CO_2$ | -94.04 | 51.09 | 8.89 | 9.86 | 10.66 | 11.32 | 12.29 | 12.98 | 13.91 | a |
| HCO | 10.11 | 53.59 | 8.29 | 8.75 | 9.29 | 9.84 | 10.85 | 11.66 | 12.94 | a |
| $CH_2O$ | -25.95 | 52.28 | 8.47 | 9.36 | 10.44 | 11.52 | 13.37 | 14.82 | 16.93 | a |
| $CH_2OH$ | -4.11 | 58.35 | 11.35 | 12.79 | 14.16 | 15.36 | 17.08 | 18.44 | 20.59 | a |
| $CH_3O$ | 5.04 | 55.98 | 10.20 | 12.05 | 13.86 | 15.47 | 17.86 | 19.70 | 22.25 | a |
| $CH_3OH$ | -48.04 | 57.51 | 10.28 | 12.07 | 14.07 | 15.98 | 19.00 | 21.38 | 25.07 | a |
| $CH_3OO$ | 2.15 | 64.44 | 12.82 | 15.05 | 17.23 | 19.17 | 22.05 | 24.20 | 27.31 | a |
| $CH_3OOH$ | -33.40 | 61.12 | 14.44 | 17.12 | 19.61 | 21.79 | 25.10 | 27.52 | 30.96 | a |
| $PO(OH)_2CH_3$ | -217.47 | 79.85 | 25.93 | 30.47 | 33.87 | 36.44 | 40.00 | 42.46 | 46.40 | b |
| $PO_2CH_3$ | -118.43 | 71.21 | 15.94 | 18.79 | 21.23 | 23.31 | 26.48 | 28.75 | 32.17 | b |
| $POOHCH_2$ | -90.64 | 71.09 | 18.44 | 21.68 | 24.10 | 25.93 | 28.53 | 30.36 | 33.27 | b |
| $PO(OH)_2CH_2$ | -164.97 | 83.16 | 25.48 | 29.56 | 32.36 | 34.32 | 36.87 | 38.63 | 41.59 | b |
| $PO_2(OH)CH_3$ | -150.68 | 78.80 | 23.69 | 27.75 | 30.96 | 33.48 | 37.03 | 39.37 | 42.78 | b |
| $PO(OH)_3CH_3$ | -212.22 | 88.53 | 31.77 | 37.62 | 41.96 | 45.23 | 49.87 | 51.65 | 58.65 | c |
| $PO(OH)_2CH_2OH$ | -247.76 | 89.79 | 30.91 | 35.58 | 39.03 | 41.60 | 45.06 | 47.42 | 51.23 | b |
| $PO(OH)_2CH_2O$ | -190.50 | 88.63 | 28.28 | 32.62 | 35.90 | 38.37 | 41.74 | 44.00 | 47.45 | b |
| $PO_2(OH)CH_2OH$ | -163.35 | 84.32 | 26.53 | 31.20 | 34.88 | 37.78 | 41.91 | 44.76 | 49.12 | b |
| $PO(OH)_2CHOH$ | -210.76 | 90.01 | 29.07 | 34.11 | 37.60 | 39.97 | 42.72 | 44.34 | 46.90 | b |
| $PO(OH)_2CHO$ | -220.13 | 88.11 | 26.08 | 29.67 | 32.28 | 34.21 | 36.93 | 38.84 | 41.88 | b |
| $PO(OH)_2CO$ | -185.33 | 89.40 | 26.28 | 28.87 | 30.69 | 32.00 | 33.80 | 35.07 | 37.17 | b |
| $PO(OH)_3$ | -271.71 | 80.55 | 21.92 | 25.06 | 27.41 | 29.16 | 31.53 | 33.15 | 35.86 | b |
| $PO(OH)_2$ | -157.03 | 74.39 | 17.31 | 19.66 | 21.33 | 22.52 | 24.07 | 25.09 | 26.78 | b |
| $PO_2OH$ | -168.45 | 66.57 | 14.42 | 16.62 | 18.27 | 19.50 | 21.15 | 22.19 | 23.68 | b |
| POOH | -111.07 | 62.39 | 11.64 | 13.17 | 14.30 | 15.14 | 16.25 | 16.97 | 18.08 | b |
| $P(OH)_4$ | -217.64 | 81.24 | 26.04 | 30.28 | 33.15 | 35.13 | 38.66 | 40.25 | 42.65 | b |
| $PO(OH)_2CH_2OO$ | -198.47 | 94.42 | 32.91 | 37.77 | 41.41 | 44.12 | 47.88 | 50.33 | 54.76 | d |
| $PO(OH)_2CH_2OOH$ | -233.11 | 97.90 | 35.12 | 40.54 | 44.49 | 47.34 | 51.10 | 53.46 | 56.99 | d |
| $PO_2(OH)CH_2OOH$ | -166.32 | 96.85 | 32.88 | 37.82 | 41.58 | 44.38 | 48.13 | 50.37 | 53.38 | d |

Sources: a) Burcat, 2003 b) CBS-Q calculations (Chapter 4) c) CBS-QB3 calculations (Chapter 4) d) estimated, this study

The thermochemistry for the peroxy compounds was estimated as follows. The $PO(OH)_2CH_2OOH$ thermochemistry was estimated from $PO(OH)_2CH_2OH$, $CH_3CH_2OOH$, and $CH_3CH_2OH$ by assuming that the change in enthalpy, entropy, and heat capacity between the following two reactions would be approximately the same.

$$CH_3CH_2OH + CH_3OOH \rightarrow CH_3CH_2OOH + CH_3OH \quad \text{(R1a)}$$
$$PO(OH)_2CH_2OH + CH_3OOH \rightarrow PO(OH)_2CH_2OOH + CH_3OH \quad \text{(R2a)}$$

The thermochemistry for $PO(OH)_2CH_2OH$ was taken from Table 5-1 and the thermochemistry for $CH_3CH_2OH$ and $CH_3CH_2OOH$ was available from Burcat (2003). With the $PO(OH)_2CH_2O_2H$ thermochemistry, the thermochemistry for $PO(OH)_2CH_2O_2^{\bullet}$ was calculated by a similar method using the two reactions below.

$$CH_3CH_2O_2H \rightarrow CH_3CH_2O_2^{\bullet} + H^{\bullet} \quad \text{(R3a)}$$
$$PO(OH)_2CH_2O_2H \rightarrow PO(OH)_2CH_2O_2^{\bullet} + H^{\bullet} \quad \text{(R4a)}$$

The thermochemistry for $C_2H_5O_2H$, $C_2H_5O_2^{\bullet}$, and $H^{\bullet}$ were all taken from Burcat (2003). Likewise, the thermochemistry for $PO_2OHCH_2O_2H$ was also calculated by comparing it to a similar reaction, as shown below.

$$PO(OH)_2CH_3 + OH^{\bullet} \rightarrow PO(O^{\bullet})OHCH_3 + H_2O \quad \text{(R5a)}$$
$$PO(OH)_2CH_2O_2H + OH^{\bullet} \rightarrow PO(O^{\bullet})OHCH_2O_2H + H_2O \quad \text{(R6a)}$$

The thermochemistry for all compounds in reaction 6a were available in Table 5-1. Due to the larger size of these peroxy compounds, their thermochemistry needed to be estimated using simpler methods.

To develop the organophosphorus reaction set, possible reaction pathways between the chosen intermediates were hypothesized. Reaction pathways were chosen from different reaction families including hydrogen atom abstraction, oxygen atom abstraction, addition of alkyl radicals to molecular oxygen, unimolecular decomposition, and non-terminating radical

collisions. The 96 hypothesized phosphorus-containing reactions included in the MPA SCWO mechanism are given in Table 5-2 along with the 150 $H_2/O_2$ and C-1 reactions. For reaction rates with no experimentally measured or *ab initio* calculated rate constants, a common rate estimation method was employed that compares specific reactions in the MPA mechanism to similar hydrocarbon reactions with well-known rate constants.

**Table 5-2: MPA SCWO mechanism**

For the estimated reaction rates, the source references are italicized. If the rate was taken directly from a similar rate constant in the literature, the species is included in parentheses. $E_a$ is in cal/mol in this table and $A$ has units of $s^{-1}$ or mol/($cm^3$s). For the pressure dependent rate constants (denoted with (+M)), the first line is the high-pressure rate constant ($k_\infty$) and the second line is the low pressure rate constant ($k_o$). When available, TROE constants are included to better estimate rate constants at intermediate pressures below the high-pressure limit. Also, third-body collision efficiencies are included for some pressure-dependent reactions as noted in the table. For pressure dependent rate constants with only +M, these are low pressure rate constants, $k_0$.

| No. | Reaction | $A$ | $n$ | $E_a$ | Source |
|---|---|---|---|---|---|
| 1 | $H_2+O = OH+H$ | 5.12E+04 | 2.67 | 6278 | a |
| 2 | $H_2O+H = H_2+OH$ | 4.52E+08 | 1.6 | 18423 | a |
| 3 | $O_2+H = HO_2$ | 2.07E+18 | -1.69 | 890 | b |
| 4 | $O_2+H = OH+O$ | 9.76E+13 | 0 | 14845 | a |
| 5 | $H_2O_2+H = HO_2+H_2$ | 1.69E+12 | 0 | 3755 | a |
| 6 | $H_2O_2+H = OH+H_2O$ | 1.02E+13 | 0 | 3578 | a |
| 7 | $H_2O_2+O = OH+HO_2$ | 6.62E+11 | 0 | 3975 | a |
| 8 | $H_2O_2+OH = H_2O+HO_2$ | 1.70E+18 | 0 | 29408 | c |
| 9 | $H_2O_2+OH = H_2O+HO_2$ | 2.00E+12 | 0 | 427 | c |
| 10 | $OH+OH = H_2O_2$ | 2.96E+28 | -5.26 | 2980 | b |
| 11 | $H+H+M = H_2+M$<br>$O_2$/0.4/CO/0.75/$CO_2$/1.5/$H_2O$/6.5/$CH_4$/3.0/$H_2$/0.0 | 1.87E+18 | -1.00 | 0 | a |
| 12 | $H+H+H_2 = H_2+H_2$ | 9.79E+16 | -0.60 | 0 | a |
| 13 | $H+O+M = OH+M$<br>$O_2$/0.4/CO/0.75/$CO_2$/1.5/$H_2O$/6.5/$CH_4$/3.0/$H_2$/0.0 | 1.18E+19 | -1.0 | 0 | a |
| 14 | $H+OH+M = H_2O+M$<br>$O_2$/0.4/CO/0.75/$CO_2$/1.5/$H_2O$/6.5/$CH_4$/3.0/$H_2$/0.0 | 5.53E+22 | -2.0 | 0 | a |
| 15 | $H+HO_2 = H_2+O_2$ | 4.28E+13 | 0 | 1410 | a |
| 16 | $H+HO_2 = OH+OH$ | 1.69E+14 | 0 | 875 | a |
| 17 | $H+HO_2 = H_2O+O$ | 3.01E+13 | 0 | 1721 | a |
| 18 | $O+O+M = O_2+M$<br>$O_2$/0.4/CO/0.75/$CO_2$/1.5/$H_2O$/6.5/$CH_4$/3.0/$H_2$/0.0 | 5.40E+13 | 0 | -1788 | a |
| 19 | $O+HO_2 = O_2+OH$ | 3.19E+13 | 0 | 0 | a |
| 20 | $OH+OH = O+H_2O$ | 1.51E+09 | 1.14 | 100 | a |
| 21 | $OH+HO_2 = H_2O+O_2$ | 1.91E+16 | -1.00 | 0 | b |
| 22 | $HO_2+HO_2 = H_2O_2+O_2$ | 4.22E+14 | 0 | 11984 | a |
| 23 | $HO_2+HO_2 = H_2O_2+O_2$ | 1.32E+11 | 0 | -1630 | a |
| 24 | $CH_4+O_2 = CH_3+HO_2$ | 3.97E+13 | 0 | 56892 | a |
| 25 | $CH_4+H = CH_3+H_2$ | 1.32E+04 | 3.00 | 8038 | a |
| 26 | $CH_4+CH_2 = CH_3+CH_3$ | 4.30E+12 | 0 | 10038 | a |
| 27 | $CH_4+CH_2(s) = CH_3+CH_3$ | 7.00E+13 | 0 | 0 | a |
| 28 | $CH_4+O = CH_3+OH$ | 7.23E+08 | 1.56 | 8485 | a |
| 29 | $CH_4+OH = CH_3+H_2O$ | 1.57E+07 | 1.83 | 2782 | a |
| 30 | $CH_4+HO_2 = CH_3+H_2O_2$ | 9.03E+12 | 0 | 24720 | a |
| 31 | $CH_4+CH_3OO = CH_3OOH+CH_3$ | 1.81E+11 | 0 | 18481 | d |

| No. | Reaction | *A* | *n* | $E_a$ | Source |
|---|---|---|---|---|---|
| 32 | $O_2+CH_3 = CH_2O+OH$ | 3.31E+11 | 0 | 8944 | a |
| 33 | $O_2+CH_3 = CH_3O+O$ | 1.32E+14 | 0 | 31398 | e |
| 34 | $CH_3+O_2(+M) = CH_3OO(+M)$ | 7.83E+08 | 1.2 | 0 | e |
| | $O_2$/0.4/CO/0.75/$CO_2$/1.5/$H_2O$/6.5/$CH_4$/3.0/$H_2$/0.0 | | | | |
| | $k_0$ | 1.55E+26 | -3.3 | 0 | |
| | TROE: 0.336/ 239 / 1.0E+05 | | | | |
| 35 | $H+CH_3(+M) = CH_4(+M)$ | 2.11E+14 | 0 | 0 | e |
| | $O_2$/0.4/CO/0.75/$CO_2$/1.5/$H_2O$/6.5/$CH_4$/3.0/$H_2$/0.0 | | | | |
| 35 | $k_0$ | 1.76E+24 | -1.8 | 0 | |
| | TROE: 0.37 / 3315 / 61 | | | | |
| 36 | $H_2+CH_2(s) = CH_3+H$ | 7.23E+13 | 0 | 0 | a |
| 37 | $CH_3+O = CH_2O+H$ | 8.43E+13 | 0 | 0 | a |
| 38 | $CH_3+O = CH_3O$ | 7.97E+16 | -2.12 | 625 | f |
| 39 | $CH_3+OH(+M) = CH_3OH(+M)$ | 2.79E+18 | -1.43 | 1330 | g |
| | $k_0$ | 4.00E+36 | -5.92 | 31400 | |
| | TROE: 0.412 / 195 / 5900 / 6394 | | | | |
| 40 | $CH_2(s)+H_2O(+M)=CH_3OH(+M)$ | 4.80E+18 | -1.16 | 1145 | g |
| | $k_0$ | 1.88E+38 | -6.36 | 50400 | |
| | TROE:0.6027 / 208 / 3922 / 10180 | | | | |
| 41 | $CH_3+HO_2 = CH_3O+OH$ | 1.80E+13 | 0 | 0 | a |
| 42 | $CH_3+HO_2 = CH_2O+H_2O$ | 1.11E+05 | 1.86 | -2460 | h |
| 43 | $CH_3+HCO = CH_4+CO$ | 1.20E+14 | 0 | 0 | a |
| 44 | $CH_2O+CH_3 = CH_4+HCO$ | 7.83E-08 | 6.1 | 1970 | a |
| 45 | $CH_3+CH_3O = CH_4+CH_2O$ | 2.41E+13 | 0 | 0 | d |
| 46 | $CH_3+CH_2OH = CH_4+CH_2O$ | 2.41E+12 | 0 | 0 | i |
| 47 | $CH_3+CH_3OO = CH_3O+CH_3O$ | 2.41E+13 | 0 | 0 | d |
| 48 | $CH_3OH+CH_3 = CH_4+CH_2OH$ | 3.19E+01 | 3.2 | 7172 | i |
| 49 | $CH_3OH+CH_3 = CH_4+CH_3O$ | 1.44E+01 | 3.1 | 6935 | i |
| 50 | $CH_2+H = CH_3$ | 2.16E+13 | 0.32 | 0 | j |
| 51 | $O_2+CH_3O = CH_2O+HO_2$ | 2.17E+10 | 0 | 1750 | a |
| 52 | $O_2+CH_2OH = CH_2O+HO_2$ | 1.57E+15 | -1.00 | 0 | a |
| 53 | $O_2+CH_2OH = CH_2O+HO_2$ | 7.23E+13 | 0 | 3578 | a |
| 54 | $H+CH_3O = CH_2O+H_2$ | 1.81E+13 | 0 | 0 | a |
| 55 | $H+CH_2OH = CH_2O+H_2$ | 3.08E+13 | 0 | 0 | a |
| 56 | $OH+CH_3O = CH_2O+H_2O$ | 1.81E+13 | 0 | 0 | a |
| 57 | $OH+CH_2OH = CH_2O+H_2O$ | 2.41E+13 | 0 | 0 | a |
| 58 | $CH_3OOH = CH_3O+OH$ | 6.00E+14 | 0 | 42330 | e |
| 59 | $O+CH_3O = CH_2O+OH$ | 1.81E+12 | 0 | 0 | a |
| 60 | $O+CH_2OH = CH_2O+OH$ | 9.03E+13 | 0 | 0 | a |
| 61 | $CH_3O+HO_2 = CH_2O+H_2O_2$ | 3.01E+11 | 0 | 0 | d |
| 62 | $CH_2OH+HO_2 = CH_2O+H_2O_2$ | 1.21E+13 | 0 | 0 | i |
| 63 | $2CH_3O = CH_2O+CH_3OH$ | 6.03E+13 | 0 | 0 | d |
| 64 | $CH_3O+CH_2OH = CH_3OH+CH_2O$ | 2.41E+13 | 0 | 0 | i |
| 65 | $CH_2OH+CH_2OH = CH_3OH+CH_2O$ | 4.82E+12 | 0 | 0 | i |
| 66 | $CH_3O+CH_3OH = CH_3OH+CH_2OH$ | 3.01E+11 | 0 | 4074 | i |
| 67 | $CH_3O+CH_2 = CH_3+CH_2O$ | 1.81E+13 | 0 | 0 | d |
| 68 | $CH_3O+CH_2(s) = CH_3+CH_2O$ | 1.81E+13 | 0 | 0 | d |
| 69 | $CH_2+CH_2OH = CH_3+CH_2O$ | 1.21E+12 | 0 | 0 | i |
| 70 | $CH_3O+CH_2O = CH_3OH+HCO$ | 1.02E+11 | 0 | 2981 | d |
| 71 | $CH_2OH+CH_2O = CH_3OH+HCO$ | 5.49E+03 | 2.80 | 5862 | i |
| 72 | $CH_3O+HCO = CH_3OH+CO$ | 9.04E+13 | 0 | 0 | d |
| 73 | $CH_2OH+HCO = CH_3OH+CO$ | 1.21E+14 | 0 | 0 | i |
| 74 | $CH_2OH+HCO = CH_2O+CH_2O$ | 1.81E+14 | 0 | 0 | i |
| 75 | $CH_3O+CO = CH_3+CO_2$ | 6.81E-18 | 9.2 | -2840 | k |
| 76 | $CH_3O+CH_3OO = CH_2O+CH_3OOH$ | 3.01E+11 | 0 | 0 | d |

| No. | Reaction | *A* | *n* | $E_a$ | Source |
|---|---|---|---|---|---|
| 77 | $CH_2OH+CH_3OO = CH_2O+CH_3O+OH$ | 1.21E+13 | 0 | 0 | i |
| 78 | $CH_3O(+M) = CH_2O+H(+M)$ | 6.80E+13 | 0 | 26171 | l |
| | $O_2$/0.4/CO/0.75/$CO_2$/1.5/$H_2O$/6.5/$CH_4$/3.0/$H_2$/0.0 | | | | |
| | $k_0$ | 5.17E+23 | -2.4 | 24307 | |
| | TROE: 8.02 / 1258 / 1022 / 454 | | | | |
| 79 | $CH_2OH(+M) = CH_2O+H(+M)$ | 7.00E+14 | 0 | 29637 | m |
| | $k_0$ | 1.26E+16 | 0 | 30020 | a |
| | $O_2$/0.4/CO/0.75/$CO_2$/1.5/$H_2O$/6.5/$CH_4$/3.0/$H_2$/0.0 | | | | |
| 80 | $CH_3OH+H = CH_2OH+H_2$ | 1.44E+13 | 0 | 6095 | n |
| 81 | $CH_3OH+H = CH_3O+H_2$ | 3.60E+12 | 0 | 6095 | n |
| 82 | $CH_3OH+O = CH_2OH+OH$ | 3.88E+05 | 2.50 | 3080 | n |
| 83 | $CH_3OH+O = CH_3O+OH$ | 1.00E+13 | 0 | 4684 | o |
| 84 | $CH_3OH+OH = CH_2OH+H_2O$ | 7.10E+06 | 1.80 | -596 | n |
| 85 | $CH_3OH+OH = CH_3O+H_2O$ | 1.00E+06 | 2.10 | 496.7 | n |
| 86 | $CH_3OH+O_2 = CH_2OH+HO_2$ | 2.05E+13 | 0 | 44900 | n |
| 87 | $CH_3OH+HO_2 = CH_2OH+H_2O_2$ | 3.98E+13 | 0 | 19400 | n |
| 88 | $CH_3OH+CH_2 = CH_2OH+CH_3$ | 3.19E+01 | 3.20 | 7172 | i |
| 89 | $CH_3OH+CH_2 = CH_3O+CH_3$ | 1.44E+01 | 3.10 | 6935 | i |
| 90 | $CH_3OH+CH_2(s) = CH_2OH+CH_3$ | 1.51E+12 | 0 | 0 | i |
| 91 | $CH_3OH+CH_3OO = CH_2OH+CH_3OOH$ | 1.81E+11 | 0 | 13712 | i |
| 92 | $CH_3OH(+M) = CH_2OH+H(+M)$ | 2.69E+16 | -0.08 | 98940 | n |
| | $k_0$ | 2.34E+40 | -6.33 | 103100 | |
| | TROE: 0.773 / 693 / 5333 / 1.0E+05 | | | | |
| 93 | $H+CH_3O(+M) = CH_3OH(+M)$ | 2.43E+12 | 0.515 | 50 | g |
| | $k_0$ | 4.66E+41 | -7.44 | 14080 | |
| | TROE: 0.7 / 100 / 9.0E+4 / 1.0E+4 | | | | |
| | $H_2$/2.0/$H_2O$/6.0/$CH_4$/2.0/CO/1.5/$CO_2$/2.0 | | | | |
| 94 | $CH_3OO+H_2 = CH_3OOH+H$ | 3.01E+13 | 0 | 26032 | d |
| 95 | $CH_3OO+H = CH_3O+OH$ | 9.64E+13 | 0 | 0 | d |
| 96 | $CH_3OO+O = CH_3O+O_2$ | 3.61E+13 | 0 | 0 | d |
| 97 | $CH_3OO+OH = CH_3OH+O_2$ | 6.03E+13 | 0 | 0 | d |
| 98 | $CH_3OO+HO_2 = CH_3OOH+O_2$ | 2.29E+11 | 0 | -1550 | p |
| 99 | $CH_3OO+H_2O_2 = CH_3OOH+HO_2$ | 2.41E+12 | 0 | 9936 | d |
| 100 | $CH_2O+CH_3OO = CH_3OOH+HCO$ | 1.99E+12 | 0 | 11665 | d |
| 101 | $CH_3OO+HCO = CH_3OOH+CO$ | 3.01E+13 | 0 | 0 | d |
| 102 | $CH_3OO+CH_3OO = CH_3O+CH_3O+O_2$ | 8.51E+12 | -0.64 | 607 | e |
| 103 | $CH_3OO+CH_3OO = CH_3OH+CH_2O+O_2$ | 3.40E+11 | -0.64 | -1718 | e |
| 104 | $CH_2+CH_3OO = CH_2O+CH_3O$ | 1.81E+13 | 0 | 0 | d |
| 105 | $CH_3OOH+H = CH_3O+H_2O$ | 7.27E+10 | 0 | 1860 | q |
| 106 | $CH_3OOH+OH = CH_3OO+H_2O$ | 7.23E+11 | 0 | -258 | r |
| 107 | $CH_3OOH = CH_2O+H_2O$ | 3.09E-02 | 4.51 | 39758 | h |
| 108 | $H+CH_2(s) = CH_2+H$ | 2.00E+14 | 0 | 0 | a |
| 109 | $CH_2+O = CO+H+H$ | 7.20E+13 | 0 | 0 | a |
| 110 | $CH_2+O = CO+H_2$ | 4.80E+13 | 0 | 0 | a |
| 111 | $O+CH_2 = H+HCO$ | 8.00E+13 | 0 | 0 | g |
| 112 | $CH_2(s)+O = H_2+CO$ | 1.50E+13 | 0 | 0 | d |
| 113 | $CH_2(s)+O = CO+H+H$ | 1.50E+13 | 0 | 0 | d |
| 114 | $CH_2+OH = CH_2O+H$ | 1.81E+13 | 0 | 0 | a |
| 115 | $OH+CH_2(s) = H+CH_2O$ | 3.00E+13 | 0 | 0 | g |
| 116 | $O_2+CH_2 = CO_2+H_2$ | 5.43E+12 | 0 | 1491 | a |
| 117 | $O_2+CH_2 = CO_2+H+H$ | 5.43E+12 | 0 | 1491 | a |
| 118 | $O_2+CH_2 = CO+OH+H$ | 8.15E+12 | 0 | 1491 | a |
| 119 | $O_2+CH_2 = CO+H_2O$ | 1.48E+12 | 0 | 1491 | a |
| 120 | $O_2+CH_2 = CH_2O+O$ | 4.20E+12 | 0 | 1491 | a |
| 121 | $CH_2+O_2 = HCO+OH$ | 4.30E+10 | 0 | -500 | q |

| No. | Reaction | *A* | *n* | $E_a$ | Source |
|---|---|---|---|---|---|
| 122 | $O_2+CH_2(s) = CO+OH+H$ | 3.13E+13 | 0 | 0 | a |
| 123 | $CH_2(s)+O_2 = CO+H_2O$ | 1.20E+13 | 0 | 0 | g |
| 124 | $HO_2+CH_2 = OH+CH_2O$ | 2.00E+13 | 0 | 0 | g |
| 125 | $HO_2+CH_2(s) = OH+CH_2O$ | 3.02E+13 | 0 | 0 | d |
| 126 | $CH_2(s)+H_2O_2 = CH_3+HO_2$ | 3.01E+13 | 0 | 0 | d |
| 127 | $CO_2+CH_2 = CH_2O+CO$ | 2.35E+10 | 0 | 0 | a |
| 128 | $CH_2(s)+CO_2 = CO+CH_2O$ | 1.40E+13 | 0 | 0 | g |
| 129 | $CH_2(s)+CH_2O = CH_3+HCO$ | 1.20E+12 | 0 | 0 | d |
| 130 | $CH_2+HCO = CH_3+CO$ | 1.81E+13 | 0 | 0 | a |
| 131 | $CH_2(s)+HCO = CH_3+CO$ | 1.81E+13 | 0 | 0 | d |
| 132 | $CH_2(s)+M = CH_2+M$ | 1.51E+13 | 0 | 0 | a |
| | $O_2$/0.4/CO/0.75/$CO_2$/1.5/$H_2O$/6.5/$CH_4$/0.48 | | | | |
| 133 | $CH_2O+H = HCO+H_2$ | 1.26E+08 | 1.62 | 2165 | a |
| 134 | $CH_2O+O = HCO+OH$ | 4.16E+11 | 0.57 | 2763 | a |
| 135 | $CH_2O+OH = HCO+H_2O$ | 3.43E+09 | 1.18 | -447 | a |
| 136 | $O_2+CH_2O = HCO+HO_2$ | 6.02E+13 | 0 | 40657 | a |
| 137 | $CH_2O+HO_2 = H_2O_2+HCO$ | 3.01E+12 | 0 | 13076 | a |
| 138 | $H+HCO(+M) = CH_2O(+M)$ | 1.09E+12 | 0.48 | -260 | g |
| | $k_0$ | 2.47E+24 | -2.57 | 425 | |
| | TROE:0.7824 / 271 / 2755 / 6570 | | | | |
| | $H_2$/2.0/$H_2O$/6.0/$CH_4$/2.0/CO/1.5/$CO_2$/2.0 | | | | |
| 139 | $H_2+CO(+M) = CH_2O(+M)$ | 4.30E+07 | 1.50 | 79600 | g |
| | $k_0$ | 5.07E+27 | -3.42 | 84350 | |
| | TROE: 0.932 / 197 / 1540 / 1.03E+04 | | | | |
| | $H_2$/2.0/$H_2O$/6.0/$CH_4$/2.0/CO/1.5/$CO_2$/2.0 | | | | |
| 140 | $H+HCO = CO+H_2$ | 9.03E+13 | 0 | 0 | a |
| 141 | $O+HCO = CO+OH$ | 3.01E+13 | 0 | 0 | a |
| 142 | $O+HCO = CO_2+H$ | 3.01E+13 | 0 | 0 | a |
| 143 | $O_2+HCO = HO_2+CO$ | 3.01E+12 | 0 | 0 | a |
| 144 | $OH+HCO = H_2O+CO$ | 1.02E+14 | 0 | 0 | a |
| 145 | $HCO+HCO = CH_2O+CO$ | 3.01E+13 | 0 | 0 | a |
| 146 | $HCO = H+CO$ | 4.50E+13 | 0 | 21500 | *s* |
| 147 | $O_2+CO = CO_2+O$ | 1.26E+13 | 0 | 47060 | a |
| 148 | $O+CO(+M) = CO_2(+M)$ | 1.80E+10 | 0 | 2385 | g |
| | $k_0$ | 6.02E+14 | 0 | 3000 | g |
| | $H_2$/2.0/$O_2$/6.0/$H_2O$/6.0/$CH_4$/2.0/CO/1.5/$CO_2$/3.5 | | | | |
| 149 | $CO+HO_2 = CO_2+OH$ | 1.51E+14 | 0 | 23666 | a |
| 150 | $CO+OH = H+CO_2$ | 6.98E+09 | 0.56 | -20 | t |
| 151 | $PO(OH)_2CH_3 = PO_2CH_3+H_2O$ | 2.20E+12 | 0.04 | 41900 | u |
| 152 | $PO(OH)_2CH_3 = PO_2OH+CH_4$ | 6.40E+11 | 0.41 | 64100 | u |
| 153 | $PO(OH)_2CH_3 = POOHCH_2+H_2O$ | 2.60E+09 | 1.31 | 73000 | u |
| 154 | $PO(OH)_2CH_3 = POOH+CH_3OH$ | 1.70E+11 | 0.73 | 105130 | u |
| 155 | $PO_2CH_3+OH = PO_2OH+CH_3$ | 1.00E+12 | 0.0 | 2000 | v |
| 156 | $PO(OH)_2CH_3+OH = PO(OH)_2CH_2+H_2O$ | 1.00E+06 | 2.39 | -1137 | u |
| 157 | $PO(OH)_2CH_3+OH = PO_2(OH)CH_3+H_2O$ | 2.13E+04 | 2.40 | 198 | u |
| 158 | $PO(OH)_2CH_3+OH = PO(OH)_3CH_3$ | 5.32+03 | 2.01 | 837 | u |
| 159 | $PO(OH)_2CH_2+H = PO(OH)_2CH_3$ | 1.00E+14 | 0 | 0 | *w* |
| 160 | $PO_2(OH)CH_3+H = PO(OH)_2CH_3$ | 1.00E+14 | 0 | 0 | *w* |
| 161 | $PO(OH)_2CH_3+H = PO(OH)_2CH_2+H_2$ | 2.80E+07 | 2.0 | 7700 | *w* |
| 162 | $PO(OH)_2CH_3+O = PO(OH)_2CH_2+OH$ | 2.20E+06 | 2.4 | 5500 | *w* |
| 163 | $PO(OH)_2CH_3+CH_3 = PO(OH)_2CH_2+CH_4$ | 6.51E+11 | 0 | 11600 | *w* |
| 164 | $PO(OH)_2CH_3+CH_3O = PO(OH)_2CH_2+CH_3OH$ | 1.58E+11 | 0 | 7000 | *w* |
| 165 | $PO(OH)_2CH_2+HO_2 = PO(OH)_2CH_3+O_2$ | 1.50E+11 | 0 | 0 | *d* ($C_2H_5$) |
| 166 | $PO(OH)_2CH_3+CH_3OO = PO(OH)_2CH_2+CH_3OOH$ | 6.06E+12 | 0 | 20430 | *w* |

| No. | Reaction | *A* | *n* | $E_a$ | Source |
|---|---|---|---|---|---|
| 167 | $PO(OH)_2CH_2OO + PO(OH)_2CH_3 = PO(OH)_2CH_2OOH + PO(OH)_2CH_2$ | 6.06E+12 | 0 | 20430 | *w* |
| 168 | $PO(OH)_2CH_3 + HO_2 = PO(OH)_2CH_2 + H_2O_2$ | 4.02E+12 | 0 | 19400 | *w* |
| 169 | $PO(OH)_3CH_3 = PO(OH)_3 + CH_3$ | 7.40E+11 | 0.05 | 2940 | u |
| 170 | $PO(OH)_2CH_2 + O_2 = PO(OH)_2CH_2OO$ | 2.94E+13 | -0.44 | 0 | $x(C_2H_5)$ |
| 171 | $PO(OH)_2CH_2 + CH_3OO = PO(OH)_2CH_2O + CH_3O$ | 1.90E+12 | 0 | -1200 | *w* |
| 172 | $PO(OH)_2CH_2 + PO(OH)_2CH_2OO = PO(OH)_2CH_2O + PO(OH)_2CH_2O$ | 1.90E+12 | 0 | -1200 | *w* |
| 173 | $PO(OH)_2CH_2 + HO_2 = PO(OH)_2CH_2O + OH$ | 3.00E+13 | 0 | 0 | $y(C_2H_5)$ |
| 174 | $PO(OH)_2CH_2 + O_2 = PO(OH)_2CH_2O + O$ | 1.00E+13 | -0.20 | 27902 | $y(C_2H_5)$ |
| 175 | $PO(OH)_2CH_2O = PO(OH)_2 + CH_2O$ | 1.10E+13 | 0 | 16700 | $z(C_2H_5O)$ |
| 176 | $PO(OH)_2CH_2O + O_2 = PO(OH)_2CHO + HO_2$ | 3.60E+10 | 0 | 1090 | $x(C_2H_5O)$ |
| 177 | $PO(OH)_2CH_2O + CO = PO(OH)_2CH_2 + CO_2$ | 4.68E+02 | 3.16 | 5380 | $aa(C_2H_5O)$ |
| 178 | $PO(OH)_2CH_2O + OH = PO(OH)_2CHO + H_2O$ | 1.00E+13 | 0 | 0 | $aa(C_2H_5O)$ |
| 179 | $PO(OH)_2CH_2OH = PO(OH)_2 + CH_2OH$ | 5.94E+23 | -1.68 | 91163 | $aa(C_2H_5OH)$ |
| 180 | $PO(OH)_2CH_2OH = PO(OH)_2CH_2 + OH$ | 1.25E+23 | -1.54 | 96005 | $aa(C_2H_5OH)$ |
| 181 | $PO(OH)_2CH_2OH = PO(OH)_2CHO + H_2$ | 7.24E+11 | 0.10 | 91010 | $aa(C_2H_5OH)$ |
| 182 | $PO(OH)_2CH_2OH + HO_2 = PO(OH)_2CH_2O + H_2O_2$ | 2.50E+12 | 0 | 24000 | $aa(C_2H_5OH)$ |
| 183 | $PO(OH)_2CH_2OH + OH = PO(OH)_2CH_2O + H_2O$ | 7.46E+11 | 0.30 | 1634 | $aa(C_2H_5OH)$ |
| 184 | $PO(OH)_2CH_2OH + H = PO(OH)_2CH_2O + H_2$ | 1.50E+07 | 1.60 | 3038 | $aa(C_2H_5OH)$ |
| 185 | $PO(OH)_2CH_2OH + O = PO(OH)_2CH_2O + OH$ | 1.58E+07 | 2.00 | 4448 | $aa(C_2H_5OH)$ |
| 186 | $PO(OH)_2CH_2OH + CH_3 = PO(OH)_2CH_2O + CH_4$ | 1.45E+02 | 2.99 | 7649 | $aa(C_2H_5OH)$ |
| 187 | $PO(OH)_2CH_2OH + HO_2 = PO(OH)_2CHOH + H_2O_2$ | 8.20E+03 | 2.55 | 10750 | $aa(C_2H_5OH)$ |
| 188 | $PO(OH)_2CH_2OH + OH = PO(OH)_2CHOH + H_2O$ | 4.64E+11 | 0.15 | 0 | $aa(C_2H_5OH)$ |
| 189 | $PO(OH)_2CH_2OH + H = PO(OH)_2CHOH + H_2$ | 2.58E+07 | 1.65 | 2827 | $aa(C_2H_5OH)$ |
| 190 | $PO(OH)_2CH_2OH + O = PO(OH)_2CHOH + OH$ | 1.88E+07 | 1.85 | 1824 | $aa(C_2H_5OH)$ |
| 191 | $PO(OH)_2CH_2OH + CH_3 = PO(OH)_2CHOH + CH_4$ | 7.28E+02 | 2.99 | 7948 | $aa(C_2H_5OH)$ |
| 192 | $PO(OH)_2CH_2OH + PO(OH)_2CH_2 = PO(OH)_2CHOH + PO(OH)_2CH_3$ | 5.00E+10 | 0 | 10400 | $bb(C_2H_5OH)$ |
| 193 | $PO(OH)_2CH_2OH + O_2 = PO(OH)_2CHOH + HO_2$ | 1.50E+13 | 0 | 50150 | $bb(C_2H_5OH)$ |
| 194 | $PO(OH)_2CHOH + O_2 = PO(OH)_2CHO + HO_2$ | 8.43E+15 | -1.20 | 0 | $aa(CH_3CHOH)$ |
| 195 | $PO(OH)_2CHOH + O_2 = PO(OH)_2CHO + HO_2$ | 4.82E+14 | 0 | 5017 | $aa(CH_3CHOH)$ |
| 196 | $PO(OH)_2CHOH + O = PO(OH)_2CHO + OH$ | 1.00E+14 | 0 | 0 | $aa(CH_3CHOH)$ |
| 197 | $PO(OH)_2CHOH + H = PO(OH)_2 + CH_2OH$ | 3.00E+13 | 0 | 0 | $aa(CH_3CHOH)$ |
| 198 | $PO(OH)_2CHOH + HO_2 = PO(OH)_2CHO + OH + OH$ | 4.00E+13 | 0 | 0 | $aa(CH_3CHOH)$ |
| 199 | $PO(OH)_2CHOH + OH = PO(OH)_2CHO + H_2O$ | 5.00E+12 | 0 | 0 | $aa(CH_3CHOH)$ |
| 200 | $PO(OH)_2CHO = PO(OH)_2 + HCO$ | 2.61E+15 | 0.15 | 80550 | $bb(CH_3CHO)$ |
| 201 | $PO(OH)_2CHO + HO_2 = PO(OH)_2CO + H_2O_2$ | 3.01E+12 | 0 | 11930 | $bb(CH_3CHO)$ |
| 202 | $PO(OH)_2CHO + OH = PO(OH)_2CO + H_2O$ | 2.34E+10 | 0.74 | -1113 | $e(CH_3CHO)$ |
| 203 | $PO(OH)_2CHO + H = PO(OH)_2CO + H_2$ | 1.34E+13 | 0 | 3300 | $bb(CH_3CHO)$ |
| 204 | $PO(OH)_2CHO + O = PO(OH)_2CO + OH$ | 5.94E+12 | 0 | 1868 | $bb(CH_3CHO)$ |
| 205 | $PO(OH)_2CHO + CH_3 = PO(OH)_2CO + CH_4$ | 2.61E+06 | 1.78 | 5911 | $bb(CH_3CHO)$ |
| 206 | $PO(OH)_2CHO + O_2 = PO(OH)_2CO + HO_2$ | 3.01E+13 | 0 | 39150 | $bb(CH_3CHO)$ |
| 207 | $PO(OH)_2CHO + CH_3OO = PO(OH)_2CO + CH_3OOH$ | 3.01E+12 | 0 | 11930 | $bb(CH_3CHO)$ |
| 208 | $PO(OH)_2CH_2OO = PO(OH)_2CHO + OH$ | 1.32E+09 | 1.37 | 41590 | $x(CH_3CH_2O_2)$ |
| 209 | $PO(OH)_2CH_2 + O_2 = PO(OH)_2CHO + OH$ | 1.60E+14 | -1.17 | 10391 | $y(C_2H_5)$ |
| 210 | $PO(OH)_2CO = PO(OH)_2 + CO$ | 3.00E+12 | 0 | 16720 | $bb(CH_3CO)$ |
| 211 | $PO(OH)_2CO + O = PO(OH)_2 + CO_2$ | 2.00E+13 | 0 | 0 | $cc(CH_3CO)$ |
| 212 | $PO(OH)_2CO + CH_3OO = PO(OH)_2 + CO_2 + CH_3O$ | 2.40E+13 | 0 | 0 | $cc(CH_3CO)$ |
| 213 | $PO(OH)_2CO + PO(OH)_2CH_2OO = PO(OH)_2 + CO_2 + PO(OH)_2CH_2O$ | 2.40E+13 | 0 | 0 | $cc(CH_3CO)$ |
| 214 | $PO(OH)_2CH_2OO + HO_2 = PO(OH)_2CH_2OOH + O_2$ | 1.62E+11 | 0 | -1987 | $x(C_2H_5O_2)$ |
| 215 | $PO(OH)_2CH_2OO + H_2O_2 = PO(OH)_2CH_2OOH + HO_2$ | 2.40E+12 | 0 | 10000 | $d(CH_3O_2)$ |

| No. | Reaction | *A* | *n* | $E_a$ | Source |
|---|---|---|---|---|---|
| 216 | $PO(OH)_2CH_2OO+CH_3 = PO(OH)_2CH_2O+CH_3O$ | 3.80E+12 | 0 | -1200 | *dd($CH_3O_2$)* |
| 217 | $PO(OH)_2CH_2OO+CH_3OO = PO(OH)_2CH_2O+CH_3O+O_2$ | 1.00E+11 | 0 | 0 | *w* |
| 218 | $PO(OH)_2CH_2OO+PO(OH)_2CH_2OO = PO(OH)_2CH_2O+PO(OH)_2CH_2O+O_2$ | 3.28E+10 | 0 | 248 | *x($C_2H_5O_2$)* |
| 219 | $PO(OH)_2CH_2OO+PO(OH)_2CH_2OO = PO(OH)_2CHO+PO(OH)_2CH_2OH+O_2$ | 1.64E+10 | 0 | 248 | *x($C_2H_5O_2$)* |
| 220 | $PO(OH)_2CH_2OO+CH_4 = PO(OH)_2CH_2OOH+CH_3$ | 1.81E+11 | 0 | 18480 | *d($CH_3O_2$)* |
| 221 | $PO(OH)_2CH_2OO+CH_2O = PO(OH)_2CH_2OOH+HCO$ | 1.99E+12 | 0 | 11660 | *d($CH_3O_2$)* |
| 222 | $PO(OH)_2CH_2OO+H_2 = PO(OH)_2CH_2OOH+H$ | 3.00E+13 | 0 | 26030 | *d($CH_3O_2$)* |
| 223 | $PO(OH)_2CH_2OO+H = PO(OH)_2CH_2O+OH$ | 9.64E+13 | 0 | 0 | *d($CH_3O_2$)* |
| 224 | $PO(OH)_2CH_2OO+HCO = PO(OH)_2CH_2OOH+CO$ | 3.01E+13 | 0 | 0 | *d($CH_3O_2$)* |
| 225 | $PO(OH)_2CH_2OO+CH_3O = PO(OH)_2CH_2OOH+CH_2O$ | 3.00E+11 | 0 | 0 | *d($CH_3O_2$)* |
| 226 | $PO(OH)_2CH_2OO+CH_2OH = PO(OH)_2CH_2OOH+CH_2O$ | 1.21E+13 | 0 | 0 | *i($CH_3O_2$)* |
| 227 | $PO(OH)_2CH_2OO+CH_3OH = PO(OH)_2CH_2OOH+CH_2OH$ | 1.81E+11 | 0 | 13712 | *i($CH_3O_2$)* |
| 228 | $PO(OH)_2CH_2OO+O = PO(OH)_2CH_2O+O_2$ | 3.61E+13 | 0 | 0 | *d($CH_3O_2$)* |
| 229 | $PO(OH)_2CH_2OO+CH_2 = PO(OH)_2CH_2O+CH_2O$ | 1.81E+13 | 0 | 0 | *d($CH_3O_2$)* |
| 230 | $PO(OH)_2CH_2OO = PO_2(OH)CH_2OOH$ | 2.00E+11 | 0 | 35250 | *ee($C_3H_7O_2$)* |
| 231 | $PO(OH)_2CH_2O = PO_2(OH)CH_2OH$ | 2.00E+11 | 0 | 32100 | *ee($C_3H_7O_2$)* |
| 232 | $PO_2(OH)CH_2OH = PO_2OH+CH_2OH$ | 1.10E+13 | 0 | 16700 | *z($C_2H_5O$)* |
| 233 | $PO(OH)_2CH_2OOH = PO(OH)_2CH_2O+OH$ | 6.31E+14 | 0 | 42300 | *bb($C_2H_5O_2H$)* |
| 234 | $PO(OH)_2CH_2OOH+OH = PO(OH)_2CH_2OO+H_2O$ | 7.23E+11 | 0 | -258 | *r($CH_3O_2H$)* |
| 235 | $PO(OH)_2CH_2OOH+H = PO(OH)_2CH_2O+H_2O$ | 7.27E+10 | 0 | 1860 | *q($CH_3O_2H$)* |
| 236 | $PO_2(OH)CH_2OOH = PO_2OH+CH_2O+OH$ | 1.10E+13 | 0 | 16700 | *z($C_2H_5O$)* |
| 237 | $PO(OH)_2CH_2OOH+OH = PO_2(OH)CH_2OOH+H_2O$ | 2.13E+04 | 2.40 | 198 | *u($PO(OH)_2CH_3$)* |
| 238 | $PO_2(OH)CH_3 = PO_2OH+CH_3$ | 1.10E+13 | 0 | 16700 | *z($C_2H_5O$)* |
| 239 | $PO(OH)_3 = PO_2OH+H_2O$ | 2.09E+07 | 1.46 | 42118 | u |
| 240 | $PO_2OH+H = PO(OH)_2$ | 3.20E+08 | 1.57 | 6190 | u |
| 241 | $PO(OH)_2+H = PO_2OH+H_2$ | 4.00E+13 | 0 | 0 | v |
| 242 | $PO(OH)_3 = PO(OH)_2+OH$ | 3.63E+15 | 0 | 120000 | *ff($PO_2OH$)* |
| 243 | $PO(OH)_3+H = PO(OH)_2+H_2O$ | 4.70E+08 | 1.69 | 37890 | u |
| 244 | $PO(OH)_2+O_2 = PO_2OH+HO_2$ | 1.30E+02 | 2.4 | 420 | u |
| 245 | $PO(OH)_3+H = P(OH)_4$ | 4.94E+06 | 2.07 | 21771 | u |
| 246 | $P(OH)_4 = PO(OH)_2+H_2O$ | 1.58E+09 | 0.91 | 26893 | u |

a) Hughes *et al.*, 2001; b) DiNaro *et al.*, 2000; c) Kappel *et al.*, 2002; d) Tsang and Hampson, 1986; e) Baulch *et al.*, 1994; f) Dean and Westmoreland, 1987; g) Smith *et al.*, 2000; h) Zhu and Lin, 2001; i) Tsang, 1987; j) Fulle and Hippler, 1997; k) Wantuck *et al.*, 1987; l) Hippler *et al.*, 2001; m) Greenhill *et al.*, 1986; n) Held and Dryer, 1998; o) Warnatz. J, 1984; p) Atkinson *et al.*, 1997; q) Slemr and Warneck, 1977; r) Baulch *et al.*, 1992; s) Benson, 1976 t) Holgate and Tester, 1994; u) *ab initio* calculations, Chapter 4; v) Glaude *et al.*, 2000; w) Curran *et al.*, 1998; x) Sheng *et al.*, 2002; y) Dean and Bozzelli, 1990; z) Caralp *et al.*, 1999; aa) Marinov, 1999; bb) Fischer *et al.*, 2000; cc) Hunter *et al.*, 1996; dd) Kaiser *et al.*, 1986; ee) Ranzi *et al.*, 1994; ff) Mackie *et al.*, 2002

Organophosphorus chemistry is different from hydrocarbon chemistry because the phosphorus is larger than carbon, it is more electronegative than carbon, and the phosphorus can form stable structures that range from monovalent to pentavalent (Quin, 2000). In Chapter 4, the

four MPA bond strengths ($PO(OH)_2CH_2$—H, $PO(OH)CH_3O$—H, $PO(OH)_2$—$CH_3$, $PO(OH)CH_3$—OH) were calculated and compared to those in other compounds (Table 4-3). The C-H bond strength in MPA was the same as that of typical hydrocarbons, such as methane or methanol, while the O-H bond strength was higher than most organic alcohols, being closer to the O-H bond strength in water. The P-C bond strength was most similar to the strongest C-C bonds, such as acetic acid, and was much stronger than other X-C bonds, such as N-C or S-C bonds. The P-OH bond strength was at least 10 kcal/mol stronger than any other X-O bond strengths examined.

When choosing similar chemistries to examine for rate estimation for the MPA SCWO model, we determined that reactions that break or form C-H bonds could be reasonably estimated from hydrocarbon chemistry because the C-H bond strength in MPA is similar to that in many hydrocarbons. For the P-C bond cleavage reactions in the mechanism, reaction rates were also estimated from hydrocarbon chemistry because C-C bonds had the closest bond strengths to the P-C bonds. For the P-O reactions, rate constants were either calculated from *ab initio* calculations or were estimated from other calculated reaction rates in the literature for $PO_y$ chemistry. No P-O reaction rates were estimated from hydrocarbon chemistry because of the much different natures of the P-O and C-O bonds. From comparisons of *ab initio* TST rate constants and estimated literature rate constants, we found that reaction rates for P-O bond cleavage in organophosphorus combustion mechanisms were typically overestimated by at least one order of magnitude.

*Detailed Rate Estimation Methodology*

A set of fourteen reaction rates was calculated using transition state theory (TST) and the CBS-Q method in Gaussian 98 as described in the *ab initio* discussion in Chapter 4. It would be

expected that reaction rates calculated using transition state theory would contain less uncertainty than rates that are estimated by general rate estimation methods. Rate constants were calculated for MPA unimolecular reactions (reactions 151 to 154), hydrogen abstraction from MPA by an $OH^{\bullet}$ radical (reactions 156 and 157), formation and dissociation of the intermediate, $PO^{\bullet}(OH)_3CH_3$ (reactions 158 and 169), and several important POy reactions (reactions 239 to 240 and 243 to 246). These reaction rates were calculated by *ab initio* methods because of their importance in the MPA SCWO mechanism.

Hydrogen abstraction rates from the $CH_3$ group on MPA were estimated for the species, $H^{\bullet}$, $O^{\bullet}$, $CH_3^{\bullet}$, $HO_2^{\bullet}$, $CH_3O^{\bullet}$, $CH_3O_2^{\bullet}$, and $PO(OH)_2CH_2O_2^{\bullet}$. These rates were estimated using the recommended values from the Curran *et al.* (1998) paper on n-heptane combustion. The majority of the remaining 73 phosphorus-containing reactions in Table 5-2 form or break C-H and C-O bonds to form oxidized intermediates, such as $PO(OH)_2CH_2O_2^{\bullet}$ or $PO(OH)_2CH_2O^{\bullet}$. These reaction rates were primarily estimated by comparison with ethyl ($CH_3CH_2^{\bullet}$) chemistry, as shown in Table 5-2. It was assumed that C-H or C-O reaction rates did not change significantly with substitution of a $PO(OH)_2$ group for a methyl group. Eleven P-C bond cleavage reactions (R175, R179, R197, R200, R210-213, R232, R236, R238) were also included in the mechanism and these reaction rates were estimated from C-C bond cleavage reactions, as noted in Table 5-2.

The following assumptions were made for estimating certain reaction rates in Table 5-2. For estimating reaction rates from hydrocarbon chemistry, adjustments were made to account for reaction path degeneracy and heats of reaction, when necessary. All phosphorus-containing reactions were assumed to be in the high-pressure limit at these conditions. For chemically activated reactions through $PO(OH)_2CH_2OOH$, the lifetime of this intermediate was estimated to be on the order of $10^{-04}$ s at $T$=800 K, so these two-step reactions were included as one step in the

mechanism. For reaction (R202), hydrogen abstraction by an $OH^{\bullet}$ radical from $PO(OH)_2CHO$, the estimated reaction rate for $CH_3CHO$ reaction from Baulch *et al.* (1994) was used because it was equal to approximately half of the hydrogen abstraction rate from formaldehyde and it seemed more reasonable than the more recent rate available from Taylor *et al.* (1996). The Taylor *et al.* (1996) rate was estimated to be one-twelfth of the formaldehyde reaction rate to account for reaction path degeneracy.

Reaction rates for the POy compounds ($PO(OH)_3$, $P^{\bullet}O(OH)_2$, $PO_2OH$, and $P^{\bullet}(OH)_4$) were also included in the current model. In the DMMP combustion models, relatively few $PO(OH)_3$ reaction rates are included because phosphoric acid is not a major intermediate in DMMP combustion (Korobeinichev *et al.*, 2000; Glaude *et al.*, 2000). Six POy rates were calculated from *ab initio* TST calculations for reactions (R239, R240, R243 to R246).

$$PO(OH)_3 = PO_2OH + H_2O \quad \text{(R239)}$$

$$PO_2OH + H^{\bullet} = P^{\bullet}O(OH)_2 \quad \text{(R240)}$$

$$PO(OH)_3 + H^{\bullet} = P^{\bullet}O(OH)_2 + H_2O \quad \text{(R243)}$$

$$P^{\bullet}O(OH)_2 + O_2 = PO_2OH + HO_2^{\bullet} \quad \text{(R244)}$$

$$PO(OH)_3 + H^{\bullet} = P^{\bullet}(OH)_4 \quad \text{(R245)}$$

$$P^{\bullet}(OH)_4 = P^{\bullet}O(OH)_2 + H_2O \quad \text{(R246)}$$

Reactions R239, R240, and R243 had been included in previous combustion mechanisms; however, the estimated rate constants were many orders of magnitude different than those calculated using transition state theory. The P-O bond is much stronger than any other C-O bonds in the literature, so it may be difficult to estimate reliable reaction rates for POy chemistry from C-O compounds. Reaction (R244) between the $P^{\bullet}O(OH)_2$ radical and $O_2$ is a new reaction that was not included in previous organophosphorus mechanisms. The combination of reactions (R245) and (R246) is a new pathway for reaction (R243) through the $P^{\bullet}(OH)_4$ intermediate. The

two-step reaction pathways through reactions (R245) and (R246) is competitive with reaction (R243) due to lower activation energies for formation of the $P^{\bullet}(OH)_4$ intermediate.

To complete this reaction subset, reaction (R241) was included from the Glaude *et al.* (2000) mechanism and reaction (R242) was estimated for unimolecular decomposition of phosphoric acid to $P^{\bullet}O(OH)_2$ and the $OH^{\bullet}$ radical.

$$P^{\bullet}O(OH)_2 + H^{\bullet} = PO_2OH + H_2 \quad \text{(R241)}$$

$$PO(OH)_3 = P^{\bullet}O(OH)_2 + OH^{\bullet} \quad \text{(R242)}$$

Both of these reactions are termination reactions for reaction of the $P^{\bullet}O(OH)_2$ intermediate. The rate for reaction (R242) was estimated by comparing it to the TST calculated rate constant from Mackie *et al.* (2002) for the following reaction:

$$PO_2OH = P^{\bullet}O_2 + OH^{\bullet} \quad \text{(R7a)}$$

For reaction (R242), the pre-exponential factor was set equal to that from reaction (R4a) and the activation energy was set equal to heat of reaction for the unimolecular decomposition of phosphoric acid.

To complete the MPA SCWO model development, updated C-1 and $H_2/O_2$ SCWO reaction rates were added to the new organophosphorus submechanism (reactions 1 through 150 in Table 5-2). The methane combustion mechanism from Leeds University by Hughes *et al.* (2001) was used as a basis for the C-1 chemistry. Under SCWO conditions, most of the reactions are in the high pressure limit. For the pressure dependent $H_2/O_2$ reactions, two QRRK calculated rate constants at 246 bar were included from a benzene SCWO model by DiNaro *et al.* (2000).

$$O_2 + H^{\bullet} = HO_2^{\bullet} \quad \text{(R3)}$$

$$OH^{\bullet} + OH^{\bullet} = H_2O_2 \quad \text{(R10)}$$

Pressure dependence was added to many of Hughes *et al.* (2001)'s rate constants in the form of high pressure rate constants and/or TROE coefficients. These higher pressure rate constants were taken from different literature sources, as noted in Table 5-2. Methanol chemistry was added from Held and Dryer's (1998) methanol mechanism and methylperoxy reactions were added from suggested rates by Tsang and Hampson (1986). Two-step chemically activated reactions through the $CH_3OOH$ intermediate were included as a one step reaction since this intermediate has a lifetime on the order of $10^{-4}$ s at the temperatures examined in this study.

Due to the lack of reliable methane and methanol SCWO data in the literature, the ability of the updated C-1 submechanism to correctly predict experimental hydrocarbon oxidation rates in SCW could not be determined. Methane oxidation in SCW was examined earlier by our group (Webley and Tester, 1991); however, several improvements have been made to the plug flow reactor since the methane study was conducted and these data may have significant uncertainty. Methanol oxidation kinetics in SCW have been examined by many researchers with a large range of results, as recently reviewed by Vogel *et al.* (2003). With the large range of data available for methanol, it was difficult to assess the model predictions correctly for this compound.

## 5.3 MPA SCWO Model Results

Given the large number of new reactions included in the model, the major reaction pathways are first presented and discussed. Then, model predictions are compared to MPA SCWO experimental data to determine how well the model predicts MPA oxidation rates and product concentrations at different operating conditions. The effects of different operating conditions on reaction fluxes are also discussed.

### *5.3.1 Reaction Path Analysis*

The dominant MPA oxidation pathways in SCW are shown in Figure 5-1 from a rate of production analysis. In Table 5-3, the reaction fluxes at $\tau$=3 s were computed are at the conditions, $T$=527 °C, $P$=246 bar, $[MPA]_0$=1 mM, and $\Phi$=1.0. Reaction fluxes corresponding to a higher fuel equivalence ratio ($\Phi$=2) and a lower water density ($\rho$=41 kg/m$^3$) are included to demonstrate how the reaction fluxes change as the oxygen or water concentration decreases. From MPA SCWO experimental data, an increase in the fuel equivalence ratio or a decrease in the water density results in a decreased MPA oxidation rate. The rate of production and concentration profiles results were calculated using the AURORA program in CHEMKIN-III (Meeks *et al.*, 1996).

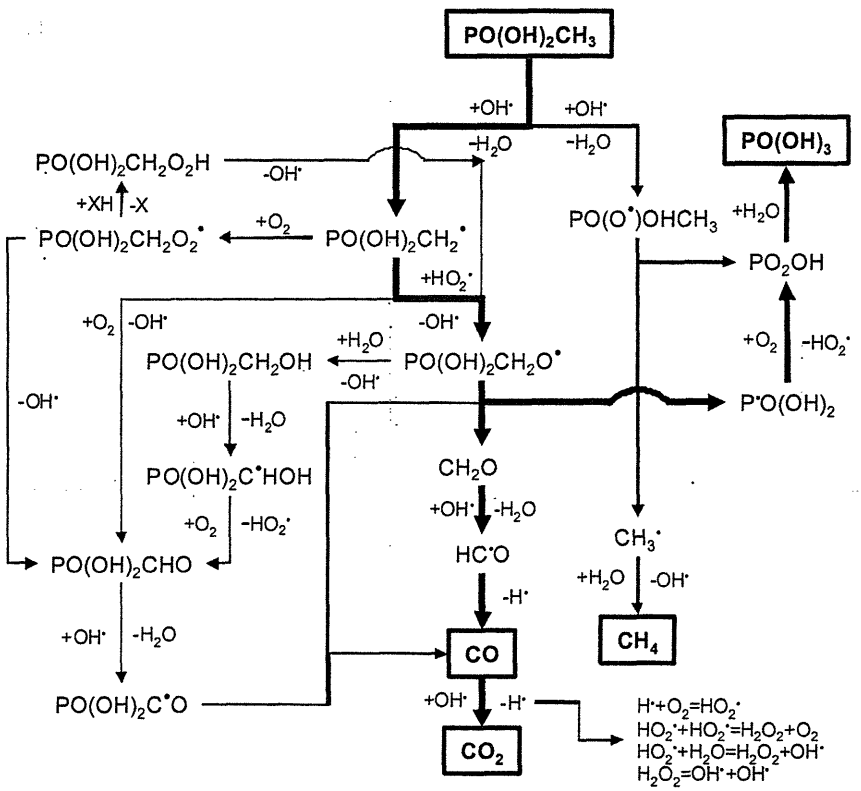


**Figure 5-1: Major reaction pathways in MPA SCWO model**

The arrows in bold indicate the dominant MPA reaction pathways to form the stable products and intermediates, CO, $CH_4$, $CO_2$, and $H_3PO_4$. At $T$<500 °C, the minor channels through $PO(OH)_2CH_2O_2$· become more important.

**Table 5-3: Computed reaction fluxes for major reaction pathways at three sets of conditions**

All net reaction fluxes are for the conditions, $T$=527 °C, $[MPA]_0$=1.0 mM, and $\tau$=3.0 s. The base fluxes are at $\Phi$=1.0 and $P$=246 bar ($\rho$=81 kg/m$^3$). The other two sets of fluxes are for a decrease in $O_2$ ($\Phi$=2) or in water density ($\rho$=41 kg/m$^3$ or $P$=138 bar).

| Reaction Groups | No. | Reaction | Fluxes ($10^{-03}$ mM/s) | | |
|---|---|---|---|---|---|
| | | | Base | $\Phi$=2 | $\rho$=41 kg/m$^3$ |
| **$PO(OH)_2CH_3$ Reactions** | 156 | $PO(OH)_2CH_3+OH = PO(OH)_2CH_2+H_2O$ | 77.7 | 67.4 | 116.3 |
| | 157 | $PO(OH)_2CH_3+OH = PO_2(OH)CH_3+H_2O$ | 21.0 | 21.4 | 21.8 |
| | 168 | $PO(OH)_2CH_3+HO_2 = PO(OH)_2CH_2+H_2O_2$ | 1.1 | 1.4 | 0 |
| **$PO(OH)_2CH_2^{\bullet}$ Reactions** | 173 | $PO(OH)_2CH_2+HO_2 = PO(OH)_2CH_2O+OH$ | 73.5 | 66.2 | 108.8 |
| | 170 | $PO(OH)_2CH_2+O_2 = PO(OH)_2CH_2OO$ | 3.3 | 1.5 | 4.5 |
| | 209 | $PO(OH)_2CH_2+O_2 = PO(OH)_2CHO+OH$ | 1.0 | 0.5 | 1.2 |
| | -180 | $PO(OH)_2CH_2+OH = PO(OH)_2CH_2OH$ | 0.6 | 0.6 | 0.5 |
| **$PO(OH)_2CH_2O^{\bullet}$ Reactions** | 175 | $PO(OH)_2CH_2O = PO(OH)_2+CH_2O$ | 74.1 | 65.2 | 111.1 |
| | -183 | $PO(OH)_2CH_2O+H_2O = PO(OH)_2CH_2OH+OH$ | 2.8 | 2.5 | 2.4 |
| **$PO(OH)_2CH_2OH$ to $PO(OH)_2C^{\bullet}O$ Reactions** | 188 | $PO(OH)_2CH_2OH+OH = PO(OH)_2CHOH+H_2O$ | 3.1 | 2.7 | 2.2 |
| | 187 | $PO(OH)_2CH_2OH+HO_2 = PO(OH)_2CHOH+H_2O_2$ | 0.3 | 0.2 | 0.3 |
| | 194/ 195 | $PO(OH)_2CHOH+O_2 = PO(OH)_2CHO+HO_2$ | 3.4 | 2.9 | 2.5 |
| | 202 | $PO(OH)_2CHO+OH = PO(OH)_2CO+H_2O$ | 4.5 | 3.3 | 3.6 |
| | 201 | $PO(OH)_2CHO+HO_2 = PO(OH)_2CO+H_2O_2$ | 0.5 | 0.3 | 0.7 |
| | 210 | $PO(OH)_2CO = PO(OH)_2+CO$ | 5.0 | 3.6 | 4.4 |
| **$PO(OH)_2CH_2O_2^{\bullet}$ Reactions** | 214 | $PO(OH)_2CH_2OO+HO_2 = PO(OH)_2CH_2OOH+O_2$ | 1.6 | 0.7 | 2.2 |
| | 208 | $PO(OH)_2CH_2OO = PO(OH)_2CHO+OH$ | 0.5 | 0.3 | 0.6 |
| | 172 | $PO(OH)_2CH_2+PO(OH)_2CH_2OO = PO(OH)_2CH_2O+PO(OH)_2CH_2O$ | 0.3 | 0.2 | 0.5 |
| | 233 | $PO(OH)_2CH_2OOH = PO(OH)_2CH_2O+OH$ | 2.4 | 1.0 | 3.3 |
| **$PO(O^{\bullet})OHCH_3$ Reactions** | 238 | $PO_2(OH)CH_3 = PO_2OH+CH_3$ | 21.0 | 21.4 | 21.8 |
| **$P^{\bullet}O(OH)_2$ and $PO_2OH$ Reactions** | 244 | $PO(OH)_2+O_2 = PO_2OH+HO_2$ | 78.5 | 67.9 | 115.0 |
| | -239 | $PO_2OH+H_2O = PO(OH)_3$ | 99.6 | 89.4 | 136.9 |
| **$CH_2O$ to CO Reactions** | 135 | $CH_2O+OH = HCO+H_2O$ | 77.1 | 66.5 | 113.6 |
| | 137 | $CH_2O+HO_2 = H_2O_2+HCO$ | 2.2 | 1.7 | 5.7 |
| | -79 | $CH_2O+H(+M) = CH_2OH(+M)$ | 10.7 | 13.7 | 19.6 |
| | 52/53 | $O_2+CH_2OH = CH_2O+HO_2$ | 11.3 | 14.0 | 2.0 |
| | 146 | $HCO = H+CO$ | 73.3 | 65.7 | 110.8 |
| | 143 | $HCO+O_2 = HO_2+CO$ | 6.4 | 2.8 | 9.4 |
| | 150 | $CO+OH = H+CO_2$ | 24.8 | 18.2 | 21.7 |
| | 149 | $CO+HO_2 = CO_2+OH$ | 1.9 | 1.2 | 2.8 |
| **$CH_3^{\bullet}$ to $CH_3O^{\bullet}$ Reactions** | -29 | $CH_3+H_2O = CH_4+OH$ | 15.8 | 18.0 | 13.5 |
| | 34 | $CH_3+O_2(+M) = CH_3OO(+M)$ | 2.0 | 0.9 | 3.1 |
| | 41 | $CH_3+HO_2 = CH_3O+OH$ | 2.4 | 2.3 | 3.8 |
| | 98 | $CH_3OO+HO_2 = CH_3OOH+O_2$ | 1.1 | 0.5 | 1.7 |
| | 58 | $CH_3OOH = CH_3O+OH$ | 1.5 | 0.7 | 2.3 |
| | 78 | $CH_3O(+M) = CH_2O+H(+M)$ | 3.9 | 2.8 | 6.4 |

The two primary reactions for consuming MPA under SCWO conditions are the hydrogen abstraction reactions with the $OH^{\bullet}$ radical.

$$PO(OH)_2CH_3 + OH^{\bullet} = PO(OH)_2CH_2^{\bullet} + H_2O \quad \text{(R156)}$$

$$PO(OH)_2CH_3 + OH^{\bullet} = PO(O^{\bullet})OHCH_3 + H_2O \quad \text{(R157)}$$

Both of these reactions are partially equilibrated at MPA oxidation conditions, with only the net flux reported in Table 5-3. Due to the high water concentration at supercritical conditions (approximately 4 to 5 M), both MPA intermediates, $PO(OH)_2CH_2^{\bullet}$ and $PO(O^{\bullet})OHCH_3$, rapidly react with water to reform MPA through reactions (R-156) and (R-157). The net reaction flux for MPA through these two pathways depends on the competing reactions of the intermediates, $PO(OH)_2CH_2^{\bullet}$ and $PO(O^{\bullet})OHCH_3$.

The only significant competing reaction for the $PO(O^{\bullet})OHCH_3$ intermediate is unimolecular decomposition through reaction (R238).

$$PO(O^{\bullet})OHCH_3 = PO_2OH + CH_3^{\bullet} \quad \text{(R238)}$$

These two products, $PO_2OH$ and $CH_3^{\bullet}$, react primarily with water to form the stable products, $PO(OH)_3$ and $CH_4$ via (R-239) and (R-29). The $CH_3^{\bullet}$ radical has minor competing oxidation pathways, including reaction with molecular oxygen (R34) or the $HO_2^{\bullet}$ radical (R41).

$$CH_3^{\bullet} + H_2O = CH_4 + OH^{\bullet} \quad \text{(R-29)}$$

$$CH_3^{\bullet} + O_2(+M) = CH_3O_2^{\bullet} \ (+M) \quad \text{(R34)}$$

$$CH_3^{\bullet} + HO_2^{\bullet} = CH_3O^{\bullet} + OH^{\bullet} \quad \text{(R41)}$$

The methyl radical has a large reaction flux through the methylperoxy reaction (R34); however, the net reaction flux for this pathway is small because the primary reaction of $CH_3O_2^{\bullet}$ is to reform $CH_3^{\bullet}$ and $O_2$ instead of reacting further to $CH_3O_2H$ or $CH_3O^{\bullet}$. Reaction fluxes through peroxy pathways are more significant at lower temperatures (below 500 °C). As the temperature increases, the equilibrium constant for peroxy radical formation decreases significantly because the entropy change to form the peroxy radical, $CH_3O_2^{\bullet}$, is negative.

For the $PO(OH)_2CH_2^{\bullet}$ intermediate, the primary reaction pathways are shown below.

$$PO(OH)_2CH_2^{\bullet} + HO_2^{\bullet} = PO(OH)_2CH_2O^{\bullet} + OH^{\bullet} \quad \text{(R173)}$$

$$PO(OH)_2CH_2^{\bullet} + O_2 = PO(OH)_2CH_2O_2^{\bullet} \quad \text{(R170)}$$

$$PO(OH)_2CH_2^{\bullet} + O_2 = PO(OH)CHO + OH^{\bullet} \quad \text{(R209)}$$

$$PO(OH)_2CH_2^{\bullet} + OH^{\bullet}(+M) = PO(OH)_2CH_2OH(+M) \quad \text{(R-180)}$$

As shown in Table 5-3, 93 to 98 % of the net $PO(OH)_2CH_2^{\bullet}$ reaction flux at $\tau$=3 s is reaction with the $HO_2^{\bullet}$ radical through reaction (R173). A large reaction flux through reaction (R170) to form the peroxy radical, $PO(OH)_2CH_2O_2^{\bullet}$, also exists. However, like (R34), this reaction is equilibrated with the equilibrium strongly favoring the reactants. Other minor pathways for $PO(OH)_2CH_2^{\bullet}$ reaction occur through (R-180) and (R209) to form the stable organophosphorus species, $PO(OH)_2CH_2OH$ and $PO(OH)_2CHO$. Formation of $PO(OH)_2CH_2OH$ through reaction (R-180) would slow MPA oxidation rates because it is a radical termination reaction. In the model, these two stable intermediates accumulate slightly to concentrations on the order of $10^{-3}$ mM.

The $PO(OH)_2CH_2O^{\bullet}$ radical reacts through the two pathways shown below with unimolecular decomposition as the primary pathway.

$$PO(OH)_2CH_2O^{\bullet} = P^{\bullet}O(OH)_2 + CH_2O \quad \text{(R175)}$$

$$PO(OH)_2CH_2O^{\bullet} + H_2O = PO(OH)_2CH_2OH + OH^{\bullet} \quad \text{(R-183)}$$

Due to the large concentration of water in the system, about 4% of the $PO(OH)_2CH_2O^{\bullet}$ reaction flux is through reaction (R-183) to form $PO(OH)_2CH_2OH$. Once formed, the $PO(OH)_2CH_2OH$ intermediate reacts primarily through the following pathways to form $P^{\bullet}O(OH)_2$ and CO, as shown in Table 5-3 and Figure 5-1.

$$PO(OH)_2CH_2OH + OH^{\bullet} = PO(OH)_2C^{\bullet}HOH + H_2O \quad \text{(R188)}$$

$$PO(OH)_2C^{\bullet}HOH + O_2 = PO(OH)_2CHO + HO_2^{\bullet} \quad \text{(R194/R195)}$$

$$PO(OH)_2CHO + OH^{\bullet} = PO(OH)_2C^{\bullet}O + H_2O \quad \text{(R202)}$$

$$PO(OH)_2C^{\bullet}O = P^{\bullet}O(OH)_2 + CO \quad \text{(R210)}$$

Reaction through the $PO(O^{\bullet})OHCH_3$ intermediate forms $PO_2OH$ as the POy product, while reaction through the $PO(OH)_2CH_2^{\bullet}$ intermediate forms $P^{\bullet}O(OH)_2$. Both of these compounds react to form the final phosphorus-containing product, $PO(OH)_3$. The major pathways for these two compounds are shown below.

$$PO_2OH + H_2O = PO(OH)_3 \quad \text{(R-239)}$$

$$P^{\bullet}O(OH)_2 + O_2 = PO_2OH + HO_2^{\bullet} \quad \text{(R244)}$$

The $PO_2OH$ intermediate reacts directly with water in (R-239) to form phosphoric acid, while the $P^{\bullet}O(OH)_2$ reacts with water in (R244) to form $PO_2OH$, which then reacts to phosphoric acid. Direct routes for $P^{\bullet}O(OH)_2$ reaction to $PO(OH)_3$ do exist in the model through reactions (R-242) and (R-243).

$$P^{\bullet}O(OH)_2 + OH^{\bullet} = PO(OH)_3 \quad \text{(R-242)}$$

$$P^{\bullet}O(OH)_2 + H_2O = PO(OH)_3 + H^{\bullet} \quad \text{(R-243)}$$

Reaction (R-242) is a termination reaction that slows MPA oxidation rates should reaction proceed through this pathway. The rate constant for reaction (R-243) was calculated from transition state theory and *ab initio* calculations. The energy barrier for this reaction was calculated to be 39 kcal/mol, a high energy barrier at SCW temperatures. Due to this high energy barrier, $P^{\bullet}O(OH)_2$ does not react with water through reaction (R-243), but instead reacts with oxygen through reaction (R244) to eventually form phosphoric acid.

Most of the carbon from MPA's methyl group enters the C-1 submechanism as formaldehyde from reaction (R175) of the $PO(OH)_2CH_2O^{\bullet}$ intermediate. Once the formaldehyde is formed, it reacts as follows.

$$CH_2O + OH^{\bullet} = HCO^{\bullet} + H_2O \quad \text{(R135)}$$

$$CH_2O + H^{\bullet}(+M) = CH_2OH^{\bullet}(+M) \quad \text{(R-79)}$$

$$CH_2OH^{\bullet} + O_2 = CH_2O + HO_2^{\bullet} \quad \text{(R52/53)}$$

$$HCO^{\bullet} = H^{\bullet} + CO \quad \text{(R-146)}$$

$$CO + OH^{\bullet} = CO_2 + H^{\bullet} \quad \text{(R150)}$$

Most of the formaldehyde reaction proceeds through (R135); however, due to the large concentrations of $CH_2O$ and $H^{\bullet}$ radical in this system, reaction also proceeds through reaction (R-79) to form $CH_2OH^{\bullet}$. The combination of reactions (R-79) and (R52/53) results in a catalytic pathway to form the $HO_2^{\bullet}$ radical since the net reaction is formation of an $HO_2^{\bullet}$ radical from the $H^{\bullet}$ radical and $O_2$.

At high pressures, CO oxidation to $CO_2$ occurs through the stabilized intermediate, the $HOCO^{\bullet}$ radical. Many earlier studies have been conducted to estimate accurate reaction rates for the following reactions (Larson *et al.*, 1988; Fulle *et al.*, 1996; Golden *et al.*, 1998; Zhu *et al.*, 2001; Senosiain *et al.*, 2003):

$$CO + OH^{\bullet} = HOCO^{\bullet} \quad \text{(R6a)}$$
$$HOCO^{\bullet} = CO_2 + H^{\bullet} \quad \text{(R7a)}$$
$$CO + OH^{\bullet} = CO_2 + H^{\bullet} \quad \text{(R150)}$$

Once the $HOCO^{\bullet}$ intermediate forms, it can react with species, such as oxygen, to form $HO_2^{\bullet}$ and $CO_2$ or it can dissociate to form $CO_2$ and $H^{\bullet}$. The $HOCO^{\bullet}$ radical has been excluded from the present model due to the large amount of uncertainty in reported thermochemical parameters (Larson *et al.*, 1988; Fulle *et al.*, 1996; Ruscic and Litorja, 2000; Duncan and Miller, 2000). Depending on the thermochemistry for $HOCO^{\bullet}$ that is chosen, results can predict that CO either completely oxidizes to $CO_2$ or does not react at all to form $CO_2$. For the MPA model, the CO reaction to $CO_2$ in reaction (R150) was taken from the CO SCWO model by Holgate and Tester (1994), who calculated an overall rate constant for reaction (R150) at $P$=246 bar and $T$=400 to 600 °C from Larson *et al.* (1988). The $CO + OH^{\bullet}$ reactions have a complex pressure and temperature dependence; however, Holgate and Tester found that these rates were essentially pressure independent in the SCWO temperature and pressure range. With this reaction rate in

their CO SCWO model, they were able to reproduce CO SCWO experimental data at temperatures greater than 500 °C and pressures between 118 and 263 bar, corresponding to a water density increase from 30 to 80 kg/m$^3$.

### *5.3.2 Comparison with Experimental Data*

Predicted concentration profiles for MPA, $CH_4$, CO, and $CO_2$ from the new MPA SCWO elementary reaction rate model are shown in Figure 5-2a at $T$=527 °C, $P$=246 bar, $[MPA]_0$=1 mM and $[O_2]_0$=2 mM ($\Phi$=1.0) and compared to MPA SCWO experimental data from Chapter 3. The updated MPA SCWO model correctly predicts the concentration profiles of MPA and its carbon-containing products and intermediates, CO, $CO_2$, and $CH_4$. The model using Glaude *et al.*'s three MPA rates is included in Figure 5-2b to compare its predicted concentrations with those from the new MPA SCWO model. Glaude *et al.*'s MPA rates correctly predict the MPA concentration profile, but incorrectly predict that most of the reacted carbon forms methane from MPA oxidation. The Glaude *et al.* (2000) MPA reactions incorrectly predict the carbon product distribution because the only carbon-containing product formed is the $CH_3^{\bullet}$ radical.

$$PO(OH)_2CH_3 + OH^{\bullet} = PO(OH)_3 + CH_3^{\bullet} \qquad \text{(R8a)}$$

$$CH_3^{\bullet} + H_2O = CH_4 + OH^{\bullet} \qquad \text{(R-29)}$$

At these conditions, the primary pathway for $CH_3^{\bullet}$ is to react with water to form methane, which is refractory at $T$ < 600 °C in supercritical water (Webley and Tester, 1991). The inclusion of the new hydrogen abstraction pathways, reactions (R156) and (R157), is necessary to predict all carbon-containing concentration profiles correctly in Figure 5-2.

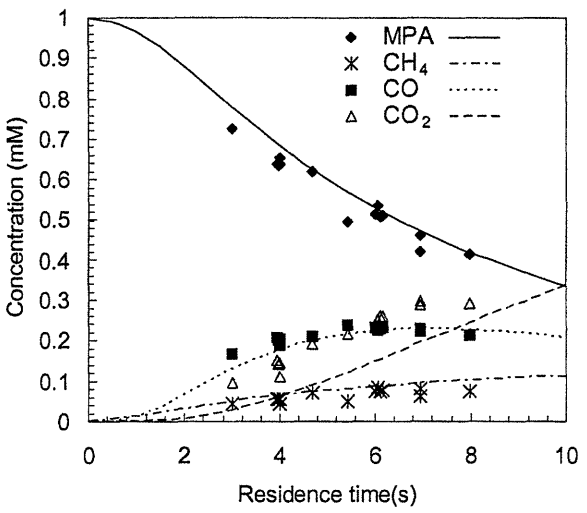


**Figure 5-2a**

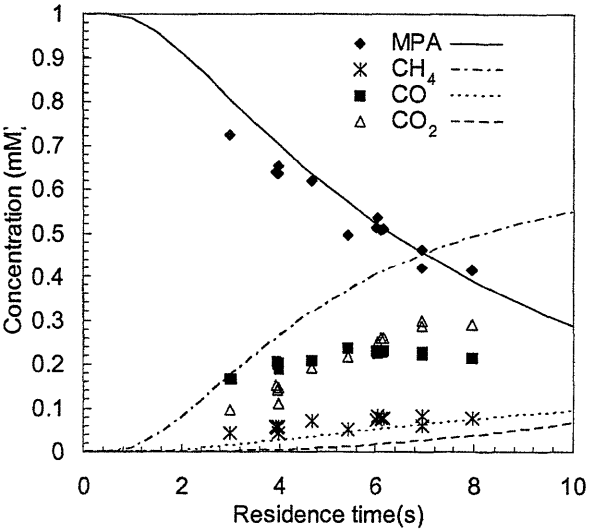


**Figure 5-2b**

**Figure 5-2: Predicted and experimental concentration profiles from the MPA SCWO model (5-2a) and the Glaude *et al.*(2000) MPA rates (5-2b) at $T$=527 °C, $P$=246 bar, $[MPA]_0$=1.0 mM, and Φ=1.0**

Plotted points represent the experimental data while the lines are the predicted concentration profiles. The Glaude *et al.* predictions were made using the C-1 SCWO model (reactions 1 to 150 in Table 5-3) and the three MPA reactions from Glaude *et al.* (2000) in Table 4-1.

The new MPA model predictions agree well with MPA conversion data in the temperature range of 478 to 571°C at the base conditions of $P$=246 bar, $[MPA]_0$=1 mM, and Φ=1.0, as shown in Figure 5-3. In Figures 5-4a to 5-4c, the concentration profiles for the carbon-containing intermediates, CO and $CH_4$, and the final product, $CO_2$, at the same conditions are also shown and compared to the experimental data. The model predictions agree well with the CO and $CH_4$ concentrations at all temperatures, but the $CO_2$ concentrations are underpredicted at higher temperatures. This underprediction occurs for two reasons: the MPA conversions are slightly underpredicted at higher temperatures and the experimental carbon balances at higher temperatures were typically around 105 %. The $CO_2$ concentrations probably contributed the most error to the high carbon balances measured at high conversions. The predicted phosphoric acid concentration profiles also agree with the experimental data. These

results are not presented in a separate figure because phosphoric acid was the only measured phosphorus-containing product and the MPA data are already shown in Figure 4-3.

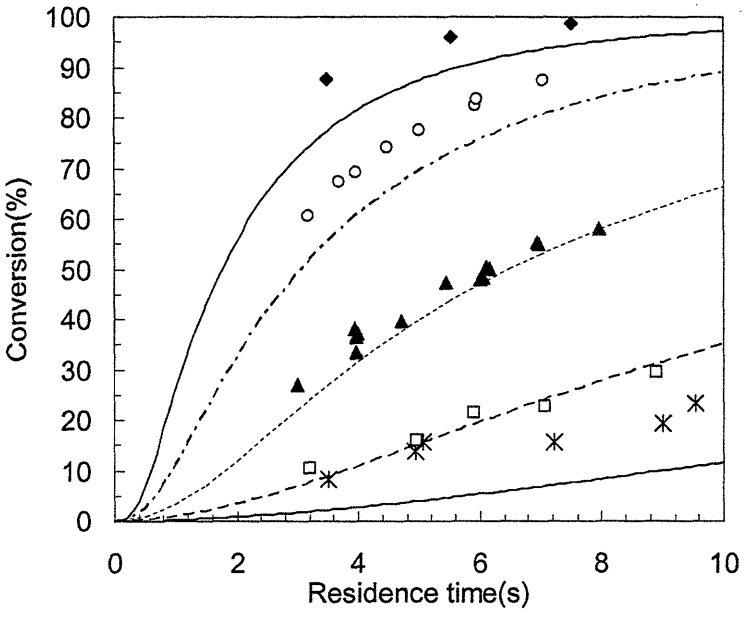


**Figure 5-3: Comparison of MPA SCWO model predictions and experimental MPA conversions over from 478 to 571 °C at $P$=246 bar, $[MPA]_0$=1.0 mM and $\Phi$=1.0**

Plotted points represent the experimental data while the lines are the predicted concentration profiles. For the graph, $T$=478 °C, *, —; $T$=503 °C, □, – –; $T$=527 °C, ▲, ···; $T$=551 °C, ○, . –; $T$=571 °C, ♦, —.

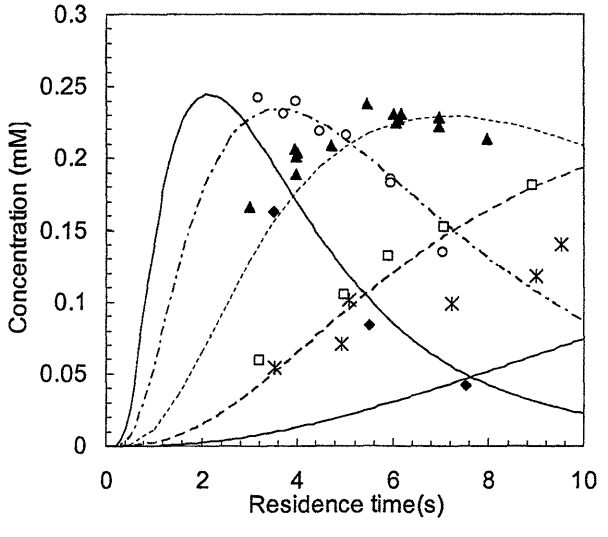


**Figure 5-4a: CO concentrations**

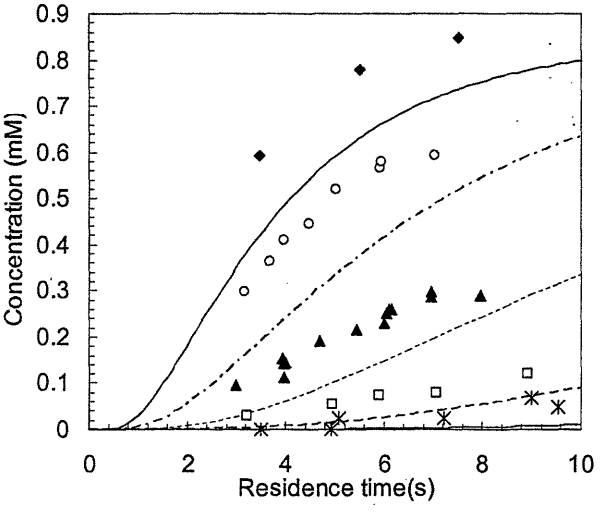


**Figure 5-4b: $CO_2$ concentrations**

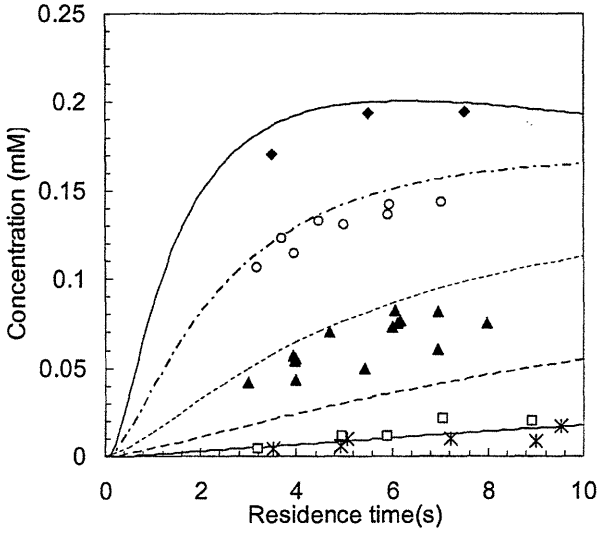


**Figure 5-4c: $CH_4$ concentrations**

**Figure 5-4: Comparison of MPA SCWO model predictions and experimental MPA carbon fractions from 478 to 571 °C at $P$=246 bar, $[MPA]_0$=1.0 mM and Φ=1.0**

Plotted points represent the experimental data while the lines are the predicted concentration profiles. In these figures, $T$=478 °C, *, —; $T$=503 °C, □, – –; $T$=527 °C, ▲, ···; $T$=551 °C, ○, . –; $T$=571 °C, ♦, —.

The ability of the model to predict the effect of oxygen concentration on MPA conversion was examined. In Figure 5-5, the fuel equivalence ratio was varied from a value of 0.7 (43 % excess oxygen) to a value of 2 (50 % sub-stoichiometric oxygen). From experimental measurements, MPA conversion decreases as oxygen concentration decreases (or as Φ increases). The elementary reaction rate model correctly predicts that MPA conversion decreases as Φ increases, as shown in Figure 5-5. According to the model, the decrease in the MPA oxidation rate occurs because the $HO_2^{\bullet}$ concentration decreases to approximately 0.86 of its value when the $O_2$ concentration decreases by half, as shown in Table 5-4. At Φ=2, the MPA reaction flux to form the $PO(OH)_2CH_2^{\bullet}$ intermediate subsequently decreases to 0.87 of its value (see Table 5-3). The MPA reaction flux is dependent on the $HO_2^{\bullet}$ concentration through the reaction of $PO(OH)_2CH_2^{\bullet}$ and $HO_2^{\bullet}$ in reaction (R173).

$$PO(OH)_2CH_2^{\bullet} + HO_2^{\bullet} = PO(OH)_2CH_2O^{\bullet} + OH^{\bullet} \qquad \text{(R173)}$$

This reaction is the primary oxidation pathway for $PO(OH)_2CH_2^{\bullet}$ and it competes with the reverse reaction of $PO(OH)_2CH_2^{\bullet}$ and $H_2O$ to reform MPA via reaction (R-156). Thus, any decrease in the reaction flux through (R173) leads to an increased reformation of MPA through (R-156) and decreased MPA oxidation rates.

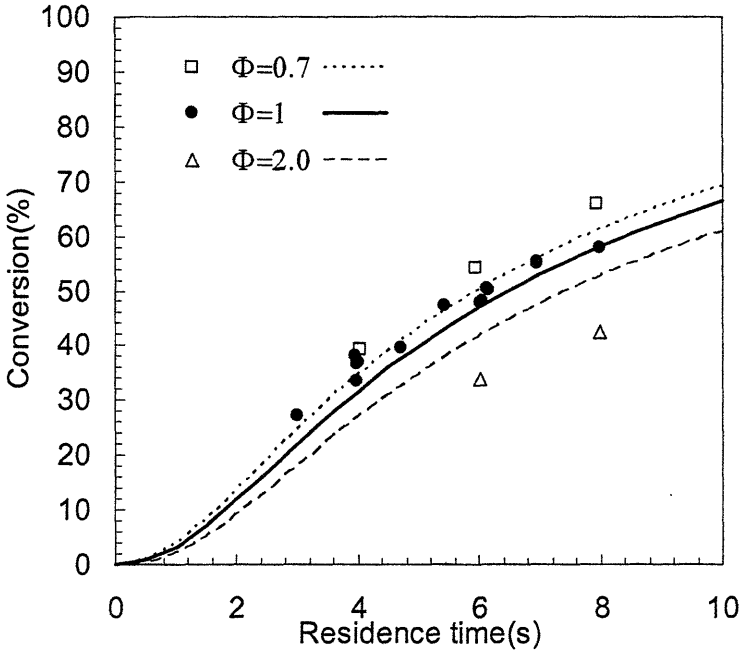


**Figure 5-5: Comparison of MPA SCWO model predictions and experimental MPA conversions at different fuel equivalence ratios at $T$=527 °C, $[MPA]_0$=1.0 mM, and $P$=246 bar**

Plotted points represent the experimental data while the lines are the predicted concentration profiles. Φ=0.70 corresponds to 43 % excess oxygen, while Φ=2.0 corresponds to 50% oxygen demand.

**Table 5-4: Computed concentrations of important H/O containing species at each of the base conditions at τ=3 s**

All concentrations are for the conditions, $T$=527 °C, $[MPA]_0$=1.0 mM, and τ=3.0 s. The base concentrations are at Φ=1.0 and $P$=246 bar (ρ=81 kg/m$^3$). The other two sets of concentrations are for a decrease in $O_2$ (Φ=2) or in water density (ρ=41 kg/m$^3$ or $P$=138 bar).

| Species | Concentrations (mol/m$^3$) | | |
|---|---|---|---|
| | Base | Φ=2 | ρ=41 kg/m$^3$ |
| $H_2O$ | $4.5\times10^{03}$ | $4.5\times10^{03}$ | $2.3\times10^{03}$ |
| $O_2$ | 1.7 | 0.84 | 1.7 |
| $HO_2$ | $2.9\times10^{-04}$ | $2.5\times10^{-04}$ | $3.4\times10^{-04}$ |
| OH | $6.7\times10^{-07}$ | $6.4\times10^{-07}$ | $4.5\times10^{-07}$ |

Other reaction fluxes that are significantly affected by decreasing oxygen concentration are the reactions with molecular oxygen shown below.

$$PO(OH)_2CH_2^{\bullet} + O_2 = PO(OH)_2CH_2O_2^{\bullet} \quad \text{(R170)}$$

$$PO(OH)_2CH_2^{\bullet} + O_2 = PO(OH)_2CHO + OH^{\bullet} \quad \text{(R209)}$$

$$CH_3^{\bullet} + O_2(+M) = CH_3O_2^{\bullet} \ (+M) \quad \text{(R34)}$$

These reaction fluxes all scale with the oxygen concentration, as shown in Table 5-3. From Figure 5-5, the model does not predict as sharp of a decrease in MPA conversion as found experimentally. This could indicate that reactions through the peroxy compounds may be more important than the current model predicts because larger reaction fluxes through peroxy compounds would lead to an increased dependence on the oxygen concentration. The predicted reaction fluxes through the peroxy pathways are strongly dependent on the peroxy thermochemistry in the model, from which the equilibrium constants are calculated. The thermochemistry for peroxy compounds is not as well known because peroxy compounds are difficult to isolate experimentally and notoriously difficult to calculate accurately using quantum calculations (Green, 1994; Wijaya *et al.*, 2002). From analyzing the model sensitivity to the heat of formation of $PO(OH)_2CH_2O_2^{\bullet}$, decreasing the heat of formation by 1 or 2 kcal/mol to further stabilize this compound would increase the net reaction flux through this peroxy compound. Improving the thermochemistry of the organophosphorus peroxy compounds could improve model predictions for the oxygen dependence of MPA oxidation rates.

The effect of pressure, or water density, on MPA oxidation rates was also measured. Given the highly compressible nature of supercritical water, system pressure and water density cannot be separately examined experimentally. For the MPA SCWO data, the pressure was varied from 138 to 277 bar and consequently, the density was varied from 41 to 94 kg/m$^3$ at $T$=527 °C. Experimentally, MPA oxidation rates decreased as the pressure, or water density,

decreased as shown by the data in Figure 5-6. However, the MPA SCWO model predicts that decreasing the water concentration increases MPA oxidation rates, contrary to the experimental data. In the model, MPA reaction fluxes could be affected by the decrease in pressure or the decrease in water concentration. Even though pressure and water could not be separately modified experimentally, we could change these two variables separately in the model by adding the inert bath gas, argon, to increase the pressure without increasing the water concentration. Modeling results showed that increasing the pressure at a constant water concentration did not affect MPA conversions. Thus, we concluded that the change in water concentration was responsible for the changing the MPA oxidation rates in the model. The hypothesis that changing the water concentration, not the system pressure, affects oxidation rates in SCW agrees with previous experimental and modeling studies in SCWO (Koo *et al.*, 1997; Holgate *et al.*, 1994; DiNaro *et al.*, 2000).

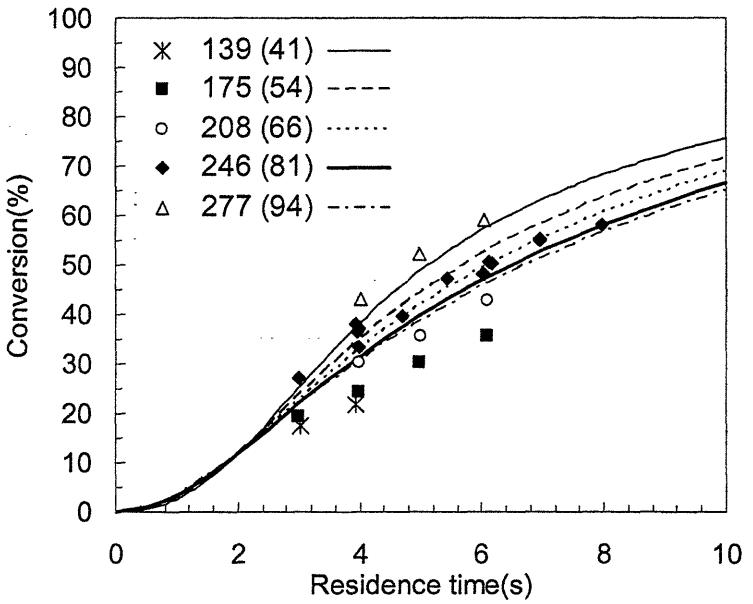


**Figure 5-6: Comparison of MPA SCWO model predictions and experimental MPA conversions at different water densities/pressures at $T$=527 °C, $[MPA]_0$=1.0 mM, and $\Phi$=1.0**
Plotted points represent the experimental data while the lines are the predicted concentration profiles. In this figure, the pressures are in bar and (the densities are in kg/m$^3$).

The water dependence may be incorrectly accounted for in the model for several reasons. First, from the governing assumptions made for this model, the only roles that water plays are as a reactant or a third-body collider (M). Water's role as a solvent, which could influence transition state energies, has not been included. For hydrocarbons, such as benzene, the SCWO elementary reaction rate model does correctly predict that oxidation rates increase with water density without including solvation effects (DiNaro *et al.*, 2000). However, for the more electronegative phosphorus-containing species included in the current model, water solvation effects could be more important. It was outside the scope of this modeling effort to attempt to include solvation effects in this model.

Since the only role that water plays in the current model is as a reactant, the decreased water concentration could slow oxidation rates by two primary ways. First, if water is a reactant in an important reaction for MPA oxidation, then a lower water concentration could decrease the flux through this pathway. For example, the methane concentration in the current model is correctly predicted to decrease with decreasing water concentration. Water is a key reactant in the formation of methane through reaction (R-29) with the $CH_3^{\bullet}$ radical. When the water concentration decreases by half at $P$=138 bar, the reaction flux decreases substantially through this pathway, as shown in Table 5-3.

The second way that water could slow oxidation rates would be if a decrease in the water concentration lowered the concentration of an important radical species. In the MPA SCWO model, the $OH^{\bullet}$ radical concentration decreases as the water concentration decreases at $P$=138 bar in Table 5-4 because water is involved in a major reaction for $OH^{\bullet}$ production. In the model, most of the $OH^{\bullet}$ radicals are produced from $HO_2^{\bullet}$ reactions that form $H_2O_2$, which dissociates quickly in SCW to form two $OH^{\bullet}$ radicals, as shown below.

$$HO_2^{\bullet} + HO_2^{\bullet} = H_2O_2 + O_2 \quad \text{(R22/23)}$$

$$HO_2^{\bullet} + H_2O = H_2O_2 + OH^{\bullet} \quad \text{(R-8/-9)}$$

$$H_2O_2 = OH^{\bullet} + OH^{\bullet} \quad \text{(R-10)}$$

When $H_2O_2$ is formed through reactions, (R22) and (R23), two $HO_2^{\bullet}$ radicals are used to form two $OH^{\bullet}$ radicals. However, when $H_2O_2$ is formed through reactions (R-8) and (R-9) involving water, one $HO_2^{\bullet}$ radical reacts and three $OH^{\bullet}$ radicals are formed, resulting in a net formation of two radicals through this pathway. When the water concentration decreases, the reaction flux through reactions (R-8) and (R-9) decreases by half, causing the $OH^{\bullet}$ concentration to decrease. This decrease in $OH^{\bullet}$ concentration does slow the reaction flux through pathways like CO reaction to $CO_2$ through reaction (R150), as shown in Table 5-3. The methane reaction from $CH_3^{\bullet}$ and the CO oxidation to $CO_2$ are examples of how the decreased water concentration decreases reaction fluxes in the model.

The MPA oxidation rates do not decrease with decreasing water concentration because water is not a reactant in many important MPA reactions, as shown in Table 5-3. Water's most common role in the model is as a product of $OH^{\bullet}$ hydrogen abstraction reactions. The reaction flux through $PO(OH)_2CH_2^{\bullet}$ increases as water concentration decreases because the primary role of water in this pathway is to react with $PO(OH)_2CH_2^{\bullet}$ to reform MPA.

$$PO(OH)_2CH_2^{\bullet} + H_2O = PO(OH)_2CH_3 + OH^{\bullet} \quad \text{(R-156)}$$

For this reaction, as water concentration decreases, the reaction flux of $PO(OH)_2CH_2^{\bullet}$ to reform MPA decreases and MPA conversion increases, contrary to the experimental data. Reaction fluxes through this reversible reaction are affected by the decrease in both the $OH^{\bullet}$ and $HO_2^{\bullet}$ concentrations. At 138 bar, the $OH^{\bullet}$ concentration decreases to 67%, while the water concentration decreases to 50% of its value at 246 bar. According to the model, the larger

decrease in water concentration causes reaction through the MPA + $OH^{\bullet}$ direction of this equilibrium to dominate more at these conditions and increases overall MPA oxidation rates.

These results indicate that there may be another important reaction with water that has either been omitted or has been incorrectly estimated in the model. One example of a pathway that could be important is the reaction of water and $PO_2OH$.

$$PO_2OH + H_2O = PO(OH)_3 \qquad \text{(R-239)}$$

Currently, no other reaction fluxes in the model are competitive with this reaction. However, if another reaction was competitive with reaction (R-239), then it could possibly become an important reaction channel as the water concentration decreased.

The model predictions do not agree with experimental MPA concversions at all conditions, but the absolute MPA oxidation rates are difficult to correctly predict because it is hard to accurately calculate the steady-state radical concentrations. In this mechanism, the radical-forming reaction pathways are very interconnected and dependent on each other. For example, the $HO_2^{\bullet}$ radical concentration is very important in this model for reaction of the $PO(OH)_2CH_2^{\bullet}$ intermediate in reaction (R173). The $HO_2^{\bullet}$ radical concentration also determines the $OH^{\bullet}$ concentration, since $HO_2^{\bullet}$ reacts to form $H_2O_2$ which dissociates to form $OH^{\bullet}$ radicals, as shown previously in reactions (R-8, R-9, R-10, R22, and R23). In the MPA mechanism, most of the $HO_2^{\bullet}$ is formed from reactions that produce $H^{\bullet}$ radicals late in the reaction mechanism through $HCO^{\bullet}$ decomposition, (R146), and CO reaction to $CO_2$ through (R150). The $HCO^{\bullet}$ and CO formation rates are themselves senstitive to the $HO_2^{\bullet}$ concentrations, particularly through reaction (R173). Any small overprediction of the MPA oxidation rate will become magnified because the radical pool is very sensitive to reactions in the entire mechanism. Thus, accurate rates for the following $HO_2^{\bullet}$ and $OH^{\bullet}$ reaction pathways are very important for this mechanism.

$$H^{\bullet} + O_2 = HO_2^{\bullet} \quad \text{(R3)}$$

$$HO_2^{\bullet} + HO_2^{\bullet} = H_2O_2 + O_2 \quad \text{(R22/23)}$$

$$HO_2^{\bullet} + H_2O = H_2O_2 + OH^{\bullet} \quad \text{(R-8/-9)}$$

$$H_2O_2 = OH^{\bullet} + OH^{\bullet} \quad \text{(R-10)}$$

The reactions shown above exhibit a marked dependence on both temperature and pressure and the pressure-dependent rate constants can be strongly dependent on the water concentration (Kappel *et al.*, 2002; Michael *et al.*, 2002; Bates *et al.*, 2001; Troe, 2000). Due to the smaller size of these species, these reactions are not necessarily at their high pressure limit at our temperature and pressure range. Thus, accurate estimation of these rate constants can be difficult because their pressure dependence with water as the collider is uncertain. In an effort to better estimate rate constants for reactions (R3) and (R10), DiNaro *et al.* (2000) calculated these reaction rates using QRRK analysis at $P$=246 bar. Determining accurate rate constants for these reactions is continually being examined in the combustion literature and improved estimates for the $HO_2^{\bullet}$ and $H_2O_2$ reactions could decrease the uncertainty in the MPA SCWO model predictions.

Even though the MPA oxidation rates are not always correctly predicted, a significant contribution of the MPA SCWO model is its ability to correctly predict the concentrations of CO, $CH_4$, and $CO_2$ (see Figure 5-4). With the MPA bimolecular rates from Glaude *et al.*, 80 to 90 % of the reacted carbon formed methane. In the new MPA SCWO model, reaction of the MPA hydrogen abstraction products, $PO(OH)_2CH_2^{\bullet}$ and $PO(O^{\bullet})OHCH_3$, controls the carbon product distribution. The reaction pathway through $PO(OH)_2CH_2^{\bullet}$ forms $CH_2O$ which reacts to CO and $CO_2$; whereas reaction through the $PO(O^{\bullet})OHCH_3$ intermediate forms $CH_3^{\bullet}$ which primarily reacts to $CH_4$, as shown in Figure 5-1 and Table 5-3. These results support the two-

pathway mechanism for MPA oxidation with a major pathway through the CO intermediate and a minor pathway leading to $CH_4$ that was regressed from the experimental data in Chapter 3.

To further demonstrate the model's ability to accurately predict the concentrations of the carbon-containing products, the predicted $CH_4$, CO, and $CO_2$ selectivities from the MPA SCWO model are compared to the experimentally measured selectivities at varying residence times (3 to 10 s), fuel equivalence ratios ($\Phi$) (0.5 to 2.0), water densities (41 to 94 kg/m$^3$) and temperatures (527 to 572 °C) in Figure 7. Even though the MPA conversions were not correctly predicted at all of these conditions, the CO, $CH_4$, and $CO_2$ selectivities agree well with experimental data. These results indicate that the major reaction pathways identified in this model appear to be correct even if the individual rate constants contain significant uncertainty. The inclusion of the MPA hydrogen abstraction reactions is necessary to correctly predict the MPA SCWO experimental data.

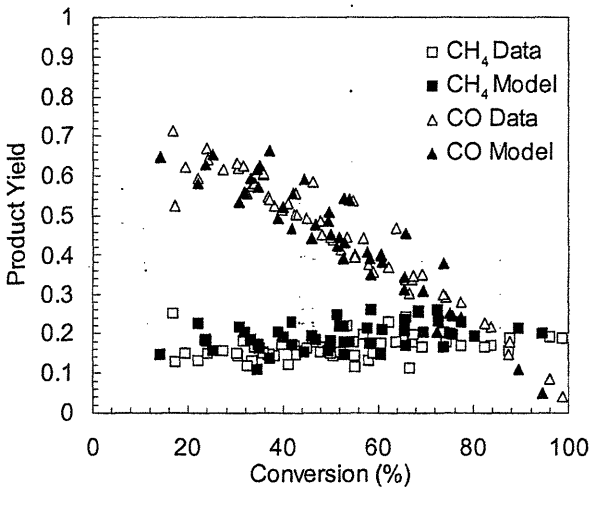


**Figure 5-7a: CO and $CH_4$ Selectivities**

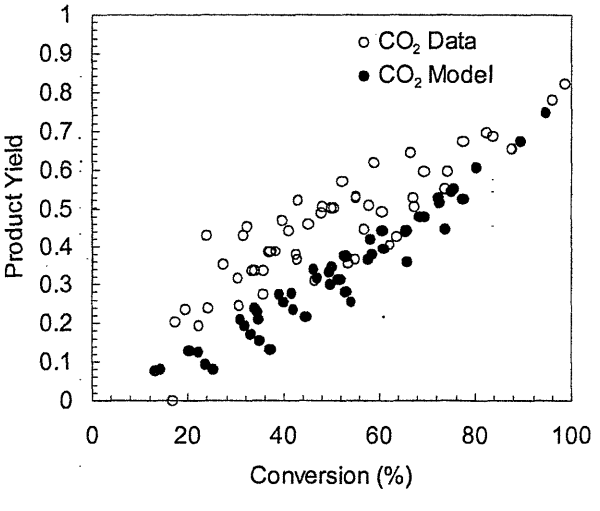


**Figure 5-7b: $CO_2$ Selectivity**

**Figure 5-7: Selectivities for the carbon-containing products in MPA oxidation**
The data were taken at $T$=527 °C to 572 °C, $\tau$ =3 to 9 s, $\Phi$=0.5 to 2.0, and $P$=139 to 277 bar

## 5.4 CONCLUSIONS

An MPA SCWO model was developed with 94 new organophosphorus reaction rates and 14 new organophosphorus species. This model improved on the current organophosphorus models available by adding important hydrogen abstraction and β-scission pathways omitted from previous mechanisms. Since MPA is only a minor intermediate during DMMP combustion (see Korobeinichev *et al.*, 2000; Glaude *et al.*, 2000), its reaction kinetics had not been previously examined in detail in the DMMP combustion models. These newly added pathways and intermediates were necessary to accurately predict experimentally measured rates and concentration profiles for MPA conversion and its products.

With these new reaction rates, the model was able to predict the SCWO concentration profiles for MPA and its products, $H_3PO_4$, CO, $CH_4$, and $CO_2$ at temperatures between 478 and 572 °C, $\tau$=3 to 10 s, $P$=246 bar, $[O_2]_0$=2.0 mM, and $[MPA]_0$=1.0 mM. The reaction channels of the two MPA hydrogen abstraction products, $PO(OH)_2CH_2^{\bullet}$ and $PO(O^{\bullet})OHCH_3$, dictated the carbon product distribution of CO and $CO_2$ versus $CH_4$ in the model. These modeling results support the two pathway MPA global model that was regressed from the experimental data. The model also predicted that MPA oxidation rates decrease with decreasing oxygen concentration, consistent with experimental observations because the MPA oxidation rate scales with the $HO_2^{\bullet}$ concentration. Our model does not correctly predict the dependence of MPA oxidation rates on water concentration. This could be due to an incomplete representation of water's role as both a solvent and a reactant in dense supercritical water solutions. One of the most significant contributions of this model is its ability to predict the product selectivities to CO, $CO_2$, and $CH_4$ over a wide range of operating conditions.

## 5.5 REFERENCES

Alkam, M., V. Pai, P. Butler and W. Pitz, "Methanol and hydrogen oxidation kinetics in water at supercritical states." *Combust. Flame* **106**(1-2), 110-130 (1996).

Atkinson, R., D. Baulch, R. A. Cox, R. F. Hampson, J. A. Kerr, M. J. Rossi and J. Troe, "Evaluated kinetic, photochemical and heterogeneous data for atmospheric chemistry: Supplement V, IUPAC subcommittee on gas kinetic data evaluation for atmospheric chemistry." *J. Phys. Chem. Ref. Data* **26**(3), 521-1011 (1997).

Bates, R. W., D. M. Golden, R. K. Hanson and C. T. Bowman, "Experimental study and modeling of the reaction $H+O_2+M->HO_2+M$ (M=Ar, $N_2$, $H_2O$) at elevated pressures and temperatures between 1050 and 1250 K." *Phys. Chem. Chem. Phys.* **3**(12), 2337-2342 (2001).

Baulch, D., C. J. Cobos, R. A. Cox, C. Esser, P. Frank, T. Just, J. A. Kerr, M. Pilling, J. Troe, R. W. Walker and J. Warnatz, "Evaluated kinetic data for combustion modeling." *J. Phys. Chem. Ref. Data* **21**(3), 411-734 (1992).

Baulch, D., C. J. Cobos, R. A. Cox, P. Frank, G. Hayman, T. Just, J. A. Kerr, T. Murrels, M. Pilling, J. Troe, R. W. Walker and J. Warnatz, "Evaluated kinetic data for combustion modeling supplement-I." *J. Phys. Chem. Ref. Data* **23**(6), 847-1033 (1994).

Benson, S. W., *Thermochemical Kinetics.* Wiley, New York (1976).

Brock, E. E. and P. E. Savage, "Detailed chemical kinetics model for supercritical water oxidation of $C_1$ compounds and $H_2$." *AIChE J.* **41**(8), 1874-1888 (1995).

Burcat, A., "Alexander Burcat's Ideal Gas Thermochemical Database." May, 2003 <http://garfield.chem.elte.hu/Burcat/burcat.thr> (2003).

Caralp, F., P. Devolder, C. Fittschen, N. Gomez, H. Hippler, M. Rayez, F. Striebel and B. Viskolcz, "The thermal unimolecular decomposition rate constants of ethoxy radicals." *Phys. Chem. Chem. Phys.* **1**(12), 2935-2944 (1999).

Curran, H. J., P. Gaffuri, W. J. Pitz and C. K. Westbrook, "A comprehensive modeling study of n-heptane oxidation." *Combust. Flame* **114**(1-2), 149-177 (1998).

Dagaut, P., B. Daney de Marcillac, Y. Tan, M. Cathonnet and J. Boettner, "Chemical kinetic modeling of the supercritical water oxidation of simple fuels: H2, CO and CH4." *J. Chim. Phys.* **92**(5), 1124-1141 (1995).

Daguat, P., M. Cathonnet and J. Boettner, "Chemical kinetic modeling of the supercritical water oxidation of methanol." *J. Supercrit. Fluids* **98**(1), 33-42 (1996).

Dean, A. M. and P. R. Westmoreland, "Bimolecular QRRK analysis of methyl radical reactions." *Int. J. Chem. Kinet.* **19**(3), 207-228 (1987).

Dean, A. M. and J. W. Bozzelli, "Chemical activation analysis of the reaction of $C_2H_5$ with $O_2$." *J. Phys. Chem.* **94**(8), 3313-3317 (1990).

DiNaro, J., J. Howard, W. Green, J. W. Tester and J. Bozzelli, "Elementary reaction mechanism for benzene oxidation in supercritical water." *J. Phys. Chem. A* **104**(45), 10576-10586 (2000).

Duncan, T. and C. Miller, "The $HCO_2$ potential energy surface: Stationary point energetics and the HOCO heat of formation." *J. Chem. Phys.* **113**(3), 5138-5140 (2000).

Fischer, S. L., F. L. Dryer and H. J. Curran, "The reaction kinetics of dimethyl ether. I: High-termperature pyrolysis and oxidation in flow reactors." *Int. J. Chem. Kinet.* **32**(12), 713-740 (2000).

Fulle, D., H. Hamann, H. Hippler and J. Troe, "High pressure range of addition reactions of HO. II. Temperature and pressure dependence of the reaction HO + CO = HOCO = H + $CO_2$." *J. Phys. Chem.* **105**(3), 983-1000 (1996).

Fulle, D. and H. Hippler, "The temperature and pressure dependence of the reaction $CH+H_2$ <->$CH_3$<->$CH_2$+H." *J. Chem. Phys.* **106**(21), 8691-8698 (1997).

Glaude, P. A., H. J. Curran, W. J. Pitz and C. K. Westbrook, "Kinetic study of the combustion of organophosphorus compounds." *Proceedings of the Combustion Institute* **28**, 1749-1756 (2000).

Golden, D. M., G. P. Smith, A. B. McEwen, C. L. Yu, B. Eiteneer, M. Frenklach, F. L. Vaghjiani, A. R. Ravishankara and F. P. Tully, "OH(OD) + CO: Measurements and an optimized RRKM fit." *J. Phys. Chem. A* **102**(44), 8598-8606 (1998).

Green, W. H., "Predictive chemical kinetics - density functional and hartree-fock calculations on free-radical reaction transition states." *Int. J. Quantum Chem.* **52**(4), 837-847 (1994).

Greenhill, P. G., B. V. OGrady and R. G. Gilbert, "Theoretical prediction of $CH_3O$ and $CH_2OH$ gas-phase decomposition rate coefficients." *Aust. J. Chem.* **39**(12), 1929-1942 (1986).

Haar, L., J. S. Gallagher and G. S. Kell, *NBS/NRC Steam Tables*. Hemisphere Publishing Corp., New York (1984).

Held, T. and F. Dryer, "A comprehensive mechanism for methanol oxidation." *Int. J. of Chem. Kinet.* **30**(11), 805-830 (1998).

Hippler, H., F. Striebel and B. Viskolcz, "A detailed experimental and theoretical study on the decomposition of methoxy radicals." *Phys. Chem. Chem. Phys.* **3**(12), 2450-2458 (2001).

Holgate, H. R. and J. W. Tester, "Fundamental kinetics and mechanisms of hydrogen oxidation in supercritical water." *Combust. Sci. Technol.* **88**(5-6), 369-397 (1993).

Holgate, H. R. and J. W. Tester, "Oxidation of hydrogen and carbon monoxide in sub- and supercritical water: reaction kinetics, pathways, and water-density effects. 2. Elementary reaction rate modeling." *J. Phys. Chem.* **98**(3), 810-822 (1994).

Hughes, K., T. Turanyi, A. Clague and M. Pilling, "Development and testing of a comprehensive chemical mechanism for the oxidation of methane." *Int. J. Chem. Kinet.* **33**(9), 513-538 (2001).

Hunter, T. B., T. A. Litzinger, H. Wang and M. Frenklach, "Ethane oxidation at elevated pressures in the intermediate temperature regime: Experiments and modeling." *Combust. Flame* **104**(4), 505-523 (1996).

Kaiser, E., C. Westbrook and W. Pitz, "Acetaldehyde oxidation in the negative temperature coefficient regime: Experimental and modeling results." *Int. J. of Chem. Kinet.* **18**(6), 655-688 (1986).

Kappel, C., K. Luther and J. Troe, "Shock wave study of the unimolecular dissociation of $H_2O_2$ in its falloff range and of its secondary reactions." *Phys. Chem. Chem. Phys.* **4**(18), 4392-4398 (2002).

Kee, R. J., F. M. Rupley, E. Meeks and J. A. Miller, *Chemkin-III: A Fortran chemical kinetics package for the analysis of gas-phase chemical and plasma kinetics,* Sandia National Laboratories, Livermore, CA, (1996).

Koo, M., W. K. Lee and C. H. Lee, "New reactor system for supercritical water oxidation and its application on phenol destruction." *Chem. Eng. Sci.* **52**(7), 1201-1214 (1997).

Korobeinichev, O. P., S. B. Ilyin, T. A. Boshova, V. M. Shvartsberg and A. A. Chernov, "The chemistry of the destruction of organophosphorus compounds in flames -III: The destruction of DMMP and TMP in a flame of hydrogen and oxygen." *Combust. Flame* **121**(4), 593-609 (2000).

Larson, C., P. Stewart and D. Golden, "Pressure and temperature dependence of reactions proceeding via a bound complex - An approach for combustion and atmospheric chemistry modelers - Application to HO + CO->[HOCO]->H+CO2." *Int. J. Chem. Kinet.* **20**(1), 27-40 (1988).

Mackie, J., G. Backsay and N. Haworth, "Reactions of phosphorus-containing species of importance in the catalytic recombination of H + OH: Quantum chemical and kinetic studies." *J. Phys. Chem. A* **106**(45), 10825-10830 (2002).

Marinov, N., "A detailed chemical kinetic model for high temperature ethanol oxidation." *Int. J. Chem. Kinet.* **31**(3), 183-220 (1999).

Meeks, E., H. K. Moffat, J. F. Grcar, and R. J. Kee, *AURORA: A Fortran Program for Modeling Well Stirred Plasma and Thermal Reactors with Gas and Surface Reactions*, Sandia National Laboratories, Report SAND96-8218 (1996).

Melius, C., "Carl Melius' Home Page." January, 2003 <http://z.ca.sandia.gov/~melius> (1997).

Michael, J. V., M. C. Su, J. W. Sutherland, J. J. Carroll and A. F. Wagner, "Rate constants for $H+O_2+M->HO_2+M$ in seven bath gases." *J. Phys. Chem. A* **106**(21), 5297-5313 (2002).

Quin, L. D., *A Guide to Organophosphorus Chemistry*. Wiley-Interscience, New York (2000).

Ranzi, E., T. Faravelli, P. Gaffuri, G. C. Pennati and A. Sogaro, "A wide-range modeling study of propane and n-butane oxidation." *Combust. Sci. Technol.* **100**(1-6), 299-330 (1994).

Rice, S. and E. Croiset, "Oxidation of simple alcohols in supercritical water III. Formation of intermediates from ethanol." *Ind. Eng. Chem. Res.* **40**(1), 86-93 (2001).

Ruscic, B. and M. Litorja, "Photoionization of HOCO revisited: A new upper limit to the adiabatic ionization energy and lower limit to the enthalpy of formation." *Chem. Phys. Lett.* **316**(1-2), 45-50 (2000).

Savage, P., J. Yu, N. Stylski and E. Brock, "Kinetics and mechanism of methane oxidation in supercritical water." *J. Supercrit. Fluids* **12**, 141-153 (1998).

Senosiain, J. P., C. B. Musgrave and D. M. Golden, "Temperature and pressure dependence of the reaction of OH and CO: Master equation modeling on a high-level potential energy surface." *Int. J Chem. Kinet.* **35**(9), 464-474 (2003).

Sheng, C., J. W. Bozzelli, A. M. Dean and A. Y. Chang, "Detailed kinetics and thermochemistry of C2H5+O2: Reaction kinetics of the chemically-activated and stabilized CH2CH2OO center dot adduct." *J. Phys. Chem. A* **106**(32), 7276-7293 (2002).

Slemr, F. and P. Warneck, "Kinetics of the reaction of atomic hydrogen with methyl hydroperoxide." *Int. J. Chem. Kinet.* **9**(2), 267-282 (1977).

Smith, G. P., D. M. Golden, M. Frenklach, N. W. Moriarty, B. Eiteneer, M. Goldenberg, C. T. Bowman, R. K. Hanson, S. Song, W. Gardiner, V. V. Lissianski and Z. Qin, "GRI-Mech 3.0." May, 2003 <http://www.me.berkeley.edu/gri_mech> (2000).

Taylor, P. H., M. S. Rahman, M. Arif, B. Dellinger and P. Marshall, "Kinetic and mechanistic studies of the reaction of hydroxyl radicals with acetaldehyde over an extended temperature range." *Proceedings of the Combustion Institute* **26**, 497-504 (1996).

Troe, J., "Detailed modeling of the temperature and pressure dependence of the reaction $H+O_2(+M)->HO_2(+M)$." *Proceedings of the Combustion Institute* **28**, 1463-1469 (2000).

Tsang, W. and R. F. Hampson, "Chemical kinetic database for combustion chemistry. 1. Methane and related compounds." *J. Phys. Chem. Ref. Data* **15**(3), 1087-1279 (1986).

Tsang, W., "Chemical kinetic database for combustion chemistry. 2. methanol." *J Phys Chem Ref. Data* **16**(3), 471-508 (1987).

Vogel, F., J. L. DiNaro, P. A. Marrone, S. F. Rice, W. A. Peters, K. A. Smith and J. W. Tester, "Critical review of kinetic data for the oxidation of methanol in supercritical water." *Ind. Eng. Chem. Res.*, accepted for publication (2003).

Wantuck, P. J., R. C. Oldenborg, S. L. Baughcum and K. R. Winn, "$CH_3O$+CO removal rate-constant measurements over the 473 K-973 K temperature range." *Chem. Phys. Lett.* **138**(6), 548-552 (1987).

Warnatz, J., "Rate coefficients in the C/H/O system." in *Combustion Chemistry*, W. Gardiner, Ed., Springer-Verlag, New York, (1984)

Webley, P. A. and J. W. Tester, "Fundamental kinetics of methane oxidation in supercritical water." *Energy and Fuels* **5**, 411-419 (1991).

Wijaya, C. D., R. Sumathi and W. H. Green, "Thermodynamic properties and kinetic parameters for cyclic ether formation from hydroperoxyalkyl radicals." *J. Phys. Chem. A* **107**(24), 4908-4920 (2003).

Zhu, R. and M.C. Lin, "The $CH_3$+$HO_2$ reaction: First-principles prediction of its rate constant and product branching probabilities." *J. Phys. Chem. A* **105**(25), 6243-6248 (2001).

Zhu, R. S., E. G. W. Diau, M. C. Lin and A. M. Mebel, "A computational study of the OH(OD) + CO reactions: Effects of pressure, temperature, and quantum-mechanical tunneling on product formation." *J. Phys. Chem. A* **105**(50), 11249-11259 (2001).

# 6 Summary and Conclusions

The oxidation kinetics of methylphosphonic acid (MPA), a refractory intermediate in the oxidation of many organophosphorus compounds, were quantitatively characterized at well-defined conditions. A multi-scale kinetic modeling approach was used to correlate and predict experimentally measured reaction rates and to obtain mechanistic understanding of important pathways. Macroscopic models were regressed as a convenient means to correlate MPA oxidation data and an elementary reaction rate model was developed to infer possible elementary reaction pathways during MPA oxidation. Certain important MPA reaction rates were estimated from *ab initio* calculations to accurately determine reaction rates for individual reaction pathways. The primary conclusions obtained from this work are included below.

***MPA Experimental Data and Macroscopic Modeling:***

An experimental study of MPA hydrolysis and oxidation in SCW was completed that systematically explored the effects of temperature (478 to 572 °C), residence time (3.0 to 9.5 s), oxygen concentration (1.0 to 3.8 mM), MPA concentration (0.5 to 1.0 mM), and pressure (138 to 277 bar) on MPA conversion and on its product distribution. Conversion in the absence of oxygen was less than 6% after $\tau$=7 s at all temperatures studied. Minimal conversion ($X$<30% at $\tau$=10 s) was measured at $T$<503 °C, while almost complete conversion ($X$=99%) was measured at $T$=571 °C and $\tau$=7 s at stoichiometric conditions and $P$=246 bar. The only phosphorus-containing product was phosphoric acid, while the carbon-containing products included carbon monoxide, methane, and carbon dioxide. At the conditions studied, methane was a minor product with a carbon yield less than 20% at all conditions examined. MPA oxidation rates exhibited a dependence on both oxygen concentration and pressure (or water density), but were relatively independent of initial MPA concentration. Data were regressed to an empirical global

rate law with a pre-exponential factor of $10^{14.0\pm1.6}$ ($s^{-1}$ $M^{-1.47}$), an activation energy of 228±22 kJ/mol, a first-order MPA dependence, an oxygen order of 0.30±0.18, and a water order of 1.17±0.30 (all parameters to 95% confidence).

MPA oxidation occurred by two pathways to form the carbon-containing intermediates, CO and $CH_4$, with the dominant pathway being through the CO intermediate to form the final carbon-containing product, $CO_2$. A four-pathway macroscopic model was regressed to estimate the relative reaction rates and oxygen dependence of these major pathways during MPA oxidation. The model predicted that the branching ratio of the two MPA pathways to form CO and $CH_4$ was approximately 10:1 at lower temperatures and decreased to 5:1 at $T$=571°C as the methane pathway became more important. MPA oxidation to CO and CO oxidation to $CO_2$ both had an oxygen dependence of approximately 0.3, while MPA oxidation to methane had an oxygen dependence of zero.

The predicted rate constants for $CH_4$ and CO oxidation during MPA oxidation were compared to the predicted rate constants from global rate laws for these compounds from earlier studies in our group (Webley and Tester (1991) and Holgate *et al.* (1992)). The regressed CO oxidation rate in the MPA model was three to four times faster than that predicted by the CO global rate law from Holgate *et al.* (1992). The CO oxidation rate is dependent on the $OH^{\bullet}$ radical concentration. A higher $OH^{\bullet}$ radical concentration in the MPA system would increase CO oxidation rates, but this effect could not be captured in the global rate law if the oxygen concentrations were the same. The model predicted that $CH_4$ was unreactive, which was also predicted by the methane global rate law at these conditions.

***Ab initio Calculations of Organophosphorus Compounds:***

The *ab initio* study was conducted to accurately estimate organophosphorus thermochemistry and reaction rates for the MPA SCWO elementary reaction mechanism. The CBS-Q method in Gaussian 98 was determined to be an accurate method for calculation of organophosphorus energies based on comparisons of predicted heats of formation with available literature values. Eleven new organophosphorus intermediates for the MPA SCWO mechanism were introduced and their thermochemistry was calculated. Bond strengths for the P-C, P-O, C-H, and O-H bonds in MPA were calculated and compared to these bond strengths in other compounds to aid in reaction rate estimation. The P-C and C-H bond strengths were both approximately equal to C-C and C-H bond strengths in other hydrocarbons. The P-O bond strength was much larger than any other X-O bond strength available and the O-H bond strength was larger than the O-H bond strength in most alcohols. From these results, it could be difficult to accurately estimate P-O and O-H bond cleavage reaction rates from analogous organic reaction rates available in the literature.

In this study, transition state theory rate constants for 14 reactions in the MPA SCWO mechanism were calculated. The MPA + $OH^{\bullet}$ potential surface was studied since these reactions could be important MPA reaction pathways in SCWO. The only MPA bimolecular reaction rate available in the organophosphorus combustion mechanisms was MPA reaction with an OH radical to form $PO(OH)_3$ and $CH_3^{\bullet}$ (Korobeinichev *et al.*, 2000; Glaude *et al.*, 2000). We calculated rate constants for hydrogen abstraction from MPA's $CH_3$ or OH group and also calculated reaction rates for the formation of $PO(OH)_3$ and $CH_3^{\bullet}$ through the $PO^{\bullet}(OH)_3CH_3$ intermediate. Reaction rates through the hydrogen abstraction pathways were two to four orders of magnitude faster than reaction through the $PO^{\bullet}(OH)_3CH_3$ intermediate to form $PO(OH)_3$ and

$CH_3^{\bullet}$, indicating that these previously ignored reaction pathways are important for MPA oxidation. Also, by comparing our calculated rate constant for $PO(OH)_3$ and $CH_3^{\bullet}$ formation with the estimated rates from Glaude *et al.* (2000) and Korobeinichev *et al.* (2000), we found that the reaction rate through this pathway is overestimated by approximately two orders of magnitude by both Korobeinichev *et al.* (2000) and Glaude *et al.* (2000).

As part of this study, certain organophosphorus reaction rates in combustion mechanisms were assessed to determine how well general rate estimation methods work for organophosphorus reaction rates. We found that certain reaction rates, such as (1) unimolecular decomposition of MPA to form methane and $PO_2OH$ and (2) the addition of an H atom to $PO_2OH$ to form $P^{\bullet}O(OH)_2$ were within an order of magnitude of the *ab initio* calculated transition state theory rate constants. However, reaction rates for several phosphorus-containing reactions that involved the P-O bond were overestimated by several orders of magnitude. The overestimation of the P-O reaction rates was probably due to the high P-O bond strength in phosphorus-containing compounds.

***MPA SCWO Elementary Reaction Rate Model:***

An MPA SCWO model was developed with 246 reactions and 41 species, including 96 phosphorus-containing reaction rates and 20 phosphorus-containing species. This model improved on the current organophosphorus rates in the literature by adding MPA hydrogen abstraction pathways and extensive oxidation pathways for the $PO(OH)_2CH_2^{\bullet}$ intermediate. Since MPA is a minor intermediate during DMMP combustion, its reaction kinetics had not been previously examined in detail in the DMMP combustion models (Korobeinichev *et al.*, 2000; Glaude *et al.*, 2000). The newly added pathways and intermediates were necessary to accurately predict experimentally measured concentration profiles for MPA and its products.

With these new reaction rates, the model was able to predict the SCWO concentration profiles for MPA and its products, $H_3PO_4$, CO, $CH_4$, and $CO_2$ at temperatures between 478 and 571 °C, $\tau$=3 to 10 s, $P$=246 bar, $\Phi$=1.0, and $[MPA]_0$=1.0 mM. The reaction channels of the two MPA hydrogen abstraction products, $PO(OH)_2CH_2^{\bullet}$ and $PO(O^{\bullet})OHCH_3$, dictated the carbon product distribution of CO and $CO_2$ versus $CH_4$ in the model. Hydrogen abstraction from MPA's $CH_3$ group produced $PO(OH)_2CH_2^{\bullet}$ which eventually oxidized to formaldehyde. In SCW, formaldehyde reacts to form CO and $CO_2$. Hydrogen abstraction from MPA's OH group formed $PO(O^{\bullet})OHCH_3$, which decomposes to form the $CH_3^{\bullet}$ radical. In SCW, the $CH_3^{\bullet}$ radical primarily reacts with water to form methane. These modeling results supported the two pathway MPA global model that was regressed from the experimental data.

Experimentally, MPA oxidation rates decreased with decreasing oxygen or water concentrations. The model predicted that MPA oxidation rates decrease with decreasing oxygen concentration due to the subsequent decrease in $HO_2^{\bullet}$ concentration. Unfortunately, the model did not correctly predict that MPA oxidation rates decrease with decreasing water concentration. In the model, the dominant effect of water is to react with $PO(OH)_2CH_2^{\bullet}$ to reform MPA and $OH^{\bullet}$. Thus, decreasing water concentration in the model increased MPA oxidation rates, contrary to the experimental data. These results indicate that water's role as both a solvent and a reactant at supercritical water conditions may not be correctly represented in the current model.

To sum up the experimental data and the modeling studies, we were able to infer possible radical pathways for MPA oxidation in supercritical water. Most of the important MPA reaction pathways that were identified had not been included in previous studies. One of the most significant contributions of this work was the introduction of the new reaction pathways that could correctly predict the carbon product distribution during MPA oxidation over a wide range

of operating conditions. Knowledge of these pathways can guide operation of an SCWO process to achieve desired results or operating conditions, such as, to minimize methane formation. Also, the results from this study could aid in the development of future organophosphorus combustion mechanisms. We were able to examine the accuracy of rate estimation methods for phosphorus-containing chemistry from our *ab initio* calculations and we also introduced new intermediates and reaction pathways that could be important during DMMP combustion.

# 7 Recommendations

The MPA SCWO elementary reaction rate model introduced many new reaction pathways and intermediates and provided substantial insight into MPA oxidation kinetics. The model was able to predict most of the MPA SCWO data correctly; however, it did not correctly capture the effect of water density on MPA oxidation rates. These results indicate that the MPA SCWO model still requires significant improvements to better predict MPA oxidation rates at all conditions. Acting on the recommendations listed below would address issues that arose from the MPA SCWO modeling studies.

1) Experimentally identify formaldehyde as a reaction intermediate during MPA oxidation. In the new MPA SCWO elementary reaction rate model, MPA oxidation proceeds through formaldehyde. However, formaldehyde was not experimentally observed at the operating conditions examined because it is highly reactive at the temperatures studied. Experimental detection of formaldehyde would provide further verification of the MPA SCWO model. At lower temperatures and longer residence times, MPA conversion would be high enough and formaldehyde conversion rates low enough to detect formaldehyde. If longer residence times are required for sufficient MPA conversion to occur, the CSTR or the batch reactor systems available in our laboratory could be used since these reactors can have residence times greater than ten seconds.
2) Experimentally measure reliable methane SCWO data. In developing the MPA SCWO model, updated C-1 reaction rates were included, but we were unable to determine the accuracy of these new rates to predict methane oxidation rates in SCW because high quality experimental data on methane oxidation rates are currently not available. Earlier in our group, Webley and Tester (1991) measured methane oxidation rates; however,

several improvements have been made to the plug flow reactor since their study was conducted and the uncertainty in experimental conditions in their study was substantial. To evaluate a model properly, data at a single temperature, methane concentration, oxygen concentration, and water concentration should be available at multiple residence times to provide concentration profiles for a single set of reaction conditions. Higher quality methane data would assist in the development of models for all organic compounds since these oxidation mechanisms include pathways through C-1 intermediates.

3) Theoretically examine the phosphorus oxide chemistry in the MPA SCWO model in more detail. Unfortunately, these rates are difficult to estimate because the P-O and O-H bonds in phosphorus-containing compounds are much different from those in other model chemistries. Thus, the best way to calculate reaction rates involving these bonds is by time consuming *ab initio* calculations. Results from the MPA SCWO model indicate that examination of new reaction rates for POy chemistry could be important. For example, the model does not currently predict the correct water dependence for MPA oxidation rates. However, the only reaction pathway for $PO_2OH$ is with water to form phosphoric acid. If a competing reaction pathway existed for the $PO_2OH$ intermediate, it could become important at lower water concentrations and possibly decrease MPA oxidation rates. Also, alternative reaction pathways could exist for this submechanism through intermediates, such as $P(OH)_3$, that are not currently included in the model. A more thorough examination of the phosphorus oxide submechanism could improve the MPA SCWO model predictions.

4) Explore the effect of water solvation on the transition state theory rate constants from *ab initio* calculations. We hypothesized that the water dependence in the model may be incorrectly predicted because water solvation effects are not included in the current model. The *ab initio* calculations conducted in this thesis were in a vacuum, following the assumption that reaction rate constants do not change significantly from combustion conditions to supercritical water conditions. *Ab initio* calculations of transition state energies at different dielectric strengths could determine if the transition state barriers are affected by the change in solvent media.

5) Determine if the new phosphorus-containing reactions and reaction rates change predictions for the DMMP combustion mechanisms. Experimental DMMP oxidation data is available from Korobeinichev *et al.* (2000) along with reaction mechanisms from Glaude *et al.* (2000) and Korobeinichev *et al.* (2000) to determine if the reactions presented here are important in DMMP combustion. For example, Nogueira and Fisher (2003) experimentally measured the effect of DMMP on a methane flame and compared their experimental data to predictions from the Glaude *et al.* (2000) DMMP model. They found that the combustion model underpredicted the $CH_2O$ and $CH_3OH$ experimental concentration profiles. Inclusion of the pathways from the MPA SCWO study could possibly improve the predictions of these concentration profiles.

6) Calculate additional transition state theory rate constants from *ab initio* calculations. The *ab initio* calculated reaction set for the MPA model was chosen during development of the model. After analyzing the sensitivity results and reaction fluxes from this model, several rate constants have been identified that are extremely important for the model predictions. For example, the decomposition of the $PO(O^{\bullet})OHCH_3$ intermediate and

reaction of the $PO(OH)_2CH_2^{\bullet}$ and $HO_2^{\bullet}$ to form $PO(OH)_2CH_2O^{\bullet}$ are both very important. Additionally, we found that $PO(OH)_2CH_2O_2^{\bullet}$ thermochemistry was very important for model predictions. Better estimation methods for the peroxy organophosphorus compounds should be investigated

7) Improved understanding of the $HOCO^{\bullet}$ chemistry would also be helpful. The potential surface for these reaction pathways has been extensively studied, but the reaction rates and thermochemistry are still not well characterized. Additionally, once formed, the $HOCO^{\bullet}$ radical could undergo hydrogen abstraction reactions with $O_2$ or peroxy compounds. It would be helpful to have better estimates for these important reaction rates.

# 8 Appendix

This appendix contains two sections. In Section 8.1, the experimental data for is presented in multiple tables. In Section 8.2, the Gaussian outputs that were used to calculate the thermochemistry and reaction rates are given.

## 8.1 MPA SCWO Experimental Data

**Table 8-1: Experimental conditions for MPA oxidation and hydrolysis experiments**
The hydrolysis experiments are noted by an NA in the Φ column (indicating no oxygen is present). All reported errors are 99% confidence intervals. The error in all temperature measurements was 3 °C.

| Run No. | T (°C) | τ(s) | e(τ) | P(bar) | e(P) | Φ | e(Φ) | $[MPA]_0$ mol/mL | e($[MPA]_0$) |
|---|---|---|---|---|---|---|---|---|---|
| 014 | 478.1 | 5.1 | 0.3 | 244.9 | 0.7 | 0.85 | 0.15 | 9.5E-07 | 5.0E-08 |
| 015 | 478.3 | 9.5 | 0.6 | 244.2 | 0.7 | 0.87 | 0.15 | 9.6E-07 | 3.4E-08 |
| 016 | 477.5 | 3.5 | 0.2 | 243.3 | 0.7 | 0.70 | 0.18 | 7.7E-07 | 2.7E-08 |
| 017 | 478.2 | 7.2 | 0.4 | 244.8 | 0.5 | 0.67 | 0.18 | 7.6E-07 | 2.9E-08 |
| 024 | 478.5 | 4.9 | 0.3 | 244.2 | 0.7 | 0.97 | 0.19 | 9.5E-07 | 3.9E-08 |
| 025 | 478.7 | 9.0 | 0.5 | 245.8 | 0.8 | 0.96 | 0.19 | 9.6E-07 | 3.8E-08 |
| 027 | 528.5 | 5.4 | 0.3 | 244.3 | 0.8 | 0.90 | 0.06 | 9.4E-07 | 2.9E-08 |
| 028 | 528.4 | 7.0 | 0.4 | 245.0 | 0.8 | 0.90 | 0.06 | 9.4E-07 | 3.0E-08 |
| 029 | 503.1 | 8.9 | 0.5 | 243.7 | 0.8 | 0.89 | 0.06 | 9.5E-07 | 3.2E-08 |
| 030 | 502.7 | 5.9 | 0.3 | 243.5 | 0.7 | 0.95 | 0.07 | 9.8E-07 | 3.1E-08 |
| 033 | 503.7 | 6.9 | 0.4 | 244.0 | 1.0 | NA | NA | 1.0E-06 | 2.5E-08 |
| 034 | 503.7 | 3.2 | 0.2 | 247.2 | 0.8 | 1.01 | 0.04 | 1.0E-06 | 2.5E-08 |
| 035 | 504.0 | 5.0 | 0.3 | 245.0 | 0.8 | 1.01 | 0.04 | 1.0E-06 | 2.3E-08 |
| 036 | 503.8 | 7.1 | 0.4 | 247.5 | 1.1 | 1.00 | 0.05 | 1.0E-06 | 3.1E-08 |
| 042 | 571.4 | 7.0 | 0.4 | 245.8 | 1.1 | NA | NA | 1.0E-06 | 2.7E-08 |
| 043 | 527.1 | 7.1 | 0.4 | 245.8 | 0.8 | NA | NA | 9.8E-07 | 2.2E-08 |
| 044 | 527.0 | 8.0 | 0.5 | 245.1 | 1.9 | 1.02 | 0.04 | 9.9E-07 | 2.2E-08 |
| 045 | 526.8 | 4.0 | 0.2 | 244.6 | 1.4 | 1.01 | 0.04 | 9.8E-07 | 2.1E-08 |
| 046 | 551.6 | 7.1 | 0.4 | 247.2 | 1.1 | NA | NA | 1.0E-06 | 2.8E-08 |
| 047 | 551.5 | 7.0 | 0.4 | 246.6 | 1.1 | 1.03 | 0.05 | 1.0E-06 | 2.4E-08 |
| 048 | 551.8 | 4.5 | 0.3 | 245.3 | 0.7 | 1.96 | 0.13 | 1.0E-06 | 2.1E-08 |
| 049 | 551.9 | 6.0 | 0.3 | 245.0 | 0.8 | 1.97 | 0.13 | 1.0E-06 | 2.2E-08 |
| 050 | 551.7 | 7.0 | 0.4 | 245.2 | 0.8 | 1.94 | 0.12 | 9.9E-07 | 2.7E-08 |
| 051 | 526.2 | 6.0 | 0.3 | 245.7 | 0.8 | 1.93 | 0.09 | 1.0E-06 | 2.2E-08 |
| 052 | 526.6 | 8.0 | 0.5 | 245.6 | 1.0 | 1.94 | 0.09 | 1.0E-06 | 2.1E-08 |
| 053 | 526.8 | 4.0 | 0.2 | 246.3 | 1.0 | 0.71 | 0.04 | 1.0E-06 | 2.2E-08 |
| 054 | 526.6 | 7.9 | 0.5 | 244.1 | 1.1 | 0.71 | 0.04 | 1.0E-06 | 2.2E-08 |
| 055 | 526.9 | 5.9 | 0.3 | 243.8 | 0.8 | 0.71 | 0.03 | 1.0E-06 | 1.8E-08 |
| 056 | 526.9 | 6.1 | 0.4 | 244.6 | 1.5 | 1.08 | 0.04 | 1.0E-06 | 2.1E-08 |
| 057 | 526.5 | 4.7 | 0.3 | 244.6 | 1.4 | 1.07 | 0.06 | 1.0E-06 | 3.1E-08 |
| 058 | 501.6 | 4.0 | 0.2 | 244.2 | 1.2 | 0.55 | 0.02 | 1.0E-06 | 2.4E-08 |
| 059 | 501.7 | 8.1 | 0.5 | 248.1 | 3.4 | 0.55 | 0.03 | 1.0E-06 | 4.0E-08 |
| 060 | 571.8 | 3.5 | 0.2 | 244.6 | 1.1 | 1.11 | 0.05 | 1.0E-06 | 2.5E-08 |
| 061 | 571.4 | 5.5 | 0.3 | 245.7 | 1.0 | 1.11 | 0.05 | 1.0E-06 | 2.5E-08 |
| 062 | 571.5 | 7.5 | 0.5 | 245.7 | 0.8 | 1.11 | 0.07 | 1.0E-06 | 4.0E-08 |

| Run No. | T (°C) | τ(s) | e(τ) | P(bar) | e(P) | Φ | e(Φ) | $[MPA]_0$ mol/mL | e($[MPA]_0$) |
|---|---|---|---|---|---|---|---|---|---|
| 063 | 552.1 | 3.7 | 0.2 | 244.0 | 0.7 | 1.07 | 0.08 | 1.0E-06 | 3.5E-08 |
| 064 | 526.9 | 3.9 | 0.2 | 244.2 | 0.7 | 1.03 | 0.07 | 1.0E-06 | 4.1E-08 |
| 065 | 527.1 | 6.1 | 0.4 | 245.5 | 0.5 | 1.01 | 0.05 | 1.0E-06 | 3.1E-08 |
| 066 | 527.1 | 7.0 | 0.4 | 244.5 | 0.8 | 1.02 | 0.06 | 1.0E-06 | 3.6E-08 |
| 067 | 527.1 | 4.0 | 0.2 | 245.5 | 0.5 | 1.01 | 0.05 | 1.0E-06 | 2.5E-08 |
| 068 | 527.2 | 6.0 | 0.4 | 243.2 | 0.8 | 1.00 | 0.06 | 9.9E-07 | 3.3E-08 |
| 069 | 527.1 | 3.0 | 0.2 | 245.5 | 0.5 | 0.99 | 0.07 | 9.9E-07 | 4.6E-08 |
| 070 | 527.2 | 4.0 | 0.2 | 245.3 | 0.7 | 1.01 | 0.05 | 1.0E-06 | 2.8E-08 |
| 071 | 527.3 | 6.2 | 0.4 | 247.6 | 0.7 | 1.01 | 0.06 | 1.0E-06 | 3.5E-08 |
| 072 | 527.1 | 3.0 | 0.2 | 173.6 | 0.7 | 1.00 | 0.04 | 1.0E-06 | 2.7E-08 |
| 073 | 526.9 | 4.0 | 0.3 | 173.7 | 1.7 | 1.00 | 0.08 | 1.0E-06 | 5.4E-08 |
| 074 | 526.8 | 5.0 | 0.3 | 174.0 | 0.8 | 1.05 | 0.07 | 1.0E-06 | 4.1E-08 |
| 075 | 526.3 | 6.1 | 0.4 | 174.2 | 0.8 | 1.05 | 0.06 | 1.0E-06 | 3.2E-08 |
| 076 | 527.2 | 4.0 | 0.2 | 276.0 | 0.8 | 0.95 | 0.04 | 9.9E-07 | 2.7E-08 |
| 077 | 528.0 | 5.0 | 0.3 | 275.9 | 1.0 | 0.96 | 0.03 | 9.9E-07 | 2.5E-08 |
| 078 | 528.3 | 6.1 | 0.4 | 276.1 | 0.8 | 0.97 | 0.04 | 1.0E-06 | 2.6E-08 |
| 079 | 526.9 | 4.0 | 0.2 | 206.3 | 0.7 | 0.99 | 0.07 | 1.0E-06 | 4.5E-08 |
| 080 | 527.0 | 5.0 | 0.3 | 207.3 | 0.8 | 1.00 | 0.05 | 1.0E-06 | 2.7E-08 |
| 081 | 526.9 | 6.1 | 0.4 | 206.6 | 0.8 | 1.01 | 0.05 | 1.0E-06 | 3.2E-08 |
| 082 | 550.7 | 3.0 | 0.2 | 172.3 | 0.7 | 1.00 | 0.04 | 1.0E-06 | 2.2E-08 |
| 083 | 550.9 | 4.0 | 0.2 | 171.9 | 0.8 | 1.01 | 0.04 | 1.0E-06 | 2.6E-08 |
| 084 | 551.4 | 5.0 | 0.3 | 172.7 | 0.8 | 1.01 | 0.06 | 1.0E-06 | 3.6E-08 |
| 085 | 526.2 | 3.0 | 0.2 | 138.9 | 0.8 | 1.02 | 0.05 | 1.0E-06 | 3.1E-08 |
| 086 | 527.1 | 3.9 | 0.2 | 136.8 | 0.7 | 1.02 | 0.05 | 1.0E-06 | 3.4E-08 |
| 087 | 550.6 | 3.2 | 0.2 | 242.6 | 0.8 | 0.98 | 0.04 | 1.0E-06 | 2.2E-08 |
| 088 | 550.9 | 4.5 | 0.3 | 243.8 | 0.7 | 0.98 | 0.05 | 1.0E-06 | 3.3E-08 |
| 089 | 550.9 | 6.0 | 0.3 | 243.6 | 0.7 | 0.99 | 0.04 | 1.0E-06 | 2.8E-08 |
| 090 | 526.0 | 3.0 | 0.2 | 245.5 | 0.7 | 0.96 | 0.06 | 5.0E-07 | 1.1E-08 |
| 091 | 525.7 | 4.0 | 0.2 | 245.1 | 0.7 | 0.97 | 0.07 | 5.0E-07 | 1.4E-08 |
| 092 | 526.3 | 6.2 | 0.4 | 245.6 | 0.7 | 1.00 | 0.09 | 5.1E-07 | 2.5E-08 |
| 093 | 551.0 | 4.0 | 0.2 | 243.1 | 0.7 | 0.97 | 0.05 | 9.9E-07 | 1.6E-08 |
| 094 | 551.1 | 5.0 | 0.3 | 245.1 | 0.7 | 0.97 | 0.07 | 1.0E-06 | 4.0E-08 |
| 095 | 551.4 | 5.9 | 0.3 | 243.0 | 0.7 | 0.97 | 0.06 | 9.9E-07 | 2.9E-08 |
| 096 | 551.6 | 3.5 | 0.2 | 244.8 | 0.8 | 1.56 | 0.10 | 1.0E-06 | 2.1E-08 |
| 097 | 551.3 | 5.0 | 0.3 | 245.7 | 0.7 | 1.58 | 0.14 | 1.0E-06 | 4.6E-08 |
| 098 | 551.6 | 6.1 | 0.4 | 246.3 | 0.7 | 1.55 | 0.10 | 1.0E-06 | 2.0E-08 |

## Table 8-2: Kinetic data for MPA hydrolysis and oxidation experiments

CBal and PBal are the carbon and phosphorus balances (%). A balance of 100% denotes that all phosphorus or carbon is accounted for in the reactor effluent. The CO, $CO_2$, and $CH_4$ values are carbon fractions with their error at the 99% confidence interval.

| Run No. | X(%) | e(X) | CBal | e(CBal) | PBal | e(PBal) | CO | e(CO) | $CO_2$ | e($CO_2$) | $CH_4$ | e($CH_4$) |
|---|---|---|---|---|---|---|---|---|---|---|---|---|
| 014 | 15.8 | 5.2 | 98.5 | 5.7 | 98.1 | 5.3 | 0.11 | 0.01 | 0.03 | 0.02 | 0.01 | 0.00 |
| 015 | 23.4 | 3.1 | 98.2 | 4.3 | 99.1 | 3.3 | 0.15 | 0.03 | 0.05 | 0.01 | 0.02 | 0.00 |
| 016 | 8.2 | 3.7 | 99.4 | 4.0 | 99.5 | 3.8 | 0.07 | 0.01 | 0.00 | 0.00 | 0.01 | 0.01 |
| 017 | 15.7 | 3.7 | 102.0 | 4.2 | 100.5 | 3.8 | 0.13 | 0.01 | 0.03 | 0.02 | 0.01 | 0.00 |
| 024 | 13.8 | 3.9 | 94.2 | 4.2 | 95.0 | 4.0 | 0.07 | 0.01 | 0.00 | 0.00 | 0.01 | 0.00 |
| 025 | 19.4 | 3.7 | 101.0 | 4.1 | 96.5 | 3.8 | 0.12 | 0.01 | 0.07 | 0.01 | 0.01 | 0.00 |
| 027 | 47.3 | 2.0 | 106.4 | 3.0 | 100.4 | 2.6 | 0.25 | 0.02 | 0.23 | 0.02 | 0.05 | 0.00 |
| 028 | 55.4 | 1.7 | 105.6 | 4.7 | 101.3 | 2.6 | 0.24 | 0.03 | 0.30 | 0.03 | 0.06 | 0.00 |
| 029 | 29.7 | 2.8 | 104.2 | 3.6 | 101.3 | 3.0 | 0.19 | 0.02 | 0.13 | 0.01 | 0.02 | 0.00 |
| 030 | 21.5 | 2.9 | 100.8 | 3.9 | 98.6 | 3.0 | 0.14 | 0.02 | 0.08 | 0.01 | 0.01 | 0.00 |
| 033 | 3.1 | 2.8 | 97.0 | 2.8 | 97.9 | 2.8 | NA | NA | NA | NA | NA | NA |
| 034 | 10.4 | 2.6 | 98.7 | 2.9 | 99.5 | 2.6 | 0.06 | 0.01 | 0.03 | 0.01 | <0.01 | 0.00 |
| 035 | 16.1 | 2.3 | 101.0 | 2.8 | 100.2 | 2.4 | 0.10 | 0.01 | 0.08 | 0.01 | 0.02 | 0.00 |
| 036 | 22.8 | 2.8 | 101.8 | 3.1 | 99.9 | 2.9 | 0.15 | 0.01 | 0.08 | 0.01 | 0.02 | 0.00 |
| 042 | 6.6 | 2.9 | 93.4 | 2.9 | 96.9 | 2.9 | NA | NA | NA | NA | NA | NA |
| 043 | 0.0 | 3.2 | 100.0 | 3.2 | 101.8 | 3.4 | NA | NA | NA | NA | NA | NA |
| 044 | 58.0 | 1.1 | 100.7 | 2.8 | 103.1 | 2.0 | 0.22 | 0.02 | 0.29 | 0.01 | 0.08 | 0.01 |
| 045 | 33.4 | 1.7 | 101.5 | 2.2 | 102.2 | 1.9 | 0.19 | 0.01 | 0.11 | 0.01 | 0.04 | 0.00 |
| 046 | 4.0 | 3.0 | 96.0 | 3.0 | 97.3 | 3.0 | NA | NA | NA | NA | NA | NA |
| 047 | 87.5 | 0.4 | 96.6 | 3.2 | 98.6 | 2.3 | 0.13 | 0.01 | 0.57 | 0.03 | 0.14 | 0.01 |
| 048 | 53.6 | 1.3 | 101.3 | 2.0 | 103.2 | 1.9 | 0.24 | 0.01 | 0.19 | 0.01 | 0.12 | 0.01 |
| 049 | 62.1 | 1.1 | 100.1 | 1.9 | 103.1 | 1.9 | 0.23 | 0.01 | 0.25 | 0.01 | 0.14 | 0.01 |
| 050 | 65.9 | 1.1 | 101.3 | 2.0 | 104.0 | 2.3 | 0.22 | 0.01 | 0.29 | 0.01 | 0.16 | 0.01 |
| 051 | 33.9 | 1.7 | 102.9 | 2.5 | 102.7 | 1.9 | 0.20 | 0.01 | 0.11 | 0.02 | 0.06 | 0.01 |
| 052 | 42.5 | 1.5 | 102.2 | 2.4 | 102.3 | 1.9 | 0.21 | 0.01 | 0.16 | 0.02 | 0.07 | 0.01 |
| 053 | 41.0 | 1.6 | 104.1 | 2.5 | 102.4 | 2.0 | 0.22 | 0.01 | 0.18 | 0.01 | 0.05 | 0.00 |
| 054 | 66.6 | 1.0 | 104.0 | 2.4 | 101.1 | 2.0 | 0.2 | 0.01 | 0.43 | 0.02 | 0.08 | 0.01 |
| 055 | 55.1 | 1.0 | 102.7 | 2.0 | 100.9 | 1.5 | 0.22 | 0.01 | 0.29 | 0.01 | 0.06 | 0.00 |
| 056 | 48.2 | 1.5 | 106.0 | 3.6 | 100.5 | 1.9 | 0.22 | 0.02 | 0.24 | 0.02 | 0.08 | 0.01 |
| 057 | 39.7 | 2.2 | 106.2 | 4.1 | 101.4 | 2.6 | 0.20 | 0.02 | 0.19 | 0.02 | 0.07 | 0.01 |
| 058 | 16.8 | 2.3 | 99.4 | 4.2 | 99.8 | 2.4 | 0.12 | 0.03 | 0.00 | 0.00 | 0.04 | 0.01 |
| 059 | 32.2 | 3.2 | 104.2 | 4.1 | 100.5 | 3.5 | 0.18 | 0.02 | 0.15 | 0.02 | 0.04 | 0.01 |
| 060 | 87.6 | 0.4 | 101.7 | 2.9 | 98.6 | 2.5 | 0.16 | 0.01 | 0.57 | 0.02 | 0.16 | 0.01 |
| 061 | 95.9 | 0.3 | 105.4 | 3.2 | 97.2 | 2.7 | 0.08 | 0.01 | 0.75 | 0.03 | 0.19 | 0.01 |
| 062 | 98.6 | 0.1 | 105.1 | 4.6 | 96.8 | 4.3 | 0.04 | 0.00 | 0.81 | 0.04 | 0.19 | 0.01 |
| 063 | 67.2 | 1.4 | 102.9 | 3.0 | 100.4 | 3.1 | 0.23 | 0.02 | 0.36 | 0.02 | 0.12 | 0.01 |
| 064 | 38.1 | 3.0 | 102.2 | 3.6 | 100.5 | 3.5 | 0.20. | 0.01 | 0.15 | 0.01 | 0.05 | 0.00 |
| 065 | 50.5 | 1.8 | 104.5 | 2.5 | 101.7 | 2.6 | 0.22 | 0.01 | 0.25 | 0.01 | 0.07 | 0.00 |
| 066 | 55.0 | 1.9 | 103.6 | 2.9 | 101.1 | 3.0 | 0.22 | 0.01 | 0.29 | 0.02 | 0.08 | 0.01 |
| 067 | 36.7 | 1.9 | 102.9 | 2.8 | 101.0 | 2.3 | 0.20 | 0.02 | 0.14 | 0.01 | 0.05 | 0.00 |
| 068 | 48.0 | 2.1 | 106.3 | 3.0 | 101.9 | 2.9 | 0.23 | 0.01 | 0.23 | 0.01 | 0.07 | 0.00 |
| 069 | 27.2 | 4.1 | 103.4 | 4.6 | 102.2 | 4.4 | 0.17 | 0.02 | 0.10 | 0.01 | 0.04 | 0.01 |
| 070 | 37.1 | 2.1 | 102.9 | 2.7 | 101.1 | 2.5 | 0.20 | 0.01 | 0.14 | 0.01 | 0.05 | 0.00 |
| 071 | 50.2 | 2.0 | 105.0 | 2.8 | 101.1 | 3.0 | 0.22 | 0.01 | 0.25 | 0.01 | 0.08 | 0.00 |
| 072 | 19.5 | 3.0 | 100.2 | 3.3 | 100.5 | 3.1 | 0.12 | 0.01 | 0.05 | 0.01 | 0.03 | 0.00 |
| 073 | 24.3 | 5.0 | 100.8 | 5.3 | 100.5 | 5.3 | 0.16 | 0.01 | 0.06 | 0.01 | 0.04 | 0.00 |
| 074 | 30.4 | 3.4 | 100.4 | 3.7 | 100.1 | 3.7 | 0.19 | 0.01 | 0.07 | 0.01 | 0.04 | 0.00 |
| 075 | 35.8 | 2.5 | 101.2 | 3.0 | 100.7 | 2.9 | 0.22 | 0.01 | 0.10 | 0.01 | 0.05 | 0.00 |
| 076 | 43.2 | 1.9 | 107.7 | 3.5 | 103.6 | 2.5 | 0.22 | 0.02 | 0.22 | 0.02 | 0.07 | 0.00 |

| Run No. | X(%) | e(X) | CBal | e(CBal) | PBal | e(PBal) | CO | e(CO) | $CO_2$ | e($CO_2$) | $CH_4$ | e($CH_4$) |
|---|---|---|---|---|---|---|---|---|---|---|---|---|
| 077 | 52.2 | 1.5 | 106.9 | 2.7 | 102.9 | 2.3 | 0.21 | 0.01 | 0.30 | 0.02 | 0.08 | 0.00 |
| 078 | 59.0 | 1.4 | 107.5 | 2.6 | 102.5 | 2.3 | 0.21 | 0.01 | 0.36 | 0.02 | 0.09 | 0.00 |
| 079 | 30.2 | 3.8 | 103.1 | 4.3 | 101.9 | 4.2 | 0.19 | 0.02 | 0.10 | 0.01 | 0.05 | 0.00 |
| 080 | 35.7 | 2.2 | 103.4 | 2.7 | 101.7 | 2.6 | 0.22 | 0.01 | 0.12 | 0.01 | 0.05 | 0.00 |
| 081 | 42.7 | 2.4 | 102.9 | 2.9 | 100.6 | 2.9 | 0.24 | 0.01 | 0.16 | 0.01 | 0.06 | 0.00 |
| 082 | 46.4 | 1.5 | 103.4 | 2.4 | 102.3 | 2.1 | 0.27 | 0.02 | 0.14 | 0.01 | 0.08 | 0.00 |
| 083 | 54.9 | 1.5 | 104.6 | 2.2 | 102.2 | 2.3 | 0.29 | 0.01 | 0.20 | 0.01 | 0.10 | 0.00 |
| 084 | 63.7 | 1.7 | 104.8 | 2.7 | 101.5 | 3.3 | 0.30 | 0.01 | 0.27 | 0.01 | 0.11 | 0.01 |
| 085 | 17.5 | 3.1 | 97.5 | 3.3 | 99.3 | 3.2 | 0.09 | 0.01 | 0.04 | 0.01 | 0.02 | 0.00 |
| 086 | 22.0 | 3.2 | 98.3 | 3.4 | 98.8 | 3.3 | 0.13 | 0.01 | 0.04 | 0.01 | 0.03 | 0.00 |
| 087 | 60.5 | 1.1 | 104.1 | 2.4 | 102.3 | 2.0 | 0.24 | 0.01 | 0.30 | 0.02 | 0.11 | 0.00 |
| 088 | 74.3 | 1.1 | 105.0 | 2.6 | 101.2 | 3.1 | 0.22 | 0.01 | 0.44 | 0.02 | 0.13 | 0.01 |
| 089 | 83.8 | 0.7 | 106.0 | 2.9 | 99.3 | 2.8 | 0.18 | 0.01 | 0.58 | 0.03 | 0.14 | 0.01 |
| 090 | 23.9 | 2.1 | 106.7 | 2.8 | 102.4 | 2.2 | 0.16 | 0.01 | 0.10 | 0.02 | 0.04 | 0.00 |
| 091 | 31.5 | 2.4 | 107.5 | 3.1 | 102.7 | 2.7 | 0.20 | 0.01 | 0.14 | 0.02 | 0.06 | 0.00 |
| 092 | 45.2 | 3.3 | 105.4 | 4.4 | 102.5 | 4.3 | 0.22 | 0.01 | 0.21 | 0.03 | 0.07 | 0.01 |
| 093 | 69.3 | 0.7 | 107.7 | 1.7 | 102.1 | 1.5 | 0.24 | 0.01 | 0.41 | 0.01 | 0.12 | 0.00 |
| 094 | 77.4 | 1.2 | 109.4 | 3.1 | 101.9 | 4.0 | 0.22 | 0.01 | 0.52 | 0.03 | 0.13 | 0.01 |
| 095 | 82.5 | 0.7 | 107.2 | 2.4 | 100.6 | 2.9 | 0.19 | 0.01 | 0.57 | 0.02 | 0.14 | 0.01 |
| 096 | 57.0 | 1.2 | 104.9 | 2.2 | 102.3 | 2.0 | 0.25 | 0.01 | 0.25 | 0.01 | 0.11 | 0.01 |
| 097 | 67.5 | 1.8 | 103.4 | 3.1 | 101.6 | 4.1 | 0.23 | 0.01 | 0.34 | 0.02 | 0.13 | 0.01 |
| 098 | 73.8 | 0.8 | 103.9 | 2.5 | 101.1 | 1.9 | 0.22 | 0.01 | 0.41 | 0.02 | 0.15 | 0.01 |

## 8.2 AB INITIO CALCULATION RESULTS

The information in this section complements the results in the tables in Chapter 4. With the information in this section and Chapter 4, the thermochemistry and reaction rates calculated in this thesis can be reproduced.

**Figure 8-1: CBS-Q structures for compounds included in MPA SCWO model**
The geometries are optimized at the MP2/6-31g(d') level. Most of the ab initio calculated structures are in Figure 4-2.

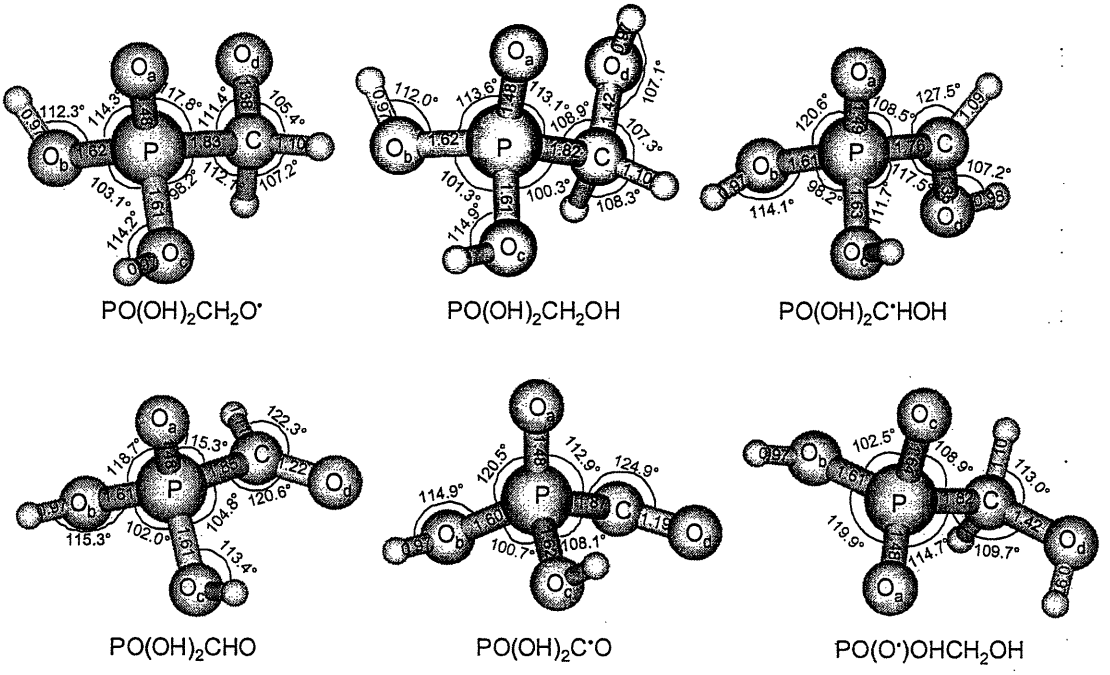

## Table 8-3: Calculated information for the phosphorus-containing species from CBS-Q calculations (calculated at the HF/6-31g(d') level)

The $PO(OH)_3CH_3$ information was calculated at the B3LYP/CBSB7 level in the CBS-QB3 method. Italicized vibrational frequencies were replaced with internal rotors to calculate the thermochemistry and partition functions.

| Species | $\sigma_{ext}$ | Vibrational Frequencies ($cm^{-1}$) | Rotational Constants ($cm^{-1}$) |
|---|---|---|---|
| $PO(OH)_2CH_3$ | 1 | *99.5*, *198.5*, 276.6, 320.6, *361.6*, 420.7, 470.9, 476.6, 787.4, 931.0, 953.0, 1010.5, 1045.6, 1089.6, 1141.0, 1393.7, 1502.7, 1591.1, 1591.6, 3216.2, 3308.9, 3309.2, 4089.6, 4094.0 | 0.150<br>0.140<br>0.133 |
| $PO(OH)_3$ | 3 | *175.1*, *175.7*, *313.6*, 409.8, 409.9, 505.9, 507.9, 507.9, 914.7, 1010.3, 1010.3, 1120.6, 1136.9, 1137.0, 1425.51, 4099.3, 4099.3, 4105.0 | 0.153<br>0.153<br>0.152 |
| $PO(OH)_2CH_2$ | 1 | *124.4*, *156.3*, 283.7, 341.9, *374.0*, 424.8, 472.9, 480.1, 560.4, 833.4, 917.3, 966.2, 1025.9, 1096.6, 1141.5, 1385.4, 1538.5, 3328.8, 3447.1, 4085.7, 4090.2 | 0.153<br>0.148<br>0.137 |
| $PO_2(OH)CH_3$ | 1 | *191.6*, 208.8, 293.2, *333.3*, 389.7, 461.1, 479.6, 777.0, 904.6, 947.9, 1000.4, 1040.5, 1111.9, 1404.4, 1502.6, 1587.4, 1589.1, 3213.4, 3304.9, 3309.3, 4077.7 | 0.155<br>0.142<br>0.137 |
| $PO(OH)_3CH_3$ | 1 | 81.0, 95.7, 205.4, 223.5, 270.1, 349.2, 378.1, 446.0, 455.3, 481.3, 529.7, 579.2, 672.4, 697.9, 860.1, 886.5, 942.9, 957.4, 1035.8, 1056.1, 1157.7, 1350.9, 1458.7, 1475.5, 3056.44, 3129.4, 3167.2, 3801.6, 3809.2, 3850.1 | 0.118<br>0.097<br>0.094 |
| $PO(OH)_2CH_2O$ | 1 | *101.5*, *167.8*, *190.5*, 273.8, 313.9, 369.6, 430.8, 475.7, 539.4, 730.6, 798.9, 948.3, 996.6, 1101.7, 1123.0, 1155.9, 1230.3, 1407.4, 1445.7, 1544.4, 3193.8, 3253.5, 4086.1, 4092.9 | 0.143<br>0.081<br>0.078 |
| $PO(OH)_2CHO$ | 1 | *78.1*, *159.2*, *208.8*, 245.1, 305.8, 387.4, 451.5, 471.9, 568.2, 810.7, 956.3, 1009.1, 1026.9, 1094.9, 1117.9, 1408.1, 1508.4, 2011.7, 3166.1, 4080.5, 4092.9 | 0.147<br>0.083<br>0.081 |
| $PO(OH)_2CO$ | 1 | *81.9*, *125.2*, 192.3, *291.2*, 345.0, 381.5, 462.3, 472.5, 553.9, 692.4, 947.2, 1008.1, 1083.6, 1118.6, 1420.8, 2166.4, 4079.0, 4083.6 | 0.149<br>0.082<br>0.081 |
| $PO(OH)_2CH_2OH$ | 1 | *93.0*, 173.4, *177.7*, 286.2, *298.8*, 370.0, 455.6, *461.1*, 481.2, 545.7, 796.9, 933.4, 962.8, 1015.5, 1103.5, 1125.8, 1192.2, 1266.2, 1394.4, 1472.1, 1537.6, 1615.0, 3208.2, 3304.9, 4089.1, 4089.9, 4096.0 | 0.143<br>0.079<br>0.076 |
| $PO(OH)_2CHOH$ | 1 | *74.8*, 206.8, *225.5*, *259.5*, *334.2*, 364.7, 409.7, 465.7, 500.5, 574.1, 615.4, 840.1, 946.5, 990.9, 1118.0, 1127.3, 1274.3, 1377.5, 1425.2, 1574.5, 3409.4, 4035.0, 4087.7, 4093.1 | 0.154<br>0.078<br>0.075 |
| $PO_2OHCH_2OH$ | 1 | 95.5, 179.3, 222.0, 299.6, 319.4, 398.8, 439.8, 468.5, 534.2, 779.5, 906.1, 964.1, 1004.5, 1095.7, 1202.7, 1268.0, 1403.5, 1471.6, 1535.5, 1611.9, 3201.9, 3295.2, 4074.4, 4089.8 | 0.148<br>0.080<br>0.076 |
| $PO_2CH_3$ | 1 | *52.0*, 323.4, 407.9, 494.3, 777.8, 955.7, 1014.8, 1290.9, 1475.7, 1574.0, 1584.6, 1600.6, 3218.0, 3300.9, 3343.6 | 0.291<br>0.260<br>0.141 |
| $POOHCH_2$ | 1 | 306.3, 367.5, 376.2, 443.8, 613.2, 739.7, 884.5, 951.1, 1082.8, 1156.2, 1465.7, 1548.4, 3351.2, 3457.4, 4101.5 | 0.299<br>0.269<br>0.142 |
| $PO(OH)_2$ | 2 | *147.4*, *291.9*, 384.4, 426.6, 517.6, 897.9, 951.7, 1070.5, 1104.2, 1351.9, 4074.3, 4090.2 | 0.296<br>0.261<br>0.151 |
| $PO_2OH$ | 1 | 443.3, 483.3, 503.9, 581.3, 1000.5, 1129.1, 1314.8, 1613.4, 4067.1 | 0.326<br>0.298<br>0.156 |
| $P(OH)_4$ | 1 | *82.0*, 152.8, 259.5, 408.1, 455.9, 469.3, 472.3, 502.0, 565.3, 621.3, 851.6, 918.6, 984.4, 1070.4, 1149.4, 1168.0, 1253.9, 4030.8, 4116.0, 4120.6, 4127.4 | 0.194<br>0.133<br>0.106 |
| POOH | 1 | 442.0, 618.8, 942.4, 1055.7, 1419.7 | 1.228<br>0.328<br>0.259 |

## Table 8-4: Internal rotation information for stable species

$\sigma_{int}$ is the internal rotor symmetry number, $I_R$ is the reduced moment of inertia about the rotor and the potential is the maximum energy calculated at the HF/6-31g(d') level

| Species | Rotor | $\sigma_{int}$ | $I_R$ | Potential (kcal/mol) |
|---|---|---|---|---|
| $PO(OH)_2CH_3$ | OH | 1 | 0.73 | 5.33 |
| | OH | 1 | 0.73 | 5.33 |
| | $CH_3$ | 3 | 3.05 | 2.25 |
| $PO(OH)_3$ | OH | 1 | 0.79 | 0.97 |
| | OH | 1 | 0.79 | 0.97 |
| | OH | 1 | 0.79 | 0.97 |
| $PO(OH)_2CH_2$ | OH | 1 | 0.80 | 4.71 |
| | OH | 1 | 0.80 | 4.71 |
| | $CH_2$ | 2 | 1.73 | 0.36 |
| $PO_2OHCH_3$ | OH | 1 | 0.78 | 6.46 |
| | $CH_3$ | 3 | 3.10 | 2.11 |
| $PO(OH)_2CH_2O$ | OH | 1 | 0.72 | 6.95 |
| | OH | 1 | 0.74 | 2.95 |
| | $CH_2O$ | 1 | 22.55 | 3.51 |
| $PO(OH)_2CHO$ | OH | 1 | 0.72 | 2.27 |
| | OH | 1 | 0.70 | 2.75 |
| | CHO | 1 | 14.96 | 2.20 |
| $PO(OH)_2CO$ | OH | 1 | 0.70 | 3.53 |
| | OH | 1 | 0.72 | 1.93 |
| | CO | 1 | 12.05 | 1.71 |
| $PO(OH)_2CH_2OH$ | OH | 1 | 0.77 | 5.92 |
| | OH | 1 | 0.74 | 3.78 |
| | C-OH | 1 | 0.76 | 3.11 |
| | $CH_2OH$ | 1 | 24.47 | 4.73 |
| $PO(OH)_2CHOH$ | OH | 1 | 0.74 | 4.37 |
| | OH | 1 | 0.71 | 4.38 |
| | C-OH | 1 | 0.79 | 5.87 |
| | CHOH | 1 | 18.45 | 3.41 |
| $PO_2CH_3$ | $CH_3$ | 3 | 2.97 | 0.02 |
| $PO(OH)_2$ | OH | 1 | 0.71 | 2.35 |
| | OH | 1 | 0.72 | 4.44 |
| $P(OH)_4$ | OH | 1 | 0.72 | 2.76 |

## Table 8-5: Internal rotation information for transition states

$\sigma_{int}$ is the internal rotor symmetry number, $I_R$ is the reduced moment of inertia about the rotor and the potential is the maximum energy calculated at the HF/6-31g(d') level

| Species | Rotor | $s_{int}$ | $I_R$ | Potential (kcal/mol) |
|---|---|---|---|---|
| $TS_1$ | $CH_3$ | 3 | 3.11 | 2.47 |
| $TS_2$ | OH | 1 | 0.80 | 8.79 |
| | $CH_3$ | 3 | 3.95 | 0.99 |
| $TS_3$ | OH | 1 | 0.78 | 3.77 |
| $TS_5$ | OH | 1 | 0.90 | 2.16 |
| | OH | 1 | 0.71 | 4.50 |
| | OH | 1 | 0.74 | 3.58 |
| | $CH_3$-OH | 1 | 54.29 | 3.12 |
| $TS_6$ | OH | 1 | 0.73 | 6.27 |
| | OH-OH | 1 | 49.03 | 8.24 |
| | $CH_3$ | 3 | 3.08 | 1.99 |
| $TS_9$ | OH | 1 | 0.79 | 5.61 |
| $TS_{10}$ | OH-H | 1 | 1.28 | 3.06 |
| | OH | 1 | 0.80 | 1.28 |
| | OH | 1 | 0.79 | 2.09 |
| $TS_{11}$ | OH | 1 | 0.71 | 3.17 |
| | OH | 1 | 0.73 | 5.96 |
| | OH | 1 | 0.73 | 3.17 |
| | OH | 1 | 1.00 | 3.26 |
| $TS_{12}$ | OH | 1 | 0.75 | 10.25 |

## Table 8-6: The MP2/6-31g(d') optimized geometric parameters for the phosphorus-containing species (distance in Angstroms)

$PO(OH)_2CH_3$

| Elements | x-coord | y-coord | z-coord |
|---|---|---|---|
| P | 0.038693 | -0.030572 | 0.137642 |
| O | 0.37766 | -0.24857 | 1.565998 |
| O | 1.337353 | 0.142602 | -0.822676 |
| O | -0.840877 | -1.230076 | -0.515247 |
| C | -0.928636 | 1.395354 | -0.349421 |
| H | 2.137319 | -0.232562 | -0.427022 |
| H | -0.757526 | -2.056786 | -0.018418 |
| H | -0.400851 | 2.3102 | -0.062621 |
| H | -1.078299 | 1.389947 | -1.433936 |
| H | -1.902315 | 1.364016 | 0.149299 |

$PO(OH)_3$

| Elements | x-coord | y-coord | z-coord |
|---|---|---|---|
| P | 0.000158 | -0.000466 | 0.122394 |
| O | 0.00208 | -0.006079 | 1.598446 |
| O | 1.423246 | -0.194758 | -0.593527 |
| O | -0.883396 | -1.132481 | -0.594088 |
| H | 2.138907 | 0.280007 | -0.14885 |
| H | -0.827721 | -1.991674 | -0.153636 |
| O | -0.542159 | 1.333981 | -0.585148 |
| H | -1.311727 | 1.713352 | -0.138882 |

$PO(OH)_2CH_2$

| Elements | x-coord | y-coord | z-coord |
|---|---|---|---|
| C | 0.101287 | -0.084518 | -1.722466 |
| P | -0.082167 | -0.085046 | 0.036317 |
| O | 1.45845 | -0.286625 | 0.498408 |
| O | -1.021783 | -1.030344 | 0.691425 |
| O | -0.449021 | 1.47171 | 0.300144 |
| H | -1.022874 | 1.583934 | 1.072086 |
| H | 1.526488 | -0.765266 | 1.337494 |
| H | -0.576218 | 0.494635 | -2.34105 |
| H | 0.796211 | -0.768427 | -2.198307 |

$PO_2OHCH_3$

| Elements | x-coord | y-coord | z-coord |
|---|---|---|---|
| C | -0.087269 | -0.045534 | -1.703572 |
| P | -0.08516 | -0.082153 | 0.087533 |
| O | 1.503766 | -0.11973 | 0.367044 |
| O | -0.938034 | -1.06924 | 0.786333 |
| O | -0.523249 | 1.421963 | 0.574771 |
| H | 1.735396 | -0.23275 | 1.301552 |
| H | -1.114264 | 0.093849 | -2.056285 |
| H | 0.538667 | 0.774048 | -2.072358 |
| H | 0.301355 | -0.993593 | -2.089663 |

$PO(OH)_2CH_2O$

| Elements | x-coord | y-coord | z-coord |
|---|---|---|---|
| P | 0.064226 | 0.16782 | -0.371604 |
| C | 0.005501 | 0.074188 | 1.450544 |
| O | 1.392419 | 0.121633 | -1.023875 |
| O | -0.813 | 1.508415 | -0.560837 |
| O | -0.951217 | -1.004444 | -0.840599 |
| O | 0.472158 | -1.142867 | 1.909198 |
| H | 0.511999 | 0.929589 | 1.92624 |
| H | -1.058427 | 0.114 | 1.753252 |
| H | -0.486392 | -1.758738 | -1.230435 |
| H | -0.766449 | 1.890826 | -1.449343 |

$PO(OH)_2CHO$

| Elements | x-coord | y-coord | z-coord |
|---|---|---|---|
| C | -0.367215 | -0.195293 | -0.027048 |
| P | 1.464368 | -0.035091 | -0.196898 |
| O | -1.075676 | -0.667364 | -1.238406 |
| O | -0.396701 | -1.115522 | 1.291209 |
| O | -0.854734 | 1.232549 | 0.548618 |
| O | 1.961272 | 1.00617 | -0.584376 |
| H | 2.073754 | -0.938484 | 0.022997 |
| H | -1.275592 | -1.412975 | 1.568957 |
| H | -1.149433 | 1.844736 | -0.141209 |

$PO(OH)_2CO$

| Elements | x-coord | y-coord | z-coord |
|---|---|---|---|
| P | 0.130537 | -0.148176 | -0.347895 |
| C | 0.152752 | -0.040963 | 1.513857 |
| O | 1.473759 | -0.014799 | -0.948146 |
| O | -0.673573 | -1.528091 | -0.456918 |
| O | -0.984382 | 0.892974 | -0.898448 |
| O | 0.023379 | 0.960651 | 2.138572 |
| H | -0.983536 | -1.750161 | -1.347495 |
| H | -0.604493 | 1.732695 | -1.197704 |

$PO(OH)_2CH_2OH$

| Elements | x-coord | y-coord | z-coord |
|---|---|---|---|
| C | 0.146129 | 0.033888 | -1.428304 |
| P | 0.139894 | 0.05602 | 0.38684 |
| O | 1.724155 | 0.061293 | 0.6794 |
| O | -1.187388 | 0.176555 | -1.895615 |
| O | -0.27425 | -1.429573 | 0.897762 |
| O | -0.706115 | 1.136468 | 0.952436 |
| H | 0.813603 | 0.831668 | -1.793496 |
| H | 0.520788 | -0.924539 | -1.801956 |
| H | -1.193319 | -1.4664 | 1.199617 |
| H | 1.966353 | -0.041675 | 1.611091 |
| H | -1.533818 | 0.999376 | -1.519898 |

$PO(OH)_2CHOH$

| Elements | x-coord | y-coord | z-coord |
|---|---|---|---|
| C | 0.062404 | 0.02578 | -1.408754 |
| P | 0.092813 | -0.048597 | 0.350419 |
| O | 1.627992 | 0.266662 | 0.70652 |
| O | -0.932411 | 0.734363 | -1.984784 |
| O | 0.040849 | -1.585425 | 0.890452 |
| O | -0.999919 | 0.812807 | 0.877687 |
| H | 0.728028 | -0.475412 | -2.101507 |
| H | -0.863055 | -1.880711 | 1.071914 |
| H | 1.908491 | -0.062429 | 1.573149 |
| H | -1.432164 | 1.165578 | -1.266323 |

$PO_2(OH)CH_2OH$

| Elements | x-coord | y-coord | z-coord |
|---|---|---|---|
| C | 0.271147 | 1.39174 | -0.101292 |
| P | -0.124386 | -0.379762 | -0.134989 |
| O | -1.012218 | -0.448937 | -1.477415 |
| O | 1.141563 | 1.666102 | 0.980479 |
| O | -1.225972 | -0.699371 | 1.033843 |
| O | 1.042877 | -1.277228 | 0.026029 |
| H | 0.697828 | 1.66932 | -1.079833 |
| H | -0.635464 | 1.987566 | 0.052647 |
| H | -1.314795 | -1.335743 | -1.726631 |
| H | 1.921337 | 1.100314 | 0.882916 |

$PO_2CH_3$

| Elements | x-coord | y-coord | z-coord |
|---|---|---|---|
| P | 0.157777 | 0 | 0.118476 |
| O | -0.127413 | 0 | 1.568173 |
| O | 1.420627 | 0 | -0.64822 |
| C | -1.318138 | 0 | -0.939778 |
| H | -2.224667 | 0 | -0.329297 |
| H | -1.289432 | 0.885782 | -1.584398 |
| H | -1.289432 | -0.885782 | -1.584398 |

$PO(OH)CH_2$

| Elements | x-coord | y-coord | z-coord |
|---|---|---|---|
| P | -0.070272 | -0.016234 | 0.115637 |
| O | -0.030697 | -0.260703 | 1.570729 |
| O | 1.389219 | 0.034549 | -0.570127 |
| C | -1.296291 | 0.213521 | -0.941069 |
| H | -2.315618 | 0.196396 | -0.572087 |
| H | -1.105561 | 0.381107 | -1.995663 |
| H | 1.384838 | 0.194111 | -1.525203 |

$PO(OH)_2$

| Elements | x-coord | y-coord | z-coord |
|---|---|---|---|
| P | -0.04439 | 0.327249 | 0.133196 |
| O | -0.439457 | -0.074864 | 1.506111 |
| O | 1.444409 | -0.042338 | -0.388572 |
| O | -0.876319 | -0.359244 | -1.104889 |
| H | 1.445934 | -0.577078 | -1.197452 |
| H | -1.809144 | -0.520085 | -0.901688 |

$PO_2OH$

| Elements | x-coord | y-coord | z-coord |
|---|---|---|---|
| P | 0.132832 | 0 | 0.054017 |
| O | -0.04023 | 0 | 1.516936 |
| O | 1.294959 | 0 | -0.840875 |
| O | -1.250247 | 0 | -0.755391 |
| H | -2.028341 | 0 | -0.175617 |

$P(OH)_4$

| Elements | x-coord | y-coord | z-coord |
|---|---|---|---|
| O | -0.757789 | -1.197483 | 0.385127 |
| P | 0.158669 | 0.012333 | -0.222943 |
| O | 1.579142 | -0.783501 | 0.065456 |
| O | -1.256916 | 0.739247 | -0.946191 |
| O | 0.342774 | 1.166428 | 0.913745 |
| H | -1.059869 | 1.130123 | -1.80714 |
| H | -0.379653 | 1.807865 | 0.861572 |
| H | 1.496439 | -1.463806 | 0.753201 |
| H | -1.694641 | -1.056712 | 0.191417 |

POOH

| Elements | x-coord | y-coord | z-coord |
|---|---|---|---|
| P | -0.367719 | 0 | -0.349335 |
| O | -0.406528 | 0 | 1.285444 |
| H | 0.463229 | 0 | 1.72366 |
| O | 1.038099 | 0 | -0.845899 |

**Table 8-7: The MP2/6-31g(d') optimized geometric parameters for the transition states in reactions (R1) to (R6) and (R9) to (R14) (distances in Angstroms)**

(R1) $PO(OH)_2CH_3 = PO_2CH_3+H_2O$

| Elements | x-coord | y-coord | z-coord |
|---|---|---|---|
| C | 1.360343 | -1.11111 | -0.14744 |
| P | 0.129912 | 0.158984 | 0.195269 |
| O | -1.0923 | -0.17135 | -1.17747 |
| O | 0.622568 | 1.551185 | 0.151627 |
| O | -1.02545 | -0.36341 | 1.073775 |
| H | -1.64128 | -0.37087 | -0.13136 |
| H | -1.36176 | 0.616556 | -1.67817 |
| H | 2.008275 | -1.21318 | 0.730963 |
| H | 0.87191 | -2.06944 | -0.34594 |
| H | 1.973583 | -0.81253 | -1.00335 |

(R2) $PO(OH)_2CH_3 = PO_2OH+CH_4$

| Elements | x-coord | y-coord | z-coord |
|---|---|---|---|
| C | -0.2457 | 0.035385 | -1.77767 |
| P | 0.077095 | -0.11807 | 0.274366 |
| O | 1.53159 | 0.312925 | 0.12111 |
| O | -0.79071 | 1.139414 | 0.785883 |
| O | -0.45748 | -1.42294 | 0.697468 |
| H | -0.33854 | -1.00684 | -2.09205 |
| H | -1.21021 | 0.548519 | -1.74735 |
| H | 0.334205 | 0.572262 | -2.55427 |
| H | -1.61558 | 0.865727 | 1.215319 |
| H | 0.880659 | 0.343849 | -1.10681 |

(R3) $PO(OH)_2CH_3 = PO(OH)CH_2+H_2O$

| Elements | x-coord | y-coord | z-coord |
|---|---|---|---|
| C | 0.074034 | 0.112446 | -1.65786 |
| P | -0.3077 | 0.101816 | -0.00159 |
| O | 1.624108 | -0.03326 | 0.291898 |
| O | -0.67182 | -1.39754 | 0.452193 |
| O | -0.73203 | 1.212797 | 0.880797 |
| H | 2.014807 | 0.741742 | 0.729675 |
| H | -0.73404 | -1.51023 | 1.412804 |
| H | 1.520911 | 0.074142 | -0.81369 |
| H | -0.18421 | -0.8002 | -2.1945 |
| H | -0.20829 | 1.036675 | -2.16233 |

(R4) $PO(OH)_2CH_3 = POOH + CH_3OH$

| Elements | x-coord | y-coord | z-coord |
|---|---|---|---|
| C | -0.230751 | 0.07024 | -1.991253 |
| P | -0.183312 | 0.351163 | 0.308939 |
| O | 1.347872 | 0.683095 | 0.801792 |
| O | 0.224026 | -1.184966 | -0.591182 |
| O | -1.093168 | -0.074863 | 1.416502 |
| H | 1.571516 | 0.246659 | 1.642747 |
| H | -0.513929 | -1.822554 | -0.50316 |
| H | 0.576057 | 0.787288 | -2.130321 |
| H | -0.108178 | -0.802065 | -2.636992 |
| H | -1.221119 | 0.515656 | -2.07574 |

(R5) $PO(OH)_2CH_3+OH=PO(OH)_2CH_2+H_2O$

| Elements | x-coord | y-coord | z-coord |
|---|---|---|---|
| C | 0.289179 | 0.013807 | -1.477428 |
| P | 0.372521 | -0.006102 | 0.318504 |
| O | 1.792264 | -0.706746 | 0.608633 |
| O | -0.660193 | -1.178073 | 0.729238 |
| O | 0.144513 | 1.320068 | 0.94305 |
| O | -2.069954 | 0.555697 | -1.220347 |
| H | 2.125405 | -0.538235 | 1.50235 |
| H | -1.568578 | -0.93333 | 0.483015 |
| H | 0.858318 | 0.816362 | -1.952936 |
| H | 0.422907 | -0.95884 | -1.958706 |
| H | -0.920949 | 0.274858 | -1.667539 |
| H | -1.893035 | 1.420296 | -0.803777 |

(R6) $PO(OH)_2CH_3+OH=PO_2OHCH_3+H_2O$

| Elements | x-coord | y-coord | z-coord |
|---|---|---|---|
| C | -0.215357 | 0.046157 | -2.09221 |
| P | -0.266985 | -0.021523 | -0.30102 |
| O | 1.316298 | -0.01956 | 0.047363 |
| O | -1.023423 | 1.030011 | 0.439011 |
| O | -0.815592 | -1.526574 | -0.06953 |
| O | 1.147377 | 0.513377 | 2.138151 |
| H | -1.237318 | -0.024808 | -2.48014 |
| H | 0.227055 | 0.996924 | -2.4051 |
| H | 0.378926 | -0.783162 | -2.48849 |
| H | -1.124784 | -1.684185 | 0.834899 |
| H | 1.674464 | 0.464111 | 1.209673 |
| H | 0.381302 | 1.098987 | 1.957717 |

(R9) $PO(OH)_3=PO_2OH+H_2O$

| Elements | x-coord | y-coord | z-coord |
|---|---|---|---|
| O | 0.240795 | -1.535624 | 0.516819 |
| P | 0.042189 | -0.224429 | -0.123839 |
| O | 1.373558 | 0.462347 | -0.686562 |
| H | 2.180275 | 0.022346 | -0.380104 |
| O | -1.157515 | 0.273486 | -0.929721 |
| H | -1.324934 | 0.998982 | 0.20122 |
| O | -0.53952 | 1.01353 | 1.109464 |
| H | -0.826719 | 0.63518 | 1.95648 |

(R10) $PO(OH)_3+H=PO(OH)_2+H_2O$

| Elements | x-coord | y-coord | z-coord |
|---|---|---|---|
| O | 1.104283 | 1.166769 | -0.569567 |
| P | 0.092193 | 0.221991 | -0.036629 |
| O | -1.076811 | 0.7635 | 0.944103 |
| O | 0.704071 | -0.916418 | 0.954111 |
| H | 1.637339 | -1.098186 | 0.775846 |
| H | -0.97887 | 0.448838 | 1.85843 |
| O | -0.724116 | -1.013603 | -1.174622 |
| H | -1.152262 | -0.517261 | -1.902646 |
| H | -0.948518 | -2.165243 | -1.414386 |

(R11) $PO(OH)_3+H=P(OH)_4$

| Elements | x-coord | y-coord | z-coord |
|---|---|---|---|
| O | 0.031299 | -0.027992 | -1.463652 |
| P | 0.001437 | -0.043172 | 0.160336 |
| O | 1.604961 | -0.068036 | 0.34777 |
| O | -0.636916 | 1.450479 | 0.358035 |
| O | -0.861963 | -1.241441 | 0.611945 |
| H | 2.087997 | 0.073462 | -0.488071 |
| H | -0.913526 | 1.607071 | 1.272838 |
| H | -1.459441 | -2.009579 | -0.144776 |
| H | -0.835631 | 0.072541 | -1.877822 |

(R12) $P(OH)_4=PO(OH)_2+H_2O$

| Elements | x-coord | y-coord | z-coord |
|---|---|---|---|
| O | -0.124586 | -0.142066 | -1.494593 |
| P | -0.039407 | 0.001038 | 0.490343 |
| O | 1.592933 | -0.126686 | 0.283442 |
| O | -0.607761 | 1.509223 | 0.311028 |
| O | -0.943493 | -1.254961 | 0.272668 |
| H | 2.044289 | -0.148836 | 1.140668 |
| H | -0.75765 | 1.712415 | -0.629977 |
| H | -0.750897 | -1.070637 | -0.949333 |
| H | 0.718617 | -0.392587 | -1.896868 |

(R13) $PO_2OH+H=PO(OH)_2$

| Elements | x-coord | y-coord | z-coord |
|---|---|---|---|
| O | -0.824527 | 1.344827 | 0.093737 |
| P | -0.127305 | 0.055658 | 0.114638 |
| O | 0.930218 | -0.516029 | 1.020251 |
| O | -0.192651 | -0.710801 | -1.292587 |
| H | 0.329639 | -1.528818 | -1.307791 |
| H | 2.275623 | -0.250028 | 1.017012 |

(R14) $PO(OH)_2+O_2=PO_2OH+HO_2$

| Elements | x-coord | y-coord | z-coord |
|---|---|---|---|
| P | 0.080608 | 0.582983 | 0.181741 |
| O | 0.061348 | 0.542392 | 1.648899 |
| O | 1.261001 | 0.560144 | -0.778657 |
| O | -1.157834 | 1.302081 | -0.521345 |
| H | -1.88523 | 1.495976 | 0.090596 |
| H | 0.965211 | -0.738217 | -1.031974 |
| O | -0.0399 | -1.222202 | -0.599568 |
| O | -0.160753 | -2.370228 | 0.02758 |

**Table 8-8: The B3LYP/CBSB7 optimized geometric parameters for $PO(OH)_3CH_3$ and the transition states in reactions (R7) and (R8) (distance in Angstroms)**

$PO(OH)_3CH_3$

| Elements | x-coord | y-coord | z-coord |
|---|---|---|---|
| C | -0.115075 | 0.334862 | -1.746364 |
| P | -0.010597 | -0.017457 | 0.026871 |
| O | 1.12566 | 0.799024 | 0.833641 |
| O | -1.048822 | -0.967971 | 0.732489 |
| O | -1.177278 | 1.2009 | 0.394648 |
| H | -1.187581 | 1.3863 | 1.342669 |
| H | 1.909297 | 0.241823 | 0.927457 |
| H | -0.692385 | 1.236344 | -1.936222 |
| H | 0.896364 | 0.434731 | -2.140207 |
| H | -0.590336 | -0.514254 | -2.242738 |
| O | 1.083649 | -1.330089 | -0.144261 |
| H | 0.648382 | -2.147176 | -0.40797 |

(R7) $PO(OH)_2CH_3+OH=PO(OH)_3CH_3$

| Elements | x-coord | y-coord | z-coord |
|---|---|---|---|
| C | -0.03477 | -0.132254 | -1.760204 |
| P | 0.168117 | 0.036031 | 0.025512 |
| O | 1.795287 | 0.151813 | 0.002647 |
| O | -1.826736 | 0.0114 | 0.233815 |
| O | 0.095609 | -1.35459 | 0.824885 |
| O | -0.212075 | 1.335026 | 0.761472 |
| H | 2.166531 | 0.250067 | 0.887383 |
| H | -0.815129 | -1.520693 | 1.103879 |
| H | 0.923672 | -0.377057 | -2.214876 |
| H | -0.771787 | -0.903707 | -1.972695 |
| H | -0.393463 | 0.817655 | -2.160773 |
| H | -2.239637 | 0.837605 | -0.046929 |

(R8) $PO(OH)_3CH_3=PO(OH)_3+CH_3$

| Elements | x-coord | y-coord | z-coord |
|---|---|---|---|
| C | -1.878769 | 0.049904 | -0.00384 |
| P | 0.056966 | 0.008577 | 0.040664 |
| O | -0.133752 | -0.159471 | 1.585044 |
| O | 0.080415 | 1.450453 | -0.69018 |
| O | 0.161286 | -1.307077 | -0.927648 |
| O | 1.733386 | 0.032643 | 0.191426 |
| H | 0.992505 | 1.7413 | -0.815534 |
| H | 2.093911 | -0.858999 | 0.236522 |
| H | -2.255269 | 0.888827 | 0.575901 |
| H | -2.125765 | 0.205993 | -1.058422 |
| H | -2.315021 | -0.877405 | 0.366634 |
| H | -0.70292 | -1.660173 | -1.161149 |